



HAL
open science

Event-driven numerical modelling of early diagenesis in coastal ecosystems : application to flood deposits in Rhône River prodelta

Stanley Nmor

► **To cite this version:**

Stanley Nmor. Event-driven numerical modelling of early diagenesis in coastal ecosystems : application to flood deposits in Rhône River prodelta. Earth Sciences. Université Paris-Saclay, 2023. English. NNT : 2023UPASJ023 . tel-04336951

HAL Id: tel-04336951

<https://theses.hal.science/tel-04336951>

Submitted on 12 Dec 2023

HAL is a multi-disciplinary open access archive for the deposit and dissemination of scientific research documents, whether they are published or not. The documents may come from teaching and research institutions in France or abroad, or from public or private research centers.

L'archive ouverte pluridisciplinaire **HAL**, est destinée au dépôt et à la diffusion de documents scientifiques de niveau recherche, publiés ou non, émanant des établissements d'enseignement et de recherche français ou étrangers, des laboratoires publics ou privés.

Event-driven numerical modelling of early diagenesis in coastal ecosystems: application to flood deposits in Rhône River prodelta

Modélisation numérique des événements lors de la diagenèse précoce dans les écosystèmes côtiers : application aux dépôts de crue dans le prodelta du Rhône

Thèse de doctorat de l'Université Paris-Saclay

École doctorale n° 129, Sciences de l'Environnement Ile-de-France (SEIF)

Spécialité de doctorat : Géosciences

Graduate School : : Géosciences, climat, environnement et planètes

Référent : Université de Versailles-Saint-Quentin-en-Yvelines

Thèse préparée dans l'unité de recherche **LSCE** (Université Paris-Saclay, CNRS, CEA, UVSQ),
sous la direction de **Christophe RABOUILLE**, Directeur de Recherche CEA,
le co-encadrement d'**Eric VIOLLIER**, MdC

Thèse soutenue à Paris-Saclay, le 13 Octobre 2023, par

Stanley NMOR

Composition du jury

Membres du jury avec voix délibérative

Didier ROCHE

Directeur de Recherche, CNRS Université Paris Saclay - LSCE

Président

Sandra ARNDT

Professeure, Biogeochemistry and Modelling of the Earth System Department of Geosciences, Environment and Society Faculty of Sciences (ULB)

Rapportrice et examinatrice

Anniet LAVERMAN

Directrice de recherche Université de Rennes

Rapportrice et examinatrice

Bruno DEFLANDRE

Maître de conférences, UMR CNRS 5805 EPOC - OASU Université de Bordeaux

Examinateur

Olivier SULPIS

Chargé de recherche, CEREGE/Aix Marseille University

Examinateur

Titre: Modélisation numérique des événements lors de la diagenèse précoce dans les écosystèmes côtiers : application aux dépôts de crue dans le prodelta du Rhône

Mots clés: Diagenèse précoce, Couplage benthique-pélagique, Modélisation numérique, Biogéochimie, Crues massives

Résumé: L'objectif principal de ce travail est d'étudier la réponse biogéochimique des fonds marins côtiers soumis à des dépôts massifs épisodiques de sédiments. Le Rhône et ses marges côtières constituent un cas d'étude important pour quantifier l'impact des dépôts de crue sur les processus diagénétiques dans les sédiments superficiels, car jusqu'à 80% des apports de sédiments sont réalisés lors d'événements courts et intenses de crues. Ces événements extrêmes sont rares et imprévisibles, et il est donc difficile d'évaluer par l'observation directe leur impact sur les processus biogéochimiques des sédiments. Afin d'étudier la réponse à court et moyen terme de la biogéochimie des sédiments dans ces conditions de changement brutal, un modèle numérique de diagenèse précoce a été spécifiquement développé au cours de cette thèse. En utilisant les données publiées de deux crues contrastées en 2008, le modèle a montré sa capacité à simuler les changements induits par l'apport de sédiments sur les profils d'eau interstitielle pour différents solutés. Le modèle suggère que ces crues pourraient produire des réponses biogéochimiques différentes, dont l'ampleur est déterminée par les caractéristiques du dépôt sédimentaire. Nous avons constaté que les taux de minéralisation du carbone organique totaux ont été multipliés par deux au cours de la crue du printemps 2008 par rapport aux conditions antérieures, et qu'ils ont encore augmenté à l'automne lorsqu'un sédiment enrichi en carbone très labile a été déposé (accroissement d'un facteur 7). Mes recherches ont démontré que ces différences étaient dues à la nature du carbone organique du delta proximal du Rhône ainsi qu'à l'épaisseur du dépôt. Ces caractéristiques intrinsèques pourraient également être responsables du temps de relaxation des divers solutés de l'eau interstitielle (par exemple l'oxygène, le carbone inorganique dissous, le sulfate) autour de quelques

mois. La thèse explore également le concept d'*effet mémoire* d'une séquence temporellement connectée de plusieurs dépôts de crue. L'occurrence multiple de ces événements peut déclencher une superposition temporelle entre les crues qui a un effet substantiel sur les processus opérant en profondeur (tels que la méthanogénèse et la réduction des sulfates) mais négligeable pour les processus oxydiques et suboxydiques superficiels. Cela a des conséquences importantes dans les scénarios futurs d'augmentation de la fréquence de ces événements extrêmes.

La récente série temporelle de composition de l'eau interstitielle obtenue au cours des campagnes hivernales de 2021-22 étudie l'évolution temporelle du sédiment après un dépôt de sédiments estimé à 25 cm. Une modification remarquable des profils de DIC, SO_4^{2-} and CH_4 a été observée, qui se distingue de la situation antérieure à la crue. Les simulations du modèle décrivent de manière adéquate l'ensemble des données et montrent que ces événements hivernaux peuvent entraîner une augmentation de 75% de la minéralisation totale du carbone, augmentant ainsi la production de DIC à plus long terme dans les sédiments. Cette crue hivernale entraîne également un découplage des deux voies de réduction du sulfate - la réduction organoclastique du sulfate et l'oxydation anaérobie du méthane - et est associée à un enfoncement dans le sédiment de la zone de transition entre le sulfate et le méthane. Ceci pourrait renforcer l'efficacité du piège de méthane (un gaz à effet de serre crucial dans le contexte du changement climatique) dans le sédiment. Dans l'ensemble, cette thèse fournit pour la première fois une synthèse issue de l'exploration numérique du rôle d'un événement épisodique tel qu'un dépôt de crue massif sur la dynamique spatio-temporelle des processus biogéochimiques dans les sédiments.

Titre: Event-driven numerical modelling of early diagenesis in coastal ecosystems: application to flood deposits in Rhône River prodelta

Keywords: Early diagenesis, Benthic-pelagic coupling, Numerical modelling, Biogeochemistry, Massive flood events

Résumé: The main purpose of this work is to study the biogeochemical response of coastal seafloor subject to episodic massive sediment deposition from floods events. The Rhône River and its connected coastal margins serve as an important case-study site for quantifying the impact of these extreme events on early diagenetic process because it receives significant inputs of sediment (estimated to be up to 80%) during short and intense events. These extreme events are rare and unpredictable, thus the assessment of their impact on sediment biogeochemical processes is difficult.

In order to study the short and intermediate term response of the sediment biogeochemistry under these abruptly changing conditions, an event-driven numerical model of early diagenesis was specifically developed during this thesis. Using published data of two contrasting floods in year 2008, the model showed reliable capability to simulate the changes induced by the sediment input on the porewater profiles for various solutes. The model suggests that these floods could produce differing biogeochemical response, the extent of which is determined by the underlying characteristics of the flood layer deposit. We found a two-fold increase in overall mineralization rates during the 2008 spring flood event from pre-flood conditions in the spring, which increased further in the fall when a very labile carbon-enrichment sediment was deposited (up to a factor of 7). My research demonstrated that these differences were due to the nature of organic carbon delivered to the proximal delta of the Rhone as well as the scale (thickness) of deposition. These intrinsic characteristics might also be responsible for constraining the relaxation timescale of the various porewater solutes (e.g oxygen, dissolved inorganic carbon, sulfate) to a few months as observed in the field. Furthermore, this research also demonstrated that the strong internal cycling and the role of secondary redox processes such as pyrite pre-

cipitation which were enhanced during these flood events might be responsible for the maintenance of non-sulfidic condition observed in Rhône prodelta sediment. The thesis also briefly explores the concept of "*memory effect*" of temporally connected sequence of flood deposition with the conclusion that the multiple occurrence of these events can also trigger temporal interaction between floods which has a substantial effect on the processes operating in the deep (such as methanogenesis and sulfate reduction) but negligible for superficial oxic and suboxic processes. This has significant ramification in the future scenarios of increasing frequency of these extreme events.

More recent time series of porewater composition obtained during winter campaigns in 2021-22 investigates the temporal evolution of the porewater following an estimated 25 cm of sediment deposition. A remarkable modification of the DIC, SO_4^{2-} and CH_4 profiles were observed which was distinguishable from the pre-flood situation. Model simulations describes adequately the dataset and showed that these winter events can result to as much as 75% increase in total carbon mineralization, thus enhancing longer-term DIC production in the sediment. This winter flood also leads to a decoupling of the two pathways for sulfate reduction - organoclastic sulfate reduction and anaerobic oxidation of methane and is associated to vertical displacement of the sulfate-methane transition zone. This observation has important implications since further deepening of the AOM maximum zone due to flood deposition could enhance the effective trapping of methane (a "green house" gas crucial in the context of climate change) flux out of the sediment.

Overall, the numerical exploration in this thesis provides for the first time, a synthesis of the role of episodic event such as the massive flood deposition on spatio-temporal dynamics of the biogeochemical processes in the sediment.

Résumé long en français: La biogéochimie des sédiments côtiers est fortement influencée par les apports terrestres et en particulier par les matériaux provenant des rivières. Ces apports sont très souvent concentrés lors d'évènements abrupts comme les crues qui contribuent largement à la sédimentation du carbone dans les deltas et aux régimes diagénétiques, ce qui entraîne souvent des conditions non-stationnaires pour les cycles du carbone et des nutriments dans les sédiments des marges océaniques dominées par les fleuves (RiOMar). L'objectif principal de cette thèse est d'étudier l'impact de la sédimentation hautement non-stationnaire générée par les dépôts de crue sur la transformation de la matière organique au cours de la diagenèse précoce. Les mesures à haute fréquence qui décrivent ce phénomène transitoire sont essentielles pour atteindre cet objectif, mais elles sont difficiles à obtenir. Ainsi, en raison de la rareté et de l'imprévisibilité de ces événements, notre compréhension de l'impact des flux massifs de carbone organique générés par les dépôts des crues sur la biogéochimie des sédiments est limitée. Des modèles numériques capables de reproduire les nombreux processus biogéochimiques clés sont nécessaires car ils peuvent combler les lacunes dans les séries de données issues de l'observation, fournissant ainsi un outil pour les études à haute résolution.

Dans cette thèse, j'ai d'abord identifié les forces et les faiblesses des modèles actuels de diagenèse précoce dans la représentation des transformations biogéochimiques induites par les inondations dans les sédiments. Mon analyse a révélé que les modèles actuels représentent de manière appropriée le transport réactif et les processus biogéochimiques. Toutefois, ils manquent de la possibilité de décrire explicitement la réponse à court terme et les caractéristiques de divers profils d'eau interstitielle typiques des sédiments de surface influencés par le flux de carbone organique dérivé du dépôts de crue.

La conclusion du diagnostic sur les modèles biogéochimiques benthiques a conduit au développement d'un outil numérique de complexité intermédiaire adapté à l'étude de l'impact de ces phénomènes transitoires sur les processus diagénétiques précoces. Des études de terrain antérieures, qui ont identifié l'occurrence de deux dépôts de crue majeurs, ont été utilisées : un dépôt de 30 cm pauvre en matière organique au printemps et un dépôt de 10 cm riche en matière organique à l'automne. Le nouveau modèle a été capable de reproduire les tendances de la base des données de terrain sur le solide et la fraction dissoute des sédiments affectées par deux événements contrastés de la crue de 2008 dans le prodelta du Rhône. Les flux et les taux de réaction biogéochimiques répondent rapidement à ce changement quasi instantané dans les sédiments. En utilisant le modèle, nous avons observé que la demande en oxygène benthique est modifiée différemment en fonction de la composition du matériau de crue. Lors de la crue du printemps, les flux d'oxygène consommé par le sédiment ont diminué de 55% par rapport à leur valeur avant la crue, alors que la consommation de O_2 a augmenté pour la crue d'automne. Mes recherches démontrent quantitativement que ces différences étaient dues à la nature du carbone organique déposé dans mes sédiments du delta proximal du Rhône et à l'épaisseur du dépôt. Ces caractéristiques intrinsèques des dépôts sont contraignant de l'échelle de temps de relaxation des différents solutés de l'eau interstitielle (par exemple, l'oxygène environ quelques jours, et entre 4 et 5 mois pour les solutés plus profonds comme le DIC et le SO_4^{2-}) dans la fenêtre temporelle telle qu'observée sur le terrain avec l'occurrence d'événements épisodiques. En outre, ces dépôts liés aux crues de 2008 ont probablement induit de forts taux de minéralisation anoxique dominés par la réduction des sulfates (72% du total) et la méthanogénèse (8%), qui ont été multipliés par plus de deux par rapport à leur valeur avant les crues. Après chaque dépôt de crue, le modèle suggère également qu'un fort cycle interne de fer (80%) et de manganèse (40%) ainsi qu'une précipitation intense de minéraux sont peut-être responsables du maintien de l'état non-euxinique (sans sulfure) des eaux porales des sédiments du prodelta du Rhône. Ma recherche explore également brièvement le concept de "l'effet mémoire" d'une séquence de dépôts de crue liés dans le

temps. J'ai montré que l'occurrence multiple de ces événements peut également déclencher des interactions temporelles entre les dépôts de crues, ce qui a un effet substantiel sur les processus opérant en profondeur (tels que la méthanogénèse et la réduction des sulfates), mais négligeable pour les processus oxydés et sub-oxydés superficiels. Cela a des répercussions importantes sur les conséquences futures de l'augmentation de la fréquence de ces événements extrêmes.

Afin de souligner l'importance de ce phénomène, l'observation d'une crue hivernale récente en 2021-22 a fourni un nouvel ensemble de données pour comprendre les variations temporelles des flux sédiments-eau, des voies biogéochimiques et de leurs taux de réaction dans le prodelta du Rhône. En utilisant une série temporelle de la composition de l'eau interstitielle obtenue après le dépôt de cette crue hivernale, un dépôt de sédiments estimé à 25 cm a été observé. Ce dépôt massif a entraîné une modification significative de la distribution des concentrations en CH_4 , DIC et SO_4^{2-} par rapport à la situation antérieure à la crue. La nature temporelle des données observées sur l'eau interstitielle a montré qu'à la suite de cette crue hivernale, une lente réorganisation des profils de concentration dans l'eau interstitielle commence à émerger, principalement sous l'effet du transport diffusif et des réactions biogéochimiques dans la colonne sédimentaire. En utilisant le modèle diagénétique développé dans cette étude pour calculer les taux et les flux de réactions biogéochimiques, mes recherches ont montré que cette crue hivernale particulière peut augmenter le taux de minéralisation du carbone organique total dans les sédiments de 75% quelques jours après le dépôt, avec une augmentation de la contribution de la réduction du sulfate à la minéralisation totale de 25% par rapport à la période de dépôt sans la crue. En outre, les résultats des modèles ont révélé que cette crue peut induire une diminution à court terme du flux de DIC hors des sédiments de 100 à 55 $mmol\ m^{-2}\ d^{-1}$ après le dépôt de la nouvelle couche, avec une augmentation à plus long terme de 4%. En reliant le cycle du carbone à d'autres cycles élémentaires, mon travail a montré qu'en comparant les variations du rapport DIC et du SO_4^{2-} aux bornes stoechiométriques et en examinant les résultats du modèle sur cette fenêtre de cinq mois, un découplage vertical dans les deux modes de réduction du sulfate après le dépôt se produit. La réduction organoclastique des sulfates (OSR) s'est intensifiée dans la couche nouvellement déposée, tandis que l'oxydation anaérobie du méthane (AOM) s'est intensifiée en profondeur sous l'ancienne interface enfouie. Cette bifurcation en profondeur des deux voies de réduction du sulfate dans la colonne sédimentaire est clairement liée à l'approfondissement de la zone de transition sulfate-méthane (SMTZ) de 25 cm après le dépôt de la crue. Cette observation a des implications importantes car un approfondissement supplémentaire de la zone maximale de l'AOM dû au dépôt de la crue pourrait renforcer le piégeage efficace du méthane (un gaz à "effet de serre" crucial dans le contexte du changement climatique) qui s'échappe des sédiments.

En conclusion, mes recherches ont jeté une lumière nouvelle sur les conséquences de ces événements épisodiques imprévisibles sur la dynamique biogéochimique des sédiments. Il est recommandé d'étendre ces travaux à d'autres marges dominées par les fleuves, au couplage avec les processus pélagiques et aux perspectives à long terme de cet événement abrupt. Je propose plusieurs feuilles de route pour atteindre cet objectif scientifique qui consiste à mieux comprendre comment ces événements peuvent affecter le fonctionnement des écosystèmes côtiers dans un monde naturel en pleine mutation.

Long Abstract in English: The biogeochemistry of coastal sediments is greatly influenced by terrestrial inputs and especially material from rivers. These inputs occur very often during special events such as floods which largely contribute to sedimentation of carbon and variable diagenetic regimes, frequently resulting in non-steady state conditions for carbon and nutrient cycles in river-dominated ocean margin (RiOMar) sediments. The primary goal of this thesis is to study the impact of highly non-stationary sedimentation generated by flooding events on the transformation of organic matter during early diagenesis. High frequency measurements that capture this transient phenomenon are essential to achieve this goal, but they are challenging to obtain. Thus, due to the rarity and unpredictability of these events, our understanding of the impact of massive flood-driven organic carbon flux on sediment biogeochemistry is limited. Numerical models capable of reproducing the numerous key biogeochemical processes are needed as they can fill gaps in observational data, thereby providing a tool for high resolution.

In this thesis, I first identified strengths and weaknesses of current early diagenetic models in capturing flood-driven biogeochemical transformations in the sediment. My analysis revealed that current state-of-the-art models are well-equipped with the appropriate reactive transport network and biogeochemical processes. However, they frequently lack the means to explicitly describe the short-term response and marked characteristics of various porewater profiles typical of surface sediment influenced by organic carbon flux derived from the flood depositional event.

The conclusion from the diagnosis of the state-of-art benthic biogeochemical models led to the development of a numerical tool of intermediate complexity suited to investigate the impact of these transient phenomena on early diagenetic processes. Insights from previous field studies that identified the occurrence of two major flood depositions were used: a 30 cm organic-poor deposition in the spring and a 10 cm organic-rich deposition in the fall. The new model was able to reproduce the basic trends from field sediment porewater data affected by these two contrasting 2008 flood events in the Rhône River prodelta. Biogeochemical fluxes and rates responded abruptly to this almost instantaneous change in the sediment. Using the model, we observed that benthic oxygen demand is modified differently depending on the composition of the flood material. With the spring flood, the oxygen flux decreased by 55% from its pre-flood value but O_2 consumption increased in the fall. My research demonstrated that these differences were due to the nature of organic carbon delivered to the proximal delta of the Rhone and the scale (thickness) of deposition. These intrinsic characteristics are also responsible for constraining the relaxation timescale of the various porewater solutes (e.g oxygen approximately few days, and between 4-5 months for deeper solutes like DIC and SO_4^{2-}) within the time-window as observed in the field with the occurrence of episodic events. Furthermore, these flood-related depositions in 2008 likely induced strong anoxic mineralization rates dominated by sulfate reduction (72%) and methanogenesis (8%) which increased by more than two-fold from its pre-flood value. After each flood deposition, the model suggests also that a strong internal cycling of iron (80%) and manganese (40%) and intense mineral precipitation were possibly responsible for the maintenance of the non-euxinic (sulfide-free) condition in the Rhône prodelta . My research also briefly explores the concept of "memory effect" of temporally connected sequence of flood deposition. I showed that the multiple occurrence of these events can also trigger temporal interactions between floods which has a substantial effect on the processes operating in the deep (such as methanogenesis and sulfate reduction) but negligible for superficial oxic and suboxic processes. This has significant ramification in the future consequences of increasing frequency of these extreme events.

In order to emphasize the importance of this phenomena, the observation of a recent winter flood event in 2021-22 provided a new dataset to understand the temporal variations of sediment-water fluxes, biogeochem-

ical pathways and their reaction rates in the Rhône prodelta. Using a time series of porewater composition obtained after this winter flood deposition, an estimated 25 cm of sediment deposition was observed. This massive deposition resulted a significant modification in the distribution of CH_4 , DIC and SO_4^{2-} concentrations relative to the pre-flood condition. The temporal nature of the observed porewater data showed that in the aftermath of this winter flood, a slow re-organization of porewater profile begins to emerge, mostly driven by the diffusive transport and biogeochemical reactions within the sediment column. Using the diagenetic model developed in this study to calculate biogeochemical reaction rates and fluxes, my research showed that this particular winter flood can increase the total organic carbon mineralization rate in the sediment by 75% a few days after deposition, with an increase of sulfate reduction contribution to the total mineralization by 25% relative to non-flood depositional period. In addition, model results revealed that this flood can induced a short-term decrease of the DIC flux out of the sediment from 100 to 55 $mmol\ m^{-2}\ d^{-1}$ after the deposition of the new layer with a longer-term increase by 4%. In connecting carbon cycle to other elemental cycles, my work showed that in examining the stoichiometric ratios of DIC and SO_4^{2-} as well as model output over this five-month windows, a vertical decoupling in the two modes of sulfate reduction following the deposition occurs. Organoclastic sulfate reduction (OSR) intensified in the newly deposited layer below the sediment surface, whereas anaerobic oxidation of methane (AOM) intensified at depth below the former buried surface. This depth-wise bifurcation of both pathways of sulfate reduction in the sediment column is clearly related to the deepening of the sulfate-methane transition zone (SMTZ) by 25 cm after the flood deposition. This observation has important implications since further deepening of the AOM maximum zone due to flood deposition could enhance the effective trapping of methane (a "green house" gas crucial in the context of climate change) flux out of the sediment.

In conclusion, my research shed new light on the consequences of these unpredictable episodic events on sediment biogeochemical dynamics. More work on upscaling the results work in other river-ocean dominated margins, coupling with pelagic processes and long-term evolution after these abrupt events is recommended and I propose several road maps for achieving this scientific goal of better understanding how these events can affect coastal ecosystem functioning in a changing world.

Acknowledgment

The last three years have been an journey worth recounting. Both on a personal and professional level. My heartfelt gratitude goes to everyone who has assisted me throughout the years. I consider myself extremely fortunate to have met some fantastic people over my academic journey, and in the practice of Ubuntu, "*I am because they are*", This is my modest way of saying thank you.

To Christophe Rabouille and Eric Viollier, for the giving me the opportunity to work with you. Without your direction, advice, and countless insights, this thesis would be impossible. The concepts in this document are the result of numerous brainstorming sessions, several lengthy and impromptu discussions, and our daily coffee table dispute. If I ever become a scientist, I owe that to you two. Merci beaucoup!

To the fantastic colleagues in the lab with whom I spent the last three years, particularly members of the OCEANIS équipe. You all welcomed me to the team with open arms, especially in the early days when I was still finding my feet in France. To Bruno Lansard, for your advise and perspective especially on sediment biogeochemistry, carbon cycle and general PhD life. My discussion with you was pivotal to the success of this thesis work. Every morning, it was a pleasure to argue with Bruno Bombléd about everything - politics, culture, science, and life. You are such a pure gentleman and I appreciate your openness. Marine, Helene, and Eva were three incredible colleagues with whom I have grown with over the years. I appreciate your company and friendship through my time in the lab and for putting up with my goofiness and opposing viewpoint on "La Vie". Now that I have completed my PhD, I will hand the baton to you; make it yours and make me proud.

To Arthur Capet, Annet Laverman for being on my thesis committee. Your suggestions and opinions were critical in determining the course of this thesis. Juliette Lauthiere, for your assistance as my COMDOC in the lab. You assisted me in developing confidence in my abilities, and your non-supervisory role always gave me clarity when the fog of lab life was thick. To Caroline and Thomas of LEGOS/LA, for the wonderful time spent in Toulouse. Despite the short duration of my visit, you both provided an excellent backdrop for some exciting science. To Karline Soetaert, who has been a mentor to me over these years and introduced me to the world of numerical modelling. See you soon in Yerseke.

To Ana, Morgan, and Camille, with whom I shared an office space during this time. You always reminding me that life is more than just work. You helped improve my French with those impromptu lectures and repetitive instructions on how certain native words were correctly pronounced. I treasured the time spent together with Marie, Bruno, and Brian, my Paleocyan/GeoTraces colleagues, during and after work.

Aside from the lab, I have had the good fortune to meet several wonderful people including Carin, whose friendship, I greatly appreciate. You took me in when I first arrived in France and offered a brotherly support over the years. Charlene, you practically fed me those delicious African meals, and your generous heart was always a breath of fresh air. Please send my love to Christ-Ethan. To Jennifer, Antoine and the people of Longjumeau for the pleasant company. You aided me in adjusting to the "French way of Life". I wish I knew French well enough to contribute more to our friendship. Many thanks to the Charlet's family for providing me with a taste of French Christmas. Those winter days spent with your family reassured me that I wasn't alone. Mrs Marie, you have been like a mother to me during these years. Saturday morning conversations with you keep me sane during the covid days. I am privileged to have known Akwuokor, Anne, Lynda, Peter, Vladmir, and the rest of the St Joe clan. I'll never forget our Saturday rendezvous, or the profound lessons on life, community and service learnt while wandering around the street of Paris with you guys for FTH. Those truths

and expression of caritas will live with me forever.

And more personally, my sincere gratitude goes to Javier. Throughout these years, you were like a brother to me. Together with Luiza, I have you both to rely on for social support. When I visit Ghent, it always feels like home to me, and I find a sense of belonging around you both. Forward my "meow" to Señoría. To Lekan and Daniel, our bond from Lagos still remains strong despite our distance. To Charles Onyema, for your wise counsel as I navigate this academic adventure. Osman and Katherine, my vacation in the Azores not only rekindle bonds from our IMBRSea days but also reenergized me ahead of this final academic year. To Alessandra, who has always been there for me. You had faith in me when few did. Our long-awaited reunion in the Balearic Island was exhilarating, and it certainly provided the last impetus to finish this thesis. To Lady L, who played Beatrice in my own unique retelling of Dante's Divine Comedy. You unintentionally directed me to dig deep within for grace and to reflect on my humanity.

And finally to my family, to whom I am eternally grateful. Your prayers and encouragement kept me going. You've all put up with my absence for the past five years. The reality is that every night when I shut my eyes, I try to hold close to my heart, recollection of the images and times spent with you all. I can hear your voices and remember your laughs and struggles. This has been my own way of staying in touch with you all. This thesis is a declaration of the love and passion that I have always attempted to convey to you. I can only hope you are as proud of me as I am of you all. I'll be coming home soon.



Table of contents

1	Introduction	1
1.1	Coastal Ocean - a seafloor perspective	1
1.2	Benthic biogeochemistry in a nutshell	2
1.3	Extreme event along river dominated ocean margins	2
1.4	A case for Rhône River delta	4
1.5	Tools of the trade	4
1.6	Objectives of thesis	5
2	Modelling sediment biogeochemistry: Current knowledge and methological approach	7
2.1	State of the Art	7
2.2	Brief overview of geochemistry of seafloor	7
2.3	Early diagenesis modelling at steady-state	11
2.4	Tracing non-stationary models of early diagenesis	13
2.5	Potential framework for event-driven modeling: Model choice and software comparison	15
2.6	Methodological approach	17
2.7	Rhône prodelta	17
2.7.1	Biogeochemical processes operating in Rhône prodelta sediments	19
2.8	FESDIA model	19
2.8.1	Description of biogeochemical processes	19
2.8.2	Primary reaction	20
2.8.3	Secondary reaction	23
2.8.4	Transport processes	25
2.9	Parameters for the biogeochemical processes	26
2.10	Evolution of biogeochemical model	27
3	Exploring temporal variations of sediment biogeochemistry under the influence of flood events using numerical modelling	29
3.1	Introduction	30
3.2	Materials and methods	31
3.2.1	Site and events description	31
3.2.2	Model development and implementation	32
3.3	Results	47
3.3.1	Qualitative model performance: Cevenol flood in the Rhône prodelta	47
3.3.2	Numerical experiment on end-member scenarios	49

3.3.3	Sensitivity of relaxation time to variation in enrichment factor (α) and sediment thickness (z_{pert})	52
3.4	Discussion	53
3.4.1	Model representation and utility	53
3.4.2	Role of end-member flood input OM in the diagenetic relaxation dynamics	54
3.4.3	Control of relaxation time by sediment deposit properties	56
3.4.4	Model limitations and future development	57
3.4.5	Relaxation time metric: Limitation and perspective	58
3.5	Conclusion	58
3.6	Appendix	59
4	Biogeochemical implication of massive episodic flood deposition: Model-Data integration	61
4.1	Summary	62
4.2	Introduction	62
4.3	Materials and Methods	64
4.3.1	Data description	64
4.3.2	Model description	64
4.3.3	Model Parameters	67
4.3.4	Characterization of flood dynamics	69
4.3.5	Model simulation	69
4.4	Results	73
4.4.1	Model-Data evaluation	73
4.4.2	Evolution of porewater profiles	73
4.4.3	Numerical experiment: Memory effect of flood deposition on biogeochemical processes	83
4.5	Discussion	84
4.5.1	Early diagenesis of Rhône prodelta sediments	84
4.5.2	Implication of extreme flood deposition in biogeochemical cycle	86
4.5.3	Interaction between successive floods	88
4.6	Conclusion	88
5	Characterization of the benthic biogeochemical dynamics after flood events in the Rhône River prodelta - A data-model	91
5.1	Summary	92
5.2	Introduction	92
5.3	Materials and Methods	94
5.3.1	Study site, Rhône prodelta	94
5.3.2	Sediment and porewater sampling and analyses	95
5.3.3	Stoichiometric ratio	96
5.3.4	Numerical modelling	96
5.3.5	Methanogenesis	98
5.3.6	Methane oxidation	99
5.3.7	Model configuration	99
5.4	Results	100
5.4.1	Water discharge, SPM concentrations	100

5.4.2	Porewater composition of dissolved inorganic carbon, sulfate and methane and its comparison to model outputs	100
5.4.3	Beryllium 7 (7Be)	102
5.4.4	Organic carbon content	104
5.5	Discussion	105
5.5.1	Disturbance identification, flood and its deposit	105
5.5.2	Transient evolution and mineralization pathways and rates	106
5.5.3	Sulfate-Methane dynamics before and after the flood	108
5.5.4	Flood induced fluxes and link to carbonate chemistry	111
5.6	Conclusion	112
6	Conclusion and perspectives	115
6.1	Conclusion	115
6.2	Perspectives	117
6.2.1	Event-driven flood typologies for Rhône River and beyond	117
6.2.2	Benthic-pelagic coupling	120
6.2.3	Long-term impact of flood deposition	122
	References	125



Chapter 1

Introduction

Follow the river and you will find the sea

French Proverb

1.1 Coastal Ocean - a seafloor perspective

The ocean covers about 71% of the globe and is a core component of the earth system playing a critical part in regulating the climate and in the biogeochemical cycles of elements necessary to sustain life on earth (Mackenzie 1999). The ocean provides human services such as food, transport and livelihood, accounting for around US\$1.5 trillion of global gross value-added economic activity (Rayner et al. 2019). However, these benefits are threatened as the ocean is already under stress from overexploitation, pollution, declining biodiversity, and climate change (Newton et al. 2012).

In the context of a changing world and from a climatic perspective, the ocean serves as a major sink of carbon dioxide (CO_2) - an important anthropogenic greenhouse gas. A core part of the ocean's ability to sequester CO_2 is the sediment. The ocean sediments represent the earth's largest reservoir of organic carbon storage and are a great indicator of past environmental conditions (Westerhold et al. 2020). Sediments are essentially unconsolidated materials, products of the modification of rocks, soils, and organic matter that have undergone weathering, transportation, transformation and deposition near the Earth's surface or in water bodies. Depending on their origin, sediments may contain particles of different sizes, shapes, minerals, and chemical compositions (Mudroch and MacKnight 1994).

Marine sediments can receive large amounts of allochthonous organic matter, mainly composed of terrestrial materials; and autochthonous organic matter, composed of algae, plants, and other animals originating from the aquatic environment itself. Continental shelves and other ocean margin deposits cover approximately 16% of global seabed area but account for 90% of total ocean organic carbon (OC) burial (Bernier 1982; Hedges and Keil 1995; Burdige 2007; Bianchi et al. 2018). Open ocean and deep-sea bottoms receive most of their organic matter from surface production, but coastal sediments, which also rely on surface production, still receive more OC from land (Hedges and Keil 1995; Middelburg and Middelburg 2019). The relative importance of terrestrially derived labile OC in coastal sediments varies widely between passive and active margins (Blair and Aller 2012), with phytoplankton contributions becoming increasingly dominant seaward on wider margins as the influence of terrestrial sources decreases (Dagg et al. 2004; McKee et al. 2004; Bauer et al. 2013). Balances between OC

supply, remineralization, and burial can vary seasonally along land-sea gradients through changes in riverine inputs, oxygen availability, and physical forcing (Blair and Aller 2012).

Sediments, especially nearshore, are deposited in the shelf regions under a wide variety of regimes that are strongly influenced by the adjacent land masses. As a result, physical, chemical and biological conditions in nearshore areas are much more variable than in deep-sea regions. Nearshore depositional environments include estuaries, fjords, bays, lagoons, deltas, tidal flats, the continental terrace and marginal basins. In general, the deposited sediment which contains organic matter can interact with the biota and provide habitat and substrate for a wide variety of organisms. These organisms, in turn, contribute to sediment organic matter degradation, which contain many organic and inorganic substances, and their transfer as dissolved elements to the water column subsidizing the trophic chains of aquatic ecosystems (Fenchel et al. 2012). The transformation of organic matter in the first meter of sediment arriving in the sediment is termed 'early diagenesis'.

1.2 Benthic biogeochemistry in a nutshell

In the first meter of the sediment, organic matter deposited undergoes several biological, chemical and physical transformations. These biogeochemical changes involve the breakdown of the organic molecules within the organic matter (OM) by microorganisms that inhabits the sediment column. This mineralization process of converting organic matter into inorganic matter, thereby generating soluble compounds, gases and energy is essential for the cycling of matter and energy in ecosystems. During the primary transformation of OM, several redox reactions take place in the sediment. These reactions involve suits of electron acceptors that release energy in decreasing amounts, ranging from the more oxidative (greater release of energy) to the less oxidative (less release of energy) (Froelich et al. 1979a) and are dependent on their availability (Fenchel et al. 2012). In the superficial layer, oxygen (O_2) is used first as part of aerobic respiration. After oxygen exhaustion, other oxidants (or electron acceptors) such as nitrate (NO_3), manganese and iron hydr(o)xides (MnO_2 , $FeOH_3$) and sulfate (SO_4^{2-}) are used sequentially. On a rudimentary level, these constitute anaerobic respiration. After the reactions, the main dissolved reduced products from these reactions (NH_4^+ , Fe^{2+} , Mn^{2+} , HS^- , CH_4) can either diffuse within the sediment and be involved in secondary reactions (re-oxidation, precipitation etc) or can be released out into the water column. Dissolved inorganic carbon (DIC) which contains all dissolved carbonate species is produced by OC oxidation and accumulates in porewaters, ultimately leading to diffusion out of the sediment. Some of the deposited sediment and its organic content can also be permanently buried. The relative importance of each of these processes determines if a system is either a sink or source of carbon or nutrients to the water column (or eventually to the atmosphere for the gaseous species).

1.3 Extreme event along river dominated ocean margins

Rivers provide the primary link between land and sea, historically discharging annually about 36 000 km^3 of freshwater and more than 20 billion tons of solid and dissolved sediments to the global ocean (Milliman and Farnsworth 2013). They impact the cycling of carbon in the ocean by providing a source of nutrients as well as trace elements that can enhance primary production, resulting in net carbon transport to the deep sea (Eppley and Peterson 1979; Raymond and Cole 2003). Ultimately, less than 50% of the terrestrial organic carbon delivered by rivers is preserved in marine systems, and as much as 80% of this amount is trapped in continental margin sediments (for reviews see Hedges and Keil (1995); Burdige (2007)).

River dominated ocean margins (RiOMar) are parts of the coastal environment that are significantly impacted by land-derived freshwater and/or sediments (Dagg et al. 2004; McKee et al. 2004) (Figure 1.1). Although RiOMars represent a relatively small fraction of the areal component of the earth's surface, their dynamic character allows for a significantly greater amount of carbon processing than other coastal and open ocean systems (Aller 1998). They are also regarded as depocenter for organic matter burial (Hedges and Keil 1995) transported from the terrestrial domain.

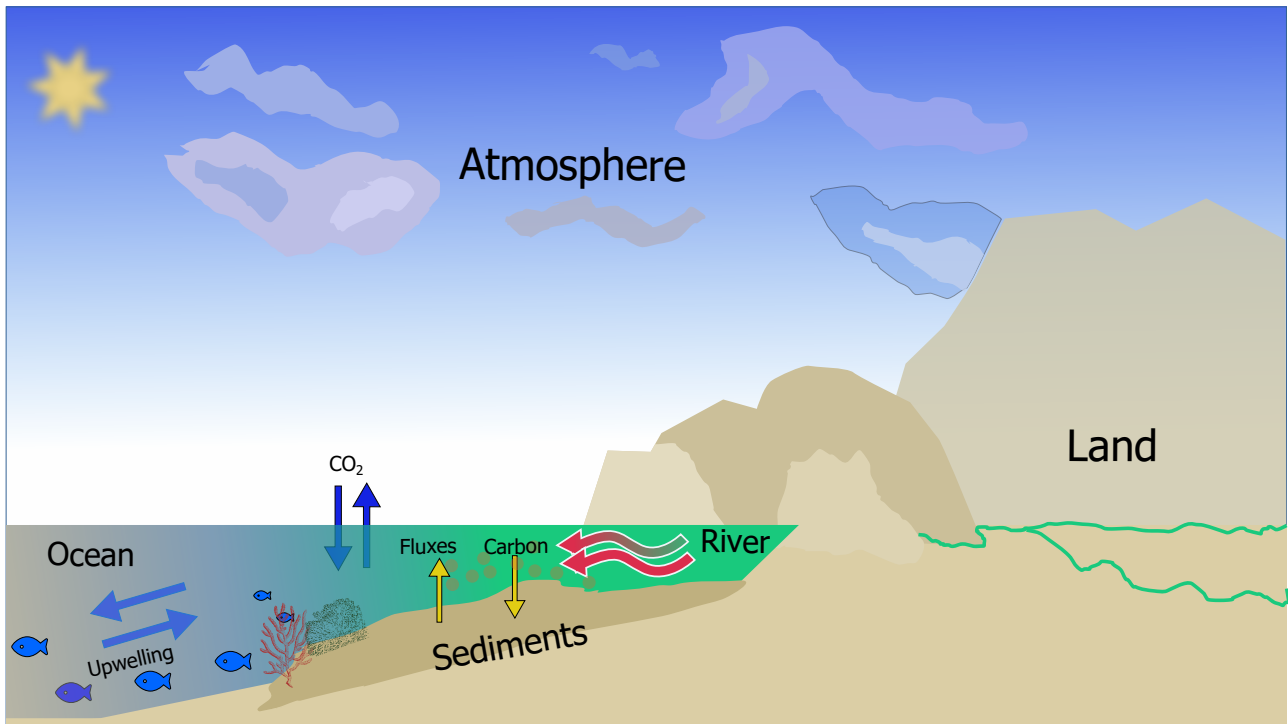


Figure 1.1: Conceptual representation of river-dominated ocean margin and connection to coastal ocean dynamics.

In RiOMar deltaic systems, the quantity and quality of carbon brought into the depocenter are dependent on several factors, mainly precipitation and riverine discharge rate (Milliman and Farnsworth 2013), watershed features, and the geochemical composition of terrestrial OM (Burdige 2007). Temporal variability in river inputs to the coastal ocean causes non-stationary OC deposition in deltas and prodeltas (Bentley and Nittrouer 2003; McKee et al. 2004). In exceptional situations, hydrological events such as intense rainfall from tropical storms or flash-floods result to disproportionate riverine organic carbon transport (Dhillon and Inamdar 2013). These extreme events are those that far exceed annual norms of intensity, duration, or impact upon the physical environment or ecosystem (McMillan et al. 2018). These intense but rare river floods and their yearly counterparts that mobilize large amounts of sediment may modify the sediment mineralization of organic matter by introducing large quantities of terrigenous organic carbon with various reactivities that determine its preservation in shallow coastal environments (Wheatcroft 1990; Tesi et al. 2012) or resulting in a variable retention capacity of the flood inputs (Sommerfield et al. 2007). This transient phenomenon leads to temporal changes in stocks and fluxes of porewaters and solids that are constrained by either the duration, magnitude and frequency of the perturbation on the seafloor (Middelburg and Levin 2009) or the nature and rates of transport and reaction (Soetaer et al. 1996). Given the high OC sequestration and oxidation potential of river dominated margins at a global scale (Blair et al. 2004; Burdige 2005), it is therefore critical to assess the behavior of the benthic system after such a massive flood event, and especially the dynamics of its OC degradation activity.

1.4 A case for Rhône River delta

In the Western Mediterranean Sea, the Rhône River is the most significant source of freshwater and particle discharge (Pont et al. 2002). This river is connected to other smaller tributaries routing materials from inland basin which then protrude outwardly to the continental shelf of the Gulf of Lions. The Rhône River mouth is characterized by a prodeltaic lobe (Got and Aloisi 1990) with three main areas based on bathymetry and sedimentation rates: a proximal (2km outward from the river mouth), prodelta (~5 km from the river mouth), and distal (extending to the larger continental shelf) domain. With an average sedimentation rate that ranges from about 30-40 $cm\ yr^{-1}$ in the prodelta domain to about 0.1 $cm\ yr^{-1}$ in the distal zone, sediments delivered are characterized by a biogeochemical gradient from the river mouth to the continental slope, leading to an offshore decrease in sediment respiration rates (Lansard et al. 2009b; Cathalot et al. 2010; Pastor et al. 2011b).

Annually, intense floods of the Rhône River can account for about 80% of terrigenous particle input in the Gulf of Lions (Antonelli et al. 2008) and have a significant influence over the continental shelf (De Madron et al. 2000; Sempéré et al. 2000; Lansard et al. 2009b). The sedimentary materials delivered during these episodic events can differ in terms of the quantity and origin of the particles transported from the various catchment areas (Eyrolle et al. 2012). As flood events are unpredictable and rare, resulting in large deposits of materials over a short duration on sediment, the role of episodic events on biogeochemistry is not wholly understood. More intriguingly, studies have shown that the prodelta sediment shows remarkably reproducible near steady-state conditions over several years in late spring and summer despite these extreme large depositions (Rassmann et al. 2016, 2020; Dumoulin et al. 2018). This begs the overarching question:

What are the primary drivers controlling the sediment response and recovery following a massive episodic flood deposition?

1.5 Tools of the trade

In order to address the questions necessary for understanding processes at the river-sea interface, observational data are crucial. In-situ measurements performed on the seafloor provide real-time information on biogeochemical changes operating in the sediment (Toussaint et al. 2014). However, their temporal and spatial coverage is limited due to logistical constraints (Viollier et al. 2003). In this thesis, we used two sets of post-flood field measurements: (i) in 2008, two flood events were captured in May-June and November-December by post-flood snapshot cruises situated a week and a month after the event respectively (Cathalot et al. 2010; Pastor et al. 2018); (ii) in 2021-22 we conducted a series of biweekly campaigns between November 2021 and March 2022 and collected time series of porewater composition before and after a winter flood (Ferreira et al. 2023).

Furthermore, as the dynamics of the cycling of materials in the seafloor are characterized by multiple timescales (e.g modified seasonality, episodic events, climatic-driven forcing), capturing the range of response of the seafloor to these drivers is unfeasible solely by field measurement. Thus, numerical models that complement observational data by providing the required extrapolation means for quantitatively analyzing and predicting OC-macrofaunal dynamics over the entire spectrum of temporally changing conditions (Bianchi et al. 2021) are needed.

Mathematical models of sediment diagenesis are idealized conceptual representation of reality and are often used to understand the dynamics of processes that affect the mineralization of organic matter and the solid and

fluid dynamics at the typical decimeter scale of the sediment deposits (Berner 1980). There are several kinds of models used to represent biogeochemical functioning in the sediment. Despite the potential importance of transient conditions for C cycling, most diagenetic models assume a steady state (Arndt et al. 2013). While there is a notable exception with models capable of including transient responses of biogeochemical processes in the sediment induced by seasonal or decadal changes in bottom water temperature, oxygen and OC flux (Soetaer et al. 1996; Rabouille et al. 2001b; Katsev et al. 2006; Sohma et al. 2008; Van de Velde et al. 2018), little effort has been made to incorporate the role of episodic events with abruptly changing boundary conditions because of the lack of observations and their unpredictability (Mermex Group et al. 2011).

1.6 Objectives of thesis

This thesis will try to address some of these questions by developing a tool for simulating organic matter transformations during early diagenesis in environments with highly non-stationary sedimentary deposits. The primary objective was to design and produce a tool of optimum complexity (spatial and temporal resolution, transport phenomena, metabolisms and chemical reactions) that can be coupled with oceanic water column models with a large spatial mesh. After calibration of the model with the measurements carried out on the sediments of the proximal station of the Rhône prodelta in the Mediterranean Sea, I used the model to provide answers to pressing questions about:

- What is/are the **biogeochemical response** of coastal sediment to extreme events such as episodic flood deposition on both short and long timescale
 - *Explicate the pattern and dynamics of short-term sediment porewater chemistry*
- What are the **primary drivers of the sediment response and recovery** in the aftermath of these massive episodic flood deposition
 - *Characterize and analyse the phase space and recovery dynamics after massive sediment deposition*
- What is the **size and scope of the biogeochemical changes** caused by significant flood events in the Rhône prodelta region
 - *Quantify of the different biogeochemical pathways, rates and fluxes in event-driven context*

In Chapter 2, I discussed the current state of the art in sediment biogeochemistry, from element cycles to the numerical tools used to explore the relevant questions. There, I introduce the biogeochemical model used in this thesis and provide a conceptual overview of the model, processes, parameterization and assumption made in developing the model. We also provide the evolution of the model in terms of the complexity added after its initial conception to the final form used in later chapters.

In Chapter 3, I showcase the model novelty in terms of expanding previous early diagenesis code to include event-driven processes. In that chapter, I discuss the part of the FESDIA model concerned with the implementation of a perturbation event. The algorithmic basis which makes the model especially capable of describing explicit flood deposition and its interaction to sediment porewater chemistry is detailed in this chapter. A sneak peek on the capability of the model to describe actual flood event is exhibited and some relevant parameters controlling the system's relaxation timescale are explored. The concept of biogeochemical attractors is introduced here and will be further expanded in another chapter.

Chapter 4 and 5 provide realistic application of the model in description of the biogeochemical feature of solid and porewater profiles in the Rhône prodelta sediment. In Chapter 5, I use the model to investigate the impact of two distinct flood deposition of 2008 (Cathalot et al. 2010; Pastor et al. 2018) with different characteristics on the carbon, sulfur and iron/manganese cycle. I also discuss the mechanisms responsible for the observed variability in the porewaters data, and briefly speculate the role of successive flood deposition on the biogeochemical pathways of carbon oxidation. In Chapter 6, I use the model with a different and more recent data collected during the winter flood season of 2021-2022. There, I show how the model could aptly describe the time-varying response of the sediment to a singular but significant deposition. This time-series data allows us to view the temporal evolution of the profile after the flood and further validate the model. The data-model perspective allows for the characterization of the role of flood deposition on sulfur-methane dynamics in the deeper sediment.

In Chapter 6, I draw the major conclusions of my work and place my research on the wider scope of coastal biogeochemistry and offer diverse perspectives on where our results fit and describe possible future trajectories to continue improving our understanding of these phenomena on the biogeochemical dynamics along river-ocean margin.

Chapter 2

Modelling sediment biogeochemistry: Current knowledge and methodological approach

The history of science is rich in example of the fruitfulness of bringing two sets of techniques, two sets of ideas, developed in separate contexts for the pursuit of new truth, into touch with one another.

J. Robert Oppenheimer

2.1 State of the Art

The development of our understanding of sediment biogeochemistry and exchange fluxes has been revolutionized by the technological advances in oceanographic research tools to determine porewater solute concentrations. This development has been met with parallel progress in reactive-transport models to quantify biogeochemical processes. Here, I briefly outline the current state of the art in sediment biogeochemistry, from element cycles to the numerical tools used to explore the relevant questions in this thesis.

2.2 Brief overview of geochemistry of seafloor

Coastal sediments are the ultimate receptacle for the export of particulate organic matter (OM) from the water column and from terrestrial origin. This flux of organic matter feeds aerobic and anaerobic respiration by all the benthic fauna and microorganisms and is responsible for the geochemical zonation of the seafloor via the rates of the various respiratory pathways (Canfield and Thamdrup 2009). The buried materials undergo rapid transformation in the upper meter of the sediment. This sedimentary transformation aptly called “*early diagenesis*”, combines chemical reactions, physical processes and biological processes. Following deposition, organic matter is degraded (or mineralized) to CO_2 and other inorganic compounds by a series of microbially mediated oxidation-reduction reactions, starting with the most thermodynamically favoured oxidant (or electron

acceptor) which yields the most free energy. When this oxidant is depleted, the remaining OM is oxidized with the next most efficient oxidant available, and so on until all oxidants are depleted. The availability of soluble oxidants is clear (O_2 , NO_3^- , SO_4^{2-}) but is more questionable for solids (MnO_x , $FeOOH$, CH_2O) which are present in different chemical forms and have different reactivities. This may modify the succession of oxidants (Canfield et al. 1993; Thamdrup et al. 1994). In marine environments, oxygen is the first electron acceptor respired by aerobic bacteria to convert OM to other reduced forms. Once the O_2 is depleted, other available oxidants proceed in a sequential manner (Nitrate NO_3^- > Mn oxy-hydroxides MnO_2 > iron oxy-hydroxides $FeOOH$ > sulfate SO_4^{2-} > CH_2O (Froelich et al. 1979a; Canfield et al. 1992; Burdige 1993) (Figure 2.1) pending oxidant availability.

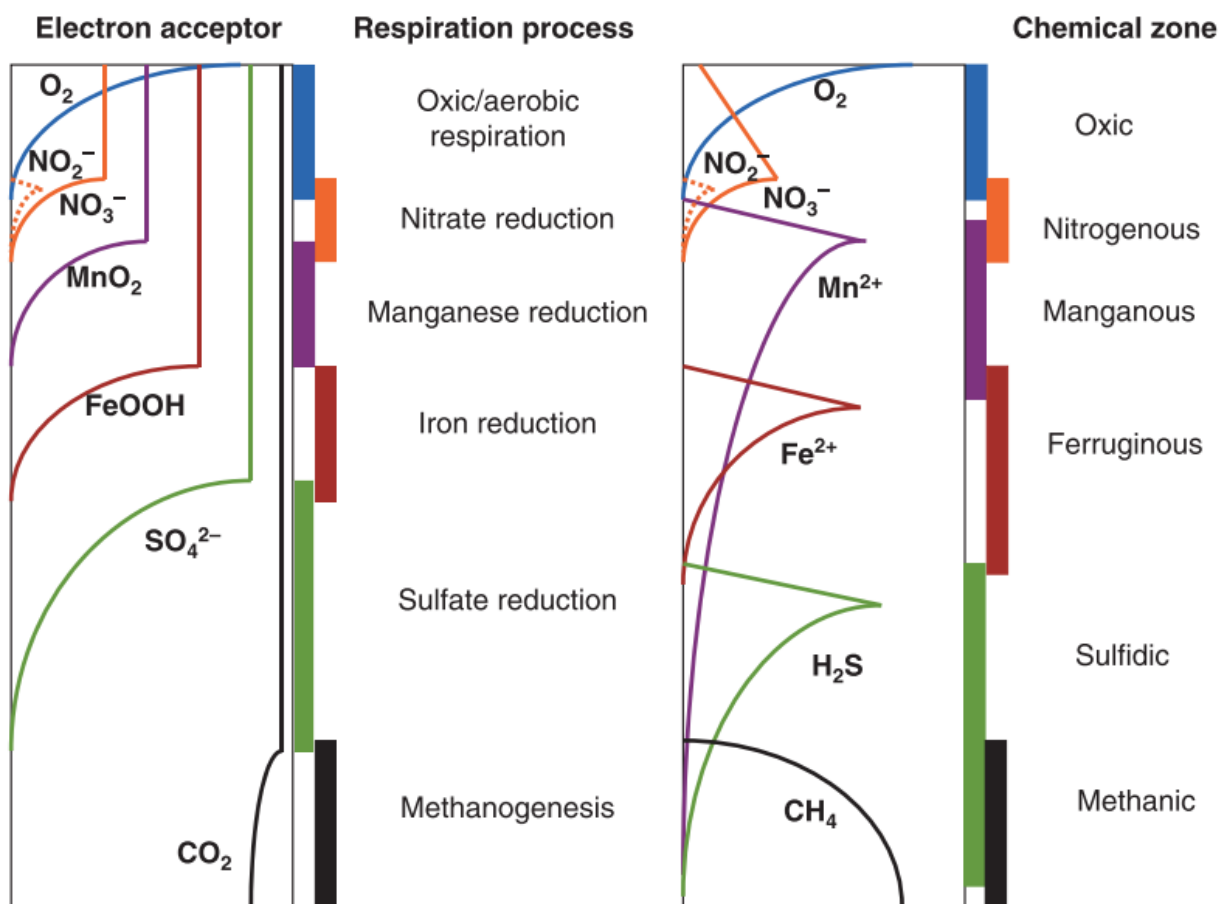


Figure 2.1: Idealized representation of the distribution of biogeochemical reaction processes in the sediment (Adapted from Canfield and Thamdrup (2009)).

This vertical cascading of oxidants for OM mineralization partitions the sediment into zones based on the presence or absence of dissolved oxygen, metals and sulfide. Sediment biogeochemists traditionally employ three zones to delineate the occurrence of biogeochemical processes in the sediment column. A superficial oxic zone where aerobic mineralization occurs, a sub-oxic zone below characterized by nitrate reduction and iron-manganese reduction, and an anoxic zone associated with sulfate reduction and methanogenesis (Middelburg and Levin 2009) (Figure 2.2). Besides such classification based on the respiratory pathways, a more chemical zonation of the sediment into distinct geochemical zones derived from the chemical species in the highest relative abundance has been proposed (Canfield and Thamdrup 2009). In either case, it is evident that the sediment constitutes a complex system with several biogeochemical interactions (Figure 2.1).

Because of high dissolved sulfate concentrations in marine environments, sulfate reduction is an important

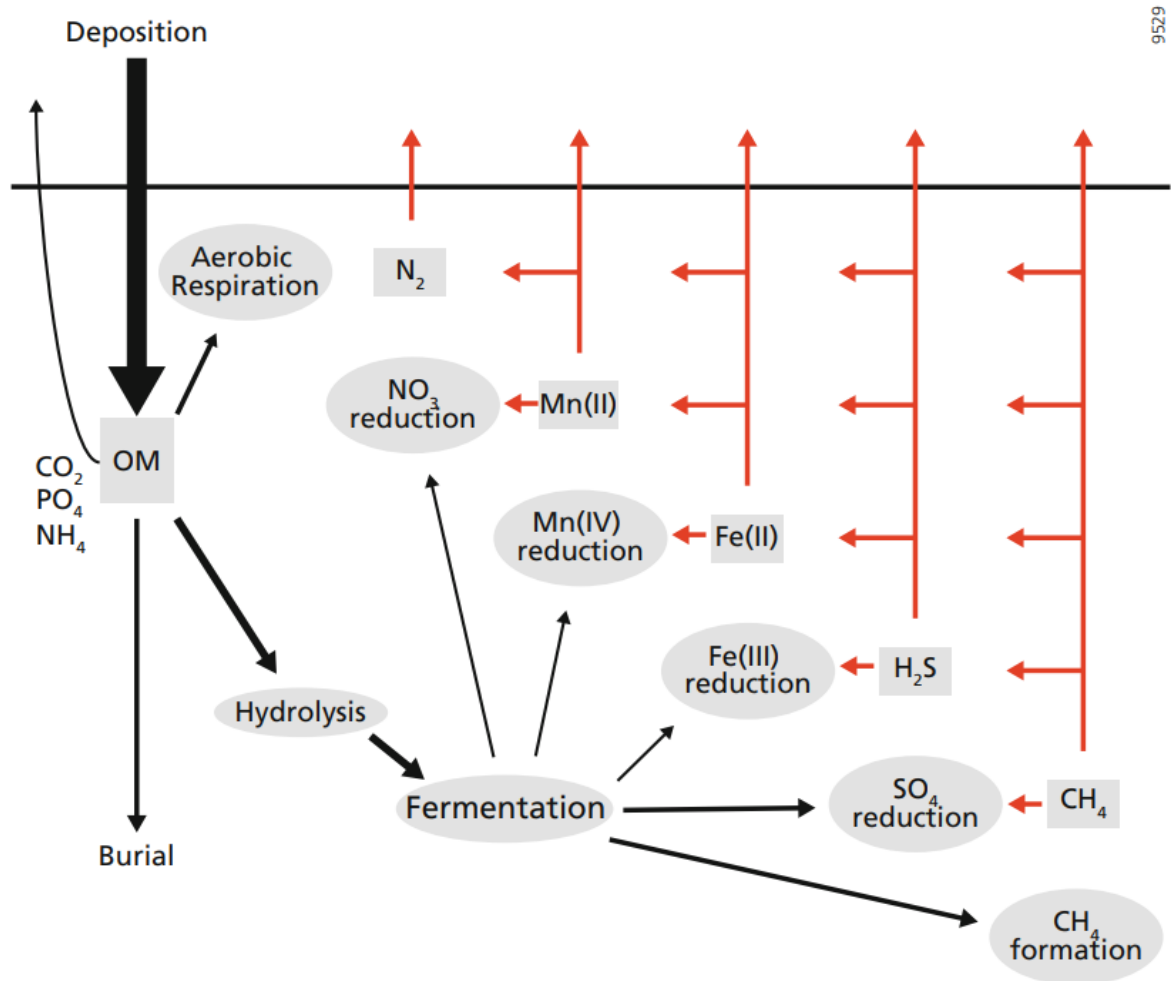


Figure 2.2: Conceptual model of organic matter (OM) degradation and reoxidation pathways in the sediment (Middelburg and Levin 2009).

metabolic pathway which accounts for 25 - 50% of the total carbon oxidation in coastal sediments (Jørgensen 1982). Away from coastal margin with declining carbon input and increasing water depth, the importance of sulfate reduction decreases. Nitrate reduction contributes less than 4% of total carbon oxidation in most marine sediments and is of low importance (Jørgensen 1982; Canfield et al. 1993). Fe (III) reduction accounts for 17% of total carbon mineralization in continental margin sediments. Mn (IV) reduction is less significant since marine sediments typically have lower Mn oxide content (Thamdrup 2000). As a byproduct of methanogenic organic matter breakdown, methane is produced below the sulfate reduction zone. Whereas sulfate-reducing activity is normally maximum in the sediment's top decimeters, depending on the quantity and quality of organic matter deposition, methane oxidation occurs deeper below the sediment surface and can account for about 35 % total carbon mineralization in coastal sediment (Egger et al. 2016).

These primary reactions promote the production of reduced species. Due to the concentration gradient, they can also diffuse through the sediment layers and react with each other (Figure 2.2). These reduced species are involved in secondary reactions in which they can be reoxidized with oxygen and other oxy-hydroxides, thus participating in redox cycling within the sediment column. Other secondary reactions include precipitation and dissolution involving carbonate (e.g. $CaCO_3$, $MnCO_3$) or sulfide (FeS , FeS_2) and adsorption (e.g. ammonium adsorption to the sediment matrix). These reactions lead to the accumulation of these mineral species in the solid phase and the consumption of dissolved species in the porewater.

Furthermore, the main physical processes operating within the sediment involve diffusive mixing (bioturbation and solute diffusion) and advection (sediment accumulation and porewater transport by bio-irrigation pumping of bottom water) (Berner 1980). These various transport mechanisms can have a significant impact on the zonation of diagenetic reactions. Many benthic organisms (fauna living on or in the sediment), for example, contribute to porewater transport via bioirrigation: they passively or actively exchange sediment porewater with the overlying water column through burrowing, pumping, ventilation, and feeding activities (Kristensen et al. 2012). Bioirrigation enables sediment-dwelling organisms to feed and exist in anoxic deeper sediment layers (Olafsson 2003; Braeckman et al. 2011) as well as radial or spherical OM-rich micro-niches (Aller 1982).

The vertical succession of early diagenesis processes is a paradigm that can be influenced by a variety of physico-chemical and biological conditions occurring at various spatial and temporal scales. The temporal variations in environmental conditions result in transient states (Sundby 2006). Such transitory states could be caused by random, small-scale disturbances like benthic faunal bioturbation as well as larger scale periodic disturbances, such as those caused by tidal cycles in estuarine/coastal sediments. In addition, large-scale episodic events, such as the deposition or resuspension of sediments by windstorms or floods, can occur. These transient states can also be seasonal, linked to temperature fluctuations, oxygen concentrations in the bottom water, or organic matter concentrations. Seasonality in remineralization rates, for example, can be seen in time-varying sediment pore-water profiles of remineralization end products (such as ammonium or sulfate). Diffusion, on these timescales, dampens any seasonal periodicity in these profiles (Lasaga and Holland 1976), and what is generally observed are smooth, asymptotic profiles with concentrations that grow in and out over the annual seasonal cycle (e.g., Aller (1980); Klump and Martens (1989); Rabouille et al. (2001b)). As such, within the community, despite this transient forcing, the sediment is sometimes assumed to be in quasi-steady state, especially over short-time period. On more shorter timescales, non-steady state processes such as episodic or event-driven events like flash floods, storms, or resuspension/deposition events can also have a sizeable impact on biogeochemical processes (Deflandre et al. 2002; Tengberg et al. 2003; Cathalot et al. 2010; Tesi et al. 2012). For example, resuspension events that transport reduced constituents from the sediments to the

water column may be more effectively reoxidized than diffusive-mediated processes (Glud 2008; Moriarty et al. 2017).

Integrating these fundamental biogeochemical interactions necessitates the application of a complex mathematical model to capture the key processes at the appropriate spatial and temporal scale. Mathematical models of sediment diagenesis are frequently used to better understand the processes that influence organic matter mineralization. These models, which might be single or multicomponent in nature, are frequently related to quantities observed in field studies or experiments. Observations can be utilized to constrain numerous processes in the model that are important to system functioning. Once validated, the model can be used to gain a better understanding of the system and forecast how changes in environmental conditions affect the biogeochemical cycles in sediment.

The type of model chosen is determined by the questions to be answered and the data available for constraining the model. The next section briefly summarizes the current state of the early diagenesis model, including its approach, assumptions, capabilities, and drawbacks.

2.3 Early diagenesis modelling at steady-state

The surface sediment is characterized by chemical, physical and biological interactions which operate on different spatial and temporal scales. This surficial sediment is also affected by natural and anthropogenic changes which pose direct concern to the functioning of coastal ecosystems. For example, severe oxygen demand by sediment and water column bacteria results in hypoxic conditions which are detrimental to aquatic organisms, in relation to eutrophic conditions that emerge when sediment bacteria digest a huge amount of organic waste (Pena et al. 2010). Other examples include the release of heavy metals by the reductive dissolution of iron minerals which may contaminate the water column (Boudreau 1999). These environmental issues necessitate a comprehensive understanding of the mechanisms and drivers of sediment biogeochemistry. To unravel these connections, computer models combined with extensive observational data have become increasingly important in recent years. Diagenetic modeling is an essential tool for investigating the interactions between sediment diagenetic processes, developing hypotheses regarding sediment-water column coupling, and predicting potential ecosystem responses (Boudreau 1997).

Early diagenetic models (Bernier 1980) are variants of the reactive-transport models (RTM) which attempt to resolve the fundamental processes affecting solid and solute species in the sediment column. This model can be mathematically described using the general advection-diffusion-reaction equation:

$$\frac{\partial \xi_i C}{\partial t} = -\frac{\partial}{\partial z} [-\xi_i \times D_i \times \frac{\partial C}{\partial z} + w_i \times \xi_i \times C] + \sum \xi_i \times REAC + \xi_i \times J_{irr} \quad (2.1)$$

where C is a generic chemical species (solid or liquid) while for solute species, ξ_i stands for porosity and for solid components, ξ_i stands for 1 - porosity. w_i is the burial rate or advection for solid and solute species respectively while D_i is the diffusive transport mechanism in the sediment which can be due to molecular diffusion (for solutes) or bioturbation (for solutes and solid). $REAC$ encompasses all source and sink terms such as production and consumption processes while J_{irr} is non-local bio-irrigation transport which affect the solutes only. More description of the of constitutive terms in this equation is given in Section 2.8 and fully covered in Chapter 3.

In the early days of sediment biogeochemical modelling, efforts were made to develop diagenetic models to answer pertinent geochemical questions. The pioneering work of (Goldberg and Koide 1962; Berner 1964; Guinasso Jr and Schink 1975; Berner 1980) laid the foundation of what is now known as early diagenesis modelling. Berner (1964) first formulated a similar diagenetic equation to model sulfate reduction in the porewater of anoxic sediments while Goldberg and Koide (1962) advanced an advective-diffusive equation for modelling solid radiotracers in surface sediments. The modelling problems were thus largely restricted to analytically tractable formulation, many simplifying assumptions and often limited number of species and processes. As such, the primary types of early diagenetic models consider one or two transport processes and one specific reaction pathway. These earlier efforts paved the way for the development of a numerical solution to early diagenetic model that provided a more realistic and mechanistic description of sediment biogeochemistry.

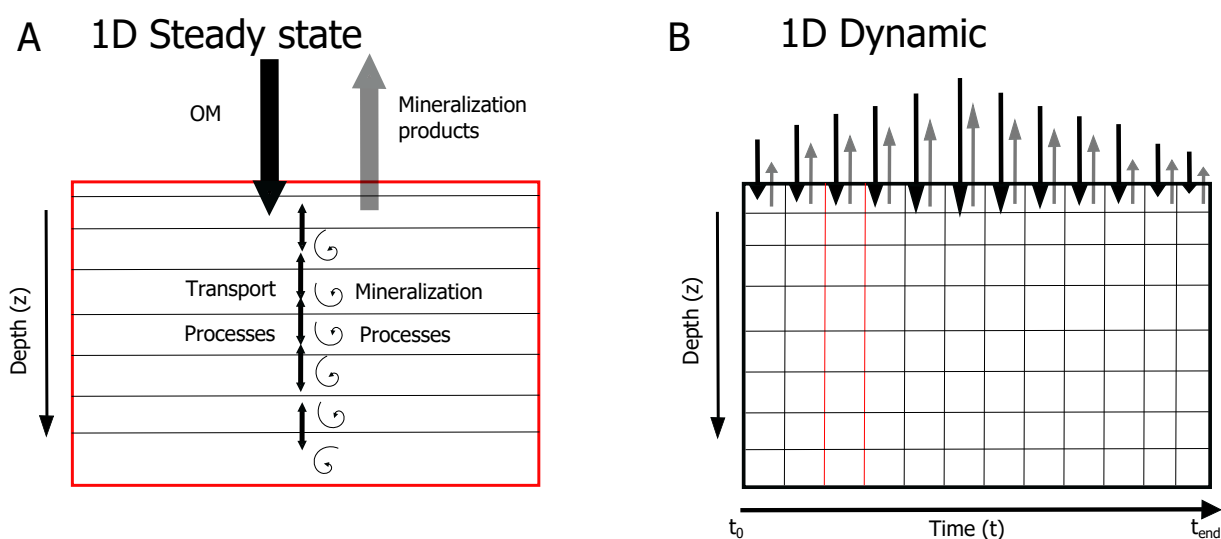


Figure 2.3: Schematic representation of difference early diagenetic paradigm used to model sediment biogeochemistry. (A) Steady-state approach (B) Transient state approach. Red lines indicate equivalent zones of sediment modelled between both approaches.

The basis of these 70's era early diagenesis models rests in the crucial assumption of the sediment in a "steady-state" which occurs when the model's concentration and boundary forcings are time-independent (Figure 2.3A). When changes at the interface occur over a much longer timescale, such as a shift in climate, or a much shorter timescale, such as bioirrigation, than the response time of the entire system subject to a perturbation, these steady state assumptions can be a valid approximation. Furthermore, the description of sediment in steady-state condition is affected by the sediment constituents. While the distribution of solutes in pore water is subject to some variability on a seasonal timescale, it is somewhat stable on a decadal scale (Pena et al. 2010). This insight has been used to simplify most diagenetic modeling work reported in the literature, thus overcoming the computational burden, especially when these models are integrated at large spatial scales (Lessin et al. 2018) or when considering processes that operate on different time scales (Soetaert et al. 2000; Hülse et al. 2018) (for example, the different time scale of organic matter reactivity or coupled biological geochemical processes). This advantage allows modelling work using this framework to provide snapshots of the time-varying rates at a particular point in time. As a result, these models have become widely used in simulating processes that exhibit relatively long-term stability of organic matter flux to the system (Rabouille and Gaillard 1991; Soetaert et al. 1996a; Wang and Van Cappellen 1996). This assumption is sufficient for the early diagenetic models used in most deep-sea research. However, in coastal marine sediments where seasonal or episodic effects are stronger, this condition is untenable, particularly when the external conditions fluctuate

on early diagenetic timescales (Rabouille and Gaillard 1990; Couture et al. 2010) and there lies the possibility of under/overestimating rates of sediment processes on appropriate seasonal or annual timescales (Burdige 2011).

In coastal settings especially along river-ocean margins, episodic events have been predicted to increase in frequency and intensity because of global climate change (Tockner and Stanford 2002). In such transitional environments, the intensity of diagenetic processes is modulated by the variable hydrodynamics of the river-ocean interface. Because of the oscillations caused by these intermittent forcings, the boundary conditions for many biogeochemical processes in the sediment change. If the system has been “reset” by an “instantaneous” and massive deposit generated by a perturbation, modeling organic matter transformation in this highly dynamic environment under the assumption of steady-state may result in under/overestimation of process rate as well as the possibility of incorrectly simulating field observations. Typical attempts to resolve the variability in benthic processes resulting from this perturbation involve the use of time-dependent early diagenetic models. This sort of models has only been validated in environments where periodic variability in key forcing parameters is the dominant source of variability. Thus, these models are readily employed to simulate seasonal and interannual variability in benthic mineralization processes. However, for highly dynamics environments with strong river-ocean connections that experience episodic pulse events at short time intervals (e.g. a few days or a week), there may be some limitations in using these time-dependent models (see Section 2.5). There is now a growing appreciation in some coastal lying areas such as deltas and coastal regions of intense sediment deposition that the assumption of steady-state dynamics as a normative condition of systems might be misleading (Tesi et al. 2012; Lessin et al. 2018).

2.4 Tracing non-stationary models of early diagenesis

A few of the published models have been applied in dynamic fashion and Paraska et al. (2014) offers a fairly recent review of these models tracing different formulations, utilities and assumptions. The success of these models rests in their ability to dynamically simulate the sediment response to the seasonal variability of carbon flux and bottom water conditions. As this thesis focuses on non-stationary diagenetic modelling with a tendency towards episodic events characterized by instantaneous deposition of organic matter and abruptly changing boundary conditions for both solid and soluble species such as in areas of high frequency perturbation (e.g. deltaic depocenter along coastal margins, abyssal plain along turbiditic canyons), the utility of these models applied to this atypical scenario is contentious. As such, a new paradigm framework that differs from the traditional approach with the ability to capture rapid depositional events characterized by stochastic and semi-continuous forcings is needed (Lessin et al. 2018). Nonetheless, here we briefly assess some of the benthic biogeochemical models developed with dynamic simulation in mind to provide some idea of the current state of the art and how this thesis builds on their successes and weaknesses.

The time-dependent analytical model of Lasaga and Holland (1976) represents one of the foundational works in applying RTM in transient mode Figure 2.3. Using a green-function approach, the effect of non-uniform distribution of decomposable organic matter on the composition of interstitial water in the sediments was explored. The model by Rabouille and Gaillard (1990) was among the first to use numerical method to explore the dynamic behavior of sediment silicate under benthic megafauna mixing and turbidite deposition in deep sea sediment. Accounting for the oxidation of particulate organic matter by a continuous sequence of electron acceptors with both limiting and inhibition terms, Rabouille and Gaillard (1991) makes the model suitable for

studying the annual and interannual variability of carbon cycle in the North Atlantic (Rabouille et al. 2001b). Concurrent efforts by Vidal and Morgui (1995) examine some physical conditions that could result in short-term pore water ammonium variability of estuarine sediment using empirical model fits. The inclusion of diagenetic processes in system-scale ecosystem model (ERSEM) was put forward to simulate biogeochemical benthic processes in space and time (Ruardij and Van Raaphorst 1995).

A renaissance in non-steady state diagenetic modelling was in full effect in the late 90s with several models developed for application with various degrees of environmental forcings. The widely used CANDI model of Boudreau (1996) was developed to stimulate the time-dependent transformation of OM, nutrients (NO_3^- , PO_4 , NH_4), oxidants (O_2 , NO_3^- , MnO_2 , Fe(III)-solid and SO_4^{2-}) and their reduced by-products, acid-base speciation and pH in aqueous sediments. Another variant of early diagenesis model which gave rise to other models still in use today was the OMEXDIA (Soetaert et al. 1996a). This model was initially developed to reproduce the cycling of carbon, oxygen and nitrogen along ocean margins both at steady and non-steady state. While it was originally developed and used in deep sea sediments, the model has enjoyed great flexibility in its usage in coastal sediments. Both CANDI and OMEXDIA gave rise to a suite of models used today.

This apex of early diagenesis modelling in the 1990s era ushers in a new phase of widespread use and the development of a more complex suite of models in the 2000s. The Berg model (Berg et al. 2003) continues this trend in developing early diagenesis models capable of resolving the cycling of different elements in the sediment at a seasonal scale. Of important peculiarity, the dynamic model of Berg et al. (2003) accounted for sixteen dissolved/or solid species with processes such as adsorption, irrigation and intricate secondary reactions involving iron-manganese-sulfur aptly included. The steady-state model of Wang and Van Cappellen (1996) (STEADYSED) evolved into the BRNS model with the capacity to be used for transient simulations (Regnier et al. 2002). This BRNS framework has been employed in a variety of problems (Thullner et al. 2005; Dale et al. 2008b; a; Smith and Matisoff 2008) and environments (Jourabchi et al. 2005; Centler et al. 2010; Nick et al. 2013). Furthermore, using an improved version of STEADYSED, Morse and Eldridge (2007) was able to investigate the response of seasonally hypoxic and anoxic shelf sediments of Louisiana. Other revisions of CANDI led to its adaptation for coupled benthic-pelagic simulation (Luff et al. 2000; Luff and Moll 2004), and recent derivations of the model have been exploited for study in deep-sea sediments with strong $CaCO_3$ dissolution driven by organic matter degradation (Sulpis et al. 2022). Other works such as Couture et al. (2010) and Couture et al. (2016) (MATSEDLAB model and its successor MEDIALAB (Steinsberger et al. 2019)) succeeded in simulating the dynamics of arsenic and sulfur cycles in non-steady state lakes, whereas progress in coupling early diagenesis model with pelagic process gained increasing momentum from the seminal work of Soetaert et al. (2000) with OMEXDIA which provided the basis for full-coupling with circulation model (Sohma et al. 2008; Capet et al. 2016) and studies accounting for lateral transport and bio-resuspension that varies with time (Radtke et al. 2019).

In application to global domain, the MUDS model of Archer et al. (2002) attempts to resolve the oxic, suboxic (via manganese, iron) and anoxic (via sulfur) remineralization pathways by simulating their time-dependent evolution toward steady state efficiently; albeit with lower vertical resolution. The different strands of HAMOCC global model include sediment diagenesis model which can be run in a time-dependent fashion (Maier-Reimer et al. 2005; Ilyina et al. 2013). Recent early diagenesis model developed for coupling with diverse ocean biogeochemical model is provided by MEDUSA (Munhoven 2021). This time-dependent model includes clay, calcite, aragonite and organic matter as solid components and CO_2 , HCO_3^- , CO_2 and O_2 as pore-water solutes.

Despite this effort, it is still unclear how these models fare in areas with high energetic dynamics characterized by short-term variability and kinetics (hours, days, weeks and months) of biogeochemical processes. In fact, the role of episodic events has been long neglected in these models because of the lack of observations and their unpredictability (Tesi et al. 2012). Future advancement in marine sediment modeling tailored to incorporating these extreme depositional feedbacks and their biogeochemical responses is thus needed. The following section briefly explores the potential models which could be used for such event-driven dynamics in sediment under episodic flood deposition of materials.

2.5 Potential framework for event-driven modeling: Model choice and software comparison

Several numerical tools have been developed over the years for the reactive transport model that will form the basis of this project. Table 2.1 compares different well-known RTM software and their comparative capacities. These models vary in their structure, solution method, and software architecture. Table 2.1 shows that while models such as CANDI, MATSEDLAB, and RAD1 contain a comprehensive reactive network involving the Fe and Mn cycles, models such as OMEXDIA and AQUASIM are less detailed in the biogeochemical processes covered. However, the latter suite of models provides some flexibility in terms of incorporating additional processes as needed. Some models suffer from software and administrative-oriented issues relating to the ease of their usage. MATSEDLAB/MEDIALAB, in particular, was written in MATLAB with a proprietary bottleneck in working with the code without an institutional license, while CANDI and AQUASIM, which are based on Fortran77, are no longer maintained or supported, limiting technical support for future development. Modeling tools, on the other hand, such as OMEXDIA and RAD1, were mostly built in R and Julia, two dynamic programming languages with an open source community that are publicly available and disseminated across all computing platforms. As a result, the ease of rapid prototyping with these models is straightforward (Soetaert and Meysman 2012a).

Another issue to evaluate is the utility of model code in terms of efficiency and entry barrier. In their current form, models such as CANDI, AQUASIM, MATSEDLAB/MEDIA, and RAD1 have a computing time (average of 20 minutes for a steady-state spin-up run) that, while small for a one-time simulation, can be resource-intensive, requiring $O(N^2)$ operations when used for parameter estimation, sensitivity analysis, and longer-time simulation. In comparison, a model like OMEXDIA runs quickly for steady-state runs and can be cost-effective in computationally demanding applications. Ultimately, there exists a trade-off in the current class of model between their default implemented reactive networks in terms of the biogeochemical processes included and the software/numerical expediency required for the task in this project.

Nonetheless, a qualitative assessment of these RTM codes in Table 2.1 indicates that none were initially designed to capture the relevant complex biogeochemical reaction system desirable for a system under abrupt sediment deposition and changing boundary conditions (personal communication with the code developers), although some like OMEXDIA have shown promise in their ability to simulate other types of event-driven processes such as bottom trawling (De Borger et al. 2021b). In Chapter 3, I exploited this advantage to design a model based on OMEXDIA which utilizes all the attributes of the other sophisticated models in Table 2.1 while adapting such event-driven process to our use case of flood deposition.

Table 2.1: Comparison of five early diagenetic model codes: OMEXDIA (Soetaert et al. 1996a), CANDI (Boudreau 1996), AQUASIM (Reichert 1994; Dittrich et al. 2009), MEDIALAB (Shafei 2012; Couture et al. 2016; Steinsberger et al. 2019), and RADII (Sulpis et al. 2022). Differences in model structure, numerical solution and source code are shown. ¹ See De Borger et al. (2021b) for implementation of bottom trawling as event process in OMEXDIA model.

	OMEXDIA	MEDIALAB	CANDI	AQUASIM	RADII
Model					
Structure					
Modelling aim	Benthic-pelagic coupling	Fe-As cycling	Nutrient cycling, Benthic-pelagic coupling	Nutrient cycling	Carbon cycle
Chemical species	9	23	27	28	19
Irreversible reactions	6	25	20	8	7
Transport processes	Advection, porewater diffusion, diffusive bioturbation	Advection, porewater diffusion, diffusive bioturbation	Advection, porewater diffusion, diffusive bioturbation, bio-irrigation	Advection, porewater diffusion, diffusive bioturbation	Advection, porewater diffusion, diffusive bioturbation, bio-irrigation
Diffusion of total species	ODU	$\sum CO_2$, $\sum H_2S$	$\sum CO_2$, $\sum H_2S$, $\sum NH_4$, $\sum PO_4$	$\sum CO_2$, $\sum H_2S$, $\sum NH_4$, $\sum PO_4$	$\sum CO_2$, $\sum H_2S$, $\sum NH_4$, $\sum PO_4$
Bioturbation	Intraphrase mixing	Intraphrase Mixing	Intraphrase mixing	Intraphrase mixing	Intraphrase mixing
Electron acceptors for organic matter oxidation	O_2 , NO_3	O_2 , NO_3 , $Fe(OH)_3$, SO_4^{2-}	O_2 , NO_3 , MnO_2 , $Fe(OH)_3$, SO_4^{2-}	O_2 , NO_3 , MnO_2 , $Fe(OH)_3$, SO_4^{2-}	O_2 , NO_3 , MnO_2 , $Fe(OH)_3$, SO_4^{2-}
Explicit formulation of the Mn and Fe redox cycles	No	Yes	Yes	No	Yes
Precipitation-dissolution	Not applied	FeS	FeS , FeS_2	$MnCO_3$, FeS , $Fe^3PO_4^2$, Calcite	Calcite, Aragonite
Solution method					

	OMEXDIA	MEDIALAB	CANDI	AQUASIM	RADI
Discretization in space	Finite differences	Finite differences	Finite differences	Finite differences	Finite differences
Dynamic model available	Yes	Yes	Yes	Yes	Yes
Dynamic solution approach	Method of Lines	variable-step, variable order (VSVO)	Method of Lines	DASSL, variable-step, variable order (VSVO)	Method of Lines
Event Handling	No ¹	No	No	No	No
Software architecture					
Programming language (PL)	R, Fortran	Matlab	Fortran	Fortran	Matlab, Julia
PL Licence	Free Open source	Propriety	Free Open source	Free Open source	Propriety/Free Open source
Average lines of code	330	2633	299	Executable file/80079	3284
CPU time	Seconds	20 mins	20 mins	30 mins	10 mins

In the following section, I will briefly discuss the Rhone prodelta area and the biogeochemical processes that operate there before moving to the explanation of the model developed for this thesis.

2.6 Methodological approach

2.7 Rhône prodelta

For the majority of this thesis work, the prodelta portion of the Rhône outlet adjoining the Gulf of Lion was the main case-study site. The Rhône River is the main source of freshwater, nutrients, organic matter and sediment for the Mediterranean Sea (Madron et al. 2000). It is characterized by a drainage basin of 97800 km^2 and an average water discharge of $1700 m^3 s^{-1}$ with a marked seasonality between low water-discharge ($>700 m^3 s^{-1}$) in summer and high water-discharge ($>3000 m^3 s^{-1}$) in fall and winter (Pont et al. 2002). South of Arles (50 km upstream from the river mouth), it splits into two channels, the Grand Rhône to the east encompassing 90% of the total discharge and the Petit Rhône to the west with the remaining 10%. The Rhône River turbidity plume extends mainly southwestward into the Gulf of Lion, with an average thickness of 1 m (up to 5 m) (Many et al. 2018). The Gulf of Lion is a microtidal, wave-dominated system, with a tidal range of 30 to 50 cm. Due to salt-induced flocculation (Thill et al. 2001), most suspended particulate matter (SPM) carried out by the Rhône River settles in front of the mouth, on the prodelta (Maillet et al. 2006; Estournel et al. 2023) (Figure 5.1).

In the prodelta located at a distance of 2 km from the river mouth, sedimentation rate at short-time scale is influenced by event-driven flood deposition and thus, sediment accumulation would not only depend on the

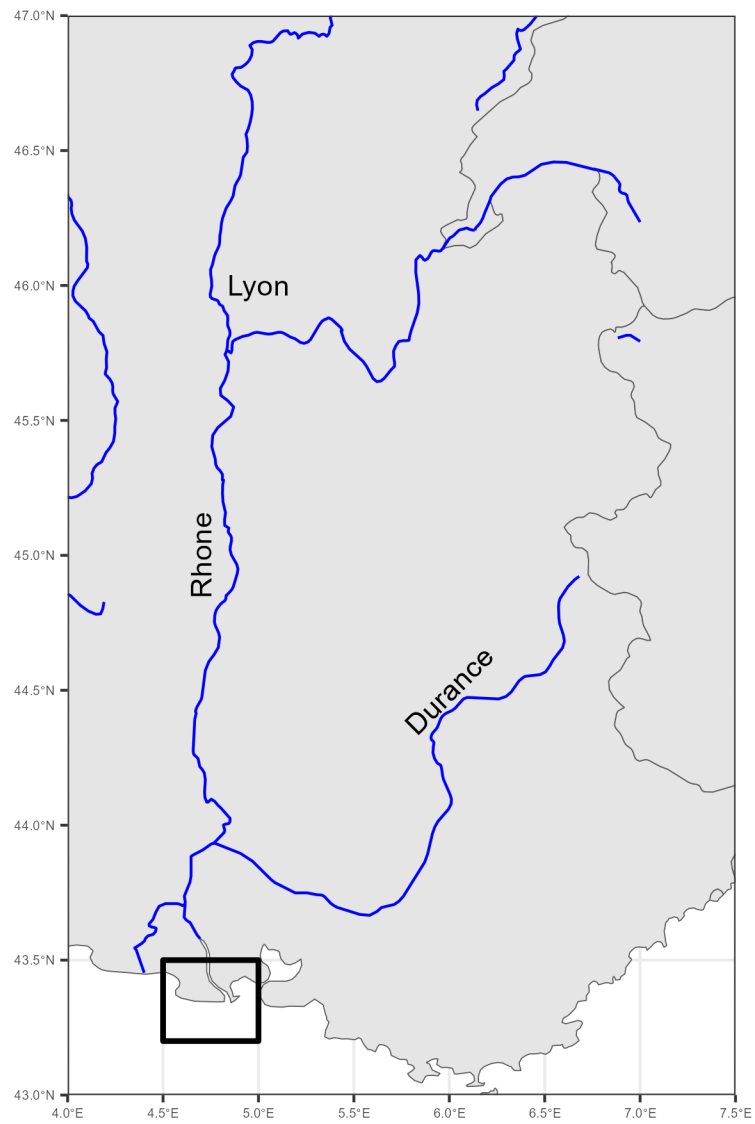


Figure 2.4: Map of the Rhone river delta. The prodelta is an area within 3 km of the Rhône River outlet with water depths of < 60 m. Stations A and Z are located inside the prodelta and are area of focus for the following chapters.

river discharge but also on the wind and wave conditions (Maillet et al. 2006). Sedimentation rates in the Rhône prodelta are characterized by a mean apparent accumulation rate of up to 35 to 48 $cm\ yr^{-1}$ (Charmasson et al. 1998). Furthermore, episodic resuspension and erosion have been observed at this location (Marion et al. 2010; Dufois et al. 2014), which has been attributed to significant strong wave-induced bottom shear stresses (Dufois et al. 2008). This deposition and erosion cycle demonstrate that the first centimeters of sediment are vulnerable to frequent physical disturbances during floods and storms. Such short-duration events (typically one day for storms and a few days for floods which most often are coupled with the storms) must therefore be fully taken into account to quantify impacts on the sediments (Madron et al. 2008) and their biogeochemistry (Moriarty et al. 2017).

2.7.1 Biogeochemical processes operating in Rhône prodelta sediments

In the Rhône prodelta, the benthic biogeochemical processes are largely driven by the flux of particulate organic matter from either terrestrial origin (Lansard et al. 2009a; Cathalot et al. 2013; Bonifácio et al. 2014) with a minor part linked to autochthonous origin from pelagic plankton export (Bourgeois et al. 2011; Pruski et al. 2015). Once deposited in the sediment, organic matter undergoes various degrees of transformation in the upper sediment - the extent of which depends on the degree of lability of the organic carbon deposited (Pastor et al. 2011b). There is substantial evidence suggesting that within the Rhône prodelta, anaerobic mineralization of carbon is dominant, with a major share being sulfate reduction (Rassmann et al. 2016). Estimate of total carbon mineralization in this region ranges from 70 - 650 $g\ C\ m^{-2}\ y^{-1}$ (Pastor et al. 2011b). Furthermore, the high deposition of more labile material close to the river is responsible for a rapid consumption of oxygen and intense OM degradation, mainly driven by anoxic processes. On the adjacent continental shelf, this predominance of anoxic processes decreases together with the decrease in organic carbon deposition, accumulation rates, and the increase in oxygen exposure time.

2.8 FESDIA model

The FESDIA model (Iron, Sulfur diagenesis) model was developed from OMEXDIA to capture the oxic and anoxic biogeochemical processes occurring in the sediment. The novelty of this model compared to early diagenetic models is in its ability to explicitly simulate non-steady early diagenesis processes in systems subject to perturbation events such as massive floods or storm deposition. Full description of the model numerical formulation and conceptual basis for adequately representing event-driven deposition is given in Chapter 3. Here, we provide the relevant biogeochemical processes described by the model and its formulation, process parameterization and the evolution of model construction to answer key questions and processes in line with the needs of this thesis.

2.8.1 Description of biogeochemical processes

Table 2.2: State variables described in the model.

State variable	Model notation	Units	Description
C_{org}^{fast}	FDET	$mmol\ C\ m^{-3}$	Fast decaying detritus
C_{org}^{slow}	SDET	$mmol\ C\ m^{-3}$	Slow decaying detritus

State variable	Model notation	Units	Description
$FeOOH_A$	FeOOHA	$mmol Fe m^{-3}$	Fast oxidized ferric iron
$FeOOH_B$	FeOOHB	$mmol Fe m^{-3}$	Slow oxidized ferric iron
MnO_{2A}	MnO2A	$mmol Mn m^{-3}$	Fast oxidized manganese
MnO_{2B}	MnO2B	$mmol Mn m^{-3}$	Slow oxidized manganese
$MnCO_3$	MnCO3	$mmol Mn m^{-3}$	Rhodochrosite
O_2	O2	$mmol O_2 m^{-3}$	Oxygen
NO_3^-	NO3	$mmol N m^{-3}$	Nitrate
NH_4^+	NH3	$mmol N m^{-3}$	Ammonium
SO_4^{2-}	SO4	$mmol S m^{-3}$	Sulfate
H_2S	H2S	$mmol S m^{-3}$	Hydrogen sulfide
Fe^{2+}	Fe	$mmol Fe m^{-3}$	Reduced ferrous iron
Mn^{2+}	Mn	$mmol Mn m^{-3}$	Reduced manganese
DIC	DIC	$mmol C m^{-3}$	Dissolved inorganic carbon
CH_4	CH4	$mmol CH_4 m^{-3}$	Methane

State variables: A set of 16 variables was included in the original FESDIA model (Table 4.1). Concentrations of dissolved and solid variables X are expressed in $mmol X m^{-3}$ (of porewater for solutes and of solid for particulates). Nine variables makes up the dissolved substances: oxygen (O_2), nitrate (NO_3^-), ammonium (NH_4^+), dissolved iron (Fe^{2+}) and manganese (Mn^{2+}), sulfate (SO_4^{2-}), hydrogen sulfide (H_2S), methane (CH_4) and dissolved inorganic carbon (DIC). In the sediment, oxygen is consumed by organic matter degradation as well as the re-oxidation of reduced substances from carbon mineralization. Nitrate can be consumed by denitrification or produced by the nitrification of ammonium. Ammonium is produced during OM degradation and a fraction of the ammonium can be adsorbed in the sediment. Dissolved manganese and iron can be produced during OM degradation as well as the reduction of their oxidized solid-bearing forms via redox processes. Sulfate reduction of OC produces dissolved sulfide, which can either accumulate in strongly anoxic condition or re-oxidized in the presence of oxygen, $FeOOH$ and MnO_2 or precipitate with iron (Figure 2.5).

Seven solid components are distinguished in the final version of FESDIA model. A fast and slow-decaying organic carbon represented by $(CH_2O)_x(NH_3)_y(H_3PO_4)_{fast}$ and $(CH_2O)_x(NH_3)_y(H_3PO_4)_{slow}$ respectively. The coefficients x and y denote the molar C/P and N/P ratios respectively. For short, these terms are decoded as C_{org}^{fast} and slow C_{org}^{slow} respectively. Oxidized form of manganese and iron are also decomposed into fast and slow fraction (MnO_{2A} and MnO_{2B}) and iron (oxyhydr)oxide ($FeOOH_A$ and $FeOOH_B$) while a single component for manganese carbonate ($MnCO_3$) was used to constrain the manganese cycle.

2.8.2 Primary reaction

The biogeochemical reactions included in this model entailed the primary processes involving organic matter degradation in the form of carbon oxidation. These primary reactions share the characteristic of taking place through bacterial respiration. The different mineralization pathways encompass aerobic mineralisation, denitrification, manganese and iron reduction, sulfate reduction and methanogenesis. The order of the primary redox reactions indicates the sequence in which they occur as sediment depth increases, in accordance with the

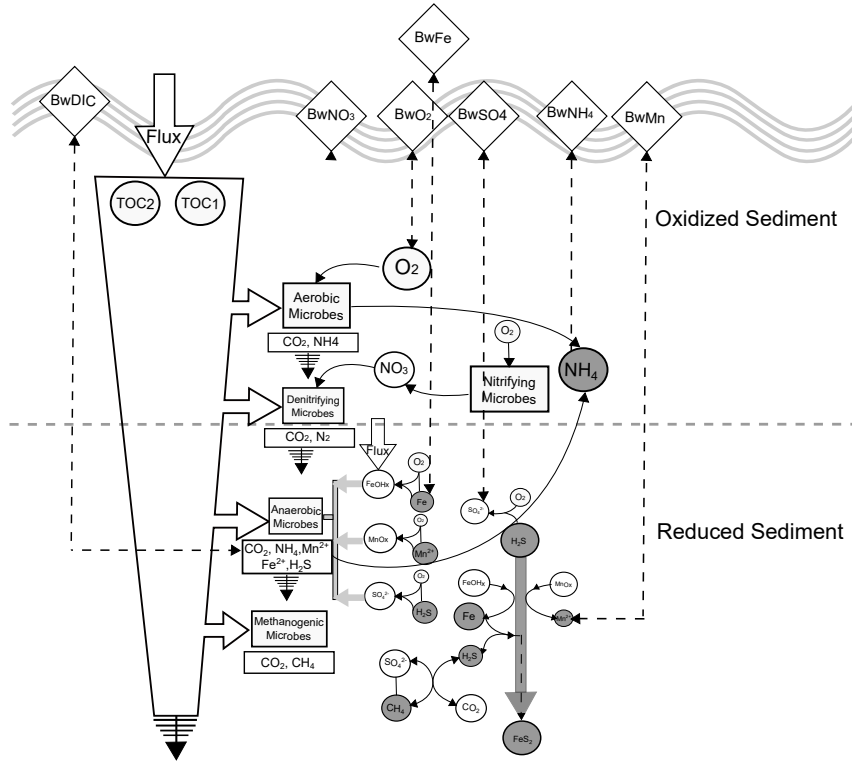
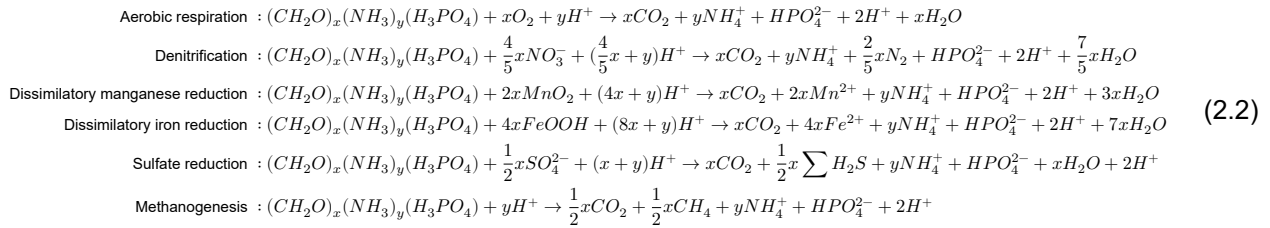


Figure 2.5: Conceptual schematic of the FESDIA biogeochemical model of organic matter (OM) degradation in the sediment. See text for description of model formulation of the different biogeochemical processes.

diminishing free energy released during OM mineralization. These mineralization pathways can be described by a set of standard overall reactions:



Unlike the model of Soetaert et al. (1996a) with an anoxic mineralization closure and the state variable, ODU , this model includes the full diagenetic pathways necessary to resolve the interactions between the carbon, sulfur, iron and manganese cycles. Together, these coupled equations uniformly produced inorganic carbon together with other reduced species in the form of a by-product which can be mathematically described as:

$$C_{prod} = \left(r_{Fast} \times C_{org}^{fast} + r_{Slow} \times C_{org}^{fast} \right) \times \frac{(1 - \phi)}{\phi} \tag{2.3}$$

and upon stoichiometric consideration, total nitrogen production is given as:

$$N_{prod} = \left(r_{Fast} \times C_{org}^{fast} \times N_{Cratio}_{C_{fast}} + r_{Slow} \times C_{org}^{fast} \times N_{Cratio}_{C_{slow}} \right) \times \frac{(1 - \phi)}{\phi} \tag{2.4}$$

where the NC_{ratio} is the redfield nitrogen to carbon ratio of the fast and slow decaying carbon. In this model, a multi-G approach to organic matter degradation is used where organic detritus is decomposed according to their reactivity which is grossly related to the age of the buried carbon. This is contrary to other approaches like the reactive continuum approach, where the spectrum of organic carbon of different degradabilities is modelled (Middelburg 1989; Boudreau and Ruddick 1991) or the power law model linking the degree of degradation process (i.e., age) to the amount of carbon consumed (Middelburg 1989; Van Cappellen et al. 1993). Our justification for using the multi-G approach stems from the ease of usage for short-term transient simulation and along shallow coastal margins (Arndt et al. 2013). Moreover, the use of sophisticated reactive continuum is limited by our poor mechanistic understanding of the controls on OM degradation in marine biosphere and lack of observation to adequately constrain the parameters inherent in the model (Arndt et al. 2013).

With this multi-G model, the rate of metabolic activity for each degradation pathway is not only substrate-limiting and dependent on the reactivity of the organic matter but also on the availability of the oxidant which places a constraint on each particular reaction. This limitation is modelled using a monod-kinetic type function with $k_{[c]}$ representing the half saturation constants and $k_{in[c]}$ the constant for inhibiting less energy-yielding oxidants by electron acceptors with greater potential for mineralization (Rabouille and Gaillard 1991):

$$\begin{aligned}
Oxicminlim &= \frac{O_2}{O_2 + k_{O_2}} \times (1 - \phi) \times \frac{1}{lim} \\
Denitrifclim &= \frac{NO_3}{NO_3 + k_{NO_3}} \times \left(1 - \frac{O_2}{O_2 + k_{inO_2}}\right) \times \frac{1}{lim} \\
Mnredminlim &= \frac{MnO_2}{MnO_2 + k_{MnO_2}} \times \left(1 - \frac{NO_3}{NO_3 + k_{inNO_3}}\right) \times \left(1 - \frac{O_2}{O_2 + k_{inO_2}}\right) \times \frac{1}{lim} \\
Feredminlim &= \frac{FeOOH}{FeOOH + k_{FeOOH}} \times \left(1 - \frac{MnO_2}{MnO_2 + k_{inMnO_2}}\right) \times \left(1 - \frac{NO_3}{NO_3 + k_{inNO_3}}\right) \times \left(1 - \frac{O_2}{O_2 + k_{inO_2}}\right) \times \frac{1}{lim} \\
BSRminlim &= \frac{SO_4}{SO_4 + k_{SO_4}} \times \left(1 - \frac{FeOOH}{FeOOH + k_{inFeOOH}}\right) \times \left(1 - \frac{MnO_2}{MnO_2 + k_{inMnO_2}}\right) \times \left(1 - \frac{NO_3}{NO_3 + k_{inNO_3}}\right) \times \left(1 - \frac{O_2}{O_2 + k_{inO_2}}\right) \times \frac{1}{lim} \\
Methminlim &= \left(1 - \frac{SO_4}{SO_4 + k_{inSO_4}}\right) \times \left(1 - \frac{FeOOH}{FeOOH + k_{inFeOOH}}\right) \times \left(1 - \frac{MnO_2}{MnO_2 + k_{inMnO_2}}\right) \times \left(1 - \frac{NO_3}{NO_3 + k_{inNO_3}}\right) \times \left(1 - \frac{O_2}{O_2 + k_{inO_2}}\right) \times \frac{1}{lim}
\end{aligned} \tag{2.5}$$

Thus, allowing for each pathway to be reformulated from the total carbon produced in Equation 2.3 using each limitation term in Equation 2.5 :

$$\begin{aligned}
Oxicmin &= C_{prod} \times Oxicminlim \times lim \\
Denitrific &= C_{prod} \times Denitrifclim \times lim \\
Mnredmin &= C_{prod} \times Mnredminlim \times lim \\
Feredmin &= C_{prod} \times Feredminlim \times lim \\
BSRmin &= C_{prod} \times BSRminlim \times lim \\
Methmin &= C_{prod} \times Methminlim \times lim
\end{aligned} \tag{2.6}$$

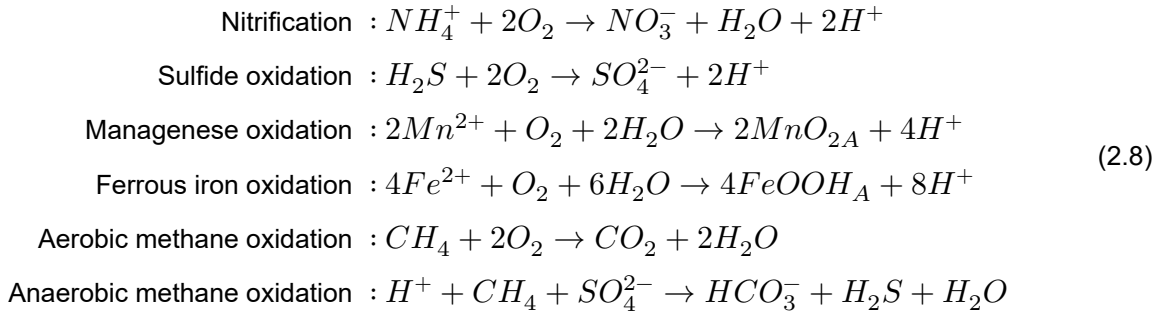
where the re-scaled limitation term, lim is given as:

$$lim = \frac{1}{Oxicminlim + Denitrifclim + Mnredminlim + Feredminlim + BSRminlim + Methminlim} \tag{2.7}$$

in order to ensure that the sum of each respiratory rate equals the total degradation rate (Soetaert et al. 1996a).

2.8.3 Secondary reaction

In contrast to primary reactions, which are all microbial respiration processes, most secondary reactions can be either microbial or purely chemical. In the previous section, the mineralization reactions produced a variety of reduced species such as NH_4 , Mn^{2+} , Fe^{2+} , H_2S and CH_4 . These reduced substances diffuse upward in the sediment column and can be re-oxidized through a series of secondary redox reactions. The secondary reactions included in the model contain several substantial differences from the ones defined by Soetaert et al. (1996a).

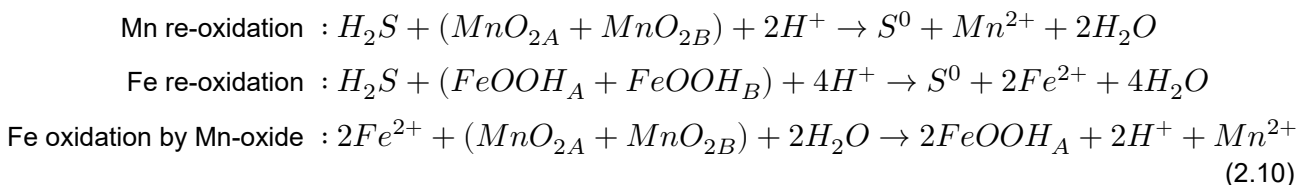


In the model, the re-oxidation of reduced species via oxygen (Equation 4.2) and metallic oxides (Equation 4.2) is included while methane formed by fermentation of OM is anaerobically oxidized (i.e., anaerobic oxidation of methane, AOM) (Dale et al. 2006). For most re-oxidation reactions, we followed Van Cappellen and Wang (1996) with a bi-molecular reaction rate law to describe the reaction kinetics.

$$\begin{aligned}
 Nitri &= R_{nit} \times NH_4 \times \frac{O_2}{(O_2 + ks_{nitri})} && \text{(Nitrification)} \\
 Feoxid &= R_{FeOOH} \times Fe \times O_2 && \text{(Iron oxidation)} \\
 Mnoxid &= R_{oxid} \times Mn \times O_2 && \text{(Mn oxidation)} \\
 H_2Soxid &= R_{H_2S} \times H_2S \times O_2 && \text{(sulfide oxidation)} \\
 CH_4oxid &= R_{CH_4} \times CH_4 \times O_2 && \text{(Methane oxidation)} \\
 AOM &= R_{AOM} \times CH_4 \times SO_4 && \text{(Anaerobic oxidation of methane)}
 \end{aligned} \tag{2.9}$$

where R_i for process i is the reaction rate of re-oxidation (d^{-1}) while ks_{nitri} is the half saturation constant ($mmol\ m^{-3}$). These dissolved species are also affected by the activities of animals, which pump water into and out of the sediment (irrigation). The importance of irrigation and bioturbation will be discussed in Section 2.8.4.

The oxidized form of iron, ferric iron (Fe^{3+}), will precipitate out as fresh iron oxide ($FeOOH_A$) minerals. Sulfide produced by organoclastic sulfate reduction is abiotically oxidized by both pools of ferric iron and manganese oxide (i.e., sulfur-mediated iron and manganese reduction) (Berg et al. 2003) whereas reduced iron is oxidized by MnO_{2A} .



As discussed in Haese (2000), the interaction between dissolved Fe^{2+} and H_2S happens in two stages, with the formation of intermediate dissolved elemental sulfur (S^0) and dissolved FeS (FeS_{aq}). However, these forms of sulfur are not modelled because of their unstable nature in marine sediment as well as the possibility of FeS_{aq} precipitating to its particulate form (FeS_p) once a solubility threshold of $\sim 2 \mu M$ is reached (Rickard 2006). Therefore, we assumed that elemental sulfur and dissolved FeS, upon formation, subsequently transform into a stable form of particulate sulfur that can be eliminated from the system via precipitation (Rickard 1997, 2006).



Implicit in this assumption is the neglect of disproportionation of S^0 (Finster et al. 1998), thus directly coupling Fe and H_2S to pyrite precipitation. This model's presumption should only apply to this particular site because precipitation of reduced species has been proposed to explain a significant removal of free sulfide from porewater in the Rhône sediment (Pastor et al. 2011a; Rassmann et al. 2020). It may need to be modified to describe sulfur dynamics in areas with different geochemical regimes. Additionally, particulate iron monosulfide is produced when dissolved iron binds with sulfide (i.e FeS production) which is explicitly accounted for as a sink pathway for sulfur in the model (Rickard 1997). The kinetic rate expressions of these secondary reactions can be described by the standard second-order rate formulation:

$$\begin{aligned} FeS_{prod} &= R_{FeS_{prod}} \times Fe \times H_2S && \text{(FeS production)} \\ H_2O_{xidMnO_2} &= R_{H_2S_{oxid}} \times H_2S \times (MnO_{2A} + MnO_{2B}) && \text{(Reoxidation of H}_2\text{S with MnO}_2\text{)} \\ H_2O_{xidFeOOH} &= R_{H_2S_{oxid}} \times H_2S \times (FeOOH_A + FeOOH_B) && \text{(Reoxidation of H}_2\text{S with FeOOH)} \\ FeO_{xidMn} &= R_{MnFe} \times (MnO_{2A} + MnO_{2B}) \times Fe && \text{(Reoxidation of Fe with MnO}_2\text{)} \end{aligned} \quad (2.12)$$

The model also includes a simple representation of the formation and dissolution of manganese carbonates ($MnCO_3$). However, iron carbonate (siderite - $FeCO_3$) formation and dissolution were not considered in the model since siderite precipitation is inhibited by low levels of sulfide (Haese 2000). In reality, despite suggestions that the Rhone pro-delta sediment is probably non-sulfidic (Pastor et al. 2018), siderite can still precipitate because of its dependency on the Eh-pH condition of the micro-environment inside the sediment matrix (Bell et al. 1987). However, such micro-scale processes are not discussed here. This kinetics of dissolution and precipitation of $MnCO_3$ follows a similar formulation in Wang and Van Cappellen (1996), where the reaction rates are dependent on the pore water saturation state. Here, the pH of the porewater was not explicitly modelled but was fixed at a constant profile of 7.5 in order to reduce the complexity of the model (Berg et al. 2003).

$$\begin{aligned} MnCO_{3diss}^{prec} &= rMnCO_3prec \times (\Omega_{rhod} - 1) && \Omega_{rhod} > 1 \\ MnCO_{3diss}^{prec} &= rMnCO_3diss \times (\Omega_{rhod} - 1) \times MnCO_3 && \Omega_{rhod} < 1 \end{aligned} \quad (2.13)$$

where $rMnCO_3prec$ and $rMnCO_3diss$ is the rate constant for precipitation and dissolution of $MnCO_3$ given as $3 \times 10^{-4} cm^3 nmol^{-1} d^{-1}$ and $6.8 d^{-1}$ respectively (Wang and Van Cappellen 1996). Ω_{rhod} is the saturation index calculated from dissolved Mn and DIC using the equilibrium constant at the specified

temperature of 15°C as:

$$\Omega_{rhod} = \frac{Mn \times CO_3^{2-}}{K_{sprod}} \quad (2.14)$$

2.8.4 Transport processes

The transport processes considered in the model include molecular diffusion for the solutes, bioturbation by macrofauna inhabiting the sediment, burial of particulate matter, and irrigative exchange of solutes between the bottom water and interstitial fluid.

The flux of solutes by molecular diffusion is calculated from Fick's first law, given the concentration gradient between the sediment and the overlying water column:

$$J_d = -\phi D_{sed} \frac{\partial C}{\partial z} \quad (2.15)$$

where the D_{sed} ($cm \ d^{-1}$) is the effective diffusion coefficient corrected for tortuosity and given as $D_{sed} = \frac{D^{sw}}{\theta^2}$, with D^{sw} the molecular diffusion coefficient of the solute in free solution of sea-water and θ is the tortuosity derived from the formation factor (F) and porosity (ϕ) of a sediment matrix (Berner 1980; Boudreau 1997).

In the model, bioturbation as a mixing process within the sediment due to animal activity is assumed to be interphase, with porosity $\phi(z)$ remaining constant over time. Thus, this intensity of this process captured as D_i in Equation 2.1 can be prescribed as:

$$D_b(z) = \begin{cases} D_b^0 & \text{if } Z \leq Z_L \\ D_\infty + (D_b^0 - D_\infty) e^{-\frac{(Z-Z_L)}{biot_{att}}} & \text{if } Z > Z_L \end{cases} \quad (2.16)$$

where D_b^0 is the bio-diffusivity coefficient ($cm^2 d^{-1}$) at the SWI and in the mixed layer, Z_L is the depth of the mixed layer (cm) and $biot_{att}$ is the attenuation coefficient (cm) of bioturbation below the mixed layer. D_∞ is the diffusivity at the deeper layer (usually specified as zero).

Depth-dependent bio-irrigation is modelled acts as a non-local exchange process between the porewater parcels and the overlying bottom water.

$$Irr(z) = \begin{cases} Irr_0 & \text{if } Z \leq Z_L \\ Irr_\infty + (Irr_0 - Irr_\infty) e^{-\frac{(Z-Z_L)}{Irr_{att}}} & \text{if } Z > Z_L \end{cases} \quad (2.17)$$

for which Irr_0 is the bio-irrigation coefficient (d^{-1}) and Irr_{att} is the attenuation of irrigation (cm) below the depth of the irrigated layer Z_{irr} (cm). At depth, the bio-irrigation coefficient (Irr_∞) is generally set to zero. The irrigation rate in $mmol \ m^{-3} \ d^{-1}$ due to bio-irrigation is given as:

$$J_{irr} = Irr(z) \times (C_0 - C(z)) \times \phi \quad (2.18)$$

with C_0 as the solute concentration of the overlying bottom water and $C(z)$ is the solute concentration at depth z .

All the equations can be arranged together with the transport term to form a system of nonlinear partial differential equations:

$$\begin{aligned}
\frac{\partial C_{org}^{fast}}{\partial t} &= transport - rFast \times C_{org}^{fast} \\
\frac{\partial C_{org}^{slow}}{\partial t} &= transport - sFast \times C_{org}^{slow} \\
\frac{\partial O_2}{\partial t} &= transport - Oximin - 1.5Nitri - 0.25FeOxid - 2H_2Soxid - 2CH_4oxid - 0.5MnOxid \\
\frac{\partial NH_3}{\partial t} &= transport + \frac{(Nprod - Nitri)}{(1 + NH_3ads)} \\
\frac{\partial NO_3}{\partial t} &= transport - 0.8Denitric + Nitri \\
\frac{\partial CH_4}{\partial t} &= transport + 0.5Methmin - CH_4oxid - AOM \\
\frac{\partial DIC}{\partial t} &= transport + Cprod + 0.5Methmin + CH_4oxid + AOM - MnCO_3^{prec} \times \frac{(1-\phi)}{\phi} \\
\frac{\partial SO_4}{\partial t} &= transport - 0.5BSRmin + H_2Soxid - AOM \\
\frac{\partial Fe}{\partial t} &= transport + 4Feredmin - Feoxid - FeSprod + (2H_2SoxidFeOOH_{A,B} - FeOxidMn_{A,B}) \times \frac{(1-\phi)}{\phi} \\
\frac{\partial FeOOHA}{\partial t} &= transport + (Feoxid - 4Feredmin) \times \frac{\phi}{(1-\phi)} - 2H_2SoxidFeOOH_A + FeOxidMn_{A,B} \\
\frac{\partial FeOOHB}{\partial t} &= transport - 2H_2SoxidFeOOH_B \\
\frac{\partial H_2S}{\partial t} &= transport + 0.5BSRmin - H_2Soxid - FeSprod + AOM - (H_2SoxidFeOOH_{A,B} + H_2SoxidMn_{O_{2A,B}}) \times \frac{(1-\phi)}{\phi} \\
\frac{\partial Mn}{\partial t} &= transport + 2Mnredmin - Mnoxid + (H_2SoxidMn_{O_{2A,B}} + 0.5FeOxidMn_{A,B}) \times \frac{(1-\phi)}{\phi} - MnCO_3^{prec} \times \frac{(1-\phi)}{\phi} \\
\frac{\partial MnO_{2A}}{\partial t} &= transport - 2Mnredmin + Mnoxid \times \frac{\phi}{(1-\phi)} - H_2SoxidMn_{O_{2A}} - 0.5FeOxidMn_A \\
\frac{\partial MnO_{2B}}{\partial t} &= transport - H_2SoxidMn_{O_{2B}} - 0.5FeOxidMn_B \\
\frac{\partial MnCO_3}{\partial t} &= transport + MnCO_3^{prec}
\end{aligned} \tag{2.19}$$

The time evolution of these systems is further modified, particularly during the flood deposition phase. The following chapter documents the whole numerical process utilized in the model as well as the boundary conditions. An explicit flood deposition procedure given in the following chapter investigates the model's ability to manage abruptly altering boundary conditions.

2.9 Parameters for the biogeochemical processes

For parameterization of the model, previous modelling efforts and parameters obtained in the Rhône prodelta area were used as a starting point for prescribing the configuration for the different applications. Notably, the steady-state modelling work of Pastor et al. (2011b) and Ait Ballagh et al. (2021) presents an optimized set of parameters employed to study the biogeochemical dynamics of the Rhône prodelta sediment. Because this thesis uses a non-steady-state approach, the parameters were further optimized in a time-dependent manner, either automatically or manually fine-tuning to match field observations.

The strategy for finding adequate parameters of the diagenetic model in each application employed as described in the subsequent chapters proceeds with the calibration of the characteristics of the newly deposited flood layer (see Chapter 4). Here, the integration of all the available knowledge which constitutes the substance of flood deposition is used. This knowledge base is gleaned either from sedimentary data describing the carbon content of the new layer (see Chapter 5), the thickness of the deposited layer diagnosed by radionuclide activities (when available - see Chapter 6) or proxy data such as the timing of the event, and the amplitude of river discharge (to provide a measure of the rough estimate of the flooded sediment characteristics). As in the model, the carbon

mineralization is independent of oxygen, nitrogen, manganese, iron and sulfur, it can be fully parameterized before considering other cycles. A glossary of literature values for iron and manganese flux (Wang and Van Cappellen 1996; Berg et al. 2003; Radakovitch et al. 2008; Dale et al. 2015; Zhao et al. 2020) to the sediment was used to constrain the reactions involving particulate oxides of metal in the model.

2.10 Evolution of biogeochemical model

Further development of the model during the course of the thesis allowed the inclusion of certain processes which were omitted from the initial version of the model. Here, I explain the developmental phase of the model as the subject and processes of the thesis evolve.

The initial version of the model entails the entire primary reaction Equation 2.2 and a subset of the secondary reaction Equation 2.9. This version opens the possibilities of including detailed anoxic-related processes in the sediment compared to the earlier OMEXDIA model (Soetaert et al. 1996a) and acts as a benchmark for verification whether the explicit flood deposition algorithm (see Chapter 4) works as intended.

As the research project evolved and the scientific questions asked were refined during the course of this thesis, additional secondary reaction pathways were added to the model. Notably, Equation 2.12 and Equation 2.13 were implemented. In addition, the initial version of the model developed in Chapter 3 and originally published as a research article was only capable of simulating multiple event-driven depositions per simulation but with a similar flood-input characteristic in all instances of the deposition. Subsequent iterations of the model build on this to simulate the sequential manifestation of flood deposition with variable flood-input characteristics across all temporal instances of the deposition.



Chapter 3

Exploring temporal variations of sediment biogeochemistry under the influence of flood events using numerical modelling

Criticize by creating

Michelangelo

Published as: Nmor, S. I., E. Viollier, L. Pastor, B. Lansard, C. Rabouille, and K. Soetaert. 2022. FESDIA (v1. 0): "Exploring temporal variations of sediment biogeochemistry under the influence of flood events using numerical modelling." *Geoscientific Model Development* 15: 7325–7351.

Abstract:

Episodic events of flood deposit in coastal environments are characterized by deposition of large quantities of sediment containing reactive organic matter within short periods of time. While steady-state modelling is common in sediment biogeochemical modelling, the inclusion of these events in current early diagenesis models has yet to be demonstrated. We adapted an existing model of early diagenetic processes to include the ability to mimic an immediate organic carbon deposition. The new model version was able to reproduce the basic trends from field sediment porewater data affected by the November 2008 flood event in the Rhône River prodelta. Simulation experiments on two end-member scenarios of sediment characteristics dictated by field observation, (1-high thickness deposit, with low TOC and 2-low thickness, with high TOC), reveal contrasting evolutions of post-depositional profiles. A first-order approximation of the differences between subsequent profiles was used to characterize the timing of recovery (i.e relaxation time) from this alteration. Our results indicate a longer relaxation time of approximately 4 months for SO_4^{2-} and 5 months for DIC in the first scenario and less than 3 months for the second scenario which agreed with timescale observed in the field. A sensitivity analysis across a spectrum of these end-member cases for the organic carbon content (described as the enrichment factor α) and for sediment thickness - indicates that the relaxation time for oxygen, sulfate, and DIC decreases with increasing organic enrichment for a sediment deposition that is less 5 cm. However, for larger deposits (> 14 cm), the relaxation time for oxygen, sulfate and DIC increases with α . This can be related to the depth dependent availability of oxidant and the diffusion of species. This study emphasizes the significance of these sediment characteristics in determining the sediment's short-term response in the presence of an episodic event. Furthermore, the model described here provides a

3.1 Introduction

Coastal margins play a crucial role in the global marine systems in terms of carbon and nutrient cycling (Wollast 1993; Rabouille et al. 2001a; Cai 2011; Bauer et al. 2013; Regnier et al. 2013; Gruber 2015). Due to their relatively shallow depth, sedimentary early diagenetic processes are critical for the recycling of a variety of biogeochemical elements which are influenced by organic matter (OM) inputs, particularly carbon (Middelburg et al. 1993; Arndt et al. 2013). Furthermore, these processes have the potential to contribute to the nutrient source that fuels primary productivity of the marine system. In river-dominated ocean margins (RiOmar, (McKee et al. 2004)), organic matter input can also be enhanced by flood events which provide a significant fraction of the particulate carbon (POC) delivered to depocenters (Antonelli et al. 2008). Organic matter derived from riverine input to sediment has biogeochemical significance in coastal marine systems (Cai 2011). As a result, the coastal environment serves as both a sink for particulate organic carbon and nutrients and an active site of carbon and nutrient remineralization (McKee et al. 2004; Burdige 2005; Sundby 2006).

In the context of early diagenetic modelling, numerical models with time-dependent capability are well established (Lasaga and Holland 1976; Burdige and Gieskes 1983; Rabouille and Gaillard 1991; Boudreau 1996; Soetaert et al. 1996a; Rabouille et al. 2001b; Archer et al. 2002; Couture et al. 2010; Yakushev et al. 2017), and they are used in many coastal and deep-sea studies. However, because of the scarcity of observations and their unpredictability, the role of massive episodic events in these models has frequently been overlooked (Tesi et al. 2012). As these rare extreme events are being currently documented in various locations, there is a growing appreciation for their impact on the coastal margin (Deflandre et al. 2002; Cathalot et al. 2010; Tesi et al. 2012).

Attempts to use mathematical models to understand perturbation-induced events such as sudden erosion/resuspension event, bottom trawling, and turbidity driven sediment deposition on early diagenetic processes have resulted in a variety of approaches that incorporate this type of phenomenon. As an example, Katsev et al. (2006) demonstrated that the position of the redox boundary (depth zone beneath the sediment-water interface that separates the stability fields of the oxidized and reduced species of a given redox couple) in organic-poor marine sediment can undergo massive shifts due to the flux of new organic matter on a seasonal basis, whereas on a longer time scale (e.g. decadal), redox fluctuation linked to organic matter deposition can induce the redistribution of solid-phase manganese with multiple peaks (due to depth-wise oxidation-reduction of Mn). Another study in a coastal system revealed that coastal sediments change as a result of an anthropogenic perturbation in the context of bottom dredging and trawling (Velde et al. 2018). More recently, using similar model, De Borger et al. (2021a) highlighted that perturbation events such as trawling can possibly decrease total OM mineralization.

In river-dominated ocean margins, episodic flood events can deliver sediment with varying characteristics depending on its source origin, frequency and intensity (Cathalot et al. 2013). Therefore, the flood characteristics have direct impact on the deposited sediment's characteristics such as scale/thickness of the deposited layer, composition (mineralogy and grain-size), OM content and so on. For example, in the Rhône prodelta, a single flash flood can deliver up to 30 cm of new sediment material in a matter of days (Cathalot et al. 2010; Pastor et al. 2018). Despite the large amount of sediment introduced by this episodic loading, vertical distribution of

porewater species like oxygen (O_2), can be restored after a few days (Cathalot et al. 2010). It has also been noticed (Rassmann et al. 2020) that spring and summer porewater compositions measured for several years following fall and winter floods show quasi-steady state profiles for sulfate and DIC. Similar massive deposition was also reported in the Saguenay Fjord (Quebec, Canada) (Mucci and Edenborn 1992; Deflandre et al. 2002). The recovery timescale from this perturbation has only been roughly estimated for short-lived species like oxygen, but this is not always the case for sulfate (SO_4^{2-}), dissolved inorganic carbon (DIC), or other redox species. Furthermore, due to the limitation in temporal resolution of the observations, the short-term post depositional dynamics in the aftermath of this flood deposition event are scarcely described, making it difficult to discern how the system responds after the event. While experimental approaches (Chaillou et al. 2007) can provide useful insight into how they work, they lack the ability to provide continuous system dynamics and are often difficult to set up. A modelling approach can assist in addressing these issues, providing useful feedback in terms of the scale and response of the sediment to this type of event.

The goal of this study is to better understand episodic events in the context of flood driven sediment deposition and their impact on benthic biogeochemistry, post-flood evolution dynamics, and relaxation timescale. As the relaxation dynamics represent a gap in our understanding of how coastal systems respond to external drivers, we characterize the timescale of the recovery of sediment porewater profiles using a first-order approximation. To accomplish this, we developed an early diagenetic model called FESDIA. The ability to explicitly simulate non-steady early diagenesis processes in systems subject to perturbation events such as massive flood or storm deposition is a novel contribution of FESDIA to early diagenetic models. In the following ways, FESDIA differs therefore from the OMEXDIA model (Soetaert et al. 1996a) by implementing:

- An explicit description of the anoxic diagenesis including (i) Iron and Sulfur dynamics, (ii) methane production and consumption. In comparison OMEXDIA has a single state variable (ODU: oxygen demand unit) to describe reduced species.
- possibility to include sediment perturbation events such as abrupt deposition of sediment.

In this paper, we only discuss part of the FESDIA model concerned with the implementation of a perturbation event as it relates to some biogeochemical indicators. The model is implemented in Fortran (for speed) and linked to R (for flexibility). We demonstrate the model's utility in describing data collected from a flood event in November/December 2008 (Pastor et al. 2018) as well as numerically investigating the impact of varying degrees of flood type characteristics on the system's relaxation dynamics. This work is a foundation for a more in-depth investigation of the model-data biogeochemistry of the porewater and solid phase components of core samples from Pastor et al. (2018), and it provides a useful baseline for understanding the spatiotemporal dynamics of coastal marine systems subject to event-driven organic matter pulses.

3.2 Materials and methods

3.2.1 Site and events description

The Rhône prodelta serves as a case study for the development of the model used to evaluate sediment perturbation dynamics. This particular coastal area acts as the transitory zone between the inland river channel and the continental shelf (Gulf of Lion) of the Mediterranean Sea. The Rhône River with a drainage basin of 97800 km^2 and mean water discharge of $1700 \text{ m}^3 \text{ s}^{-1}$ delivers up to $1.6 \times 10^{10} \text{ moles C}$ of particulate carbon (POC) annually (Sempéré et al. 2000) to the pro-deltaic part (i.e., where the river meets the sea). The

Rhône prodelta covers an area of approximately 65 km^2 with depth ranging from 2 to 60 m (Lansard et al. 2009a) and is characterized by high sedimentation rates reaching up to 41 cm yr^{-1} in the proximal zone (Rassmann et al. (2016); Lat - $43^\circ 18.680' \text{ N}$, Long - $4^\circ 51.038' \text{ E}$ and average depth of 21 m) (Radakovitch et al. 1999; Miralles et al. 2005). The organic matter delivered to the depocenter typically reflects the different compositional materials derived from the terrestrial domain (Pastor et al. 2018), whereas the magnitude of material transported and the quantity of organic carbon transferred laterally vary according to seasons and the period of massive instantaneous deposition (Lansard et al. 2008; Cathalot et al. 2013).

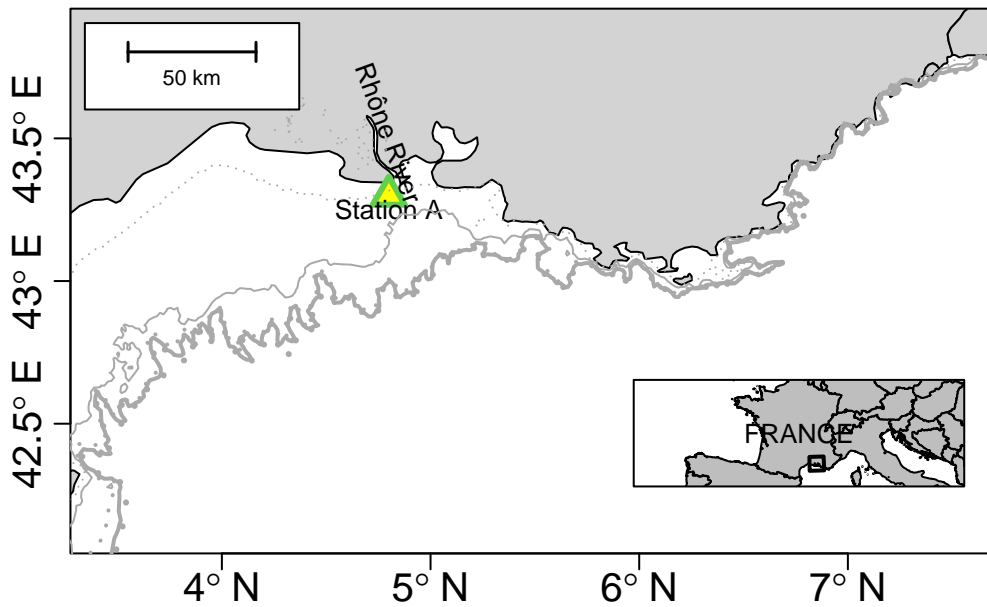


Figure 3.1: Map showing the locations of sampling sites in the proximal area off the Rhône River mouth.

Relating to the episodic pulse of organic matter, numerous studies have documented instances of flood-driven deposition from the Rhône River from a hydrographic perspective (Hensel et al. 1998; Boudet et al. 2017; Pont et al. 2017). Pastor et al. (2018) goes beyond sedimentology and hydrographic characteristics to provide a concise description of the various flood types, their diagenetic signatures, and biogeochemical implications. Furthermore, published porewater chemistry and solid phase data have highlighted sediment characteristics following such an event (Cathalot et al. 2010; Cathalot et al. 2013; Toussaint et al. 2013a; Pastor et al. 2018).

3.2.2 Model development and implementation

Following the description of the Rhône River flood types and the composition of the flood deposit (mainly in terms of organic carbon) at the proximal station A (Pastor et al. 2018), we proceed to describe the model developed to explore the observed data and their diagenetic implications in terms of relaxation times and their evolution following this transient perturbation.

Table 3.1: Description of notations, phrases, acronyms, and abbreviations, as used in this paper.

Symbols	Description
TOC_{ref}	Asymptotic carbon content. This is equal to the refractory component of sedimentary carbon not modelled explicitly by FESDIA.
Δz	Thickness of vertical layer. Unequal in each layer of the modelled domain.

Symbols	Description
N_{cur}	Number of grid layer. Equal to default modelled layer ($N = 100$).
N	
N_{pert}	Depth of sediment deposition. This corresponded to the observed depth of sediment deposited due to flood input.
Z_{pert}	
$TOC_{z_{pert}}$	Organic carbon content in the deposited layer. This corresponds to the TOC (total organic carbon) content introduced by the flood layer and differs from the ancient layer depending on its concentration of carbon.
TOC_{old}	Organic carbon content in the ancient layer. This corresponds to the TOC content in the previous layer prior to the flood deposition.
t^-	Time index prior to the flood event deposition.
α	Carbon enrichment factor. This is a multiplicative coefficient for which the solid component of the sediment in the newly deposited layer can be increased dynamically during the simulation. As such, a “new initial condition” for the deposition can be realized without stopping the simulation using this factor.
C_{org}	Concentration of fast and slow degradable organic matter. This is the sum of both model variables (C_{org}^{fast} and C_{org}^{slow})
C_{org}^{flood}	This variable symbolically specifies concentration of fast and slow degradable organic matter immediately after the event.
$flux_{org}$	Daily flux of organic carbon flux derived from the annual average flux.
$\varphi(t)$	Time-dependent, differential operator of successive depth integrated over the modelled domain.
$\tau(t)$	Relaxation time derived from $\varphi(t)$.

Our model combines the development of the OMEXDIA model (Soetaert et al. 1996a), applied in the Rhône prodelta area (Pastor et al. 2011a; Ballagh et al. 2020) and which has recently been equipped with event-driven processes (De Borger et al. 2021a). In De Borger et al. (2021a), the authors specifically addressed the issue of bottom trawling as a mixing and an erosional process that removes an upper layer of sediment and mixes a certain layer below. In addition, the model considers a bulk categorization of reduced substances in a single state variable, ODU (oxidative oxygen unit). For our approach, the event is defined by an addition of a new layer on top of the former sediment-water interface. Furthermore, we explicitly modelled pathways involving sulfur and iron. Following this preamble, the following sections expand on aspects of the model description and parameterization. Table 3.1 provides some key glossaries of mathematical notations used in the model.

3.2.2.1 Model state variables

The complete model describes the concentration of labile (C_{org}^{fast}) and semi-labile (C_{org}^{slow}) decaying organic matter, oxygen (O_2), nitrate (NO_3^-), and ammonium (NH_4^+), dissolved inorganic carbon (DIC), following the classic early diagenetic equation of (Berner 1980; Boudreau 1997). In addition to the model from De Borger et al. (2021a), our model includes sulfate (SO_4^{2-}), hydrogen sulfide (H_2S) and methane (CH_4), as well as iron species (Fe^{2+} and $Fe(OH)_3$) (Table 4.1).

Table 3.2: State variables described in the model.

State variable	Model notation	Units	Description
Solid			
C_{org}^{fast}	FDET	$mmol\ C\ m^{-3}$	Fast decaying detritus
C_{org}^{slow}	SDET	$mmol\ C\ m^{-3}$	Slow decaying detritus
$Fe(OH)_3$	FEOOH	$mmol\ Fe\ m^{-3}$	Fast oxidized ferric iron
Liquid			
O_2	O2	$mmol\ O_2\ m^{-3}$	Oxygen
NO_3^-	NO3	$mmol\ N\ m^{-3}$	Nitrate
NH_4^+	NH3	$mmol\ N\ m^{-3}$	Ammonium
SO_4^{2-}	SO4	$mmol\ S\ m^{-3}$	Sulfate
H_2S	H2S	$mmol\ S\ m^{-3}$	Hydrogen sulfide
Fe^{2+}	Fe	$mmol\ Fe\ m^{-3}$	Reduced ferrous iron
DIC	DIC	$mmol\ C\ m^{-3}$	Dissolved inorganic carbon
CH_4	CH4	$mmol\ CH_4\ m^{-3}$	Methane

In some coastal settings, oxidation via sulfate reduction has been highlighted as the primary pathway for organic carbon (OC) mineralization, with minor contributions from manganese and iron oxidation (Burdige and Komada 2011). In addition, the flux of integrated remineralization products such as DIC has previously been estimated to contribute up to 8 times that of diffusive oxygen uptake (Rassmann et al. 2020) - thus highlighting its importance in describing the amplitude of benthic recycling in coastal water. As such in this paper, we focus our analysis on these proxy variables (O_2 , SO_4^{2-} , DIC) because they serve as indicators of the integrated effect of the main diagenetic processes.

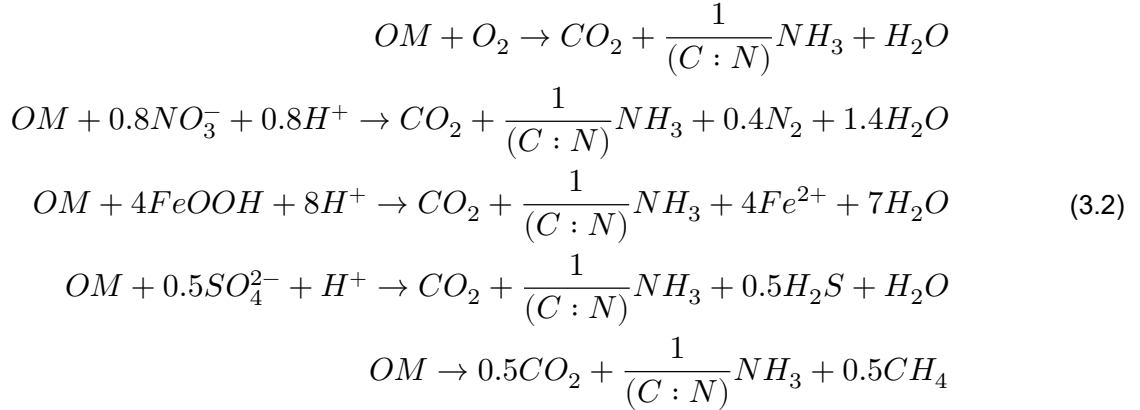
3.2.2.2 Biogeochemical reaction

Early diagenesis processes on the seafloor are driven by organic matter deposition. For areas such as the Rhône prodelta, continental organic carbon input is dominant, and it is difficult to identify the fraction of labile fraction responsible for fast OM pool consumption (Pastor et al. 2011a). Moreover, observations show that some organic compounds are preferentially degraded and become selectively oxidized (Middelburg et al. 1997; Pozzato et al. 2018). As a result, the model assumed solid phase organic carbon with two reactive fractions with different reactivities and C/N ratios (Westrich and Berner 1984; Soetaert et al. 1996a). The mineralization of OM occurs sequentially, with the labile fraction mineralizing faster than the slow decaying carbon. During the timescales considered here, the refractory organic matter class is not reactive. To compare with the observation, we consider an asymptotic OC constant (TOC_{ref}) for the inert fraction that scales the model calculated TOC output to the observation (Pastor et al. 2011a) (see Section 3.2.2.8). This organic carbon degradation requires oxidants, and the depth-dependency in sequential utilization of terminal electron acceptors assumption first proposed by (Froelich et al. 1979a) is used here. Oxygen is consumed first, followed by nitrate, iron oxides, sulfate and finally methanogenesis occurs (Equation 3.3). Because the quantity of organic matter, the relative proportions of fast and slow degrading materials, and the reactivities decrease with depth, the overall organic matter degradation rate decreases and eventually ceases. In the formulation of the individual biogeochemical processes, we use a similar paradigm as (Soetaert et al. 1996a) (Equation 4.1).

This rate of carbon mineralization of organic matter ($mmol\ m^{-3}\ d^{-1}$) can be expressed as:

$$C_{prod} = (r_{Fast} \times C_{org}^{fast} + r_{Slow} \times C_{org}^{slow}) \times \frac{(1 - \phi)}{\phi} \quad (3.1)$$

Where the r_{Fast} and r_{Slow} are the decay rate constant (d^{-1}) for the fast and slow detritus component. ϕ and $(1 - \phi)$ are the volume fraction for both solutes and solid respectively. This process is mediated by microorganisms and oxidant availability. The primary redox reaction includes (1) Oxidic respiration (2) Denitrification (3) Fe (III) reduction (4) Sulfate reduction and (5) Methane production:



where OM is simply represented as $(CH_2O)(NH_3)_{N:C}$ and N:C is the redfield nitrogen to carbon ratio respectively ($N:C = \frac{16}{106}$). This reaction can be modelled using a Monod type relationship with each oxidant having a half-saturation constant ($k_{s[C]}$) represented as k_{s*} in the model code. The inhibition of mineralization by the presence of other oxidants is also modelled with a hyperbolic term (subtracted from 1) where $k_{in[C]}$ is the concentration at which the rate drops to half of its maximal value. Using these limitation and inhibition functions, a single equation for each component across the model-depth domain can be realized (Rabouille and Gaillard 1991; Soetaert et al. 1996a; Wang and Van Cappellen 1996), together with some possible overlap (Froelich et al. 1979b; Soetaert et al. 1996a). For a generic species, this can be described mathematically as:

$$lim = \frac{[C]}{(k_{s[C]} + [C])} \prod \left(1 - \frac{[C]}{(k_{in[C]} + [C])} \right) \quad (3.3)$$

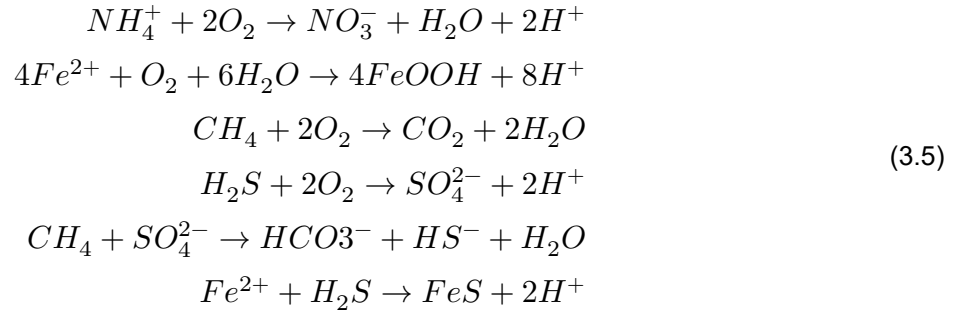
Where C is an oxidant. Formulation for individual pathways as well as values of half-saturation and inhibition constants for each oxidant can be found in Appendix (A1). With this limitation term, mineralization rate per solute can be estimated using potential carbon produced via OM degradation in Equation 3.1:

$$rate_{min} = C_{prod} \times lim \times \frac{1}{\sum lim} \quad (3.4)$$

with the $\sum lim$ the sum of all limitation terms which normalizes the term in order to always achieve the maximum degradation rate. See Soetaert et al. (1996a) for more details on the derivative of this equation.

Secondary redox reactions include reoxidation of reduced substances (nitrification, Fe oxidation, H_2S oxidation, methane oxidation) (Equation 4.2) and the precipitation of FeS. Anaerobic oxidation of methane occurs in the absence of O_2 following upward diffusion of methane to the sulfate-methane transition zone (SMTZ)

(Jørgensen et al. 2019):



These reactions are mathematically described using a coupled reaction formulation. Nitrification is limited by the availability of oxygen and the other reactions are described with a first-order term.

$$\begin{aligned}
Nitri &= R_{nit} \times NH_4 \times \frac{O_2}{(O_2 + ks_{nitri})} && \text{(Nitrification)} \\
Feoxid &= R_{FeOH_3} \times Fe \times O_2 && \text{(Iron oxidation)} \\
H_2Soxid &= R_{H_2S} \times H_2S \times O_2 && \text{(sulfide oxidation)} \\
CH_4oxid &= R_{CH_4} \times CH_4 \times O_2 && \text{(Methane oxidation)} \\
AOM &= R_{CH_4} \times CH_4 \times SO_4 && \text{(Anaerobic oxidation of methane)}
\end{aligned} \tag{3.6}$$

where R_{nit} is the rate of Nitrification (d^{-1}), R_{FeOH_3} , R_{H_2S} , R_{CH_4} are the rate of oxidation of Iron, sulfide and methane via oxygen respectively ($mmol^{-1} m^3 d^{-1}$). Because sulfide precipitation can occur in some coastal sediments, we accounted for this sink process by removing produced sulfide from sulfate reduction as a first order FeS formation.

$$FeSprod = R_{FeSprod} \times Fe \times H_2S \quad \text{(FeS production)} \tag{3.7}$$

with $R_{FeSprod}$ the rate of production of FeS ($mmol^{-1} m^3 d^{-1}$).

3.2.2.3 Transport processes

Transport processes in the model are described by molecular diffusion and bio-irrigation for dissolved species whereas bioturbation is the main process for mixing the solid phase. In addition, advection occurs in both solid and dissolved species. The model dynamics described as a partial differential equation (PDE) is the general reaction-transport equation (Berner 1980). We use a similar paradigm and formulations to those of (Soetaert et al. 1996a). For substances that are dissolved:

$$\frac{\partial \phi C}{\partial t} = -\frac{\partial}{\partial z} \left[-\phi \times D_{sed} \times \frac{\partial C}{\partial z} + w_{\infty} \times \phi_{\infty} \times C \right] + \sum \phi \times REAC + \phi \times J_{irr} \tag{3.8}$$

With special consideration of ammonium adsorption to sediment which reaction kinetic is linear and accompanied by diffusion and reaction:

$$\frac{\partial \phi C}{\partial t} = -\frac{\partial}{\partial z} \left[-\frac{\phi \times D_{sed}}{(1 + k_{ads})} \times \frac{\partial C}{\partial z} + w_{\infty} \times \phi_{\infty} \times C \right] + \sum \frac{\phi \times REAC}{(1 + k_{ads})} \tag{3.9}$$

where we assumed that the immobilization of NH_4^+ is in instantaneous, local equilibrium (i.e., any changes caused by the slow NH_4^+ removal process results in an immediate adjustment of the NH_4^+ equilibrium; so, it can be modelled with a simple chemical species) and k_{ads} is the adsorption coefficient. The inclusion of this formulation for the diffusion and reaction term has the effect of slowing down ammonium migration in sediment. Derivation of this formulation is given in Berner (1980) and Soetaert and Herman (2009).

For the solid phase:

$$\frac{\partial(1-\phi)S}{\partial t} = -\frac{\partial}{\partial z}[-(1-\phi) \times D_b \times \frac{\partial S}{\partial z} + w_\infty \times (1-\phi)_\infty \times S] + \sum (1-\phi) \times REAC \quad (3.10)$$

where C is the concentration of porewater (unit of $mmol\ m^{-3}liquid$) for Equation 3.8 and S for solid (unit of $mmol\ m^{-3}solid$) Eq. Equation 3.10. w ($cm\ d^{-1}$) and D_{sed} ($cm^2\ d^{-1}$) represent the burial/advection and molecular diffusion coefficient in the sediment respectively and REAC is the source/sink processes linked to biogeochemical reactions in the sediment. This term include both biological and chemical reactions within the sediment column while J_{irr} is act as a non-local bio-irrigation transport term (see next section). D_b is the bioturbation term for solid driven by the activities of benthic organisms. For dynamic simulation, w can change as a function of time but in most cases we assumed a constant value.

Diffusive fluxes of solutes across the sediment-water interface are driven by the concentration gradients between the overlying seawater and the sediment column. Fick's first law is used to describe the solute flux due to molecular diffusion:

$$J_d = -\phi D_{sed} \frac{\partial C}{\partial z} \quad (3.11)$$

where the D_{sed} ($cm\ d^{-1}$) is the effective diffusion coefficient corrected for tortuosity and given as $D_{sed} = \frac{D^{sw}}{\theta^2}$, with D^{sw} the molecular diffusion coefficient of the solute in free solution of sea-water and θ is the tortuosity derived from the formation factor (F) and porosity (ϕ) of a sediment matrix (Berner 1980; Boudreau 1997). This molecular diffusion coefficient is calculated as function of temperature and salinity using compiled relation of (Boudreau 1997), implemented in the R package `Mare1ac` (Soetaert and Petzoldt 2020).

As a simplifying assumption, material accumulation has no effect on porosity. We further assumed the porosity profile decreased with depth but invariant with time. Although, this assumption is restrictive as the site of flood deposition can undergo variation in grain size, which might affect their porosity (Cathalot et al. 2010), we proceed noting that the fixed parameters which define the porosity curve can be changed when necessary. Thus, using optimized parameters fitted with data in the proximal sites of the Rhône prodelta (Ait Ballagh et al. 2021), porosity ($\phi(z)$) in Eq. Equation 3.10 - Equation 3.8 is prescribed as an exponential decay:

$$\phi(z) = \phi_\infty + (\phi_0 - \phi_\infty) e^{-\frac{(z-z_{swi})}{\delta}} \quad (3.12)$$

Where ϕ_0 and ϕ_∞ is the porosity surface and at deeper layer respectively while Z_{swi} is the depth of the SWI and δ (cm) is the porosity coefficient with depth.

3.2.2.4 Bioturbation and Bio-irrigation

Bioturbation in the model is characterized by the movement and mixing of particles by benthic organisms. This is parameterized as a diffusivity function in space ($D(z)$) and acts on the concentrations of the different solid species in the sediment. In our model, this bioturbation flux is assumed to be intraphase, with porosity $\phi(z)$ remaining constant over time. Thus, this process is prescribed as:

$$Db(z) = \begin{cases} D_b^0 & \text{if } Z \leq Z_L \\ D_\infty + (D_b^0 - D_\infty)e^{-\frac{(Z-Z_L)}{biot_{att}}} & \text{if } Z > Z_L \end{cases} \quad (3.13)$$

where D_b^0 is the bio-diffusivity coefficient (cm^2d^{-1}) at the SWI and in the mixed layer, Z_L is the depth of the mixed layer (cm) and $biot_{att}$ is the attenuation coefficient (cm) of bioturbation below the mixed layer. D_∞ is the diffusivity at the deeper layer, usually specified as zero. In the model, we did not account for the mortality of benthic fauna following the deposition as in De Borger et al. (2021a) where they focus on habitat recolonization after trawling.

Bio-irrigation is modelled in an identical manner to that of biodiffusion and acts as a non-local exchange process between the porewater parcels and the overlying bottom water.

$$Irr(z) = \begin{cases} Irr_0 & \text{if } Z \leq Z_L \\ Irr_\infty + (Irr_0 + Irr_\infty)e^{-\frac{(Z-Z_L)}{Irr_{att}}} & \text{if } Z > Z_L \end{cases} \quad (3.14)$$

for which Irr_0 is the bio-irrigation coefficient (d^{-1}) and Irr_{att} is the attenuation of irrigation (cm) below the depth of the irrigated layer Z_{irr} (cm). At depth, the bio-irrigation rate (Irr_∞) is generally set to zero.

3.2.2.5 Model vertical grid

The model is vertically resolved with a grid divided into 100 layers (N) of thickness (Δz) increasing geometrically from 0.01 cm at the sediment-water interface to 6 cm at the lower boundary. The result is a 100 cm model domain comprising a full grid with non-uniform spacing and maximum resolution near the SWI. Depth units are in centimeters. This choice of modelled depth allows for complete carbon degradation. This modelled grid is generated by the grid generation routine of the ReacTran R package (Soetaert and Meysman 2012a) - which implements many grid types used in early diagenesis modelling. During the time instance of the event specification, the added grid of new layers ($N_{pert} \approx Z_{pert}$) unit of sediment and the current grid ($N_{cur} \approx N$) are rescaled to the model's common grid of N layer by linear interpolation (see Section 3.2.2.6 and Fig. S1). The concentration of state variables is defined at the layer midpoints, whereas diffusivities, advection (sinking/burial velocities), and resulting transport fluxes are defined at the layer interfaces.

3.2.2.6 Deposition event

The inclusion of the deposition event as a separate external routine to modify the sediment properties (i.e., porewater species, C_{org}) is a fundamental difference between our approach and the other previous early diagenesis model applied in the Rhone Delta, but it bears similarity to De Borger et al. (2021a). We assume the event occurred as an instantaneous deposition of organic carbon (C_{org}^{fast} and C_{org}^{slow}) over a depositional layer, Z_{pert} (Figure 3.2).

The event calculation was carried out dynamically within the same simulation time. For the solid species, following the flux of organic carbon via the boundary condition (see Section 3.2.2.7), the portion of organic carbon is split between the fast and slow decaying components using a proportionality constant ($pfast$) as in Ait Ballagh et al. (2021). $pfast$ varies from 0 to 1 and it is expressed in percentage of carbon flux deposited associated with either fraction (fast and slow). However, at the time when the event is prescribed, the integrated profile of the solid specie, C_{org}^{fast} and C_{org}^{slow} from the previous time step, defined as t^- , are used to create a virtual composite of the deposited layer. This integral calculation was performed over a specified sediment thickness (Z_{pert}), which corresponded to the vertical extent of the depositional event. This average concentration for the solid, which we define exclusively at the time of deposition as (C_{org}^{flood}) is scaled with an enrichment factor (α see below) and then nudged on top of the old layer, which is supposed to be buried beneath after the event. To avoid numerical issues caused by the discontinuity of both layers with different properties, an interpolation of the composite profile was performed over the modeling domain. This smooths the interface between the deposited layer's base and the current model grid's upper layer. This algorithmic procedure is schematically shown in Figure 3.2, and we summarized this process mathematically as:

$$C_{org}^{flood} \approx \alpha C_{org}^i(t) \Big|_0^{z_{pert}} = \alpha \frac{\int_0^{z_{pert}} C_{org}^i(t^-) dz}{Z_{pert}} \begin{cases} \alpha < 1, & \text{if } TOC_{z_{pert}} < TOC_{old} \\ \alpha > 1, & \text{if } TOC_{z_{pert}} > TOC_{old} \end{cases} ; \quad i = 1(fast), 2(slow) \quad (3.15)$$

where $TOC_{z_{pert}}$ corresponds to the TOC content introduced by the flood layer and TOC_{old} represents the TOC in the previous layer prior to the flood deposition. The carbon enrichment factor (α) denoted as `confac` in the model code is introduced here in order to scale the deposited OC with those observed from field data. This helps in calibrating the deposited organic matter concentration (C_{org}^{fast} and C_{org}^{slow}) in the new layer relative to the previous sediment fraction, simulating the wide range of TOC content observed in the field. For instance, when the newly deposited organic matter is similar to the former sediment topmost layer (average pre-flood layer concentration over an equivalent Z_{pert} depth), an α value of 1:1 is used. If the new material is lower in organic carbon content compared to what is near the sediment-water interface, then $\alpha < 1$, while if the newly deposited material is higher in carbon content than the sediment surface, $\alpha > 1$. This flexibility can be used to constrain the simulation to match the corresponding TOC profile from field observation. In the modelling application, this parameter is generally specified by using different values for the magnitude of OC in each fraction depending on the empirical observation of the TOC data. This quantity is therefore tunable, and the upper bound of this parameter is dictated by the maximum TOC in the sediment sample.

It is important to note that this parameter differs from $pfast$. This OC flux partitioning by $pfast$ occurs regardless of the event and is related to the carbon flux received at the boundary, but the carbon enrichment factor occurs only during the event. The carbon enrichment factor (α) can be viewed as a method of imposing a new initial condition only at the time of the event by using the integral concentration from the previous time. However, using the approach described here, all calculations can be done dynamically without stopping the model.

For the solutes species (O_2 , NO_3^- , NH_4^+ , DIC , SO_4^{2-} , H_2S , CH_4), the bottom water concentration is mainly imposed through the perturbed layer at the time of the event by assuming this new layer is homogeneously mixed.

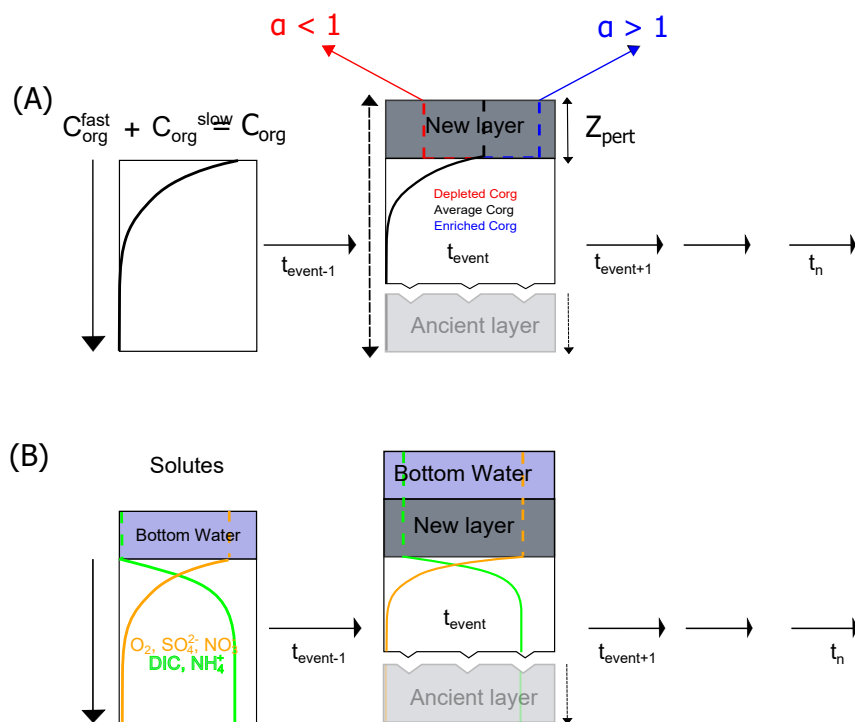


Figure 3.2: Schematic of model implementation for the deposition event scenario. Profile from previous time step (left) and after addition of new layer over a predefined depth layer (right). For the solid (A), the new layer can be enriched (blue) or depleted (red) relative to the old (average) (black). The dissolved substance (B) are set equal to the bottom water concentration during the deposition. Thereafter, the profile is integrated forward with time. The whole sequence of step occurs dynamically with time capitalizing on the integrator ability to simulate dynamic event process. α is the carbon enrichment factor applied over depth Z_{pert} (see text for details).

3.2.2.7 Boundary Conditions

The boundary conditions for the model are of three type:

- At the sediment-water interface, a Dirichlet concentration condition for most solutes equaling the bottom water concentration was used.

$$C|_{z=0} = C_{bw} \quad (3.16)$$

- Both pore water and solid have a zero-flux boundary condition at the bottom of the model:

$$\left. \frac{dC}{dz} \right|_{z=z_\infty} = 0 \quad (3.17)$$

- For solid, an imposed flux at the upper boundary for most of the year is used:

$$flux_{org}|_{z=0} = -(1 - \phi_0)Db_0 \left. \frac{dC}{dz} \right|_{z=0} + (1 - \phi_\infty)w_\infty C \Big|_{z=0} \quad (3.18)$$

The model also includes the ability to include time-varying organic carbon flux with a user-specific time-series or a functional representation such as a sinusoidal pattern. In the latter case, this carbon flux varies over the annual carbon flux (\overline{flux}_{org}) in the region in question. This was expressed mathematically as:

$$flux_{org}(t)|_{z=0} = \left[\overline{flux}_{org} \times \left(1 + \sin\left(\frac{2 \cdot \pi \cdot t}{365}\right) \right) \right] \quad (3.19)$$

At the time of the instantaneous deposition, this deposited carbon is treated as described in Section 3.2.2.6.

3.2.2.8 Model parameterization and verification

The model parameters in Table 3.3 (for full model parameters see Table S1 in supplementary) were derived from previously published models in the Rhône Delta (Pastor et al. 2011a; Ait Ballagh et al. 2021). The organic matter stoichiometry for both fractions is represented here by the NC ratio (NCrFdet and NCrSdet) with values of 0.14 and 0.1 respectively. The flux of carbon in the upper boundary of the model was defined using a yearly mean flux (\overline{flux}_{org}) of $150 \text{ mmol m}^{-2} \text{ d}^{-1}$ in Rhône prodelta (Pastor et al. 2011a). TOC (in % dw) is estimated from both carbon fractions (C_{org}^{fast} and C_{org}^{slow}) assuming a sediment density (ρ) of 2.5 g cm^{-3} and conversion from the model unit for detrital carbon fraction of mmol m^{-3} to unit percent mass. The model diagnostic TOC value is then computed as follows:

$$TOC = (C_{org}^{fast} + C_{org}^{slow}) \times 1200 \times \frac{10^{-9}}{2.5} + TOC_{ref} \quad (3.20)$$

with TOC_{ref} the asymptotic TOC value at the deeper layer of the sediment, thus representing the concentration of refractory carbon not explicitly modelled. The sedimentation rate used in this modelling study was kept constant at 0.027 cm d^{-1} (Pastor et al. 2011a). The decay rate constants for the labile and semi-labile detritus matter are set as 0.1 and 0.0031 d^{-1} respectively with both fractions split equally with a proportionality constant (p_{fast}) of 0.5. Using parameters fitted by the model of Ballagh et al. (2020) to data observed in

the Rhône prodelta area, the rate of bioturbation and bio-irrigation is fixed as $0.01 \text{ cm}^2 \text{ d}^{-1}$ and 0.23 d^{-1} with these fauna-induced activities occurring down to a depth of 5 and 7 cm respectively.

Table 3.3: Core parameters used in the model.

Model parameters	Model notation	Values	Units	Description	References
\overline{flux}_{org}	CFlux	150	$mmol \text{ m}^{-2} \text{ d}^{-1}$	total organic C deposition	Pastor et al. (2011a)
pfast	pFast	0.5	-	part FDET in carbon flux	Pastor et al. (2011a)
$\overline{flux}_{Fe(OH)_3}$	FeOH3flux	0.01	$mmol \text{ m}^{-2} \text{ d}^{-1}$	deposition rate of FeOH3	Assumed
rFast	rFast	0.1	d^{-1}	decay rate FDET	Ait Ballagh et al. (2021)
rSlow	rSlow	0.0031	d^{-1}	decay rate SDET	Ait Ballagh et al. (2021)
NCrFdet	NCrFdet	0.14	$molN/molC$	NC ratio FDET	Pastor et al. (2011a)
NCrSdet	NCrSdet	0.1	$molN/molC$	NC ratio SDET	Pastor et al. (2011a)
$O_{2_{bw}}$	O2bw	197	$mmol \text{ m}^{-3}$	upper boundary O_2	Ait Ballagh et al. (2021)
$NO_{3_{bw}}$	NO3bw	0.0	$mmol \text{ m}^{-3}$	upper boundary $NO_{3_{bw}}$	Ait Ballagh et al. (2021)
$NH_{3_{bw}}$	NH3bw	0.0	$mmol \text{ m}^{-3}$	upper boundary NH_3	Ait Ballagh et al. (2021)
$CH_{4_{bw}}$	CH4bw	0.0	$mmol \text{ m}^{-3}$	upper boundary CH_4	Rassmann et al. (2016)
DIC	DICbw	2360	$mmol \text{ m}^{-3}$	upper boundary DIC	Pastor et al. (2018)
Fe^{2+}_{bw}	Febw	0.0	$mmol \text{ m}^{-3}$	upper boundary Fe^{2+}	Pastor et al. (2018)
H_2S_{bw}	H2Sbw	0.0	$mmol \text{ m}^{-3}$	upper boundary H_2S	Pastor et al. (2018)
$SO_{4_{bw}}^{2-}$	SO4bw	30246	$mmol \text{ m}^{-3}$	upper boundary SO_4^{2-}	Pastor et al. (2018)
w	w	0.027	$cm \text{ d}^{-1}$	advection rate	Pastor et al. (2011a)
D_0	biot	0.01	$cm^2 \text{ d}^{-1}$	bioturbation coefficient	Ait Ballagh et al. (2021)
Z_L	biotdepth	0.01	cm	depth of mixed layer	Ait Ballagh et al. (2021)

$biot_{att}$	biotatt	1.0	cm	attenuation coef below biotdepth	Ait Ballagh et al. (2021)
Irr_0	irr	0.2	d^{-1}	bio-irrigation rate	Ait Ballagh et al. (2021)
Z_{irr}	irrdepth	7	cm	depth of irrigated layer	Ait Ballagh et al. (2021)
temp	temperature	16	°C	temperature	Ait Ballagh et al. (2021)
sal	salinity	38	psu	salinity	Ait Ballagh et al. (2021)
TOC_{ref}	TOC0	1.1	%	refractory carbon conc	Pastor et al. (2018)
ϕ_0	por0	0.8	•	surface porosity	Ait Ballagh et al. (2021)
ϕ_∞	pordeep	0.6	•	deep porosity	Ait Ballagh et al. (2021)
δ	porcoeff	2	cm	porosity decay coefficient	Ait Ballagh et al. (2021)
k_{ads}	Kads	1.3	•	adsorption coefficient	Soetaert et al. (1996a)

The bottom water temperature was fixed at 20°C. The bottom water salinity is nearly constant below the Rhône River plume, ranging from 37.8 to 38.2. In the model, the average temperature and salinity are used to calculate the diffusion coefficient for the solute chemical species (Section 3.2.2.3). Bottom water solute concentrations were constrained using previously reported values in previous modelling efforts (Ait Ballagh et al. 2021) and adapted with new data for the time corresponding to the flood deposit event (see Section 3.2.2.6). Porosity decreases exponentially with depth, from 0.9 at the sediment water interface to 0.5 at the deeper layer with a decay coefficient of 0.3 cm (Lansard et al. 2009a).

For the verification of the model output, data from (Pastor et al. 2018) corresponding to the diagenetic situation 26 days after an organic-rich flood were used. We restricted our benchmark to data from the proximal station (Station A) near the river mouth, where the impact of this flood discharge is more visible (Figure 3.1).

3.2.2.9 Numerical Integration, Application & Implementation

Because the procedure is based on OMEXDIA, complete details of the derivation can be found in that paper and are referenced therein (Soetaert et al. 1996a). Here we recap the mathematical formulation of the method-of-lines (MOL) algorithm used by FESDIA. Direct differencing of Equation 3.8 - Equation 3.10 results to:

$$\begin{aligned}
\frac{\partial C_i}{\partial t} = & \frac{\Phi_{i,i+1} D_{\Phi_{i,i+1}} (C_{i+1} - C_i)}{\Phi_i \Delta z_{i,i+1} \Delta z_i} - \\
& w_\infty \Phi_\infty \frac{\lambda_{i,i+1} C_i + (1 - \lambda_{i,i+1}) C_{i+1}}{\Phi_i \Delta z_i} - \\
& \frac{\Phi_{i-1,i} D_{\Phi_{i-1,i}} (C_i - C_{i-1})}{\Phi_i \Delta z_{i-1,i} \Delta z_i} + \\
& w_\infty \Phi_\infty \frac{\lambda_{i-1,i} C_{i-1} + (1 - \lambda_{i-1,i}) C_i}{\Phi_i \Delta z_i} + REAC_i + J_{irr}
\end{aligned} \tag{3.21}$$

for a generic tracer C with a phase properties index Φ and D_Φ denoting porosity and dispersive mixing term respectively for solid or liquid. This equation is calculated such that the variables and parameters are defined both at the centre of each layer z_i and at the interface between layers $z_{i-1,i}, z_{i,i+1}$. The position at the centre of the grid is then given as $z_i = \frac{z_{i-1,i} + z_{i+1,i}}{2}$. Δz_i represents the thickness of the i -layer and $\Delta z_{i,i+1}$ is the distance between two consecutive grid layers. A Fiadeiro scheme (Fiadeiro and Veronis 1977) based on the model's Peclet number (a dimensionless ratio expressing the relative importance of advective over dispersive processes) is used to set $\lambda_{i,i+1}$, thus providing a weighted difference of the transport terms which reduces numerical dispersion.

Equations Equation 3.8 - Equation 3.10 implemented as Eq. Equation 3.21) are integrated in time using an implicit solver, called Isodes, that is part of the ODEPACK solvers (Hindmarsh 1983). This solver uses a backward differentiation method (BDF), has an adaptive time step, and is designed for solving systems of ordinary differential equations where the Jacobian matrix has an arbitrary sparse structure. The model output time and its timestep (dt) are set by the user and are generally problem specific. Because of the aforementioned challenge in observability of the massive flood event deposition, daily resolution is most often used for dt . However, there is the possibility of obtaining higher resolution by decreasing dt .

The model application starts by estimating the steady-state condition of the model using the high-level command `FESDIAperturb()`. This steady-state condition is calculated using iterative Newton-Raphson method (Press et al. 1992) and is then used as a starting point for a dynamic simulation, with perturbation times as in `perturbTimes` and depth of perturbation given as `perturbDepth` in the model function call. As the event can be given as a deposit and mixing process, further specification of the perturbation type (`deposit` and `mix`) is provided as an argument to the simulation routine. In our case, we used only the deposit mode. The event algorithm is used at the stated time point to estimate the model pore-water and solid properties driven by the instantaneous change in the boundary condition. The concentrations are successively updated by their diagenetic contributions during this time step. Afterward, this modified profile is integrated forward in time. The model is written in Fortran for speed and integrated using the R programming language (R Core Team 2021) via the method-of-lines approach (Boudreau 1996). In addition, the model made use of the event-handling capabilities specific numerical solvers written in the R `deSolve` package (Soetaert et al. 2010b). The R programming language is used in the preprocessing routine for model grid generation (Soetaert and Meysman (2012b)), porewater chemistry parameter (Soetaert et al. (2010a)), steady state calculation (Soetaert (2014)), and time integration (Soetaert et al. (2010b)). Further information about the model usage can be found in the model user vignette found on the code development page (R-forge).

3.2.2.10 Quantification of sediment diagenetic relaxation timescale

3.2.2.10.1 Quasi-relaxation timescale

Given the strong non-linearity and coupled nature of the biogeochemical system in question, we used an approximate approach to define the timescale of relaxation. Recognizing that in a nonlinear system, a perturbed trajectory is frequently arbitrarily divided into a fast, transient phase and a slow, asymptotic stage that closes in on the attractor (i.e., steady state concentration; Kittel et al. (2017)), we proceeded to estimate the relaxation timescale by using the time for which the memory of the perturbed signature disappears. We estimate the relaxation timescale by first calculating the absolute difference ($\varphi(t)$) between successive model outputs after the event, assuming that a slowly evolving state will eventually converge to the pre-perturbed state as time after the disturbance approaches infinity. This point-by-point concentration difference between two successive discretized profiles is then terminated at the point where the sum of absolute differences at each time point is less than the threshold ($\varphi_{threshold}$) (i.e., given by the median over the entire time duration). The relaxation time, τ for each porewater profile species is then defined as the first time this threshold is crossed. Similar technique was employed by (Rabouille and Gaillard 1990).

$$\varphi(t) = \frac{1}{N} \sum_{i=1}^N \|X_{t+1}^i - X_t^i\|$$

$$\text{In the limit of time } (t): \tag{3.22}$$

$$\tau(t) \Rightarrow \varphi(t) \leq \varphi(t)_{threshold}$$

$$\text{where } \varphi(t)_{threshold} = \overline{\varphi(t)} \approx \text{seasonal background}$$

where N is the total number of grid points (i) used to discretize the depth profile (X_t) and X_{t+1} is the depth profile at $t + 1$ after the event.

This relaxation timescale calculation based on the disappearance of the perturbed signal (via successive profile similarity) may differ from an approach in which the profile returns to a pre-defined “old profile”. Because the exactness of pre-flood and post-flood profiles is difficult to quantify numerically (Wheatcroft 1990), and the return to the former is frequently driven by slow dynamics, the approach used here can provide a window of estimate for which a particular signal fades toward the background of a theoretically pre-perturbed signal.

3.2.2.10.2 Uncertainty in relaxation timescale estimate

The uncertainty introduced by this technique is quantified using a non-parametric bootstrap of the τ statistics. The objective of bootstrapping is to estimate a parameter based on the data, such as a mean, median, or any scalar or vector statistic but with less restrictive assumptions about the form of the distribution that the observed data came from (Efron 1992).

In this case, we employ a modified bootstrapping technique to estimate the uncertainty in the relaxation timescale by resampling on the cutoff point introduced in Equation 3.22 (i.e., median, $\overline{\varphi}$ of a given reference simulation). This calculation takes advantage of the fact that the timeseries will be dominated by the slowly varying seasonal cycle over a long time period away from the point of perturbation, with the influence of the perturbation fading to the background. The variation of this reference time series over time reflects the uncertainty in this median threshold point. This variance, along with the reference cutoff value, can be used to generate n random perturbations varying about the normative threshold value. We can proceed to

create a histogram of the replicate threshold(s) distribution. The histogram of this distribution is depicted schematically in the left margin of Figure 3.3). The relaxation time in each realization of the threshold is calculated ($\hat{\tau}_i$). The median absolute deviation from this ensemble of relaxation times is then used to calculate the level of uncertainty in the statistics of interest (timescale of relaxation - $\hat{\sigma}_\tau$). Figure 3.3 depicts this concept schematically. It should be noted that this method eliminates the need to rerun the deterministic model for each, reducing the computational burden of this technique.

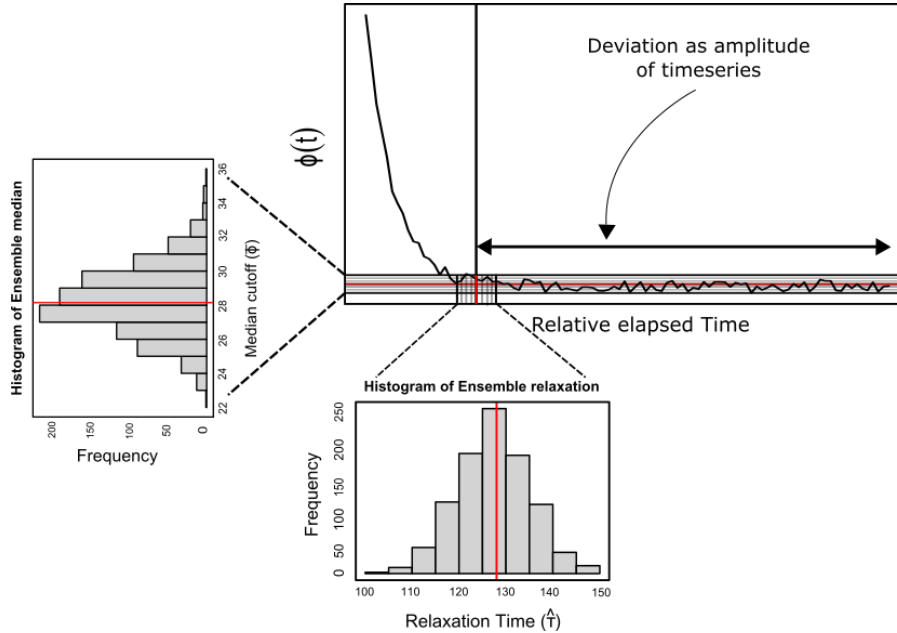


Figure 3.3: The bootstrapping technique used to calculate the uncertainty in the relaxation timescale. The resampled median about a reference provides a replicate over which the standard error estimate is defined. The solid red represents the expected value of the quantity estimated while the vertical red line is the deviation from this expected value.

The 95 % confidence intervals ($\hat{\sigma}_{\tau(level/2)}$ and $\hat{\sigma}_{\tau(1-level/2)}$) are reported in this paper by calculating the quantiles of this empirical distribution of $\hat{\sigma}_\tau$.

3.2.2.11 Model simulation

The model is initialized as explained in Section 3.2.2.9. Thereafter, for the dynamic simulation, the model is spin-up for a sufficiently long-time to attain dynamic equilibrium (≥ 5 years). A 2-yr run is carried out for the respective model application. The timestep (dt) for dynamic simulation is daily in order to match the frequency at which observation of field data is possible. For specific numerical experiment, model configuration required for the simulation will be detailed in Section 3.2.2.11.1.

3.2.2.11.1 End-member type numerical experiment

For the numerical model experiment, we investigate the sediment's response to two end member types of deposition that can represent actual field observations in the Rhône prodelta (Pastor et al. 2018).

- **Low OC content with high sediment thickness scenario (EM1):** In this scenario, we assume that a 30 cm new layer of degraded sediment was deposited. This scenario can describe old terrestrial material and is similar to the extreme case of flood event of May/June 2008 in the proximal outlet of Rhône River where lateral transfer of low TOC sediment (around 1%) was deposited on top of the previously deposited sediment (OC around 1.5-3%) (Cathalot et al. 2010). Using the partitioning of the carbon as explained in

Section 3.2.2.6, An α value of 0.5 and 0.7 for C_{org}^{fast} and C_{org}^{slow} respectively was used to scale the TOC profile in order to mimic this type of trend.

- **High OC with low sediment thickness scenario (EM2):** For this, we assumed a moderate 10 cm deposition of a new layer enriched in carbon during a flood discharge event. This scenario can correspond to the end-member case of November 2008 flood type with high TOC around 2.5%, reaching more than 6% in some sediment cores from the prodelta (Pastor et al. 2018), (most likely composed of freshwater phytoplankton detritus, debris and freshly dead organisms) overlain on a less labile layer. In order to simulate this type of pattern, an α value of 20 and 10 for C_{org}^{fast} and C_{org}^{slow} respectively was used to adjust the TOC profile to such high deposit OC scenario.

Except for the α and the thickness of the flood deposit, all other parameters were held constant in all numerical experiments. The time of the event occurrence in both scenarios was initialized at the period corresponding to the published date for May and November 2008 flood deposition as reported in (Pastor et al. 2018). This helps to provide some realism to this hypothetical case study as well as appropriate context for the environmental regime when these events occur.

3.2.2.11.2 Sensitivity analysis

Lastly, we conducted a sensitivity analysis of the relaxation timescale for oxygen, sulfate, and DIC concentrations in terms of their variation with the thickness of the new sediment layer as well as the quantity of organic carbon introduced by the deposition.

We assumed a 15 cm average deposit thickness and conducted simulations with a thickness scale of 1 cm to 30 cm. A 5 cm increment was used for the sensitivity analysis. The α value is calculated in the same way: assuming a 1:1 ratio in the fast and slow OC fractions, and because deposited sediment can be highly refractory in nature, we geometrically conducted simulations with values ranging from 0.3 to 35. This was done only by changing the α corresponding to C_{org}^{fast} with the slow fraction fixed at 1. We also made sure that both series are equilateral in length, and that the values were chosen to span the range of values in EM1 and EM2, thus bracketing the normative value for the end-member case. This range encompasses the large spectrum of flood deposits such as those experienced in the Saguenay Fjord, Canada (Mucci and Edenborn 1992 - landslide event; Deflandre et al. 2002), the Rhône prodelta, France (Pastor et al. 2018), and in the Po River, Italy (Tesi et al. 2012).

3.3 Results

3.3.1 Qualitative model performance: Cevenol flood in the Rhône prodelta

In order to compare the model evolution to field data, we made a comparison between the simulated profiles 26 days after a flood layer deposition and data collected in the Rhône prodelta in December 2008 (observed data collected 26 days after a cevenol flood). During this flooding period, riverine discharge delivered 0.4×10^6 t of sediment which amounted to approximately 10 cm of sediment deposited in the site A of depocenter (Figure 3.4).

The general pattern of the simulated profile agrees well with the observed data (Figure 3.4). The newly introduced organic carbon-rich sediment resulted in rapid oxygen consumption. The data for Total organic carbon (TOC) shown in Figure 3.4 suggests a good agreement with the model, with high TOC (2.5wt% - 2.0 wt%) de-

posited at the upper 10 cm. 26 days after the flood, the oxygen concentration dropped from $250 \mu M$ at the new sediment interface to nearly zero at 0.2 cm depth, and oxygen may have already returned to pre-flood levels; the simulated porewater profile was within the data's range (Figure 3.4). The model diffusive flux of oxygen at this period was $18 \text{ mmol m}^{-2} \text{ d}^{-1}$ while the measured DOU flux was $16.6 \pm 2.9 \text{ mmol m}^{-2} \text{ d}^{-1}$.

Table 3.4: Short term response and flux of Oxygen penetration depth (OPD), O_2 , SO_4^{2-} and DIC for end-member scenario experiment. Time one day before the event is denoted by -1 and Time 1 – 26 is the elapsed time, in days after the perturbation. Positive fluxes are directed IN the sediment while negative fluxes are directed OUT from the sediment to the overlying water.

Time (days)	OPD (cm)	O_2 flux ($\text{mmol } O_2 \text{ m}^{-2} \text{ d}^{-1}$)	SO_4^{2-} flux ($\text{mmol } SO_4^{2-} \text{ m}^{-2} \text{ d}^{-1}$)	DIC flux ($\text{mmol DIC m}^{-2} \text{ d}^{-1}$)
Observation -				
Model				
Measured	0.6 ± 0.03	16.6 ± 2.9	-	-
Simulated	0.2	18	142	-203

Overall, the model-Data trend was satisfactory, with observed depth distribution of sulfate (SO_4^{2-}) 26 days after the flood event fitted well, without much parameter fine-tuning. Only the advection rate of the sediment was changed from 0.027 to 0.06 cm d^{-1} in order to match the observed distribution at depth. Sulfate reduction was high in the new layer. However, below the flood layer, the SO_4^{2-} concentration in the data seems to asymptote to a value of 10 mM at 25 cm, while the model simulates complete sulfate depletion below 20 cm (Figure 3.4).

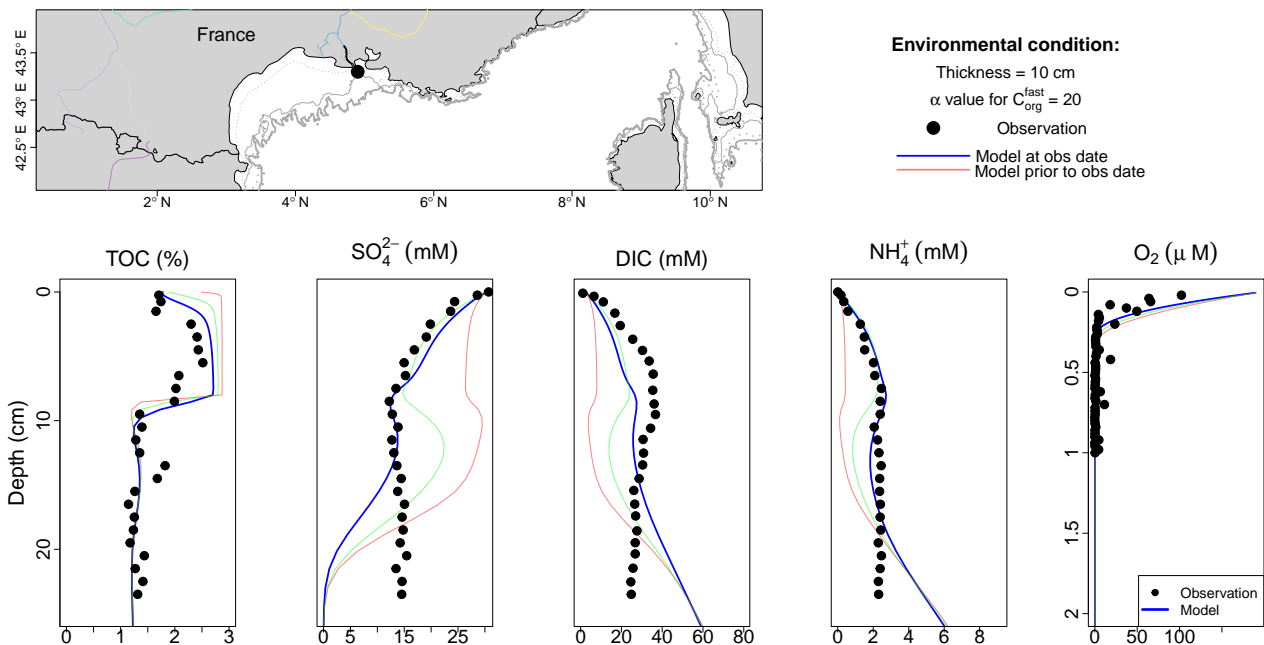


Figure 3.4: Model and observation depth profile of TOC (%), SO_4^{2-} , DIC, NH_4^+ and O_2 for November/December Event in Station A (Rhône Prodelta). Model results are at 26 days after flood event in blue line. Data collected in December 8, 2008 showed in black circle. The red lines represent the evolution of the model from the deposition (day - 0 and 10).

The DIC profile shows a similar trend to the data collected after the flash flood. Within the depth interval of the data, the model tends to follow the data. It drifts at lower depths, on the other hand, by overestimating the

concentration of DIC observed at deeper layers. Similarly, the modeled NH_4^+ shows a gradual increase with depth, and the model overestimates the production of NH_4^+ below 15 cm (Figure 3.4).

3.3.2 Numerical experiment on end-member scenarios

3.3.2.1 Low carbon, High Thickness scenario (EM1)

With a test case of 30 cm of new material deposited during the event (EM1) in the spring, the sediment changes as follows: Prior to the event, the oxygen penetration depth (OPD) was about 0.17 cm. The OPD increases to 1.17 cm after the deposition of these low OC materials. The model showed a gradual return to its previous profile within days, with the OPD shoaling linearly with time (Table 3.4). By day 5, oxygen had returned to the pre-flood profile with similar gradient to the pre-flood state.

Against a background OM flux following the introduction of the flood layer, the sediment responded quickly. As a result, the perturbation has a significant effect on sulfate penetration depth, with concentration remaining nearly constant within the perturbed depth (≈ 20 cm). This corresponds to the bottom water concentration (30 mM) trapped within the flood deposit. Within that layer, sulfate reduction rate was low with an estimated integrated rate of $2.14 \text{ mmol C m}^{-2} \text{ d}^{-1}$ from the surface to 30 cm.

Below the interface with the newly deposited layer, the sediment is enriched in OM whose mineralization results in a higher sulfate reduction rate (SRR) at the boundary that delineates the newly deposited layer and the former sediment-water interface. The simulated SRR falls from $437 \text{ mmol C m}^{-3} \text{ solid d}^{-1}$ at the former sediment-water interface (now re-located at 26 cm) to $24 \text{ mmol C m}^{-3} \text{ solid d}^{-1}$. This high interior sulfate consumption at the boundary correlates well with the higher proportion of reactive organic material buried by the new layer containing less reactive material. From day 10, the consumption of this OM stock by sulfate controls the shape of the profile (Figure 3.5). This anoxic mineralization via sulfate reduction will continue until the entire stock of carbon is depleted 50 days after deposition. Following that, OM mineralization via sulfate reduction shifts; becomes more intense at the top layer by day 60 (two months after the event), then it begins to gradually evolve to the typical depth decreasing sulfate profile. By day 115 (~ 4 months), the profile had almost completely returned to its pre-flood state. We estimate that it took approximately 4 months for sulfate to relax back to within the range of background variability (with lower and upper bootstrap estimate between 92 - 139 d).

Correspondingly, OC mineralization products (such as DIC) were significantly lower in the newly deposited layer as a consequence of the reduced quantity of OC brought by the flood. This concentration increased with depth to about 80 mM. Starting from the deposition, higher production of DIC below the former SWI led to a distinct boundary in the sediment: a DIC depleted layer above an increasing DIC layer with concentrations up to 75 mM trapped in the region below the new-old sediment horizon 20 days after deposition (Figure 3.6). This increased DIC production continued despite complete exhaustion of the buried labile carbon fraction, with mineralization driven by the slow decaying component. The depth gradient caused by the increased DIC production enhances diffusive DIC flux. Following that initial period, DIC began to revert to its previous state. This slow re-organization, mostly driven by diffusion continues, with an estimated recovery time of 5 months (with a 95 % bootstrap confidence interval of 137 - 147 days respectively), as it temporarily lags behind SO_4^{2-} in its return to the previous pre-flood state.

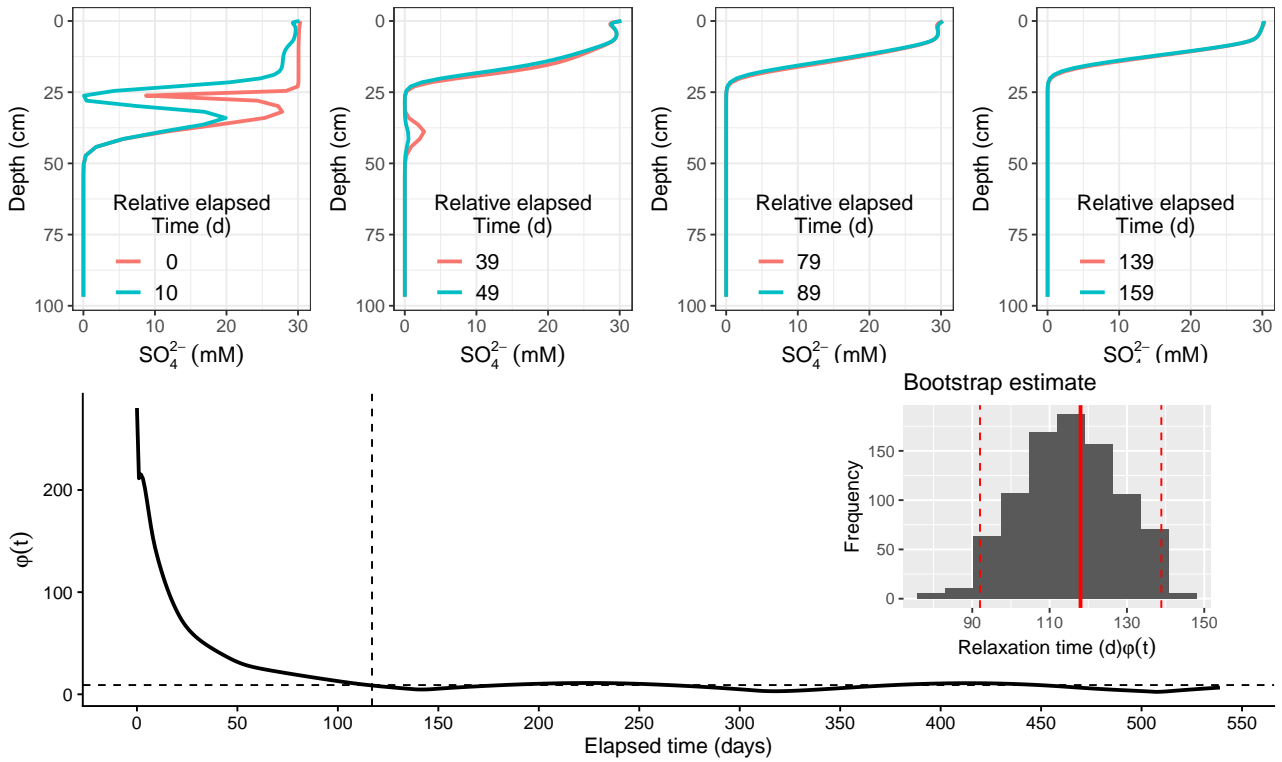


Figure 3.5: Scenario 1 (EM1): Model evolution for sulfate following deposition. Relative deviation of successive profile with time shown below. Dashed vertical line signify cutoff point by the median (Dashed horizontal line). Inset: Histogram of bootstrap estimate of sulfate relaxation timescale for EM1 with 95 % confidence interval.

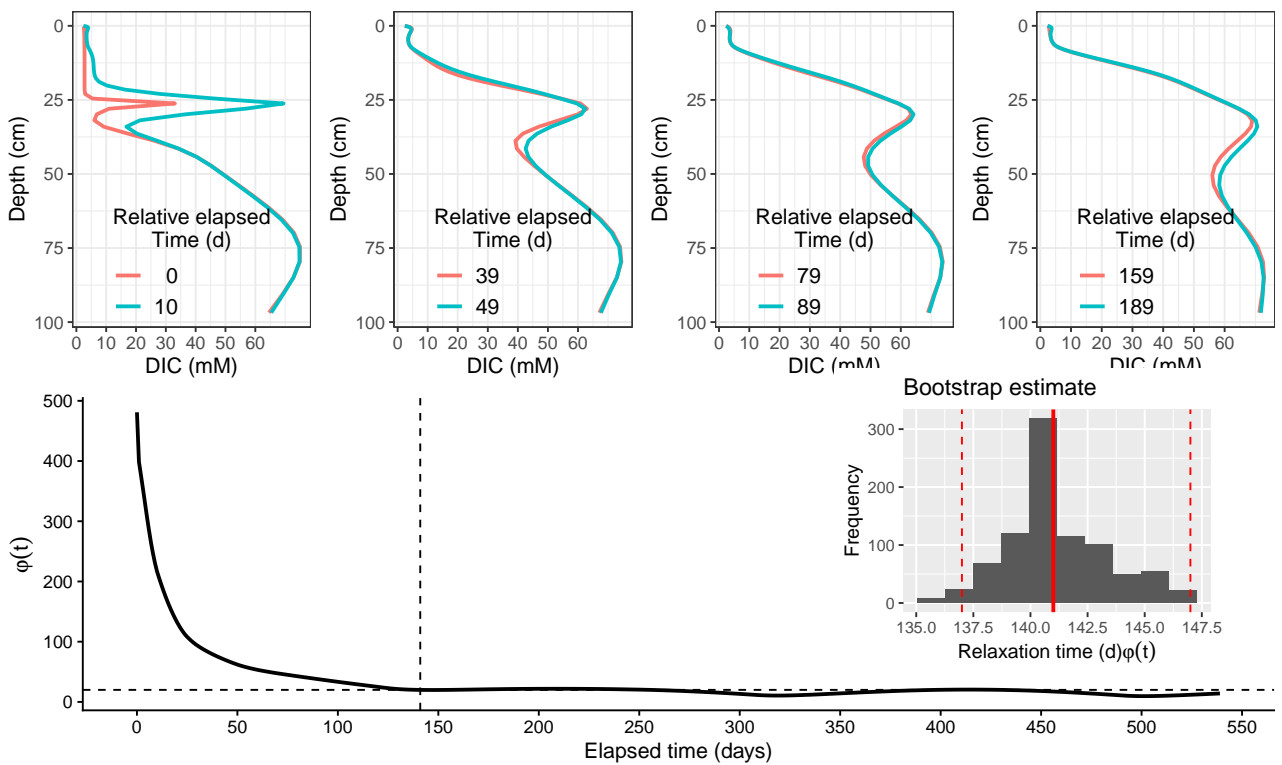


Figure 3.6: Scenario 1 (EM1): Model evolution for DIC following deposition. Relative deviation of successive profile with time shown below. Dashed vertical line signifies cutoff point by the median (Dashed horizontal line). Inset: Histogram of bootstrap estimate of DIC relaxation timescale for EM1 with 95 % confidence interval.

3.3.2.2 High carbon, Low Thickness scenario (EM2)

A flood deposition scenario of 10 cm thick material with enhanced OC content was used for the other end-member case experiment (EM2) in autumn. In this scenario, the modelled sediment exhibits a variety of response characteristics. The newly introduced sediment resulted in rapid oxygen consumption. The OPD decreased to 0.74 cm shortly after the event, according to the model, and stabilized there for days. There was no visible deformation in the shape of oxygen during its recovery trajectory, and total oxygen consumption for organic matter mineralization decreased by 8 % during the first two days after the event, from 12 to 11 $mmol O_2 m^{-2} d^{-1}$.

The SO_4^{2-} concentration that developed as a result of the deposition showed two gradients: a concentration gradient from 30 mM at the “new” sediment water interface to 26 mM in the newly deposited layer (Figure 3.7). Accordingly, the DIC in the corresponding depth layer gradually increased up to 20 mM (Figure 3.8). An intermittent increase in SO_4^{2-} was simulated below the new interface, at the boundary with the “old” sediment-water interface (SWI), reaching up to 29 mM from 9 cm to 12 cm (Fig. Figure 3.7). This layer, which corresponded to the depth horizon where the new layer gradually mixed with the old layer, resulted in less sulfate reduction and DIC production in comparison to the new layer. Porewater SO_4^{2-} concentrations decreased monotonically with depth from this interface, with a corresponding increase in DIC. Within 26 d of the event, the sulfate profile appears to be returning to its original shape. By then, 75 % of the newly introduced fraction of OM had been depleted, with OM remineralization in the upper layer fueled by the small amount of remaining detrital materials. As the temporal memory of the deposition fades, the profile continues to gradually evolve towards the background, fed by the slow decaying OM, up to day 90, when the sulfate profile appears to have reached a similar pre-flood state. In this scenario, the estimated SO_4^{2-} and DIC relaxation timescales were around 3 months (91 d for SO_4^{2-} and 102 d for DIC) (Figure 3.8).

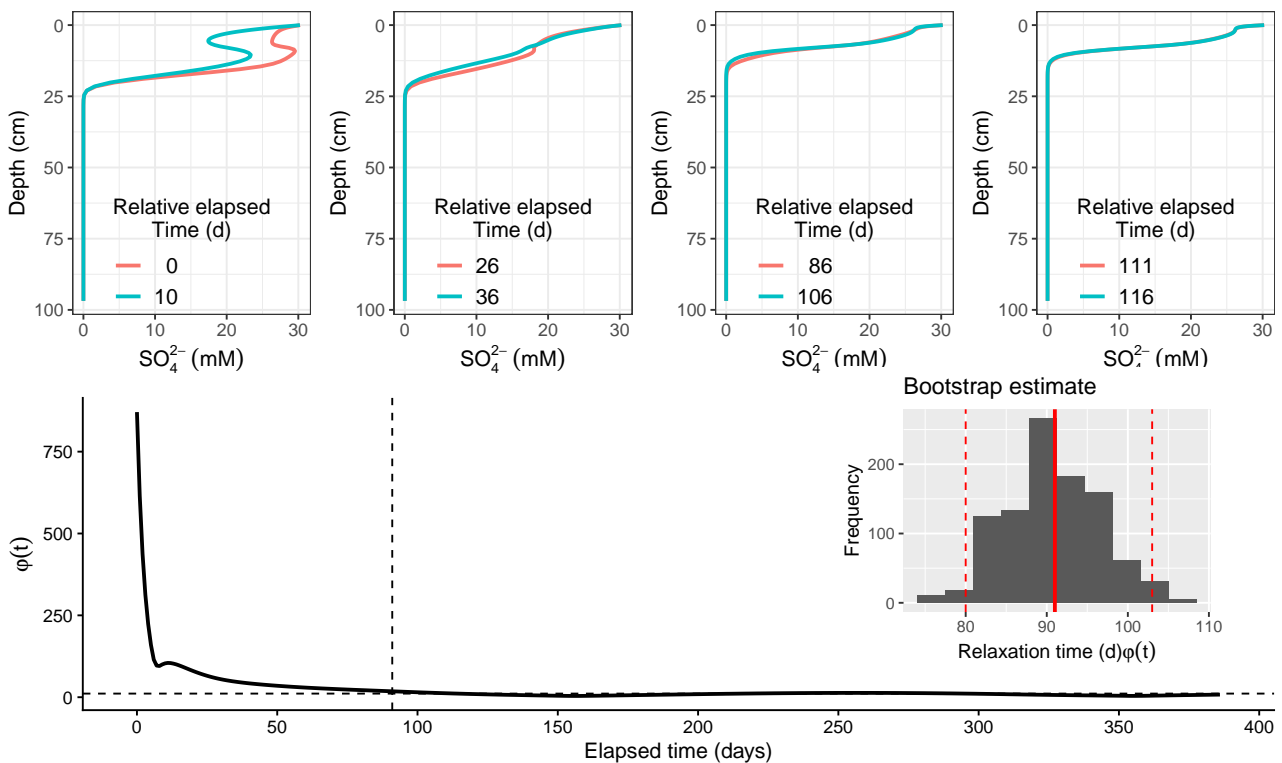


Figure 3.7: Scenario 2 (EM2): Model evolution for sulfate following deposition. Relative deviation of successive profile with time shown below. Dashed vertical line signifies cutoff point by the median (Dashed horizontal line). Inset: Histogram of bootstrap estimate of sulfate relaxation timescale for EM2 with 95 % confidence interval.

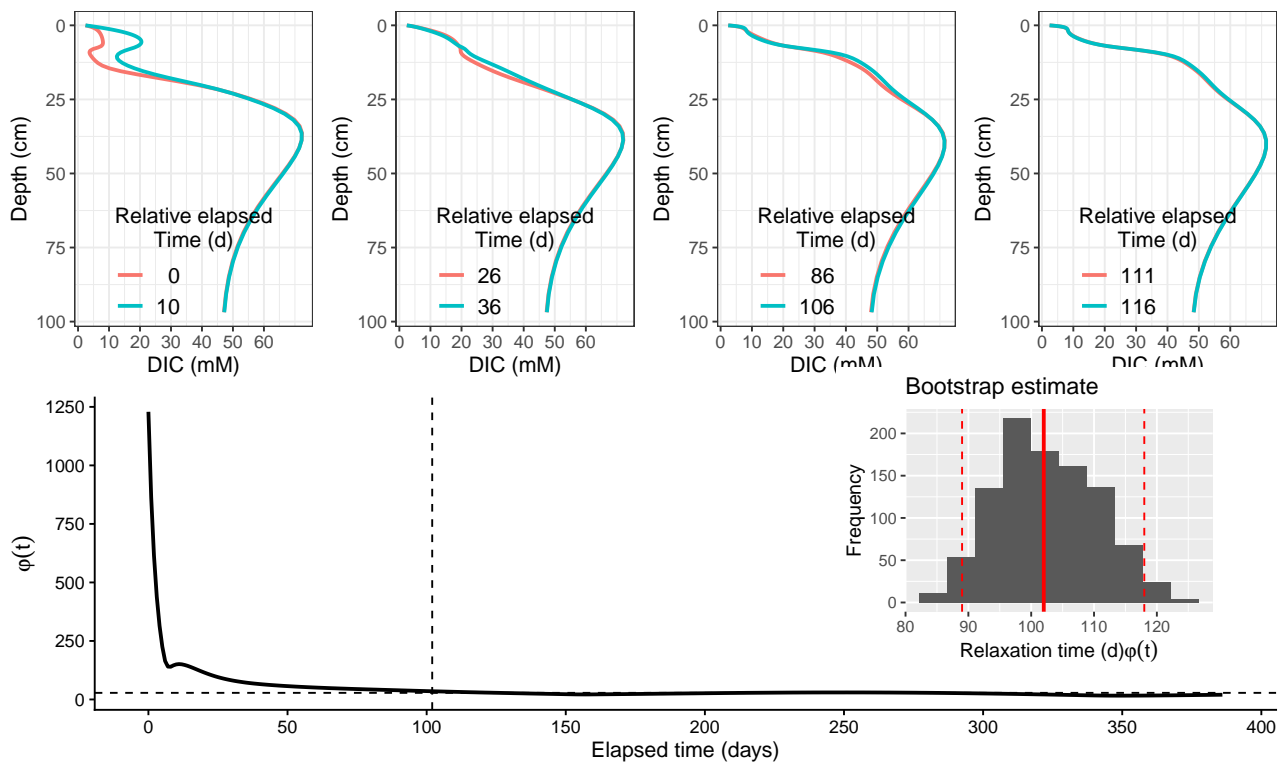


Figure 3.8: Scenario 2 (EM2): Model evolution for DIC following deposition. Relative deviation of successive profile with time shown below. Dashed vertical line signify cutoff point by the median (Dashed horizontal line). Inset: Histogram of bootstrap estimate of DIC relaxation timescale for EM2 with 95 % confidence interval.

3.3.3 Sensitivity of relaxation time to variation in enrichment factor (α) and sediment thickness (Z_{pert})

We then examine the sensitivity analysis of the relaxation timescale (τ) for oxygen, sulfate, and DIC for variation in sediment deposit thickness (Z_{pert}) and the concentration factor for C_{org}^{fast} enrichment (α) covering values ranging between the two EM scenarios.

Over all runs varying the enrichment factor (α) and the thickness of the flood input layer, relaxation time for oxygen varied from 2 d for a flood deposited layer consisting of a thin layer of high concentration of labile OC to 9 d for a thicker deposited layer with low concentration of labile OC. In contrast, the relaxation timescales for SO_4^{2-} and DIC were significantly longer than those for O_2 (3 to 4 months). In addition, the relaxation timescale surface structure for SO_4^{2-} appears complex with divergence gradient at mid-depth of 15 cm. For deposited depth layers above 5 cm and at low α value, the relaxation time for SO_4^{2-} varied between 75 - 100 days (2 - 3 months). Below 5 cm (bioturbated depth imposed in the model), relaxation time was constant across all α variations (100 d). As organic enrichment (α) and thickness increase, the model estimates a longer relaxation time with a maximum time span of 105 d.

Similar variations of relaxation time for DIC were simulated for different α and sediment deposit thicknesses. However, unlike SO_4^{2-} , relaxation time for DIC varies smoothly across the range of α and thickness combinations, with relatively constant relaxation time (100 d) at low thickness and α combinations. The relaxation time increased exponentially as sediment deposit thickness and labile OC concentration increased (α), with maximum recovery time (171 d / 6 months) simulated at the extremes of both combinations (Figure 3.9).

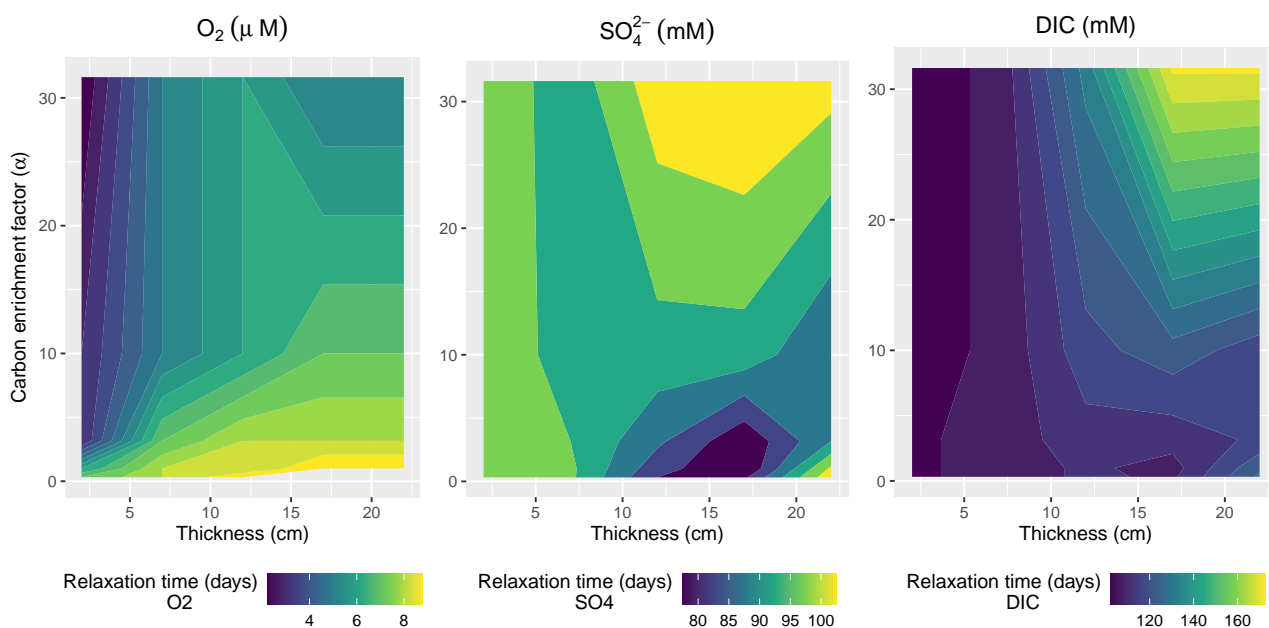


Figure 3.9: Relaxation timescale (τ) in days as function of deposited sediment thickness and enrichment factor (α) for degradable OM.

3.4 Discussion

In highly dynamic coastal ecosystems, such as river-dominated ocean margins (RiOmar systems), driven by seasonal variability and meteorologically extreme events, the response of early diagenetic processes to time-varying deposition of organic matter is generally non-stationary (Tesi et al. 2012). While dynamic equilibrium as a steady state condition may be reasonable in the case of seasonal variability, such an assumption may fail in cases of instantaneously event-driven deposition. An intermittent supply of sediment and OC, like those presented here, can cause a change in the system's properties on a short- or long-term basis. Previous works have highlighted excursions in sediment redox boundary (Katsev et al. 2006), flux of solutes at the sediment-water interface (Rabouille and Gaillard 1990) as well as modification of other system properties due to depositional flux of organic matter. Thus, the premise of steady state conditions in early diagenetic processes, which often depends on the temporal resolution of the observation, might need revisiting especially in areas of episodic sedimentation (Wheatcroft 1990; Tesi et al. 2012). Here, we discuss the evolution and dynamics of a non-stationary sedimentary system following a singular perturbation.

3.4.1 Model representation and utility

Non-steady state models are increasingly being applied in dynamic coastal environments, but they are still primarily based on forcing from smooth varying boundaries that mimic seasonal forcing or long-term variability (Soetaert et al. 1996b; Rabouille et al. 2001b; Zindorf et al. 2021). Explicit consideration of abrupt changes in the upper boundary of the model caused by events such as landslides, flash flooding, turbiditic transfer of materials on a continental slope, and trawling is still relatively uncaptured by these models (but see De Borger et al. (2021a) for inclusion of erosion events). In this paper, we adapt OMEXDIA (Soetaert et al. 1996a), a well-known reaction transport model, to investigate the changes in the solid and liquid phases during massive deposition and mixing event. Our efforts highlight the algorithm's utility in incorporating this process with minimal numerical issues. The model represented the basic characteristics of the data derived from the November/December 2008 flood event at Station A in the Rhône Delta's depocenter (Figure 3.4). The simulated flux

was also in agreement with the estimate from field data, as the diffusive oxygen uptake (DOU) rate sampled 26 d after the event (8th December 2008) was $16.6 \pm 2.9 \text{ mmol m}^{-2} \text{ d}^{-1}$ (Cathalot et al. 2010) while the estimate from the model was $18 \text{ mmol m}^{-2} \text{ d}^{-1}$. As the inclusion of such discontinuity in PDE(s) presents numerical challenges in classic solvers, the implementation utilized by our model ensures such difficulties are overcome. This is the result of improved development of solvers adapted to such problems (Soetaert et al. 2010b). This difference in the approach employed here distinguishes ours from other published models (e.g. Berg et al. (2003), Velde et al. (2018)) with similar scientific motivation for time dependent simulation. Overall, the validation of the model output with field observations lends some confidence in using the model in scenarios involving abrupt changes in boundary conditions and investigating biogeochemical changes in the sediment as a result of such an event. This is despite the model under-estimation of the amplitude of sulfate and DIC at depth which can be improved with better optimization of some parameters, especially those derived from previous studies that might not be suited for such a flooding regime or with better process resolution relating to these pathways. Nonetheless, there are advantages to this model especially in the case of episodic flood deposit event, where only a snapshot of data is available at any given time. Modelling tools capable of simulating this event with high fidelity can provide continuous information of the system state and help fill in data gaps needed to understand the sediment's response on different timescales.

3.4.2 Role of end-member flood input OM in the diagenetic relaxation dynamics

Flooding events can transport large amounts of material through the river to transitional coastal environments such as deltas and estuaries. River floods can account for up to 80% of terrigenous particle inputs (Antonelli et al. 2008; Zebracki et al. 2015), and they can have a significant impact on geomorphology (Meybeck et al. 2007), ecosystem response, and biogeochemical cycles (Group et al. 2011). If the source materials have a different organic matter composition (Dezzeo et al. 2000; Cathalot et al. 2013), the rapid deposition of these flood materials can alter diagenetic reactions and resulting fluxes.

Furthermore, the relaxation timescale associated with the sediment recovery following this external perturbation can be important in terms of the process affecting the biogeochemistry of solid and solute species. With a series of numerical experiments ranging in between two end-members of the input spectrum for flood events such as those in the Rhône prodelta (Pastor et al. 2018), our study revealed contrasting sedimentary responses as well as associated typical time scales at which porewater profiles relax back to undisturbed state. Using a simple metric for estimating relaxation timescale of the perturbation, our calculations for the first end-member scenario (EM1) show that the upper bound of the timescale of relaxation for oxygen is $5 \pm 3 \text{ d}$, whereas it was approximately $2 \pm 2 \text{ d}$ for the second end-member scenario (EM2). This reflects the property of oxygen, which quickly approaches a steady state situation after an event (Aller 1998). This viewpoint is supported by an *ex situ* controlled laboratory setup. In their studies, Chaillou et al. (2007) demonstrated that after gravity levelled sediment was introduced, oxygen consumption quickly recovered to its first-day level, with a sharp response time of 50 minutes and gradual shoaling of OPD within five days. We conclude that the tiny difference in oxygen relaxation and diagenetic response between the two scenarios can be attributed to the slow kinetic degradability of the refractory carbon deposited in the first scenario versus the labile nature of the deposit in the second scenario. This kinetically driven OM degradation has been extensively studied and provides the basis for the reactive continuum in early diagenesis models (Jørgensen and Revsbech 1985; Middelburg 1989; Burdige 1991).

Other terminal electron acceptors (TEAs) such as SO_4^{2-} , relax toward natural variation over a longer timescale

than oxygen. For EM1, our simulation predicts a sulfate relaxation time of 117 days with a 95 % confidence interval (CI) estimate between 92 days (lower CI) and 139 d (upper CI) days) while in the case of EM2, we estimate a sulfate relaxation time of 91 d with comparatively low temporal variability (lower CI - 80 and upper CI - 103 d). This difference in relaxation time is caused by the differences in sediment characteristics and how their mineralization occurs over the sediment layer. In the first scenario, organic-rich sediment is buried by less reactive new material. The buried sulfate fraction is reduced faster than in the new layer above, and controls the short-term recovery. As the buried carbon stock depletes and the physical imprint of the flood deposition fades, the profile begins to revert to its pre-flood shape. The post-flood evolution for the second scenario (EM2), on the other hand, differs in that the OM is consumed in the classical manner, with decreasing sulfate consumption with depth, caused by top-down control of the OM flux that adds OM to the sediment surface.

Such a long-time lapse for the recovery of an element with a complex pathway, such as SO_4^{2-} , has been reported in the literature (Anschutz et al. 2002; Chaillou et al. 2007; Stumm and Morgan 2012). Similarly, estimates from our simulation for each end-member scenario indicate that mineralization products such as DIC have a longer relaxation time. This is especially true for the first scenario as opposed to the second, with evidence of slow convergence at depth within the simulation timescale for the first scenario. We estimate that DIC will recover to its pre-deposition state in 141 d or about 5 months for EM1 and in a comparatively shorter time for EM2 (102 d or about 3 months). This lag in DIC recovery could be attributed to the fact that its post-flood dynamics are governed by the slow decaying detrital material that contributes to the already buried refractory carbon. This long-term quasi-static behaviour of the porewater concentrations despite such dynamic introduction of flood input can be understood by introducing the concept of a “*biogeochemical attractor*” effect - a similar analogy to the Lorenz attractor (Lorenz 1963). This idea derived from the mathematical theory that describes chaos in the real world (Strogatz 2018; Ghil 2019). The existence of a “biogeochemical attractor” may explain why multiple temporal data sets in the Rhône River prodelta show a similar diagenetic signature from spring to summer (Rassmann et al. 2016; Dumoulin et al. 2018). Our timescale analysis estimates that such rapid system restoration is indeed plausible and of the correct order of magnitude, based on the range of uncertainty reported here.

In addition, our calculations show that the timescale of return to the previous “pre-flood” profile is bracketed by the range of recovery due to purely molecular diffusion, putting an upper bound on our estimate. For example, a species such as oxygen with a sediment diffusion coefficient (D_s) of $1.52 \text{ cm}^2 \text{ d}^{-1}$ takes approximately 300 d to be transported solely by diffusion through a 30 cm sediment column and approximately 30 days for a 10 cm sediment column. Similar scaling argument could be made for species such as SO_4^{2-} ($D_s = 0.86 \text{ cm}^2 \text{ d}^{-1}$) with > 500 d to be transported through 30 cm and ≈ 60 d for 10 cm. Because our estimates are less than these values, it suggests that processes other than diffusion (Thickness effect) may contribute to relaxation control. It emphasizes the importance of biogeochemistry (OM kinetic) in modulating the response after the event. Besides that, any long-term recovery timescale is governed by the solid deposited. In comparison to the time scale of relaxation roughly estimated from field data (Cathalot et al. 2010), our estimate shows the right order of magnitude.

The relaxation time may also vary depending on the diagenetic interaction, and the characteristics of the organic matter available for degradation. This difference in characteristics was partially imposed in our study by assuming variations of α value in the new deposit. The empirical observation of sediment characteristics associated with flood input dictates this parametric turning to match the TOC characteristics (Mucci and Edenborn 1992; Deflandre et al. 2002; Bourgeois et al. 2011; Tesi et al. 2012; Pastor et al. 2018). However, more data

from the field and laboratory experiments that resolve the OM composition of flood deposits are required to constrain the choice of this numerical parameter.

3.4.3 Control of relaxation time by sediment deposit properties

With the sensitivity analysis, we further explore the variation of relaxation timescale under variation of the thickness of the layer and enrichment factor of the input material given by α in our model. The model's sensitivity analysis reveals that the thickness and concentration of the reactive fraction of TOC control the relaxation time across a wide range of deposited sediment perturbation characteristics (Figure 3.9).

In terms of the recovery time as a function of the availability of labile OC, our results revealed a contrasting pattern for oxygen and sulfate. Several factors related to how different oxidants react with sediment matrix disturbances can explain these differences:

- With oxygen that has a high molecular diffusion coefficient, variations in relaxation time depend on the levels of labile OC, with thin sediments containing a high level of labile OC showing a shorter recovery time than thicker sediments with a low OC content. This pattern can be attributed to the higher relative importance of oxygen consumption in OM poor sediment relative to OM rich sediment.
- For low thickness deposits, sulfate and DIC relaxation times were more or less constant. However, a longer relaxation time was simulated for larger deposits and higher labile OC. This can be attributed to the increased distance required for solutes to migrate back after the event. This is clearly the case for sediment thicknesses greater than 14 cm. Such two-way dynamics could be explained by the fact that biological reworking and physical mixing within the surface mixing layer (SML) can improve OC degradation by promoting the replenishment of electron acceptors (i.e., oxygen, sulfate, nitrate, and metal oxyhydroxides) (Aller and Aller 1992; Wheatcroft and Drake 2003; Aller 2004); resulting in a shorter recovery time for the porewater profile to reorganize when perturbed above this depth.

This critical depth could also be the distance horizon at which the slow diffusion of the profile when retracting back to its pre-flood profile becomes an important factor in controlling the relaxation timescale. This is especially true for DIC, where the connection is more obvious. It has been proposed that when flood deposits extend beyond the sediment bio-mixing depth, the relaxation time for the constituent species is determined by the concentration gradient between the historic and newly deposited layers (Wheatcroft 1990). In our sensitivity analysis, higher α corresponds to higher C_{org}^{fast} concentrations at depth, resulting in a case of enhanced OC degradation (both at the surface and within the sediment matrix). This depletes electron acceptors such as sulfate, which are required for OM mineralization at this depth. The slow diffusion across the displaced distance, on the other hand, cannot quickly compensate for its demands, which may explain the longer relaxation time. In other words, a higher concentration of OC in a region where all oxidants are nearly consumed results in a profile that takes a relatively longer time to recover to its previous state due to the constraints imposed by oxidant availability. This viewpoint is consistent with previous research from the Rhône prodelta area, where a minimum transport distance of 20 cm is suggested for efficient connection with the SWI; above which several processes are decoupled (Rassmann et al. 2020) as well as other eutrophic systems, where evidence of large accumulations of organic matter in subsurface sediments serves as a constraint on system restoration (Mayer 1994; Pusceddu et al. 2009). Indeed, more observational and experimental studies are needed to better understand these processes.

3.4.4 Model limitations and future development

Because it is based on the well-established OMEXDIA model, FESDIA has several capabilities that make it suitable for a wide range of application domains for non-steady state early diagenetic simulation. However, due to assumptions made during model development, some limitations in model usage must be considered.

- First, we assumed that porosity is time independent. This may not be the case in some coastal systems that receive sediment materials from regions with distributary channels, which contribute particles of varying origin and grain size (Grenz et al. 2003; Cathalot et al. 2010). The composite sediment that is eventually transported to the depocenter by a flood event may differ in porosity and thus vary temporarily depending on when and where the source materials are derived during the flood event. In this case, model estimates of fluxes in dissolved species may be over/underestimated. However, the temporal variation in porosity is typically small, ranging from 0.6 to 0.9 in sediment depocenter sites such as the Rhône prodelta (Cathalot et al. 2010), allowing us to justify our assumption.
- Second, in our examples, we assumed that the burial rate and bioturbation were constant. With the introduction of these flood events, such assumptions may be called into question (Tesi et al. 2012). In addition, benthic animals respond to other perturbation events such as trawling in ways that may warrant explicit description of their recovery, which is linked to bioturbation (Sciberras et al. 2018; De Borger et al. 2021a). While some coastal sediment burial rates have been shown to vary seasonally (Boudreau 1994; Soetaert et al. 1996b), in the proximal zone of the Rhône prodelta, approximately 75% of sediment deposition can occur during the flood (e.g., 30 cm d^{-1}), with the remaining 25% distributed throughout the year at a low range daily constant rate (0.03 cm d^{-1}). The dominance of flood deposition over non-flood sedimentation, as well as the low bioturbation rate observed in the Rhône prodelta (Pastor et al. 2011a), prompted the use of a constant rate in the application shown here. Moreover, we designed the FESDIA model to allow for the use of a temporarily varying rate constant and coefficient for these processes, as well as the possibility of imposing an observational time series in cases where such data exists.
- The current FESDIA version does not include a diffusive boundary layer, which can be important for material exchange between the overlying bottom water and the sediment. This is critical for calculating fluxes of species such as O_2 , where the depth extent of the DBL (diffusive boundary layer) zone is comparable to the depth at which oxygen consumption occurs (Boudreau and Jorgensen 2001). As a result, the current version of FESDIA may overestimate the flux of O_2 . However, because the primary focus of this paper is on the relaxation dynamics of species (SO_4^{2-} and DIC), where the DBL has negligible impact on the relaxation time and overall diagenetic processes (Boudreau and Jorgensen 2001), the simplification presented here is justified. Even for oxygen, the inclusion of DBL which might result in a corresponding change in the concentration at the SWI only has a marginal effect on its relaxation time ($< 2 \text{ d}$ - within the range of uncertainty reported here), so the conclusion drawn in the case-studies discussed here is still valid.

In terms of future development, we hope to improve the model's diagenetic pathways, particularly for the Iron and Sulfur cycles. Furthermore, processes such as calcite formation have been shown to affect DIC profile by 10-15% in the proximal sites of Rhône prodelta (Rassmann et al. 2020), thus might necessitate inclusion in future version of the model. This will enable FESDIA to account for carbonate system dynamics in marine sediment which can play an important role in the coastal carbon cycle (Krumins et al. 2013).

3.4.5 Relaxation time metric: Limitation and perspective

While one main focus of this study is on providing a quantitative estimate of relaxation time, the difficulty of objectively defining what “*relaxation*” means necessitates some commentaries. This difficulty is not unique to marine biogeochemistry, as accurate quantification of recovery time is an open research question in other fields. In the context of a sedimentary system, Wheatcroft (1990) proposed that determining “dissipation time” (analogous to our “relaxation time”) can be subjective when it comes to signal preservation after sediment event layer deposition. The difficulties are exacerbated by previous work on episodic pulse on sediment biogeochemistry (Rabouille and Gaillard 1990), in which two metrics for estimating relaxation timescales for silica were proposed. Outside benthic early diagenesis, Kittel et al. (2017) proposed two generic metrics for systems with well-defined asymptotic properties that can be applied to a distance function from a given target (subject to certain mathematical assumptions). Because porewater profiles are inherently nonlinear and biogeochemical pathways in sediment are tightly coupled, the mathematical suggestion of asymptoticity using such a distance metric for an evolving profile converging toward the “*target*” proposed in that paper is frequently not met. This is the case for our investigation. Overall, while we provide a first-order approximation of relaxation time following perturbation for some model state variables, these studies also highlight some of the challenges associated with defining the timescale at which a signal can be validly assumed to have returned to its prior state. However, our method allows a full discussion of relaxation times for the main biogeochemical pathways.

3.5 Conclusion

The need to comprehend extreme events and their relationship to marine biogeochemistry prompted the development of novel methods for diagnosing flood-driven organic matter pulses in coastal environments. In this paper, we propose a new model for characterizing flood deposition events and the biogeochemical changes that result from them. This type of event can have an impact on the benthic communities and the response of the whole ecosystem (Gooday 2002; Bissett et al. 2007; Smith et al. 2018). Our modelling study shows that the post-depositional sediment response varies depending on the input characteristics of the layer deposit. For instance, we tested the combined effect of enrichment of labile organic carbon and deposit thickness on the space-time distribution and relaxation time of key dissolved species. This integral timescale of relaxation is constrained by the intrinsic properties of the solutes (diffusion) as well as the characteristics of the flood input (thickness and concentration of labile organic carbon). In essence, the findings from this study highlight the importance of the quantity and quality of organic carbon in modulating the sediment response following such a singular perturbation, as well as the role of flood events with heterogeneous quantitative contributions in the coastal ocean.

Author contributions

All authors contributed to the paper in several capacity. The project was supervised by CR and EV. SN, CR, EV conceptualized the method design, result interpretation, and assist in the initial draft of the paper. Model development was jointly designed by KS and SN. LP and BL provided insight on the data used in the model.

Code availability. As a whole, the model is bundled as a R package for easy accessibility and the current version is developed in (R-forge) with subsequent expected release in CRAN. Full R vignette illustrating the capabilities of the model can be found on the model doc folder. The version used to produce the results used in this paper is archived on Zenodo, along with the input data and scripts to recreate the simulation presented

in this paper. FESDIA users should cite both this publication and the relevant Zenodo reference.

Data availability. The data and paper used to evaluate the model (Pastor et al., 2018) can be found in the Zenodo link (). Users of the data should cite the Pastor et al., 2018 and Ait-Ballagh et al 2021. This paper was developed with literate programming concept in mind to encourage open-science and reproducibility. Full Rmarkdown files and model pipeline to fully reproduce the results here is available on Github.

Financial support This research has been supported by grant from INSU EC2C0 DELTARhône and PhD grant from Ecolé doctorale des science de l'environnement, Ile de France (SEIF) N° 129.

3.6 Appendix

Reaction	Kinetic Rate
Primary reaction	
Aerobic respiration	$R_{min} \times \frac{O_2}{O_2+k_{O_2}} \times (1 - \phi) \times TOC_i \times \frac{1}{lim}$
Denitrification	$R_{min} \times \frac{NO_3}{NO_3+k_{NO_3}} \times (1 - \frac{O_2}{O_2+k_{O_2}}) \times TOC_i \times \frac{1}{lim}$
Iron reduction	$R_{min} \times \frac{FeOH_3}{FeOH_3+k_{FeOH_3}} \times (1 - \frac{NO_3}{NO_3+k_{NO_3}}) \times (1 - \frac{O_2}{O_2+k_{O_2}}) \times TOC_i \times \frac{1}{lim}$
Sulfate reduction	$R_{min} \times \frac{SO_4}{SO_4+k_{SO_4}} \times (1 - \frac{FeOH_3}{FeOH_3+k_{FeOH_3}}) \times (1 - \frac{NO_3}{NO_3+k_{NO_3}}) \times (1 - \frac{O_2}{O_2+k_{O_2}}) \times TOC_i \times \frac{1}{lim}$
Methane formation	$R_{min} \times (1 - \frac{SO_4}{SO_4+k_{SO_4}}) \times (1 - \frac{FeOH_3}{FeOH_3+k_{FeOH_3}}) \times (1 - \frac{NO_3}{NO_3+k_{NO_3}}) \times (1 - \frac{O_2}{O_2+k_{O_2}}) \times TOC_i \times \frac{1}{lim}$
Secondary reaction	
Nitrification	$R_{nit} \times NH_4 \times O_2$
Iron Oxidation	$R_{FeOH_3} \times FeOH_3 \times O_2$
Sulfide Oxidation	$R_{H_2S} \times H_2S \times O_2$
Methane oxidation	$R_{CH_4} \times CH_4 \times O_2$
FeS production	$R_{FeSprod} \times Fe \times H_2S$



Chapter 4

Biogeochemical implication of massive episodic flood deposition: Model-Data integration

Reality is superior to ideas

Blaise Pascal

Nmor, S. I., E. Viollier, L. Pastor, B. Lansard, C. Rabouille: "Biogeochemical implication of massive episodic flood deposition: Model-Data integration" In: *Journal of Geophysical Research: Ocean*. (to be submitted)

Abstract:

Coastal deltas play an important role in the fate of materials transported to the sea through riverine channels. Under regime of extreme flood and storm events, this zone can experience large sediment deposition or resuspension within a short period. However, the biogeochemical consequences of such disturbances on the carbon and other element cycles are not fully understood. Using a coupled data-model approach, we explore the early diagenesis responses of shallow water sediment under the influence of massive flood-driven sediment inputs. The impact of this abrupt deposition of sediment is investigated using a case study of two intense flood discharges (in spring and fall) by the Rhône river in 2008 and a new numerical model of early diagenesis. The model provides a reliable representation of the observed porewater profiles over time and a comparison to profiles measured before and after the flood. The data set from 2008 shows that biogeochemical fluxes and rates responded abruptly to this almost instantaneous change in sediment deposition. Using the model, we observed that the oxygen fluxes reacted differently depending on the composition of the flood material, with the spring flood decreasing by 55% from its pre-flood value but increasing O_2 consumption in the fall, a prominent feature in the dataset. The occurrence of these flood-related depositions induced an increase of anoxic mineralization by a factor of 2 to 6 from its pre-flood value which was previously dominated by sulfate reduction (72%) and methanogenesis (8%). After each flood deposition, the model suggests that strong internal cycling of iron (> 80%) and manganese (> 40%) and intense mineral precipitation were possibly responsible for the maintenance of the non-euxinic (sulfide-free) condition in the sediment. Examining the sequential manifestation of these flood-related depositions reveals a temporary memory effect (i.e. an interaction between two successive floods), which becomes more pronounced as the sequence of terminal electron acceptors for organic carbon oxidation increases. This effect is stronger for methane (44

4.1 Summary

The goal of this section of the thesis is to provide the first realistic application of the model developed in the previous section. We show how the model may be used to describe the biogeochemical dynamics peculiar to the response of porewater profiles observed following the massive flood events encountered in the proximal zone of the Rhône delta in 2008 (Cathalot et al. 2010; Pastor et al. 2018). A spring event with 30 cm thick sediment of old calcareous material and a fall event with 10 cm of fresh detrital material were both studied in depth. The interaction of the carbon, iron, manganese, and sulfur cycles was the subject of our discussion in this section.

Our findings suggest that these floods could indeed produce differing biogeochemical responses, the extent of which is determined by the underlying characteristics of the flood layer deposit. We found a 55% decrease in oxygen flux across the SWI during the 2008 spring flood event, as well as a two-fold increase in overall mineralization rates from pre-flood conditions in the spring, which increased further in the fall when a very labile carbon-enrichment sediment was deposited (up to a factor of 7). In addition, we showed that the significant internal redox cycling was possibly responsible for the distinct dissolved iron and manganese profiles reported in the Rhône prodelta sediment for the two floods. Furthermore, we suggest that the significant precipitation of sulfide release from sulfate reduction contributes to the maintenance of the ferruginous condition in such a high organic carbon flux site.

Our findings further highlight the importance of successive flood deposition feedback on biogeochemical carbon mineralization pathways. We show that cumulative flood deposition has negligible effect on oxic and suboxic pathways, especially if their occurrence is temporally disconnected, but can be discernible for anoxic pathways like sulfate reduction and methanogenesis. This cumulative flood deposition effect on biogeochemical processes, referred to here as the “*memory effect*”, may be significant in coastal sediments subject to increasing intensification of extreme flood and particulate matter discharge.

4.2 Introduction

River-dominated ocean margins (RiOMar) are important for connecting the terrestrial and marine organic carbon cycles (OC) (Mackenzie et al. 2004; Regnier et al. 2022) by filtering the transfer of material from the River systems on continent margins to the open ocean. They also serve as a major organic matter (OM) deposition center, which has implications for preservation and burial. Indeed, continental margins account for more than 85 % of all organic carbon burial in the ocean, with deltas (RiOMars) representing half of the shelf burial (Burdige 2005). At the same time, river deltas are active biogeochemical reactors that emit large quantities of CO_2 to the atmosphere (Cai 2011; Dai et al. 2022).

These RiOMar systems are also vulnerable to extreme flood events, which are known to transport large amounts of sediment, carbon and nutrients from the land to the oceans, with their primary depositional zone occurring preferentially in the connecting deltas (McKee et al. 2004). Massive sediment inputs driven by these flood events have been observed in many of such systems: for example, Amazon River (Aller et al. 1996; Montanher et al. 2018), Mississippi River (Morse and Rowe 1999), Atchafalaya River (Allison et al. 2000), Eel River (Bentley and Nittrouer 2003), Po River (Palinkas et al. 2005; Tesi et al. 2012; Tesi et al. 2013), Têt River (Bourrin et al. 2008), Rhône River (Cathalot et al. 2010). These large and nearly instantaneous transfers of sediment are projected to occur with increasing frequency due to changing environmental landscapes and

climate change (Tockner and Stanford 2002). Indeed, the current trend in extreme precipitation from hurricanes and other storm events can result in large amounts of sediment being delivered in a short period of time, as documented in some coastal margins: Tropical Storm Lee transported sediment to a large portion of Cheapeake Bay via the Susquehanna River (Cheng et al. 2013), extreme precipitation events in the Mississippi River basin transferred a large volume of terrestrial organic carbon to the northern Gulf of Mexico (Bianucci et al. 2018), large volumes of sediment were transported on the Northeastern Australian coast during Cyclone Winifred (Carter et al. 2009), to name a few. All of these events have been shown to have a short (daily)-to-medium (yearly) impact on the ecosystem productivity, such as degrading water clarity and growth of phytoplankton (Cheng et al. 2013), increasing mineralization in bottom waters of the coastal ocean inducing hypoxic condition (Cheng et al. 2013; Moriarty et al. 2021), or increased CO_2 flux to the atmosphere (Osburn et al. 2019).

In the Gulf of Lions (the southern part of France), about 80% of the annual terrigenous particulate input is delivered by Rhône river floods (Antonelli et al. 2008) with a large majority of the materials deposited in the prodeltaic zone (Ulses et al. 2008b). The sediment delivered by these flood events can differ in terms of its quantity and quality, as they represent a conglomeration of different particles originating from different regions of the catchment (Eyrolle et al. 2012; Pont et al. 2017). In addition, given the unique sedimentary characteristics of the prodelta (high sedimentation up to 40 cm yr^{-1} , high carbon flux up to $650\text{ gC m}^{-2}\text{ yr}^{-1}$), the underlying diagenetic sequence of sediment shows remarkable stationarity (high concentration of DIC, dissolved iron and manganese, strong sulfate reduction) during spring and summer (Rassmann et al. 2020) despite short-term biogeochemical response linked to fall and winter floods (Cathalot et al. 2010). The reason for such long-term stability but short-term response is still unknown (Pastor et al. 2018), but has been linked to a rather short system's relaxation timescale (4-5 months) and the existence of a possible "*Biogeochemical attractor*" - a hypothetical concept basically associated with the rapid reorganisation of the perturbed porewater profiles to their pre-flood condition despite being affected by such massive depositional event (Nmor et al. 2022). The latter would help explain the maintenance of the same diagenetic characteristic for multi-temporal data in non-steady conditions (Nmor et al. 2022). While a proper understanding of the characteristics of this type of perturbation requires continuous monitoring and observation in both long- and short-term basis (Toussaint et al. 2014; Ferreira et al. 2023), there is still a scarcity of data on the estimated biogeochemical fluxes and rates caused by these flood events. Combination of available data (Cathalot et al. 2010; Bourgeois et al. 2011; Bonifácio et al. 2014; Pastor et al. 2018), with appropriate spatio-temporal scale, and numerical modelling can thus help to answer some of these questions.

This study aims to quantify the size and scope of biogeochemical changes brought about by significant flood events in the Rhône prodelta region. A reactive transport model with a non-steady state approach was used to investigate how the diagenetic mineralization of organic matter can explain porewater data obtained from observations of two distinct flood deposition events in 2008. We also calculated the biogeochemical fluxes and rates associated with these events, as well as the system's temporal evolution after this perturbation. The effect of this phenomenon on carbon, iron, manganese, and sulfur cycling was then determined. The results of this model-data investigation give new insights on the consequences of these extreme events on sediment biogeochemical dynamics.

4.3 Materials and Methods

4.3.1 Data description

The dataset discussed in this paper entails the flood driven deposition events which occurred in the Rhône prodelta in the year 2008 (Cathalot et al. 2010; Pastor et al. 2018). The data described the hydro-sedimentological and chemical situation of the sediment in the proximal station within 2 km from the river mouth (Station A: 4°51.099 °E and 43°18.751 °N). The average depth at this location is 23 m (Pastor et al. 2018) with high apparent accumulation rates up to 40 $cm\ yr^{-1}$ (Charmasson et al. 1998).

Our concern in this work is the flood events of May/June 2008 (Generalized flood) and November/December 2008 (Cenevol flood) (Pastor et al. 2018). These two floods have been dubbed the spring and fall floods, respectively. The sampling dates are specified in Figure 4.1. In the spring flood, 30 cm of sediment was deposited. The average organic carbon content in this layer of sediment (1% d.w.) was lower than the average OC in pre-flood sediment (> 2% d.w.; Cathalot et al. (2010)), with deposited materials primarily composed of aggregated siliceous and carbonate crystalline rocks from nearby tributaries (Durance and Isère rivers) containing large amounts of refractory carbon (Cathalot et al. 2013; Copard et al. 2018). During the fall flood, a sediment layer of 10 cm thickness was deposited mostly composed of silicate minerals and organic debris with a high OC content sediment containing large amounts of young OC (5% d.w.; Cathalot et al. (2010)). Pore-water composition including dissolved iron (Fe^{2+}) and manganese (Mn^{2+}) profiles in both events showed evidence of this flood perturbation, with these species responding sequentially to the deposition (Pastor et al. 2018). This response was characterized by a slow build-up of iron following manganese release in the first 30 cm of porewater. Furthermore, significant sulfate reduction was observed within the sediment, with sulfide concentrations below the detection limit. Full description of the dataset can be found in Cathalot et al. (2010) and Pastor et al. (2018).

4.3.2 Model description

The model used for this study is the time dependent, one dimensional reactive transport model, FESDIA (Nmor et al. 2022). This model described the transformation of OC within the sediment column with well adapted capabilities for usage in sudden flood depositional scenarios. The full description of the model can be found in Nmor et al. (2022) and detailed mass balance equations and reaction kinetic is provided in the Appendix. Here, we basically recap the key biogeochemical reactions and pathway necessary to simulate the flood datasets derived from Pastor et al. (2018).

The reactive transport model includes 16 state variables: fast (C_{org}^{fast}) and slow C_{org}^{slow} degradable organic matter, two pools of manganese oxide (MnO_{2A} and MnO_{2B}) and iron hydroxide ($FeOOH_A$ and $FeOOH_B$), manganese carbonate ($MnCO_3$) all constitute the particulate solid modeled (Table 4.1). The choice of iron and manganese fractions was dictated by the assumption that the short-term path of Fe and Mn dynamics is driven by the reactive pool of their respective oxides. In practice, iron oxide pool broadly consists of highly reactive (amorphous and crystalline) oxides - ferrihydrite, goethite, lepidocrocite and hematite) with half-life of < 1 yr (Canfield et al. 1992; Raiswell and Canfield 1998), moderately reactive component (magnetite and reactive silicate of half-life of 10^2 yr), poorly reactive iron oxide with longer half-life, > 10^5 yr (Canfield et al. 1992; Poulton et al. 2004). Detrital iron fraction bound within sheet silicates are nonreactive on the timescale of early diagenetic processes of concern to the model (Poulton and Raiswell 2002) while particulate iron bound

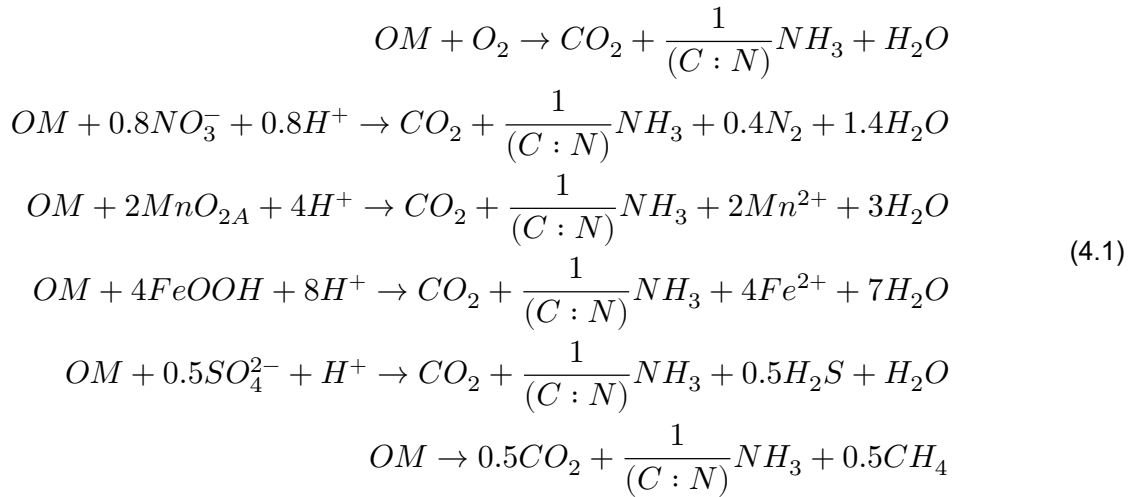
to sulfide (FeS and FeS_2) when formed via precipitation have high stability and low solubility, thus can be permanently buried (see below and Rassmann et al. (2020)). As such, these solid phases of iron are not modeled. Similarly, manganese oxides or (oxyhydroxides) in the sediment span different reactive timescales and only the reactive fractions are considered in the model. Our modeling strategy is analogous to other diagenetic models that describe metal cycling in marine sediment (Berg et al. 2003; Dale et al. 2015; Zhao et al. 2020).

Dissolved species included in the model are oxygen (O_2), nitrate (NO_3), ammonium (NH_4^+), dissolved iron (Fe^{2+}) and manganese (Mn^{2+}), sulfate (SO_4^{2-}), hydrogen sulfide (H_2S), methane (CH_4) and dissolved inorganic carbon (DIC) (Table 4.1).

Table 4.1: State variables described in the model.

State variable	Description	Model notation	Units
C_{org}^{fast}	Fast decaying detritus	FDET	$mmol\ C\ m^{-3}$
C_{org}^{slow}	Slow decaying detritus	SDET	$mmol\ C\ m^{-3}$
$FeOOH_A$	Fast oxidized ferric iron	FeOOHA	$mmol\ Fe\ m^{-3}$
$FeOOH_B$	Slow oxidized ferric iron	FeOOHB	$mmol\ Fe\ m^{-3}$
MnO_{2A}	Fast oxidized manganese	MnO2A	$mmol\ Mn\ m^{-3}$
MnO_{2B}	Slow oxidized manganese	MnO2B	$mmol\ Mn\ m^{-3}$
O_2	Oxygen	O2	$mmol\ O_2\ m^{-3}$
NO_3^-	Nitrate	NO3	$mmol\ N\ m^{-3}$
NH_4^+	Ammonium	NH3	$mmol\ N\ m^{-3}$
SO_4^{2-}	Sulfate	SO4	$mmol\ S\ m^{-3}$
H_2S	Hydrogen sulfide	H2S	$mmol\ S\ m^{-3}$
Fe^{2+}	Reduced ferrous iron	Fe	$mmol\ Fe\ m^{-3}$
Mn^{2+}	Reduced manganese	Mn	$mmol\ Mn\ m^{-3}$
DIC	Dissolved inorganic carbon	DIC	$mmol\ C\ m^{-3}$
CH_4	Methane	CH4	$mmol\ C\ m^{-3}$
$MnCO_3$	Mn carbonate	MnCO3	$mmol\ Mn\ m^{-3}$

Degradation of organic matter (OM) occurs via the sequence of energy utilization of electron acceptors, with oxygen used first, followed by oxidation via NO_3 . Thereafter, the model includes microbially mediated reduction by the oxides of Mn and Fe (MnO_2 and $FeOOH_3$) with this justification largely dictated by the substantial release of their respective reduced solutes during flood deposition (Pastor et al. 2018). Sulfate reduction and methanogenesis close the carbon-based cycle of OM remineralization in the model (Equation 4.1).

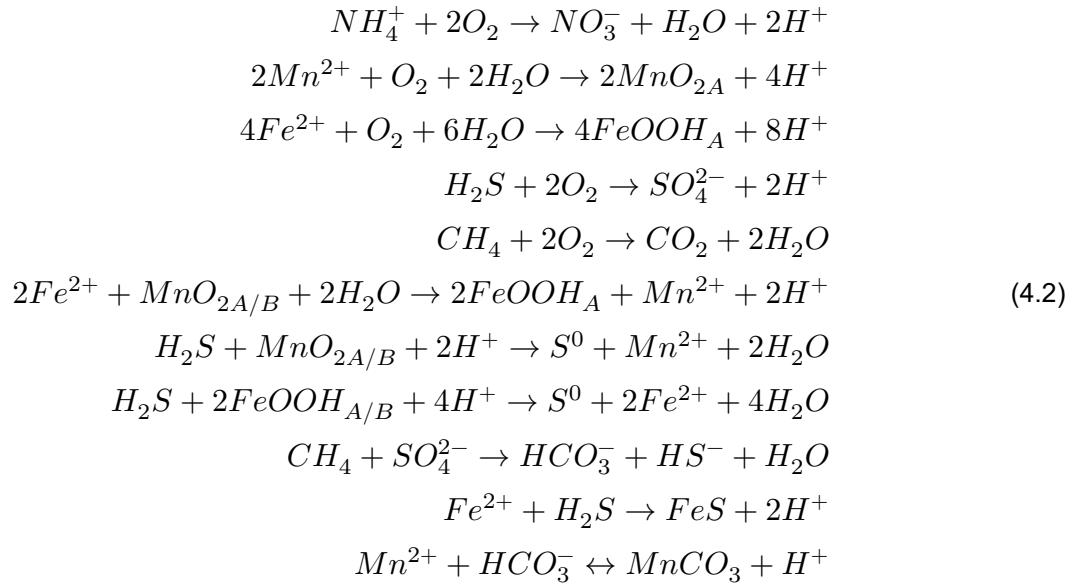


where OM is simply represented as $(CH_2O)(NH_3)_{N:C}$ and N:C is the redfield nitrogen to carbon ratio respectively ($N:C = \frac{16}{106}$). The reactive rate is represented by a Michaelis-Menten type relationship with respect to the oxidant concentration (see Appendix).

The direct consequence of organic matter remineralization in the model is the production of reduced substances (Equation 4.1). The model considers a series of subsequent processes connected to these reduced species (Equation 4.2). In order to reduce the degree of freedom for calibrating poorly constrained parameters and processes which govern many of the secondary reaction in the Rhône prodelta sediment, a simplified representation of the iron, manganese and sulfur interactions was made.

Re-oxidation of reduced species from OM mineralization via oxygen (Equation 4.2) and metallic oxides (Equation 4.2) is included while methane formed by fermentation of OM can be anaerobically oxidized (i.e anaerobic oxidation of methane, AOM) (Dale et al. 2006). Fe^{2+} is oxidized to ferric iron (Fe^{3+}), which precipitates out as fresh iron oxide ($FeOOH_A$) minerals. Sulfide produced by sulfate reduction is abiotically oxidized by both pools of iron oxyhydroxides and manganese oxides (i.e sulfur-mediated iron and manganese reduction) (Berg et al. 2003). As discussed in Haese (2000), the interaction between dissolved Fe^{2+} and H_2S happens in two stages, with the formation of intermediate dissolved elemental sulfur (S^0) and dissolved FeS (FeS_{aq}). However, these forms of sulfur are not modeled because of their unstable nature in marine sediment as well as the possibility of FeS_{aq} to precipitate to its particulate form (FeS_p) once a solubility threshold of $\sim 2 \mu M$ is reached (Rickard 2006). Therefore, we assumed that dissolved FeS, upon formation, is subsequently transforms into a stable form of particulate sulfur that can be eliminated from the porewaters via precipitation (Rickard 1997, 2006). The kinetic rate expressions of all re-oxidation processes and other secondary reaction are described by standard second-order rate formulation.

The model also includes a simple representation of the formation and dissolution of Mn carbonates. However, iron carbonate (siderite) formation and dissolution was not considered in the model since siderite precipitation is inhibited by low levels of sulfide (Haese 2000). This is precisely the situation in the Rhône pro-delta sediment in which FeS precipitation is the dominant sink for dissolved iron and is produced through the sediment column (Rassmann et al. 2020). This kinetics of dissolution and precipitation follow a similar formulation in Wang and Van Cappellen (1996), where the reaction rates are dependent on the pore water saturation state. Here, the pH of the porewater was not explicitly modeled but was fixed at a constant value of 7.5 in order to reduce the complexity of the model (Berg et al. 2003).



4.3.3 Model Parameters

The key rate parameters for the biogeochemical processes are tabulated in Table 4.2 . The environmental parameters and boundary conditions were derived from previous steady-state modelling studies investigated in the Rhône prodelta sediment (Pastor et al. 2011a; Ait Ballagh et al. 2021). For our model-data calibration, parameters associated with the transport processes were first adjusted before pathways involving the carbon dynamics were fine-tuned.

The specification of the carbon-based parameters was carried with respect to range of value reported in the aforementioned studies with little modification. Thus, for the processes associated with OM mineralization, our model fitting procedure was constrained to these prior best-fit (Pastor et al. 2011a; Ait Ballagh et al. 2021). Thereafter, the processes affecting the iron and manganese cycle were then parameterized. As these previous modelling studies only capture the anaerobic diagenesis processes by considering a lumped term, ODU (oxygen demand unit), nominal additional parameters pertaining to the coupled iron-sulfur-manganese cycle is derived from other published works (Berg et al. 2003; Dale et al. 2015; Zhao et al. 2020).

However, because the boundary flux for other particulate species besides carbon in the Rhône prodelta sediments is largely unknown, the parameters involving sulfur, iron and manganese interactions were fine-tuned to adapt to the data at hand using both manual and automatic fitting procedures provided by the R package FME (Soetaert and Petzoldt 2010), while accounting for the constraints present in the study site (e.g low sulfide system (Pastor et al. 2018), high sedimentation rate and carbon flux (Pastor et al. 2011a), low bioturbation (Pruski et al. 2015) and possibly high iron flux (Roussiez et al. 2011).

Table 4.2: Summary of parameters used in the FESDIA model. (I) independent parameters derived from experiment or field observation external to actual data being simulated (C) constrained parameters obtained from range of literature sources (M) model-derived parameters fitted to the observed data. FDET stands for Fast detritus (labile carbon) and SDET for slow detritus, semi-refractory carbon. Literature sources includes (1) Pastor et al. (2011a), (2) Soetaert et al. (1996a), (3) Ait Ballagh et al. (2021), (4) Rassmann et al. (2020), (5) Wang and Van Cappellen (1996) and (6) Wijsman et al. (2002).

Description	Model		Units	Type	Source
	name	Parameters			
total organic C deposition	Cflux	10000	$nmol C cm^{-2} d^{-1}$	I	1
part FDET in carbon flux	pFast	0.5	-	C	1
deposition rate of FeOH3	FeOH3flux	5000	$nmol cm^{-2} d^{-1}$	M	-
decay rate FDET	rFast	0.05	d^{-1}	C	1
decay rate SDET	rSlow	0.0031	d^{-1}	C	1
NC ratio FDET	NCrFdet	0.14	molN/molC	I	2
NC ratio SDET	NCrSdet	0.1	molN/molC	I	2
upper boundary O2	O2bw	238	$mmol m^{-3}$	M	-
upper boundary NO3	NO3bw	0	$mmol m^{-3}$	M	-
upper boundary NH3	NH3bw	0	$mmol m^{-3}$	M	-
upper boundary CH4	CH4bw	0	$mmol m^{-3}$	M	-
upper boundary DIC	DICbw	2360	$mmol m^{-3}$	M	-
upper boundary Fe2	Febw	0	$mmol m^{-3}$	M	-
upper boundary H2S	H2Sbw	0	$mmol m^{-3}$	M	-
upper boundary SO4	SO4bw	30246	$mmol m^{-3}$	M	-
upper boundary Manganese	Mnbw	0	$mmol m^{-3}$	M	-
advection rate	w	0.027	$cm d^{-1}$	M	-
bioturbation coefficient	biot	0.05	$cm^2 d^{-1}$	C	1
depth of mixed layer	biotdepth	5	cm	I	3
attenuation coeff below biotdepth	biotatt	1	cm	I	3
bio-irrigation rate	irr	0.3	d^{-1}	M	-
depth of irrigated layer	irrdepth	7	cm	I	3
attenuation coeff below irrdepth	irratt	1	cm	I	3
Max nitrification rate step1 (NH3ox)	rnitri	10	d^{-1}	M	-
temperature	temperature	15.6	dgC	M	-
salinity	salinity	37.8	psu	M	-
refractory Carbon conc	TOC0	1	%	I	5
maximum rate FeS production	rFeS	0.5	$cm^3 nmol^{-1} d^{-1}$	I	4
Max rate anaerobic oxidation Methane	rAOM	30×10^{-6}	$cm^3 nmol^{-1} d^{-1}$	I	1/4
surface porosity	por0	0.83	-	I	1/4
deep porosity	pordeep	0.65	-	M/C	-/5
porosity decay coefficient	porcoeff	2	cm	M/C	-/5
Rate of Sulphide-mediated iron reduction (oxyhydr)oxides	rH2Sfeox	0.00121	$cm^3 nmol^{-1} d^{-1}$	M/C	-/5
Flux of Mn Oxides	MnO2flux	1000	$nmol cm^{-2} d^{-1}$	M/C	-/5

Description	Model		Units	Type	Source
	name	Parameters			
Rate of Reoxidation of H ₂ S by MnOx	rH2SMnox	0.001728	$cm^3 nmol^{-1} d^{-1}$	C	6
Rate of Reoxidation of Fe with MnOx	rMnFe	6.5×10^{-6}	$cm^3 nmol^{-1} d^{-1}$	C	2

4.3.4 Characterization of flood dynamics

As introduced in Nmor et al. (2022), the dynamics of the flood deposition events is driven by the characteristics of the sediment delivered (such as the deposit thickness, organic carbon content and reactivity). In that study, the mechanism of flood-induced sediment deposition was modeled as a single massive event against an underlying background variation. However, in this paper, this singular flood prescription is expanded to include multiple events in one simulation run, thereby allowing a chain of event-driven simulation to be performed with their respective characteristics. As a consequence, the so-called enrichment factor (α) - a scaling parameter linked to the quantity of carbon within the flood layer - becomes a time dependent parameter ($\alpha(t)$) in tandem with the thickness extent of the depositional depth ($Z_{pert}(t)$). This advance in the event-depositional algorithm provides some realism to how natural dynamic sedimentary systems work, albeit with an extra layer of complexity and parameterization constraint to the model.

4.3.5 Model simulation

4.3.5.1 Simulation strategies

4.3.5.1.1 Nominal simulation for flood deposition 2008

The numerical procedure for solving the underlying reactive transport equation capturing the processes in Section 4.3.2 have been previously discussed (Nmor et al. 2022). In summary, the simulation was carried out in the sediment grid layer of 100 cm thickness with intermittent deposition events treated as an abrupt change to the model dynamics at specified time interval (see Figure 4.1).

The model simulation was conducted over two years starting in January 2008 in order to capture the hydrological regime of this particular year. It was started with a steady-state simulation and dynamic spin-up for two years to achieve a dynamic equilibrium. Thereafter, the main simulation was run for two years (January 2008 - December 2009). Because the model can be configured to include multiple events, the decision on when, where, and how many such depositions to implement to adequately describe the observed data was made considering the prevailing hydrodynamical and sedimentological constraints within the sampling time-window (Cathalot et al. 2010; Pastor et al. 2018). We used data from the nearest river monitoring site in Arles (40 km upstream the river mouth) to calculate river discharge and total suspended matter (TSM). Figure 4.1 depicts the constraints on the timing and magnitude of the deposits. A detailed analysis of the river discharge and the corresponding TSM data suggests a power law relationship (Pont et al. 2002), and examination of the temporal variability in both datasets indicates the occurrence of a minor flood event between the two major depositions (spring and fall deposition) (Figure 4.1). Following this analysis, three sequential flood deposition simulations were performed. The first corresponds to a *major* spring flood event with low organic carbon content and a sediment deposition of 30 cm. The second event is associated with a *minor* flood depositions of limited thickness (Cathalot et al. 2010) and organic carbon. The fall flood, which delivered 10 cm of sediment enriched in organic carbon and reactive

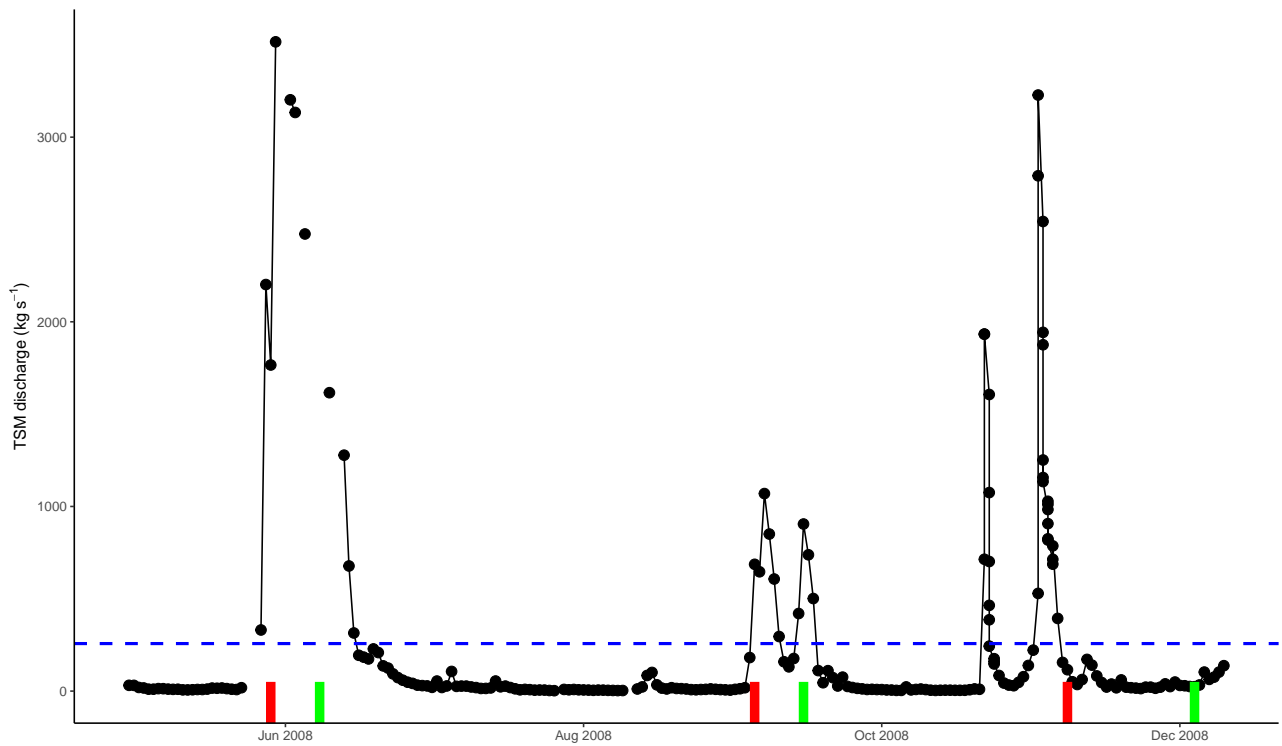


Figure 4.1: Timeseries of total suspended matter (TSM) river discharge by the Rhône River in year 2008. Red bar denotes the day of deposition used in the model and green bar is the sampling date when measurement was carried out. Blue dashed line is the annual mean of TSM discharge. Data was obtained from the Mediterranean Oceanic Observing System from the Environment (MOOSE database) provided by Mediterranean institute of oceanology.

minerals, was described as the third event (see Cathalot et al. (2010) for sediment deposition in May and November 2008).

Because the intermediate second event was missed by the sampling campaign in 2008, we chose a simple approach by assuming that the event is relatively mild in comparison to the two major floods, as evidenced by discharge and TSM data, as well as down core sediment retrieved in September and October (around the limited deposition event) which show little evidence of deposition (Cathalot et al. 2010). The enrichment factor (α) used in the simulations as well as the thickness of the deposited layer is provided in Table 4.3. These enrichment factors are basically parameterization of the carbon content in the newly deposited sediment layer relative to the ancient layer and is dependent on the source region of the flood (Nmor et al. 2022).

Table 4.3: Event specific enrichment factor (α) used in model simulation for spring and fall flood

	C_{org}^{fast}	C_{org}^{slow}	$FeOOH_A$	$FeOOH_B$	MnO_{2A}	MnO_{2B}
Spring	0.5	0.7	0.3	0.3	1	2
Intermediate	0.5	0.7	1.0	1.5	1	2
Fall	20.0	5.0	8.0	2.0	10	5

Furthermore, model analysis performed within this simulation was decomposed into 2 components corresponding to the spring and fall flood event. This calculation was done by integrating any model quantity, variable or metric of interest over a relaxation timescale window. The relaxation interval is defined as the timescale over which a particular variable subject to the perturbation signal caused by flood deposition becomes indistin-

guishable from background variation (see Nmor et al. (2022) for introduction and Section 4.3.5.1.2). Thus, the biogeochemical effects of the different flood deposition events can be compared.

4.3.5.1.2 Relaxation time

The relaxation timescales of the various biogeochemical pathways are calculated in the same way as Nmor et al. (2022). However, a minor change in the methodology is presented using a more analytical rather than numerical approach in order to consider processes or rates which may have a longer timescale of relaxation beyond the interval of two successive deposition. Thus, given that the shape of the so-called “point-by-point” concentration difference between two successive profiles (ϕ) following the perturbation can be approximated as a first order exponential decay:

$$\frac{d\phi}{dt} = -\lambda\phi \quad (4.3)$$

a secular rate of decay λ can be estimated from the curve. This is especially true for situations where there is no internal background forcing, such as the configuration investigated in this work. This decay coefficient can be calculated by fitting the distance function $\phi(t)$ to the solution of this exponential decay, such as:

$$\phi = \phi_0 e^{-\lambda t} \quad (4.4)$$

where ϕ denotes the point-by-point differences in successive profiles for any given variable/rate for which the relaxation timescale is estimated (see Eq 22 in Nmor et al. (2022)), and ϕ_0 denotes the initial value of the difference between the preflood profile and just after the deposition. This equation can be used to fit a non-linear regression to determine λ . The distance function's characteristic timescale can then be defined as the timescale over which a fixed percentage of the profile is said to be similar to previous profiles. For example, if the profile has recovered 95% of its pre-flood state, then for all practical purposes, the variable/rate profile in question is more or less indistinguishable from its pre-flood state.

An advantage of this approach is that we can derive an analytical formulation of this relaxation timescale using Equation 4.4. For example, a relaxation timescale ($\hat{\tau}_\eta$) for any arbitrary time threshold η can be written as:

$$\hat{\tau}_\eta = \frac{1}{\lambda} \ln \frac{100}{100 - \eta} \quad (4.5)$$

where τ_η is the relaxation timescale required to restore the system to η % of its preflood state. This analytical derivation allows us to infer the long-term outcomes of these repeated transient responses to constant environmental perturbation. Another advantage of this method is the possibility to investigate the temporal characteristics of the variability of the sediment biogeochemistry if a perturbed system never reaches an ultimate asymptotic state (as in the case of an environment that is sufficiently variable).

4.3.5.1.3 Memory effect for flood deposition 2008

A natural consequence of the chain of instantaneous flood depositions at various times in the simulation is the possibility of the different biogeochemical processes incorporating a memory effect (i.e. processes at previous time-step might affect processes at future time). Given that relaxation times for some species such as DIC and

SO_4^{2-} are up to 5 months (Nmor et al. 2022), they may overlap with other deposition events. The occurrence of these multiple flood deposition events and their interactions could be important drivers of biogeochemical processes in coastal sediment and the resulting fluxes.

We investigate to what extent these sequential flood events might influence the biogeochemical pathways of carbon by conducting another slightly different simulation from the nominal reference simulation detailed above by omitting the first deposition (i.e. spring flood). This provides a way to quantify the changes in the reaction pathways with regard to different situations in a given hydrological year: two successive floods (spring and fall) which relaxation may overlap or one flood only (fall). The comparison of the two situations can provide some suggestion of the possibility of flood-feedback dynamics on the biogeochemistry (Figure 4.2).

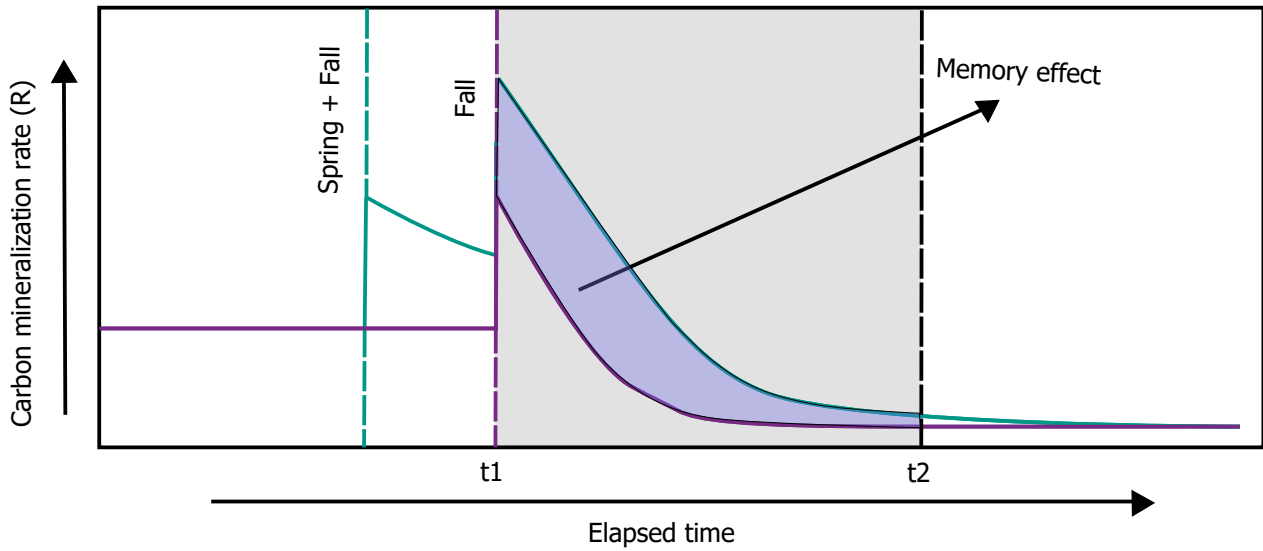


Figure 4.2: Schematic of the interaction between two flood on biogeochemical process in the sediment. The memory effect of the spring flood on subsequent fall period flood is defined as the time-integrated rate of biogeochemical process between t_1 and t_2 .

Given the occurrence of two characteristic flood events in one hydrological year, we proceeded to diagnose the effect of succession of floods on the biogeochemical rates. To this end, we estimated the memory effect of the flood by simulating two flood events: The first simulation is the same as the simulation performed above where the two depositions occurred within the simulation window, i.e. initialized with spinup profiles and two sequential flood event). The second simulation is performed without the first spring flood (i.e. only second flood effect initialized from the spinup profiles) (Figure 4.2). The difference in the integrated rates of biogeochemical processes averaged from the start of the fall flood deposition (t_1) to the end of the relaxation (t_2) in both scenarios indicates the magnitude of the memory effect (ME):

$$ME = \frac{\int_{t_1}^{t_2} R^{spring+fall} dt - \int_{t_1}^{t_2} R^{fall} dt}{\int_{t_1}^{t_2} R^{fall} dt} \times 100 \quad (4.6)$$

where t_1 and t_2 is the time interval in which the memory effect of the spring flood on the fall flood is estimated. The numerator in Equation 4.6 is basically the time-integrated difference of any vertical integrated rate biogeochemical process R^i within a time window between t_1 and t_2 . t_1 is the fall flood deposition and t_2 is 6 months later, encompassing the relaxation time of the system. In essence, this numerical experiment implicitly

assumed no other intense deposition occurs in between the period when this calculation is performed.

4.4 Results

4.4.1 Model-Data evaluation

4.4.1.1 Global performance of model prediction

The model was validated with the complete data presented in the two flood events in 2008 as described in Pastor et al. (2018) for station A. The skillfulness of the model in describing the observed vertical distributions and their temporal variations was diagnosed using a Taylor diagram (Taylor 2001), which summarizes the goodness of model fit relative to the data. We considered the depth-dependence variability, model-data bias and model-data correlation as three different measures of the model's performance. The variability is represented by the standard deviation of the observed and modeled values (x and y axis of the graphs) with its magnitude measured as the radial distance from the origin of the plot (dashed line in Figure 4.3). A value of 1 indicates a fair representation of vertical variability in the data while value above and below 1 signifies an over or under-estimation of the true variability in the data. The bias measured as the model-data difference (Root Mean Square, RMS) as well as the model standard deviation are normalized by dividing the RMS and standard deviation by the observation's standard deviation (N.sd). The centred root-mean square error (RMSE) is the concentric dashed lines originating from the "observed" point. The further the model is from the observed point, the bigger its bias is. As such, a value close to 0 reflects a good fit of the model to the observation. The "observed" point is plotted on the x-axis at a unit length distance from the origin in this case. As such, we can succinctly visualize, by how much the model under/over-estimates the variability in the data. This non-dimensional deviation also has the advantage of allowing model-data statistics for different flood types/events to be compared on the same plot. The model-data correlation is captured by the correlation coefficient and is shown on the arc line; with points which lies closest to the x-axis, having the highest correlation.

Here, the simulation of oxygen profiles during the spring flood show lesser bias to the oxygen data compared to the fall despite the fact that both events display reasonably high and similar correlations. The model prediction for SO_4^{2-} performed better in both deposition periods with a correlation of 0.66 and 0.96 for spring and fall flood respectively with a better overall metrics in the fall compared to the spring (Figure 4.3). Similarly, DIC simulated by the model during the fall deposition showed better correspondence with the measured data (high correlation = 0.96) and reasonable representation of the variability in the porewater DIC (± 0.5 from true variation i.e half the true variability observed in the data) in comparison to the spring model prediction (Nsd ± 0.8). Among the reduced metal species, the predicted profile for dissolved Mn was significantly more faithful to the data across both events (with a higher correlation coefficient and lower RMSE) than the predicted profile for dissolved Fe. The vertical variability observed in the fall porewater data is better captured in both cases. Ammonium showed decent model fit with the data in both events with moderate correlation ($r > 0.4$) (Figure 4.3).

4.4.2 Evolution of porewater profiles

4.4.2.1 Preflood situation

The porewater profiles prior to the occurrence of the massive flood input in May-June indicated a fairly steady-state condition Figure 4.4. In this preflood situation, the model captured the main biogeochemical features of the

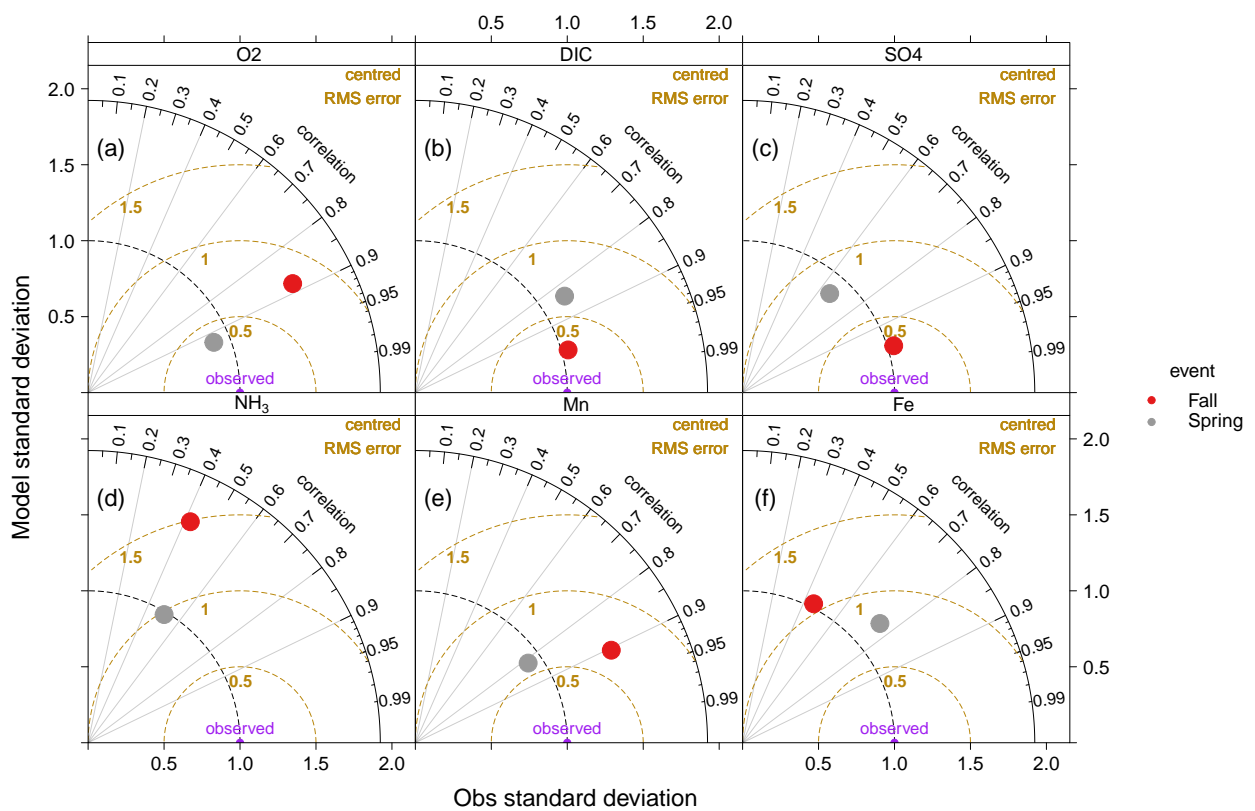


Figure 4.3: Taylor diagram of Goodness of fit between model simulation and data for (a) Oxygen, O_2 (b) Dissolved inorganic carbon DIC (c) Sulfate SO_4^{2-} (d) Ammonium NH_4^+ (e) Manganese Mn^{2+} and (f) Iron Fe^{2+} . Red and grey dots denote the spring and fall deposition simulation with the normalized observed standard deviation shown in purple. See text for explanation and interpretation.

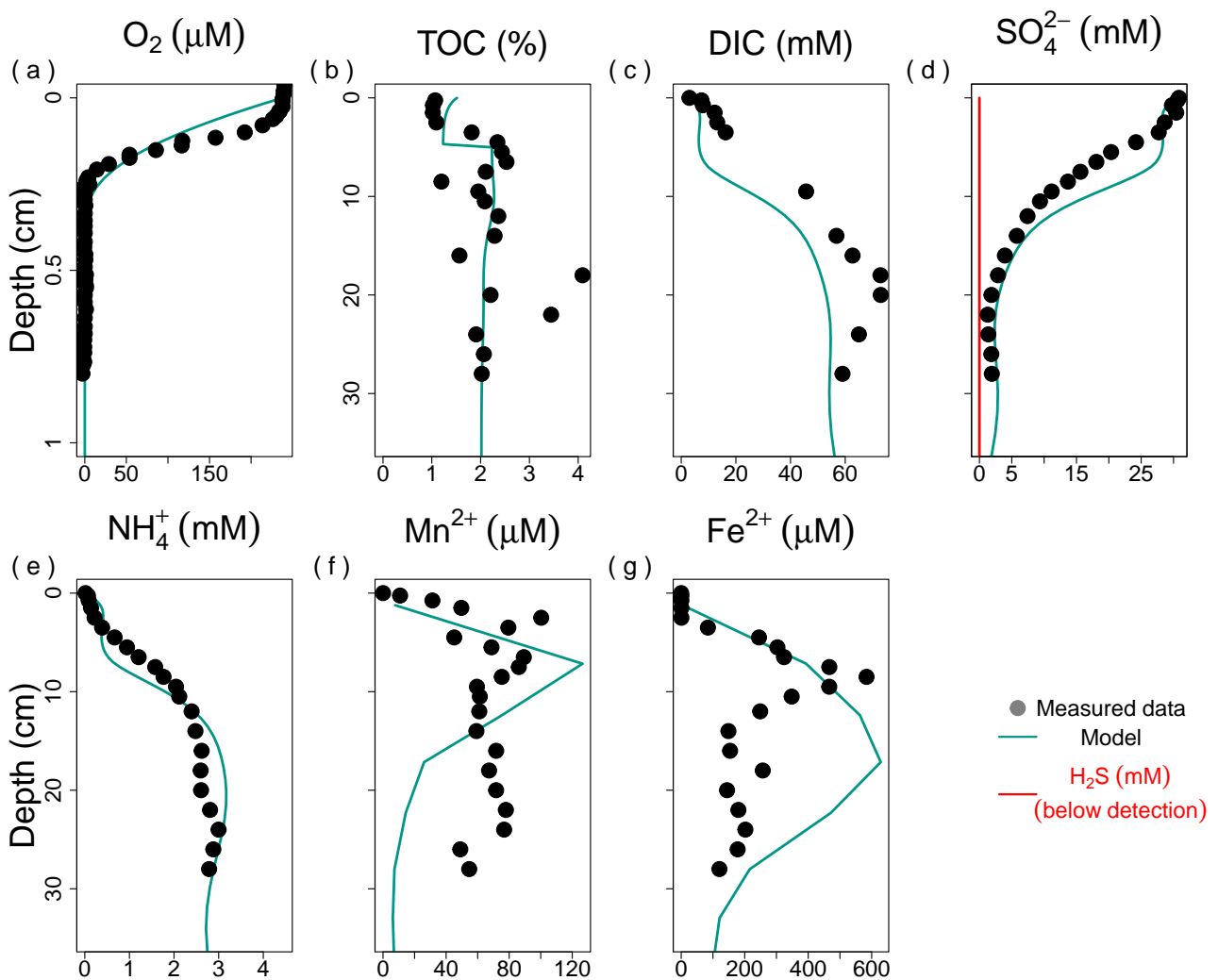


Figure 4.4: Model data fit against observed data for (a) Oxygen, O_2 (b) Total organic carbon, TOC (c) Dissolved inorganic carbon DIC (d) Sulfate SO_4^{2-} (e) Ammonium NH_4^+ (f) Manganese Mn^{2+} (g) Iron Fe^{2+} (h) Hydrogen sulfide H_2S . Data collected the 29th of May 2008 at Station A before spring flood (Pastor et al. 2011a).

prodelta sediment. Simulated TOC profile follows the basic trend in TOC with higher OC content (2%) below 5 cm and high concentration around 20 cm. This variability is typical of sediment accumulation under flood regimes. The deposition of sediment initiated the oxidation of OC which led to a shallow oxygen penetration depth (3.5 mm) before the flood and complete sulfate exhaustion around 20 cm. DIC and NH_4^+ increased with depth to an asymptotic concentration of 60 mM and 3 mM respectively. Furthermore, dissolved Mn was observed with enhanced concentration between 5 and 10 cm with maximum concentration of 100 μM . However, this Mn maximum (127 μM) was overestimated by the model (Figure 4.4). The model dissolved Fe profile, on the other hand, demonstrated better agreement with the measured porewater Fe, with a subsurface maximum of 629 μM fed by iron reduction linked to the mineralization of organic carbon-enriched sediment. This peak is however shifted at 20 cm depth in the model versus 10 cm in the data. It is noteworthy that no dissolved sulfide is simulated which reflects the observed absence of sulfide in porewaters.

4.4.2.2 Generalized flood deposition (Spring 2008)

The delivery of terrestrially-derived sediment particles peaked within ten days after the flood began, with a massive accumulation of sediment as high as 30 cm observed at the study site (Cathalot et al. 2010).

The simulated profiles 10 days after the flood event were able to capture the dominant spatial variation in the porewater species. Given the refractory nature of the deposited sediment, oxygen was present in the surface sediment down to 9.2 mm (Figure 4.5). The model estimate of the oxygen penetration depth is 3.8 mm. Modelled total oxygen flux across the sediment-water interface (SWI) during this period was 13 $mmol O_2 m^{-2}d^{-1}$ while the measured diffusive flux was $9.2 \pm 3.1 mmol O_2 m^{-2}d^{-1}$. The spatial variation of ammonium was well captured by the model with the low but constant (NH_4^+) at the surface down to the depth of the newly deposited layer (30 cm). However, the model seems to suggest a subsurface peak in NH_4^+ at the former sediment water interface (SWI) which is unobserved in the data.

Sulfate concentration during this spring event was constant in the upper 30 cm of the sediment, equaling the value of the bottom water concentration trapped in by the flood layer (Figure 4.5). Underneath the layer, the sulfate concentration in the model as well as the data decline with depth characterized by strong sulfate reduction ($160 mmol C m^{-2}d^{-1}$) within this zone. The by-product of this mineralization, dissolved inorganic carbon (DIC) showed a mirrored pattern: with a low but almost constant concentration from the surface down to the depth of 30 cm. Total DIC production beyond this depth was 183 $mmol C m^{-2}d^{-1}$ and was majorly driven by the relatively rich buried OM below the former interface. As for other compounds, the presence of a subsurface peak in the model is noteworthy. The model-calculated correlation between porewater SO_4^{2-} and DIC indicates that the additional flood deposition induced an enhanced DIC due to the complete exhaustion of SO_4^{2-} and a growing importance of methanogenesis ($20 mmol m^{-2}d^{-1}$), especially just slightly below the zone of sulfate depletion (45 cm) (Figure 4.5).

4.4.2.3 Cenevol flood deposition (fall 2008)

The contrasting flood deposition observed in the fall of 2008 and the subsequent evolution of the sediment and porewaters, were well-reproduced by the model. One month after the flood, oxygen penetrated down to a depth of 9.6 mm with stronger oxygen demand due to the labile nature of the deposited OM. The total oxygen uptake rate calculated by the model during this fall flood was higher ($21 mmol O_2 m^{-2}d^{-1}$) in comparison to the spring deposition. DIC increased with depth, with the model matching the spatial variation of the measured

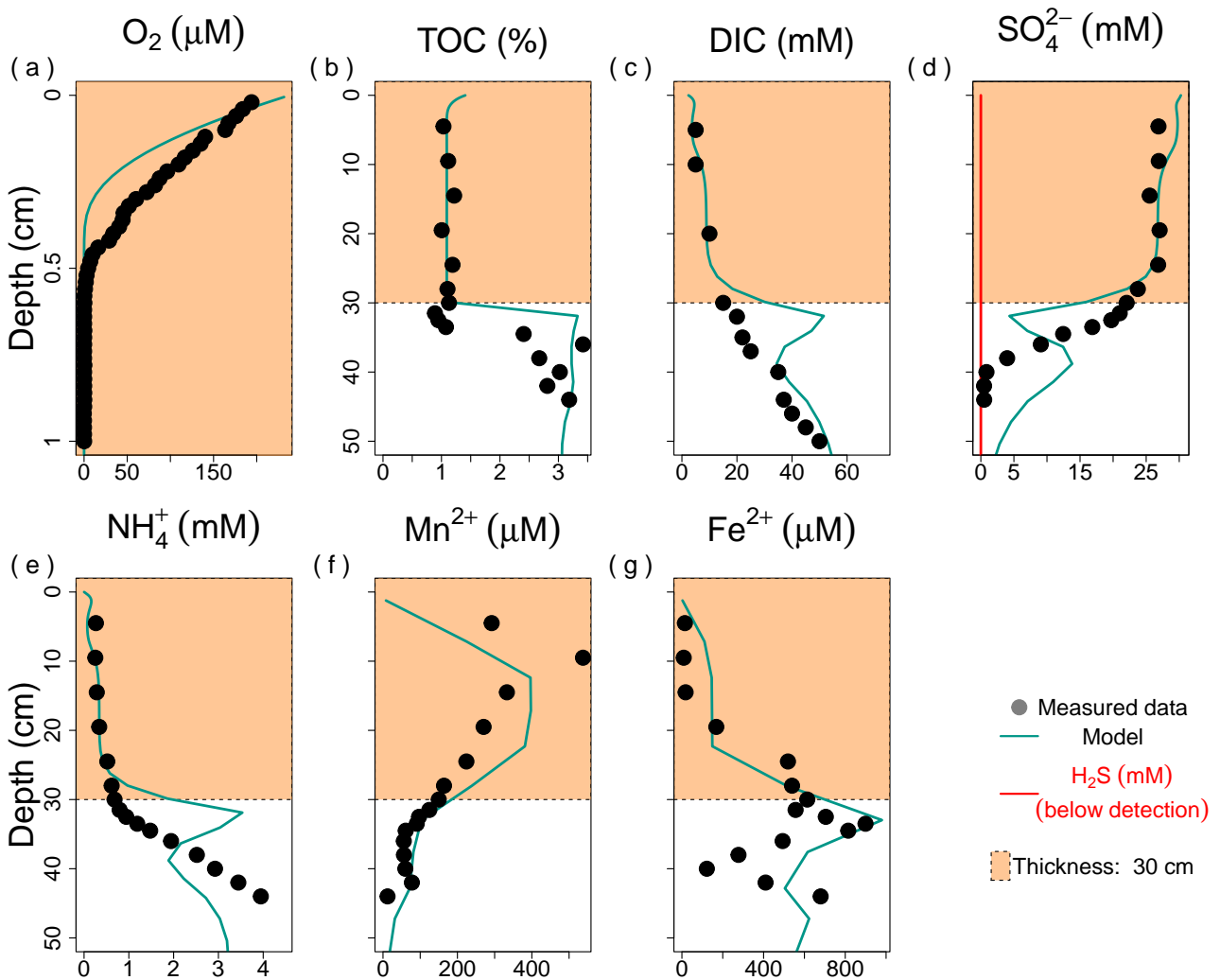


Figure 4.5: Model data fit against observed data for (a) Oxygen, O_2 (b) Total organic carbon, TOC (c) Dissolved inorganic carbon DIC (d) Sulfate SO_4^{2-} (e) Ammonium NH_4^+ (f) Dissolved manganese Mn^{2+} (g) Dissolved iron Fe^{2+} (h) Hydrogen sulfide H_2S during the May/June flood. Data were collected the 6th of June 2008 at Station A. The orange section represents the new flood deposit.

porewater DIC. The sulfate concentration decreased from 30 mM at the SWI to about 15 mM at a depth of 10 cm (Figure 4.6). During this period, sulfate reduction accounted for 94 % with flood-induced mineralization rate of 450 $mmol\ m^{-2}\ d^{-1}$. Below this gradient, SO_4^{2-} was largely constant with porewater concentration of 15 mM (Figure 4.6).

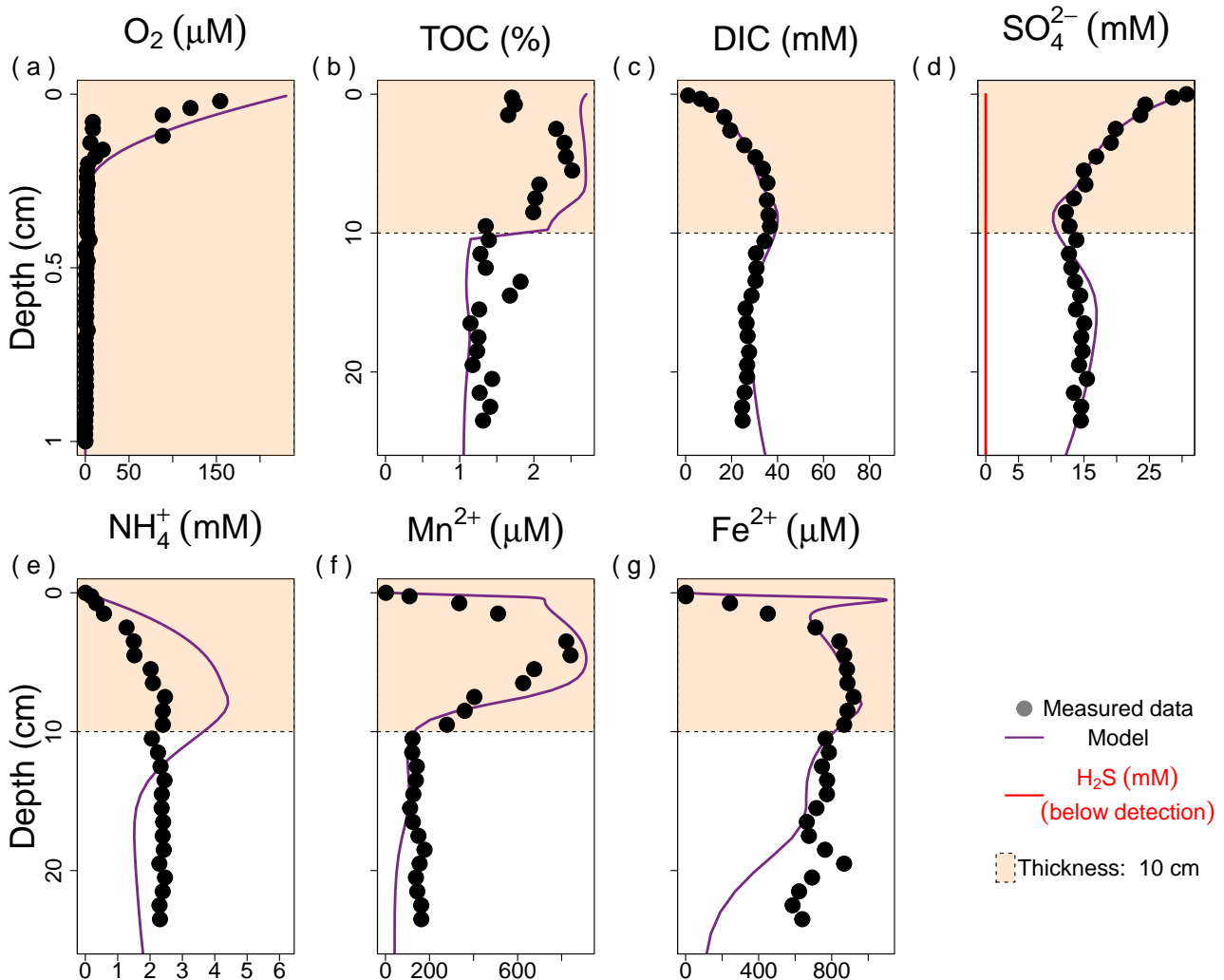


Figure 4.6: Model data fit against observed data for (a) Oxygen, O_2 (b) Total organic carbon, TOC (c) Dissolved inorganic carbon DIC (d) Sulfate SO_4^{2-} (e) Ammonium NH_4^+ (f) Manganese Mn^{2+} (g) Iron Fe^{2+} (h) Hydrogen sulfide H_2S during the November/December flood collected the 8th of December 2008 (26 days after the flood event - 11th of November 2008) at station A.

4.4.2.4 Fe-Mn cycling under episodic flood event

The difference between the flood deposits of the spring and fall floods can also be revealed in the distribution and concentration of dissolved iron and manganese. In general, when compared to the measured porewater profiles during the spring flood, the model simulation in the fall event moderately reproduced the vertical structure of the data and suggest a transiently, non-steady state condition of the dissolved Fe and Mn. In order to simulate this different flood deposit, a fixed particulate oxide flux of 50 and 10 $mmol\ m^{-2}\ d^{-1}$ for iron and manganese respectively was imposed in the model upper boundary. The availability of this particulate Fe and Mn as well as organic carbon generates a release of dissolved metal in the porewater. Our model simulation indicates that at the time of sampling in June 2008, the peak Mn concentration had already migrated from a depth of 30 cm (below the newly deposited layer) to around 10 cm where the observed Mn maximum was detected (Figure 4.5).

At this particular depth of 10 cm, the model matches the trend but not exactly the amplitude of the observed variation (data - 537 vs model - 399 μM). Below this reactive front, Mn decrease with depth was observed and simulated. Both the measured data and model prediction suggest a complete exhaustion of MnO_2 and negligible release of dissolved Mn at depth.

In contrast, dissolved Fe in the spring flood period was comparatively low at the surface in the measured data and increased with depth to a concentration of 980 μM at the former SWI (now buried underneath the deposited layer) (Figure 4.5). In this zone, non-steady dynamics was simulated by the model as can be seen in Figure 4.5, probably driven by a combination of diagenetic processes involving microbial iron oxide reduction, dissolved sulfide reoxidation by Fe oxides and FeS precipitation Equation 4.2. This geochemical horizon in the subsurface layer where dissolved Fe is maximum only migrate slowly and persist for a longer period after the spring flood deposition.

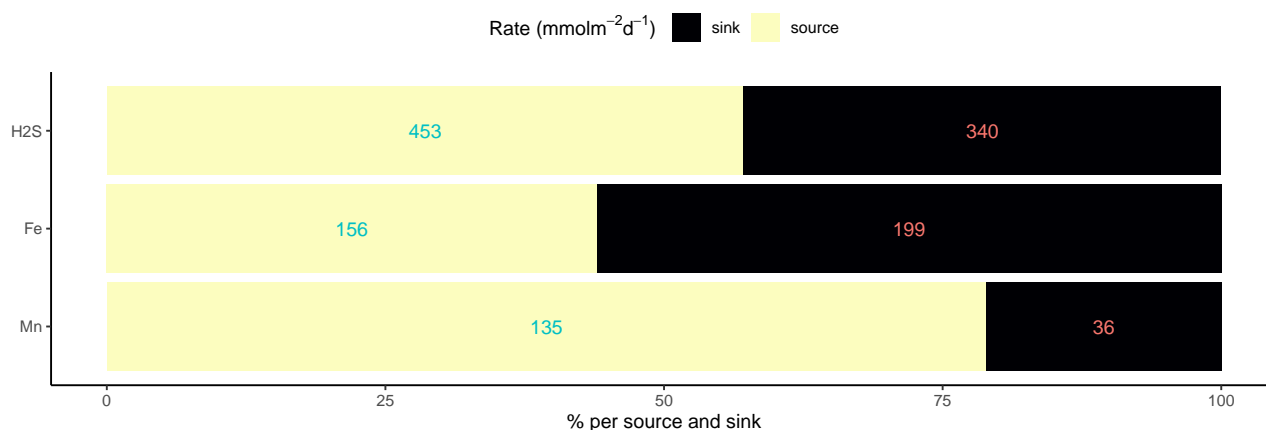


Figure 4.7: The geochemical balance between source and sink for Fe^{2+} , Mn^{2+} and H_2S for fall flood event. The value inside the bar represents the vertically integrated time-snapshot rate.

In the fall flood, a different vertical profile of the reduced metabolites emerged. Like the measured data, the model predicted a sub-surface Mn peak of 912 μM within the vicinity of 5 cm which shows a good correspondence with the data (840 μM). Dissolved iron (Fe^{2+}) gradually increased from the surface up to 834 μM at 5 cm in contrast with the spring flood where dissolved iron was confined below the new flood layer. This gradient in measured and simulated Fe^{2+} data stabilized to this asymptotic concentration albeit with a tendency of a slight departure from the model (Figure 4.6). Comparison of combined source and sink of the biogeochemical rate involving iron corresponding to the time of fall sampling (8th December 2008), indicates that the source term for iron contribute to a total depth integrated rate of 156 $\text{mmol Fe m}^{-2} \text{d}^{-1}$ compared to the sink (199 $\text{mmol Fe m}^{-2} \text{d}^{-1}$) (Figure 4.7). On the other hand, the source of Mn (135 $\text{mmol Mn m}^{-2} \text{d}^{-1}$) was by far greater than the sink (36 $\text{mmol Mn m}^{-2} \text{d}^{-1}$) (Figure 4.7).

The source of these metals in porewaters is linked to the reduction of iron and manganese oxides which differs from the other oxidants utilized because of the relative importance of microbial-mediated and chemical reduction pathways. The depth-integrated rate of microbial iron reduction during the spring flood event (39 $\text{mmol Fe m}^{-2} \text{d}^{-1}$) was lower than in the fall (44 $\text{mmol Fe m}^{-2} \text{d}^{-1}$) while microbial manganese reduction varies little across time but chemical Mn reduction was three times higher in the fall (45 $\text{mmol Mn m}^{-2} \text{d}^{-1}$) compared to spring (19 $\text{mmol Mn m}^{-2} \text{d}^{-1}$). The model calculation suggests that more than two-third of the depth-integrated reduction of FeOOH during the spring deposition is due to the chemical oxidation of H_2S (83 $\text{mmol Fe m}^{-2} \text{d}^{-1}$) while it increased to 82 % during the fall flood event (207 $\text{mmol Fe m}^{-2} \text{d}^{-1}$). This

is linked to the internal cycling involving changes in redox state of Mn and Fe.

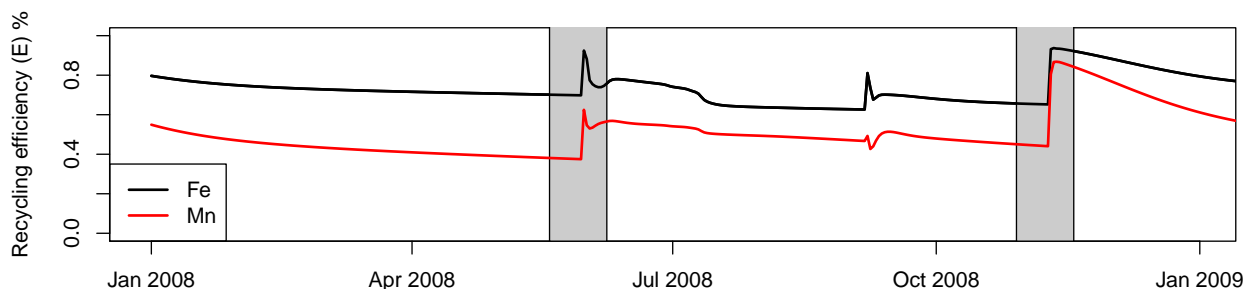


Figure 4.8: Temporal evolution of recycling efficiency of the metals (iron and manganese) in the sediment. Increasing efficiency numbers imply that the sediment has a high recycling capacity, with a limiting value of 1 indicating that ions cycle only between oxidized and reduced forms inside the sediment without external inputs. The gray bar indicates the time of the flood deposition.

This redox cycling in the sediment can be quantified using the recycling efficiency number, E^i (Equation 4.7) (Rabouille and Gaillard 1991; Wang and Van Cappellen 1996) adapted for a time dependent model:

$$E^i = \frac{R_{red}^i}{J + R_{red}^i} \quad (4.7)$$

where R_{red}^i is the depth integrated rate of Fe or Mn reduction at each time point, i and J is the deposition flux of reactive metal oxides. Values near 1 indicate a very strong internal cycle, whereas values below 0.2 indicate flux dominated metal oxide reduction. Using this calculation, the model suggested that the sediment reactivity is under intense recycling in both flood events (> 0.5) especially after the flood deposition. In this case, the efficiency number jumps from 0.7 to 0.92 for Fe and 0.38 to 0.62 for Mn in the spring. The recycling potential was slightly higher during the fall flood event for both Mn and Fe (0.87 and 0.94 respectively) compared to the Spring flood (Figure 4.8).

4.4.2.5 Mineralization pathways and biogeochemical fluxes

Following calibration of the model with the data, we extracted timeseries fluxes of dissolved species across the SWI, as well as calculated vertically integrated rates.

4.4.2.5.1 Exchange across the sediment-water interface

The model indicates that a reduced oxygen consumption follows the introduction of the 30 cm deposit of the spring flood as observed by the oxygen flux across the SWI. Model sediment O_2 flux declined from 18.43 to 8.4 $mmol O_2 m^{-2}d^{-1}$ immediately after the first major deposition; rebounding back within 15 days to its pre-flood level. It is worth noting that this range of O_2 flux encompasses the measured flux snapshot (see: Section 4.4.2.2 and Figure 4.9). The fall perturbation induced a 39 % increase in oxygen flux which relaxes in 40 days. Oxygen consumption was dominated by oxic mineralization accounting for 76 and 71 % of the total oxygen consumption during the spring and fall flood event respectively. Aerobic oxidation of methane doubled between the spring and fall flood accounting for 0.3 and 2 % respectively. This shift in methane reoxidation is

caused by the dynamic modification of the sediment, which results in a greater amount of CH_4 produced by different flood types.

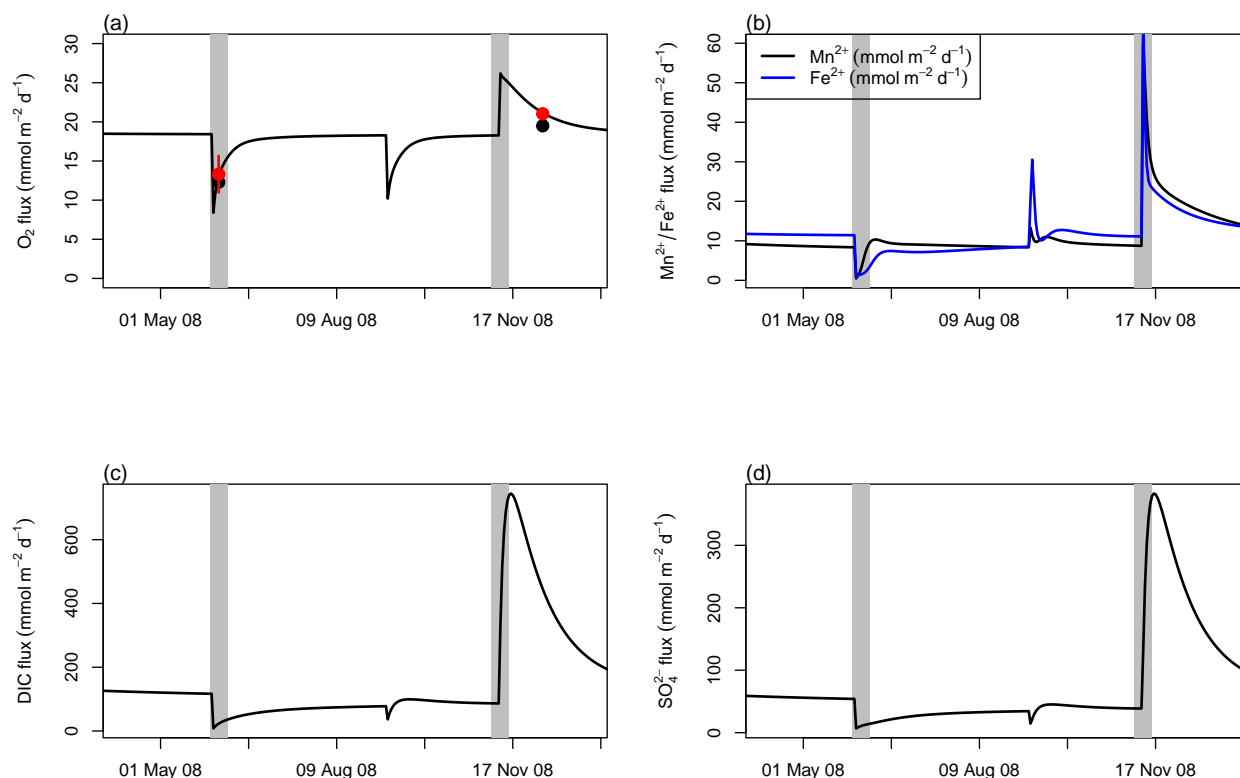


Figure 4.9: Temporal magnitude of flux (in absolute value) across the sediment-water interface for (a) Oxygen (b) iron and manganese (c) DIC (d) Sulfate. Black dot in O_2 flux signifies measurement made during this sampling point while red dot is the model equivalent as the measured sampling date. Vertical error bar represents the flux uncertainty in the exact date when this flood occurs. Flux for DIC, Iron and Manganese are directed out of the sediment while Sulfate and Oxygen flux are directed into the sediment. The gray bar indicates the time of the major flood deposition

Over the same interval, the flux of SO_4^{2-} into the sediment follows the same pattern as above but with a larger increase during the fall flooding where SO_4^{2-} exchange across the SWI first jumped to a very high values ($\times 7$), then decreases, thus temporarily increasing the overall sediment stock of SO_4^{2-} with an increased consumption afterwards. Throughout the simulation period, the sediment was a source of DIC for the bottom water. The DIC exchange showed a strong contrast between the two floods: during the spring depositional event, the DIC flux dropped to a very low value ($139 \text{ mmol C m}^{-2}d^{-1}$ to $8 \text{ mmol C m}^{-2}d^{-1}$) whereas it jumped to a much higher efflux estimated after the fall flood ($745 \text{ mmol C m}^{-2}d^{-1}$) (Figure 4.9).

The magnitude of dissolved Fe and Mn release associated with the spring flood deposit was weakened. In contrast, the sediment acted as a strong source of dissolved Fe and Mn to the bottom water during the fall which can be driven by the reduction of freshly supplied oxides. As this new layer is smaller in thickness in the fall (10 cm), the diagenetic transformations of OM and associated oxides result in an instant enhancement of the sediment inventory of dissolved Fe and Mn (Figure 4.9). A burst in Fe and Mn release was simulated immediately after the deposit, which quickly rebounds to its background flux of $11 \text{ mmol Mn m}^{-2}d^{-1}$. For manganese, this stock of reduced metabolites was quickly re-oxidized within the sediment.

4.4.2.5.2 Temporal evolution of biogeochemical pathways

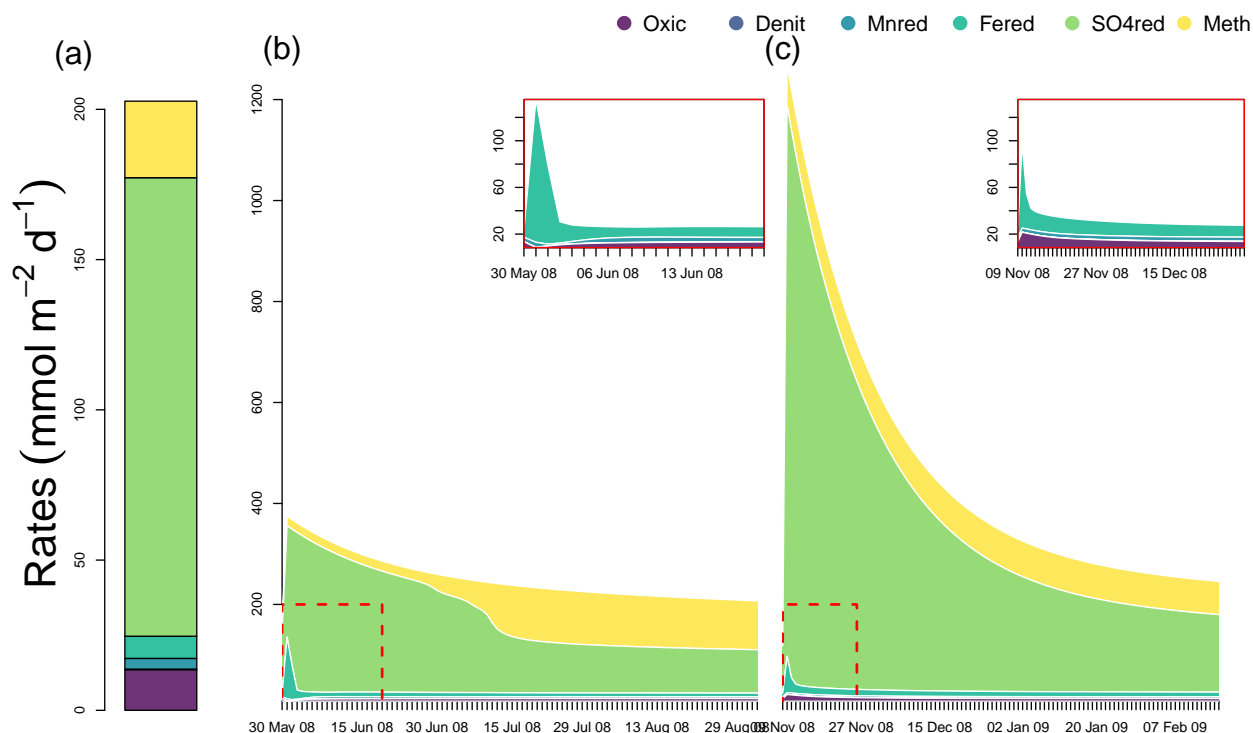


Figure 4.10: Dynamic evolution of total organic carbon mineralization rate. (a) steady state of total organic carbon mineralization rate and different portion of the mineralization pathways. Oxic = aerobic mineralization, Denit = Denitrification, Mnred = Mn oxides reduction, Fered = Fe oxides reduction, SO4red = Sulfate reduction, Meth = Methanogenesis. (b and c) Dynamic evolution of total organic carbon mineralization rate and relative importance of the carbon biogeochemical pathways following the successive flood in spring (b) and fall (c) period. The beginning date is the day of major flood deposits for each event. The insert zooms in on the pathways with lower carbon mineralization rate.

The dynamics of the TOC mineralization and the partitioning in the different biogeochemical pathways are shown in Figure 4.10. Before the event, the pre-flood sulfate reduction (75 %) was the dominant mechanism of carbon oxidation, with minor contribution from aerobic respiration (7 %) and methanogenesis (13 %). The contribution from metal reduction was equally low (3 %). During the first 10 days after the spring flood deposition, oxic mineralization dropped to 5 % with similar marginal change in metal reduction. After this initial drop, aerobic respiration increased up to pre-flood level and stabilized. Similar asymptoticity of reaction rate was observed in metal reduction at short interval after the deposition.

The most remarkable change occurring during this flood is observed in the change in anoxic contribution to carbon mineralization rate (sulfate reduction and methanogenesis). The model simulated 50 % increase (227 $mmol\ m^{-2}\ d^{-1}$ versus 151 $mmol\ m^{-2}\ d^{-1}$) in sulfate reduction from its pre-flood rate due to the perturbation while methanogenesis doubled as a result of the deposition (Figure 4.10). About 20 days after this spring perturbation, both pathways for total carbon mineralization begins to decline as the signature of the deposition begins to wane. Beyond two months, methanogenesis becomes more prominent equaling the contribution of sulfate reduction.

In fall, the large delivery of labile OM produces the greatest change in sulfate reduction (increased from 94 to more than 1000 $mmol\ m^{-2}\ d^{-1}$) and although the rate of methanogenesis almost doubled, the contribution of methanogenesis to total mineralization declined by six-fold from its pre-flood level (Panel b 41 % to 7 % Panel c). During this fall flood, only minor changes in aerobic mineralization as well as metal reduction were

simulated except in the very first days.

4.4.3 Numerical experiment: Memory effect of flood deposition on biogeochemical processes

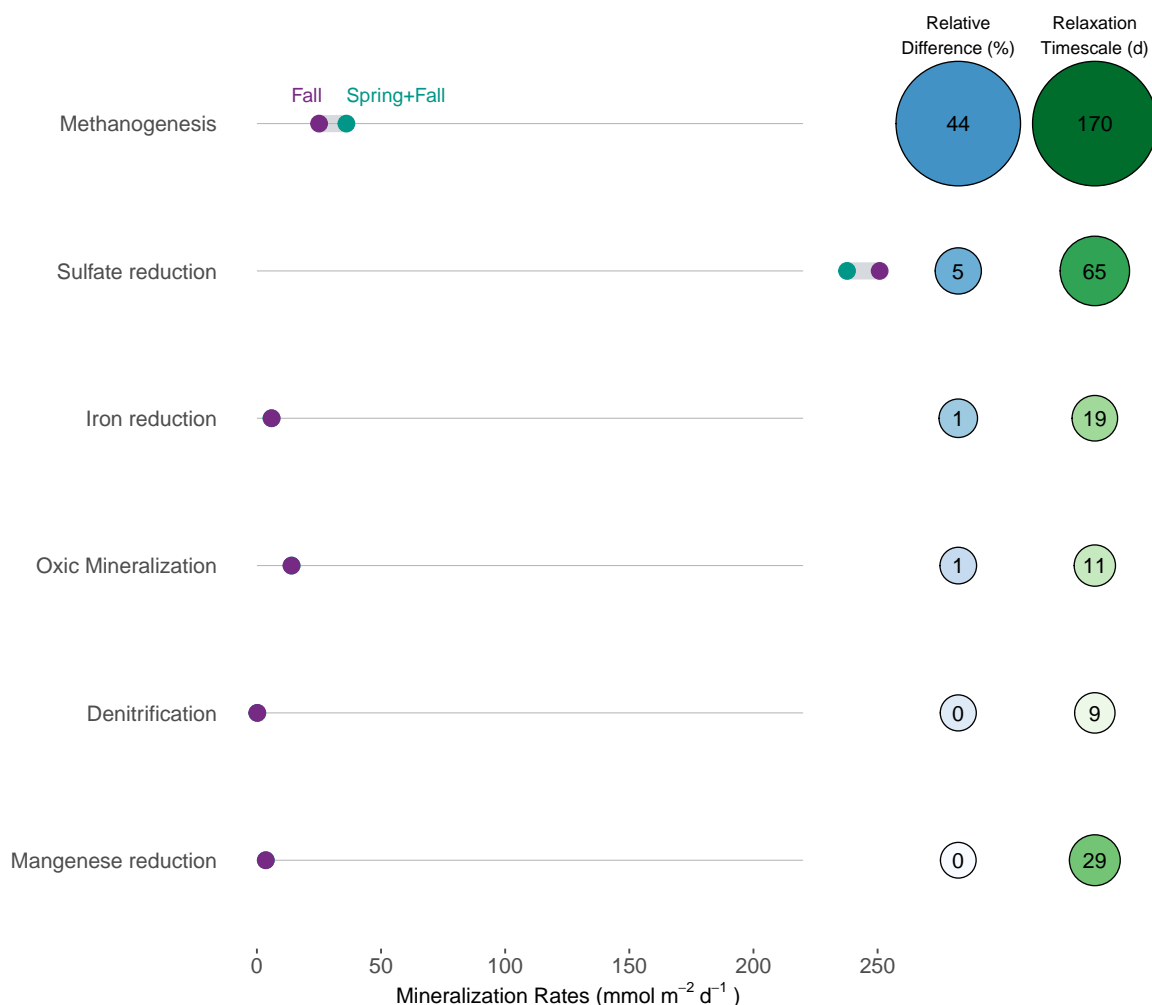


Figure 4.11: Differential 'memory effect' of flood deposition on biogeochemical pathways of carbon. This is calculated as the relative difference between a reference simulation with both spring and fall flood versus another simulation with only the fall flood (green dots) deposition (purple dots).

We examine the effect of cumulative floods (spring and fall) compared to a single fall flood. The memory effect is the relative difference of the cumulative fluxes for the two scenarios (see methods). Results from this analysis show that within the time window after the event, the residual effect of the first flood on biogeochemical pathways is large for the anoxic pathways but limited for the other pathways. The succession of two floods lead to limited increase/decrease of mineralization rates for all oxidants between the spring+fall floods scenario compared to second flood (fall event) alone. Our results indicate that methanogenesis has the largest of the residual effect of the flood with memory-induced influence of 44 %. Aerobic mineralization rate shows little sign of memory effect of the flood deposition (Figure 4.11). In similar manner, the relaxation timescale calculated for these processes in the first scenario shows that the recovery period ranges from 6 months for methanogenesis and less than 2 weeks for oxic mineralization.

4.5 Discussion

In RiOMar systems prodeltas and depocenters are zones of rapid accumulation of sediment along the continent-ocean interface that are typically of terrestrial origin (Blair and Aller 2012). The quantity and quality of sediment deposited in these depocenters are determined by a variety of parameters, including precipitation pattern in the watershed and river discharge, river network and size, and the sedimentological composition of the watershed from which it originates (Aller 1980; Chakrapani 2005). As a result, the materials deposited in the river-ocean margins reflect the source and transit path taken, and so differ in the properties of organic matter supplied in the majority of depocenters (LaRowe et al. 2020).

The amount of organic matter deposited near the river mouth in the Rhône prodelta varies with the flood type. The component of the material deposited in 2008, for example, distinguishes the spring flood from the fall flood (Cathalot et al. 2010). In comparison to the fall flood, which was characterized by labile OM with enriched $\Delta^{14}C$ (Cathalot et al. 2013), the spring consists primarily of refractory debris with depleted $\Delta^{14}C$ (-500 ‰) whereas the fall flood has $\Delta^{14}C$ of -90‰, indicating a mix with labile organic matter. These disparities in OM properties can lead to distinct sediment responses, as evidenced by discrepancies in porewater profiles. The difference is reflected in the model by the carbon enrichment factor (α) imposed in both events, with a greater value in the fall compared to the spring (Table 4.3), indicating that the organic matter delivered during these events can have significantly different features. However, this relationship is not known and certainly complex as other factors like deposit thickness might influence sediment dynamics in response to flood deposition (Nmor et al. 2022). Here we discuss the implication of these flood event deposition and their types on the biogeochemical processes in the sediment.

4.5.1 Early diagenesis of Rhône prodelta sediments

The Rhône prodelta sediment is a highly dynamic environment driven by episodic flood discharge. This flood-driven phenomenon delivers considerable amounts of sedimentary materials which drives the biogeochemical characteristics of the zone. Integrating observed data with numerical modelling as done here sheds light on the different diagenetic processes that operate during periods of flood-induced organic matter input. However, this data-driven modelling approach can only be validated by the fidelity of the model in capturing the observed trend and variability present in the data. In this study, we provide some objective metrics to assess the skillfulness of the numerical model in reproducing the spatio-temporal pattern of the dataset (Figure 4.3). Our findings demonstrate that the model porewater profile for sulfate, DIC and manganese were well represented in both flood events in term of their adjustments to the data as well as the variability with depth.

In contrast, despite their correlation with the data, the overall model skillfulness of the simulated results for ammonium and iron during spring deposition is less impressive. This is especially true for iron, where the vertical variability of the porewater profile suggests a system still in the process of slow evolution that is tightly coupled to other cycles (Figure 4.5). With more data constraints for such evaluation (i.e. FeOx and MnOx deposition flux and reactivity), the model's performance could be improved through better characterization of the Fe dynamics during this time period. The lesser known dynamics and forcings (transient phases, OM lability) at the start of the perturbation, as well as the uncertainty about when this specific event occurred, may also be responsible for the bias in the May-June flood. Furthermore, our preliminary test carried with and without the inclusion of an intermediate flood deposition (around September) between the two events highlights the important of data coverage and timescale of investigation for capturing the key features of the interstitial

porewater signature arising from this type of event (Romans et al. 2016).

Moreover, the model-data assessment showed much better fit in the fall flood suggesting that the model is not far off from describing the general pattern in sediment dynamics during this flood year. Furthermore, the O_2 flux temporal patterns have been well-studied in this region in 2008 and shows temporal variability linked to extreme events (Cathalot et al. 2010). Our model O_2 flux (accounting for both diffusive and irrigative flux) in both flood event slightly overestimate the observed diffusive oxygen uptake (DOU) flux reported in Cathalot et al. (2010) and Pastor et al. (2018) for this particular prodelta site but much closer to the average TOU observed in this site (about $24 \text{ mmol C m}^{-2} \text{ d}^{-1}$) (Lansard et al. 2008, 2009b; Pastor et al. 2011b). This range of oxygen flux compared favorably to other RiOMar systems characterized by high sedimentation rate and particulate carbon flux: Amazon delta ($6 - 25 \text{ mmol C m}^{-2} \text{ d}^{-1}$ Aller et al. (1996)), Mississippi delta ($2 - 56 \text{ mmol C m}^{-2} \text{ d}^{-1}$ Morse and Rowe (1999)) and other coastal areas with pulse cycle of resuspension and deposition such as in Göteborg harbour, Sweden ($8 - 23 \text{ mmol C m}^{-2} \text{ d}^{-1}$ Tengberg et al. (2003)), Gulf of Finland, Baltic sea ($5 - 20 \text{ mmol C m}^{-2} \text{ d}^{-1}$ Almroth et al. (2009)), Gulf of Mexico ($7 - 50 \text{ mmol C m}^{-2} \text{ d}^{-1}$ Moriarty et al. (2018)).

Within the Rhône prodelta, the sediment biogeochemical dynamics is closely coupled to the underlying transport and biogeochemical changes linked to massive depositional event. As in the case described in the fall flood, a strong oxygen consumption ensued in the first few days after the events via immediate degradation of organic carbon driven by oxic mineralization. Our model in agreement with the data showed substantial temporal variability in the O_2 flux driven by the variability in organic carbon input associated with the flood event. Especially, the lowering of O_2 fluxes observed after the spring flood is well represented by the model. Organic carbon mineralization in general was dominated by sulfate reduction in both spring and fall events. In both cases, the total mineralization increased by a factor of 2 in spring and 7 in winter reflecting the amount and lability of the OM deposited with a much larger increase to the total carbon mineralization during the fall depositional event compared to the spring one. During the spring event, a significant portion of the total mineralization was induced at the old sediment-water interface where a layer of degradable organic matter was buried by the flood deposit. This layer is located at 30 cm depth after the flood, therefore lowering the transfers at the present sediment-water interface. This organic-rich material fuels the intense subsurface sulfate reduction. Similar trapping and enhanced biogeochemical activities have also been reported in flooded organic rich sediment in the Saguenay fjord (Deflandre et al. 2002; Mucci et al. 2003).

This trend, however, was in contrast with the fall flood where the majority of the mineralization took place in the first 10 cm of the sediment. This is the result of the deposition of organic-rich material during this fall flood. As a result of this dissimilar pattern, DIC production revealed that with organic-rich sediment deposition, particularly during the fall period, a strong DIC efflux across the sediment-water interface ($445 \text{ mmol DIC m}^{-2} \text{ d}^{-1}$) can be expected. On the contrary in spring, recycling is internal (below the 30 cm flood layer) and leads to reduced exchange with the water column. While benthic release of DIC in this proximal zone of the Rhône delta is not as frequently measured as oxygen flux (and especially in the flood period), reported measurement estimate that DIC flux ranges between 18 and $78 \text{ mmol DIC m}^{-2} \text{ d}^{-1}$ before the usual flood season of late summer (Rassmann et al. 2020). As the model is dynamic in time and linked by successive episodic flood event, an hindcast of DIC flux before this flood season showed better correspondence ($55 \text{ mmol DIC m}^{-2} \text{ d}^{-1}$) with reported values for this site.

Short term dynamics in manganese and iron redox cycling was assessed with the model constrained by the available data and empirical observations at this proximal site. The porewater chemistry in the prodelta was

altered by the spring (generalized) and fall (evenol) floods, with differing responses for Mn and Fe. Model Mn oxides reduction rate was estimated around $26 \text{ mmol Mn m}^{-2} \text{ d}^{-1}$ in the spring compared to 52 in the fall. Chemical reduction via oxidation of sulfide accounted for about 72% while microbially mediated reduction of organic carbon accounted for 28% during the spring deposition. The latter had a much lower contribution in fall (14%) despite having a slightly higher organoclastic Mn reduction rate compared to the spring event with a stronger contribution by H_2S oxidation via Mn oxides. This fall enrichment of dissolved Mn in the upper sediment layer (up to $800 \mu\text{M}$ Figure 4.6) is driven by the strong imbalance between the sources and sinks (Figure 4.7) resulting in its unique shape with the contribution from the reoxidation of dissolved Fe^{2+} by MnO_2 as the major driver. In contrast, dissolved iron porewater profile is primarily controlled by the reoxidation of sulfides (68 %). However, in the fall event, this large iron release is balanced in deeper layers by precipitation to a stable form of FeS and lost by burial to deeper layers. This dynamic diagenetic balance could be responsible for the peculiarity of the observed pattern of the dissolved iron profile (Figure 4.5). Indeed, other previous studies in the Rhône prodelta have alluded to this routing of iron-sulfide precipitation as a possible mechanism for the maintenance of the observed ferruginous condition and the alkalinity fluxes (Pastor et al. 2018; Rassmann et al. 2020).

Furthermore, recent research by Van de Velde et al. (2020) has demonstrated that oscillating redox circumstances can affect remineralization processes where a dominating Fe state with regard to sulfide can occur due to the sediment's inherent bistability. This bistability condition is determined by the particulate carbon to iron input ratio. In our example, with significant carbon (Pastor et al. 2011a; Ait Ballagh et al. 2021) and iron flux (Marin and Giresse 2001; Radakovitch et al. 2008; Roussiez et al. 2011), this ratio is 5, and such Fe-rich and sulfide-free condition is observed, as theoretically predicted by Van de Velde et al. (2020) when combined with kinetically fast FeS formation as in the natural environment. Thus, our results highlight the suggested possibility of chemical reduction of the metal oxides as well as precipitation of FeS (and subsequent pyrite formation) (Pastor et al. 2011a; Rassmann et al. 2020). These secondary reactions (especially chemical reduction of manganese oxide by reduced iron) may help explain the elevated Mn^{2+} concentration in the sediment after both floods with higher values in the fall (Pastor et al. 2018).

In general, the high metal reduction is a consequence of two factors: Firstly, the large deposition of terrigenous materials linked to high sedimentation rate and possibly large concentrations of reducible iron terrestrially transferred to this depocenter (Roussiez et al. 2011; Pastor et al. 2018) as implied by the relatively higher α value imposed in November deposit in order to simulate such observed trend. Secondly, the importance of secondary reactions involving cycle of Fe and Mn as an efficient metal cycling in the area (Figure 4.8). This view of metal cycling has also been previously suggested to be responsible for the rapid recycling of manganese and iron in the seafloor (Rabouille and Gaillard 1991; Van Cappellen and Wang 1996; Wang and Van Cappellen 1996). These two factors could be critical in sustaining the porewater profiles of the dissolved species as observed in Figure 4.5 and Figure 4.6 and the absence of $\sum H_2S$ in the porewater (Pastor et al. 2011a). This modelling insight on the role of combined factor in redox cycle of metals is also supported by observation in other dynamic sedimentary systems subject to episodic of flood events (Blair and Aller 2012).

4.5.2 Implication of extreme flood deposition in biogeochemical cycle

As discussed previously, river dominated margins serve as retention zones for riverine borne particulate matter and are subject to both anthropogenic and natural perturbation (Dai et al. 2022). These extreme events bring large quantities of sediment within a short timeframe which has the possibility to induce changes in the biogeo-

chemical properties of the sediment. In the Rhône River prodelta, the annual flood can deliver up to 5.4×10^6 tons of sediment in 10 days period (Antonelli et al. 2008). This large volume of sediment delivered is also seen in similar river systems with rapid sedimentation of riverine materials: Pô river flood in 2007 (Miserocchi et al. 2007), Saguenay Fjord, Canada (Mucci and Edenborn 1992; landslide - Deflandre et al. 2002). Thus, the introduction of these new materials can affect not only the carbon cycle but also the other elemental cycles such as iron and manganese as demonstrated in this paper.

Under this flood regime, biogeochemical processes undergo sudden change linked to biogeochemical conditions in the sediment. For example, the oxygen flux decreases by 55 % during the spring flood event and depending on the prevailing characteristics of the particulate input, strongly anoxic condition with greater propensity for methanogenesis can be induced. Our result shows that this is the case for pathways affecting the carbon cycle where sulfate reduction and methane production can double or even quadruple at short time interval following these massive sediment depositions. The substantial changes in carbon mineralization results to enhanced DIC production and can have a considerable effect on DIC flux across the sediment-water interface. Our findings reveal that the intensity of DIC exchange varies with the flood type, with a much higher flux of DIC in the fall compared to the spring, reflecting the contrast in the nature of materials deposited. Such abrupt changes in the recycling of carbon in the sediments has been observed in other region where the seafloor is disturbed by anthropogenic forcing such as disposal activities and dredging where average OC mineralization rate can be enhanced by a factor 2.5 Van de Velde et al. (2018).

Furthermore, the difference in DIC flux simulated by these floods indicates that different carbon cycling mechanisms are at work in the deposited materials. The spring deposition resulted in slow internal production and porewater storage of the DIC, possibly due to the mineralization of trapped reactive materials buried beneath the newly deposited refractory layers, resulting in a decrease in exchange across the SWI. Mineralization of carbon-rich OM in the fall resulted in a significant increase in DIC release in the flood layer and an increased exchange with the bottom water. These two dissimilar responses demonstrate that these floods might have a diverse impact on material exchange with the water column, which has a considerable impact on coastal carbon dynamics (Cai 2011; Bauer et al. 2013).

In addition, the sediment acting as a bioreactor for exchange of flux of dissolved metals can change depending on the characteristics of the flood type: serving as a large source of iron and manganese during the organic-rich fall flood event and a reduced to insignificant source during the spring flood that is characterized mostly of refractory material. This exchange of flux when coupled to other elemental pathways, such as phosphate can play a role in the retention and mobilization of phosphorus in marine sediment (Reed et al. 2011; Slomp et al. 2013). Massive sediment deposition can also trigger changes in metal recycling efficiency of the sediment. This can result in a diagenetic response of iron and manganese which has consequences on the long-term fate of their respective cycle. For example, metal reduction during non-steady state condition have been shown to be a source of dissolved organic carbon accumulation (Deflandre et al. 2002). Furthermore, some of the reduced Fe within the sediment column is sequestered with sulfides which can be critical for the perennial burial of sulfur in the sediment (Jørgensen et al. 2019). This might be the case in deltaic systems connected to river mouths which are dominated by anoxic diagenesis, with intense sulfate reduction and iron oxide reduction which generates an efficient precipitation and burial of FeS/FeS_2 . This is actually the scenario for the Rhône prodelta sediment. This precipitation of particulate FeS (FeS_p) have also been detected in the proximal and prodelta stations which indicates that the immobilization of iron bound sulfide could well be active in this sediment and be related to a large alkalinity release (Rassmann et al. 2020). Flood inputs can deeply modify the internal

Fe/S cycling, favor FeS production and contribute to reduced species burial, thus controlling alkalinity fluxes to the water column (Rassmann et al. 2020).

4.5.3 Interaction between successive floods

As our understanding of rapidly accumulating sedimentary system continues to improve as a result of better observing systems (Viollier et al. 2003; Maillet et al. 2006; Toussaint et al. 2014; Zebracki et al. 2015) and greater appreciation for the non-stationarity in benthic biogeochemical processes (Mucci et al. 2003; Tesi et al. 2012; Pastor et al. 2018; Nmor et al. 2022), the influence of successive depositions of OM materials via these extreme flood events needs to be investigated. One widely recognized consequence of this phenomenon is the decoupling of oxygen consumption from carbon mineralization during transient flood condition (Aller 1998). Another ramification of this back-to-back occurrence of flood deposition is the cumulative impact induced on the biogeochemical processes. This is demonstrated in our experimental simulation Figure 4.11 where the co-occurrence of sequential flood deposition initiates a temporal lag in the carbon mineralization pathway. Interestingly, the memory effect is visible only for the slow relaxing species (methane). For sulfate, the memory effect is limited because its relaxation time nears 5 month which is the interval between the two floods in 2008.

The successive use of terminal electron acceptors for the breakdown of organic matter in the sediment appears to have an intriguing side effect related to these series of flood and follows in the opposite direction of their energy yield (Froelich 1988). As such, anaerobic processes (methanogenesis and sulfate reduction) have a longer memory lag brought forth by the sediment deposition. This might be the case because the activities involving this pathway take place significantly deeper in the sediment generating a longer relaxation time dictated by their longer diffusive time (Nmor et al. 2022). Such timescale-dependent recovery of the mineralization pathways has also been attributed to either the depletion of electron acceptors or colonization due to microbial community (Van Velde et al. (2018)). In general, our results show that episodic events such as those observed in the Rhône prodelta and other similar regions can lead to transient states within a perturbation window (Velde et al. 2018). Although in the scenario explored here, the interval between the flood input are far apart for the effect to be consequential and thus the system might have been reset Figure 4.11. The possibility of this “memory effect” on the carbon mineralization pathways and even in other cycles will therefore raise a pertinent question: To what extent does increasing frequency and magnitude of the flood deposition influence the biogeochemical functioning of the coastal sediment especially in the context of changing environmental forcings? Further investigation on the role of this flood-modulated interaction should be conducted to ascertain the biogeochemical implication of this phenomenon.

4.6 Conclusion

Floods in the river-ocean continuum can deposit sediment materials of several tens of centimeters in a short period of time. As particulate OM is tightly coupled to carbon mineralization in the Rhône River prodelta sediment, this study focuses on two unique flood depositions with variable sediment characteristics, resulting in distinct biogeochemical responses. The labile nature of the OM provided during the 2008 fall season leads in increased oxygen consumption when compared to the spring flood. The porewater profile of sulfate and DIC also vary between the two flood periods, indicating a differing degree of oxidation of organic carbon. Furthermore, total carbon oxidation, which is dominated by sulfate reduction, was much higher in the fall than in the spring. The different nature of the two floods (thick organic-poor in spring versus thin organic-rich in fall) induced opposite

effects on DIC release from sediments with burst of DIC release in the fall versus a decrease in spring. This highlights the importance of internal vs near surface recycling of carbon in controlling the solute exchange across the SWI. Despite the substantial sulfate reduction, no dissolved sulfide was detected in the porewater, indicating strong precipitation with Fe and, eventually, reoxidation with manganese/iron oxides. The model supporting this paradigm emphasizes the involvement of secondary redox mechanisms (representing > 75% of metal reduction) in sustaining the observed profiles in both flood situations. In addition, the sequential accumulation of sediment can also trigger an interaction between two independent flood deposition if the frequency of their occurrence is high enough to cause an overlap between them. In this case, we demonstrated that anoxic mineralization processes such as sulfate reduction and, in particular, methanogenesis can be influenced by this consecutive flood if it occurs more frequently in the future.



Chapter 5

Characterization of the benthic biogeochemical dynamics after flood events in the Rhône River prodelta - A data-model

In seed time learn, in harvest teach, in winter enjoy.

William Blake

Ferriera, E, Nmor, Stanley, Eric Viollier, Bruno Lansard, Bruno Bombled, Edouard Regnier, Gael Monvoisin, C Grenz, C Gauthier, Peter Van Beek, and Christophe Rabouille: "Characterization of the benthic biogeochemical dynamics after flood events in the Rhône River prodelta - A data-model" In: *Biogeosciences*. (in review)

Abstract:

At the land-sea interface, the benthic carbon cycle is strongly influenced by the export of terrigenous particulate material across the river-ocean continuum. Episodic flood events delivering massive sedimentary materials can occur, and their short-term impact on carbon cycling is poorly understood. In this paper, we use a coupled data-model approach to estimate the temporal variations of sediment-water fluxes, biogeochemical pathways and their reaction rates, during these abrupt phenomena. We studied one episodic depositional event in the vicinity of the Rhône River mouth (NW Mediterranean Sea) during the fall-winter season of 2021-2022. The distribution of dissolved inorganic carbon (DIC), sulfate (SO_4^{2-}) and methane (CH_4) were studied in sediment porewater collected every 2 weeks. The impact of 25 cm sediment layer deposition was studied after the main winter flood event. Significant changes in the distribution of CH_4 , DIC and SO_4^{2-} concentrations were observed. The use of an early diagenetic model (FESDIA) to calculate biogeochemical reaction rates and fluxes revealed that this type of flooding event can increase the total organic carbon mineralization rate in the sediment by 75% a few days after deposition, with an increase of sulfate reduction contribution to the total mineralization by 25% relative to non-flood depositional period. It predicts a short-term decrease of the DIC flux out of the sediment from 100 to 55 $mmol\ m^{-2}\ d^{-1}$ after the deposition of the new layer with a longer-term increase by 4%. Furthermore, examination of the stoichiometric ratios of DIC and SO_4^{2-} as well as model output over this five-month window shows a decoupling in the two modes of sulfate reduction following the deposition - organoclastic sulfate reduction (OSR) intensified in the newly deposited layer below the sediment surface, whereas anaerobic oxidation of methane (AOM) intensified at depth below the

former buried surface. This depth-wise bifurcation of both pathways of sulfate reduction in the sediment column is clearly related to the deepening of the sulfate-methane transition zone (SMTZ) by 25 cm after the flood deposition. Our findings highlight the significance of short-term transient biogeochemical processes at the seafloor and provide new insights on the benthic carbon cycle in the coastal ocean.

5.1 Summary

The objective of this section of the thesis is to expand our knowledge of flood events and their impact on anoxic diagenesis. In this paper, we broaden our technique to include longer, continuous time-series data from the Rhône prodelta. This chapter offers new datasets collected during the winter sampling session of 2021. The dataset contains sulfate (SO_4^{2-}), Dissolved inorganic carbon (DIC) and Methane (CH_4) measured repeatedly during 4 months at a biweekly period. Furthermore, data from the radionuclide Beryllium-7 (7Be) and organic carbon content were used to better constrain the thickness and content of the new deposit. This data-driven approach is supplemented by the numerical model built in the thesis to comprehend the function of major depositional events in the temporal dynamics of porewater solutes. Of emphasis in this section is the role of flood deposition on the anoxic processes operating deep down in the sediment. In this chapter, we look at the potential mechanisms that govern the response of sulfate, DIC, and methane in porewater after a winter deposition. Our findings show that this flood deposition event can result in substantial modification of the porewater solutes. Following deposition, we observed an enhanced mineralization of carbon characterized by a 75% of total carbon mineralization rate, with sulfate reduction dominating the biogeochemical pathway.

We also observed a limited sensitivity of DIC flux to the introduction of this new deposit with a 4% increase experienced shortly afterward. Because of the temporal nature of the data collected in this winter campaign, we were able to detect transient features involving sulfate reduction in the sediment. A distinct spatial decoupling of organoclastic sulfate reduction, mostly occurring in the first few cm of the sediment, and anaerobic oxidation of methane occurring at depth was found after the flood deposited. This separation, which is linked to the movement of the sulfate-methane transition zone (SMTZ) as a result of this deposition, indicates that biogeochemical processes such as AOM, which functions as a “filter” to the methane flux diffusing from below, may be influenced in the short term. Because the relative position of this SMTZ and the magnitude of the AOM maximum determine the flux of methane reaching the sediment-water interface, the occurrence of this type of perturbation at the seafloor can thus play a role in the modulation of biogeochemical cycles of carbon, sulfur and methane.

5.2 Introduction

River-dominated ocean margins (RiOMars) are crucial areas linking land and open ocean. They play a key role in marine nutrient and carbon cycles (Rabouille et al. 2001b; McKee et al. 2004; Cai 2011; Bauer et al. 2013; Gruber 2015; Bianchi et al. 2018). These dynamic environments are known to have high riverine input and sedimentation rate (Aller 1998). Furthermore, coastal sediments account for 85% of long-term oceanic organic carbon burial, with deltaic environments accounting for the majority (Burdige 2005), but they are also powerful biogeochemical reactors (Aller et al. 1996; Rassmann et al. 2016). The large deposition of riverine (or terrigenous) particulate organic matter (POM) on the seafloor can result in strong benthic mineralization

rates, dominated by sulfate reduction and methanogenesis (Mucci et al. 2000; Burdige and Komada 2011). In deltaic sediments, which receive large amounts of POM, anaerobic respiration is one of the most important pathways for the remineralization of organic carbon (Canfield 2004; Canfield and Thamdrup 2009; Pastor et al. 2011a). As an example, the prominent anoxic pathway in the Rhône River prodelta is sulfate reduction accounting for approximately 70% of the total organic carbon mineralization rate in sediments (Pastor et al. 2011a). This anoxic mineralization of organic carbon is supplemented by methanogenesis which can account for up to 35% of total organic matter degradation in sediment where a portion of reactive organic matter remains after complete sulfate exhaustion (Egger et al. 2016). The methane fluxes are controlled by the anaerobic oxidation of methane (AOM) in the subsurface sulfate-methane transition zone (STMZ; Boetius et al. (2000)). Together, these processes modulate anoxic-based carbon cycling in coastal and deltaic sediments, therefore generating large quantities of dissolved inorganic carbon (DIC), and RiOMar systems are considered as CO_2 sources to the atmosphere (Cai 2011; Bauer et al. 2013).

Flood events are especially significant along river-dominated margins and particularly for smaller river systems where sediment transport to the ocean preferentially occurs during extreme precipitation events (Bourrin et al. 2008; Lee et al. 2015). These materials can be subjected to secondary transport by waves and currents with a repeated cycle of resuspension and deposition (Moriarty et al. 2017) as they discharge to the adjacent shelves and deltas. Furthermore, episodic events can be important in determining the locations and magnitude of hotspots for OC burial on the coastal margin. This is especially true during large storms that can greatly increase both river discharge and sediment load, resulting in increased sediment discharge to depositional zones along the shelf (Eglinton 2008). During flood periods, large amounts of sediment and terrigenous OM are delivered to the adjacent delta and shelf. For example, the Eel river, in Northern California serves as a major source-to-sink conduit for large sediment transport, delivering between 60-80 % of discharged fine-grained sediment to the adjacent marine depocenter during large winter storms (Wheatcroft and Sommerfield 2005). Similar large deposition of sediment over a relatively short period of time have been documented elsewhere: Mekong delta (Manh et al. 2014) or the Yangtze river-estuary depositional system (Dai et al. 2018) to name a few.

In the Rhône River, these flood events can account for 80% of annual terrigenous particle inputs (Antonelli et al. 2008; Eyrolle et al. 2012), which at times can deliver up to 30 cm of sediment to the Rhône River prodelta in the Gulf of Lion (Antonelli et al. 2008; Cathalot et al. 2010; Eyrolle et al. 2012). These sediments are mostly deposited in the prodelta as previously shown by Wu et al. (2018) using beryllium-7 (7Be), natural short-life radionuclide to trace deposits of riverine suspended particulate matter (SPM). These winter events are abrupt and therefore difficult to document precisely. As a result, few studies have been conducted on the biogeochemical response of coastal sediment following intense export of sediment and organic carbon (Cathalot et al. 2010; Pastor et al. 2018). Furthermore, we can expect that these types of extreme events will increase as a result of climate change (Day et al. 2019; Lionello et al. 2023). However, due to the unpredictable nature of meteorological and flood events, it is difficult to monitor these intense events.

Many efforts have been made to incorporate biogeochemical processes operating in the sediment into mathematical models (Bernier 1980). These early diagenetic models have been heavily used to investigate the fate and transport of a selected set of chemical species in the seafloor (Aguilera et al. 2005). Recent non-steady-state diagenetic models based on previous numerical representations of sediment transport and reactions (Rabouille and Gaillard 1991; Soetaert et al. 1996a; Wang and Van Cappellen 1996; Berg et al. 2003) have demonstrated the importance of explicitly depicting event-driven processes (De Borger et al. 2021b; Nmor

et al. 2022). The benefit of these models is that they take deposition thickness into consideration as a vital parameter for reproducing such an episodic event (Nmor et al. 2022). Combining sediment and porewater data can help constrain model inputs and aid in the simulation of such depositional events.

The goal of this study is to examine the transient evolution of benthic carbon mineralization processes and their impact on sediment-water exchange during a flood event marked by large sediment deposition. We intend to characterize and quantify the changes that occur on several biogeochemical pathways and fluxes during these periods of substantial deposition of sedimentary material. We use a dualistic approach to solve this question by combining bi-monthly observational data on sediment evolution with a non-steady state early diagenetic model that calculates biogeochemical rates and fluxes. This multivariate perspective gives us a better understanding of the factors that control anaerobic oxidation of methane (AOM) and organoclastic-related sulfate reduction (OSR), as well as how massive material deposition affects coastal sediment.

5.3 Materials and Methods

5.3.1 Study site, Rhône prodelta

The Rhône River is the main source of freshwater, nutrients, organic matter and sediment for the Mediterranean Sea (Madron et al. 2000). It is characterized by a drainage basin of 97800 km^2 and an average water discharge of $1700 \text{ m}^3 \text{ s}^{-1}$ with a marked seasonality between low water-discharge ($<700 \text{ m}^3 \text{ s}^{-1}$) in summer and high water-discharge ($>3000 \text{ m}^3 \text{ s}^{-1}$) in fall and winter (Pont et al. 2002). The Rhône River turbidity plume extends mainly southwestward into the Gulf of Lion, with an average thickness of 1 m (up to 5 m) (Many et al. 2018). The Gulf of Lion is a microtidal, wave-dominated system, with a tidal range of 30 to 50 cm. Due to salt induced flocculation (Thill et al. 2001), most suspended particulate matter (SPM) carried out by the Rhône River settle in front of the mouth, on the prodelta (Maillet et al. 2006; Estournel et al. 2023). The study site (station Z, water depth 20 m, Figure 5.1) is located on the delta front, at a distance of 2 km from the river mouth, and is characterized by a mean apparent accumulation rate of up to 35 to 48 cm yr^{-1} (Charmasson et al. 1998). The site is defined by geographic coordinates (lat. $43^{\circ}19.135\text{N}$ / long. $04^{\circ}52.974\text{E}$), but the constraints of sea work (e.g. ship drift) lead to a positioning variability estimated at a perimeter of 60m around these coordinates.

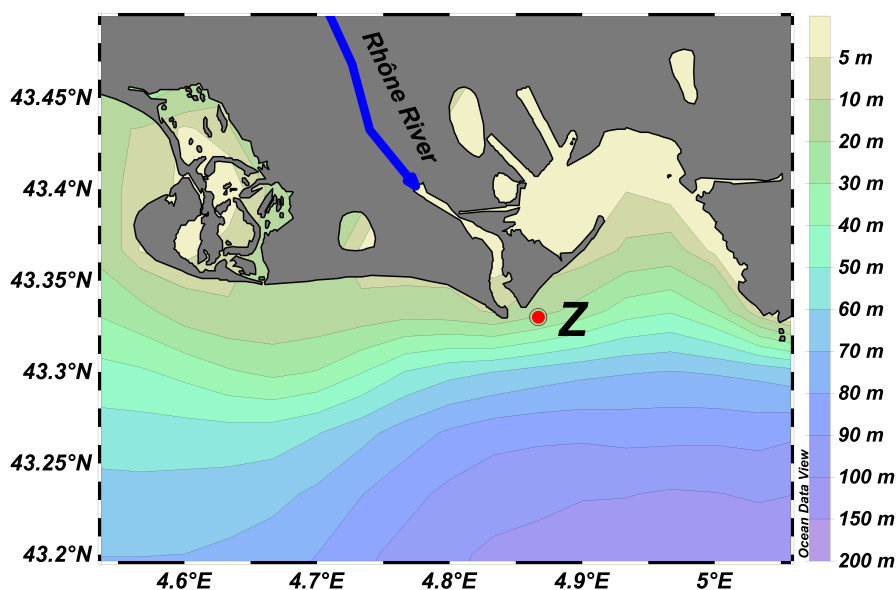


Figure 5.1: Map of the Gulf of Lion (Rhône prodelta) including the location of the sampling station (Z).

Table 5.1: Temporal sampling coverage and location of sampling sites during the winter season of 2021-2022.

Cruises	Date (dd-mm-yy)	Rhône river water flow			
		($m^3 s^{-1}$)	Lat (°N)	Lon (°E)	Depth (m)
SB7	03-Nov-2021	2057	43°19.066'	4°52.023'	20
SB7bis	19-Nov-2021	830	43°19.066'	4°52.023'	20
SB8	01-Dec-2021	905	43°19.032'	4°51.952'	20
SB9	07-Jan-2022	2533	43°19.111'	4°52.048'	20
SB9bis	19-Jan-2022	1318	43°19.096'	4°52.034'	20
SB10bis	23-Feb-2022	1972	43°19.131'	4°52.071'	20
SB11	08-Mar-2022	1110	43°19.108'	4°52.089'	20

The fall-winter monitoring (AMOR SB) took place bi-monthly from November 2021 to March 2022 (Table 5.1) with the sampling cruises onboard the RV Antédon II (IFREMER-FoF). The Rhône River flows were recovered from the Hydroréel database at the Tarascon-Beaucaire station (hydrometric station V720001002). The SPM content was recovered from the database of the Rhône sediment observatory. Missing data are estimated empirically using the relationship between flows and Cs determined from sediment rating curves (Horowitz 2003; Sadaoui et al. 2016; Lepage et al. 2022).

5.3.2 Sediment and porewater sampling and analyses

Sediment cores were collected at each of the cruises reported in Table 5.1 with an UWITEC single corer (USC 09000) equipped with a weight of 30 kg. The length of the coring tubes was 120 cm with an internal diameter of 9 cm. At least, two sediment cores were retrieved with a well-preserved sediment-water interface (SWI). One core was dedicated to the sampling of sediment porewaters and the second core was cut into slices for further laboratory analysis. Sediment porewaters were extracted using syringes connected to porous Rhizon with an average pore diameter of 0.1 μm (Seeberg-Elverfeldt et al. 2005). The vertical sampling resolution was 2 cm for the first 10 cm and then 4 cm down to the end of the core. At each sampled depth between 12 and 15 mL of porewater were extracted. The content of each syringe was immediately subsampled after extraction. For dissolved inorganic carbon (DIC) analysis, 5 mL samples were poisoned with 10 μL of supersaturated mercuric chloride (HgCl_2) and stored in 10 mL glass vials and stored at 4°C until analysis. Concentrations of DIC were analyzed by a LI-COR infrared detector with a DIC Analyzer ASC-1 (Apollo SciTech) on 0.75 mL samples, as described in (Rassmann et al. 2016). The relative uncertainty was $\pm 0.2\%$. For sulfate analysis, 2 mL were subsampled and acidified with 8 μL HNO_3 and stored in Eppendorf tubes at 4°C until analysis. Concentrations of SO_4^{2-} were analyzed on 100 μL samples with a liquid phase ion chromatography (ICS 1000 *Dionex*TM) with AG14 precolumn, AS14 column and AERS 500 suppressor configuration at Geosciences Paris-Saclay laboratory, as described in (Rassmann et al. 2020). The relative uncertainty was $\pm 0.3\%$.

On the same core, sub-core samples were taken for CH_4 with a 5 cm resolution in side holes using two sharpened 5 mL syringes of 1 cm diameter. The contents of two syringes of the same level were quickly introduced into empty pre-weighed 60 mL vials with 35 mL of potassium hydroxide ($\text{KOH } 1 \text{ mol } L^{-1}$). The vials were then directly sealed, shaken and stored in the dark. Back in the laboratory, CH_4 concentrations were analyzed with a micro-gas chromatograph Agilent Technologies® 490 GC. Measurements were made in three 60-second analyses, with 1.5 mL gas samples taken from the “headspace”. The calibration was performed

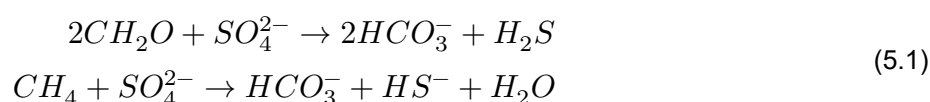
with a standard gas of CH_4 at 104 ppm with a reproducibility of 0.1 %. Data obtained indicate a percentage of CH_4 in the headspace which allows the calculation of CH_4 quantity in headspace by dividing the volume of CH_4 by the molar volume of a gas at 1 atm. This quantity is the used to calculate the CH_4 concentration in the porewater using porosity and sediment weight, with an estimated accuracy of 5 %.

The second sediment core was sliced as follows: every 0.5 cm for the first 2 cm of the core, every 1 cm down to the 10 cm, every 2 cm down to the 20 cm and finally 5 cm on the rest of the length. Sediment samples were stored in freezer bags preserved at -20 °C. One part of the sediment samples was used to determine the organic carbon (OC) content, reported in % dry weight sediment. Sediment layers were freeze-dried, crushed and decarbonated by successive acidification baths (HCl 1%) over several days after rinsing. Homogenized and accurately weighed subsamples were analyzed by a Carlo-Erba NA-1500 Elemental Analyzer. The average OC contents are calculated for the first 30 cm sediment before and after the flood.

Another part of this sediment core was used to analyze the beryllium-7 (7Be) activity within three months after sample collection by using low-background gamma-ray spectrometry at the LAFARA underground laboratory (Van Beek et al. 2013). Between 8.0 and 12.5 g of dry sediment were analyzed during 48 h using a Mirion-Canberra planar detector (germanium crystal of 230 cm^3) equipped with LYNX (Mirion-Canberra) electronics and an electric cooling system (CryoPulse® 5 plus provided by Mirion-Canberra). The 7Be activities are reported with 2 sigma uncertainties.

5.3.3 Stoichiometric ratio

The aerobic mineralization of buried organic matter by sulfate reduction (Equation 5.1) and the anaerobic methane oxidation (AOM, Equation 5.1) reactions provide theoretical, stoichiometric ratio ($r_{c:s}$) of SO_4^{2-} consumption to bicarbonate ion production.



This ratio can be used to identify the key process that dominates mineralization in sediments from porewater measurements (Burdige and Komada 2011). The $r_{c:s}$ (Equation 5.2) were calculated as described by Burdige and Komada (2011). The slope of the property-property plot of ΔDIC versus ΔSO_4^{2-} was corrected by the diffusion coefficient ratio at in situ temperature (Yuan-Hui and Gregory 1974) in order to eliminate the effect of transport by diffusion (Burdige and Komada 2011).

$$r_{c:s} = \frac{D_{HCO_3^-}}{D_{SO_4^{2-}}} \cdot \frac{\Delta DIC}{\Delta SO_4^{2-}} \quad (5.2)$$

Before the flood event $r_{c:s}$ were calculated on the whole core. After the deposition event, two $r_{c:s}$ were calculated as a function of depth, the first on a surface layer between 1 and 25 cm and the second from 25 cm to the bottom of the core.

5.3.4 Numerical modelling

The model used here is FESDIA, an early diagenesis model designed for perturbation studies. This model is made up of a set of coupled nonlinear partial differential equations that describe the distribution of porewater

species at different depths. This model is notable for its ability to simulate event-driven dynamics such as sudden sediment deposition as a result of flood input. Details of the model formulations and equations are described in Nmor et al. (2022). Here, we briefly outline important processes involving sulfur and methane cycle as well as parameterization considered necessary for the representation of the winter flood situation in the Rhône River prodelta.

The model considers the entire sequence of OM remineralization pathways in the sediment, including OM remineralization coupled to oxygen, nitrogen, iron and manganese oxides, sulfate, and, finally, methane production. In general, organic matter oxidation follows the formalism of a cascading sequence of these terminal electron acceptors. The organic matter modelled is made up of two degradable fractions with different reactivities. This decay is modelled as a first-order rate law and is dependent on the limitations of specific oxidants and their inhibition. Secondary reactions involving reduced species include nitrification, reoxidation of reduced metals, methane oxidation (see below) via oxygen, sulfide reoxidation by iron and manganese hydr(oxides), and iron-sulfide precipitation. Table 5.2 contains a summary of the parameters used in the model. These values were either derived from previous steady-state modeling works in the Rhône prodelta sediment (Pastor et al. 2011a; Ait Ballagh et al. 2021) or in other cases, where no model parameter value was known a priori in the Rhône prodelta sediment, values from other literature sources were calibrated with the observed data.

Table 5.2: Summary of parameters used in the FESDIA model. (I) independent parameters derived from experiment or field observation external to actual data being simulated (C) constrained parameters obtained from range of literature sources (M) model-derived parameters fitted to the observed data. Literature sources includes (1) Pastor et al. (2011a), (2) Soetaert et al. (1996a), (3) Ait Ballagh et al. (2021), (4) Rassmann et al. (2020) and (5) Wang and Van Cappellen (1996).

Description	Model				
	name	Parameters	Units	Type	Source
total organic C deposition	Cflux	15000	$nmol C cm^{-2} d^{-1}$	I	1
part FDET in carbon flux	pFast	0.5	-	C	1
deposition rate of FeOH3	FeOH3flux	7000	$nmol cm^{-2} d^{-1}$	M	-
Flux of Mn Oxides	MnO2flux	1500	$nmol cm^{-2} d^{-1}$	M/C	-/5
decay rate FDET	rFast	0.5	d^{-1}	C	1
decay rate SDET	rSlow	0.0031	d^{-1}	C	1
NC ratio FDET	NCrFdet	0.14	molN/molC	I	2
NC ratio SDET	NCrSdet	0.1	molN/molC	I	2
temperature	temperature	15.6	dgC	M	-
salinity	salinity	37.8	psu	M	-
upper boundary O2	O2bw	238	$mmol m^{-3}$	M	-
upper boundary NO3	NO3bw	0	$mmol m^{-3}$	M	-
upper boundary NH3	NH3bw	0	$mmol m^{-3}$	M	-
upper boundary CH4	CH4bw	0	$mmol m^{-3}$	M	-
upper boundary DIC	DICbw	2360	$mmol m^{-3}$	M	-
upper boundary Fe2	Febw	0	$mmol m^{-3}$	M	-
upper boundary H2S	H2Sbw	0	$mmol m^{-3}$	M	-
upper boundary SO4	SO4bw	33246	$mmol m^{-3}$	M	-
upper boundary Manganese	Mnbw	0	$mmol m^{-3}$	M	-

Description	Model		Units	Type	Source
	name	Parameters			
advection rate	w	0.08	$cm\ d^{-1}$	M	-
bioturbation coefficient	biot	0.05	$cm^2\ d^{-1}$	C	1
depth of mixed layer	biotdepth	5	cm	I	3
attenuation coeff below biotdepth	biotatt	1	cm	I	3
bio-irrigation rate	irr	0.3	d^{-1}	M	-
depth of irrigated layer	irrdepth	7	cm	I	3
attenuation coeff below irrdepth	irratt	1	cm	I	3
refractory Carbon conc	TOC0	1	%	M	-
surface porosity	por0	0.83	-	I	4
deep porosity	pordeep	0.65	-	I	1/4
porosity decay coefficient	porcoeff	2	cm	I	1/4
maximum rate FeS production	rFeS	0.5	$cm^3\ nmol^{-1}\ d^{-1}$	I	5
Max rate anaerobic oxidation Methane	rAOM	30×10^{-6}	$cm^3\ nmol^{-1}\ d^{-1}$	I	5
Rate of Sulphide-mediated iron reduction (oxyhydr)oxides	rH2Sfeox	0.00121	$cm^3\ nmol^{-1}\ d^{-1}$	M/C	-/5
Rate of Reoxidation of H2S by MnOx	rH2SMnox	0.001728	$cm^3\ nmol^{-1}\ d^{-1}$	M/C	-/5
Rate of Reoxidation of Fe with MnOx	rMnFe	6.5×10^{-6}	$cm^3\ nmol^{-1}\ d^{-1}$	M/C	-/5
Enrichment factor for FDET	alphaFDET	4	-	M	-
Enrichment factor for SDET	alphaSDET	1.8	-	M	-
Enrichment factor for FeOH3A	alphaFeOH3A	1	-	M	-
Enrichment factor for FeOHB	alphaFeOHB	1	-	M	-
Enrichment factor for MnO2A	alphaMnO2A	1	-	M	-
Enrichment factor for MnO2B	alphaMnO2B	1	-	M	-

5.3.5 Methanogenesis

Below the sulphidic zone, organic carbon that remains is subsequently remineralized via methanogenesis. The product of this fermentation of organic matter in depth by anaerobic archaea is methane (CH_4) and can be represented in Equation 5.3:



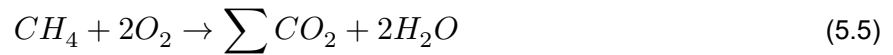
In the Rhône river proximal prodelta, evidence of high apparent sedimentation deposition ($> 30\ cm\ yr^{-1}$) and high particulate organic carbon flux ($657\ gC\ m^{-2}\ yr^{-1}$) has been observed (Madron et al. 2000; Pastor et al. 2011b). As a result, high methane production in deeper sediment is likely (Garcia-Garcia et al. 2006; Pozzato et al. 2018; Rassmann et al. 2020). In the model, the accumulation of methane derived from carbon remineralization is limited by the equilibrium between dissolved and free gas, which can occur at around 90 ppm (or 6 mM) in shallow sediments of Rhône prodelta (Garcia-Garcia et al. 2006). This is done by considering methane removal into either free gas as Equation 5.4:

$$CH_{4gas} = \max(0, k_{gas} * (CH_4 - CH_{4equil})) \quad (5.4)$$

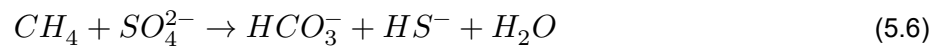
where CH_{4equil} is the equilibrium concentration for which observed/simulated methane transition to hydrate or gas phases.

5.3.6 Methane oxidation

The methane produced deep down in the sediment can diffuse upward and be re-oxidized in the presence of oxygen with a simple first-order rate expression used in the model:



However, an important part of this investigation involves the interaction between the sulfur and methane cycle. Critical to this link is the role of anaerobic oxidation of methane (AOM) (Equation 5.1). The AOM is a vital microbial process which acts as a barrier to the extent of the upward methane flux from the deeper sediment. The AOM occurs at the nexus of sulfate depletion and methane production; at a depth horizon typically referred to as the sulfate-methane transition zone (SMTZ). In this SMTZ, methane produced below the sulfate depleted sub-surface sediment diffuses upward and is oxidized by sulfate according:



This reaction is modelled as a first-order process involving both CH_4 and SO_4^{2-} .

$$AOM = R_{AOM} \times CH_4 \times SO_4^{2-} \quad (5.7)$$

where R_{AOM} is the apparent rate constant for reaction and as this pathway of sulfate reduction occurs at a much slower rate than the sulfate reduction coupled to organic carbon oxidation (Van Cappellen and Gaillard 2018), a value R_{AOM} set to $3 \times 10^{-5} \text{ cm}^{-3} \text{ mmol}^{-1} \text{ d}^{-1}$.

5.3.7 Model configuration

The model was implemented in a 1 m sediment domain with variable depth resolution. Sediment thickness increases from 1 mm at the surface to about 6 cm at the base of the domain. For our application, we used a sedimentation rate of 30 cm yr^{-1} (Lansard et al. (2009b)) and the degradation constant of the labile carbon (r_{Fast}) was also tuned to 0.05 d^{-1} . Other parameters relevant for this particular simulation were derived from other literature sources and a listing is provided in Table 5.2.

Porosity was modelled as an exponential decay with depth increasing from 0.83 at the surface to an asymptotic value of 0.65 at depth following the obtained data. Bioturbation was constant in the first 5 cm with a rate of $0.05 \text{ cm}^2 \text{ d}^{-1}$ and exponentially attenuated below with reduced fauna activity. Based on the low bioturbation rate observed at station Z and the dominance of flood deposition on sedimentation (Pastor et al. 2011a), the FESDIA model is used with a constant bioturbation rate over the study period (Nmor et al. 2022). Solutes

pumping via bio-irrigation was also modelled. A summary of the parameters used in the model is described in Table 5.2.

The deposition of flood materials was carried out in a similar manner as described in Nmor et al. (2022). Here, we imposed a singular flood scenario with a thickness of 25 cm. The inclusion of this single event was dictated by the dominant presence of an abnormally high suspended particulate matter (SPM) observed during the winter flooding season recorded at the SORA monitoring station located in Arles, 40 km upstream from the river mouth (Figure 5.2). As such, we assumed that deposition during this flood period only lagged by a few days from the observance of high TSM load. This forces the date used for the deposition in the model (2022-01-03). The deposited material thickness in the model is indirectly diagnosed using measurement of porewater solute distribution and strengthened by Beryllium-7 (${}^7\text{Be}$) data collected after particle settling (see Section 5.4).

As described in Nmor et al. (2022), the deposited flood layer can have a different particulate composition than the pre-existing sediment. Depending on the nature of the flood, it can be enriched or depleted in reactive compounds (two pools of organic matter (C_{fast}^{org} , C_{org}^{slow}), of manganese (MnO_{2A} and MnO_{2B}) and amorphous iron ($FeOOH_A$ and $FeOOH_B$)) which is translated in the model by the enrichment factor (α). This α factor was set to the values reported in Table 5.2.

5.4 Results

5.4.1 Water discharge, SPM concentrations

During the sampling period (November 2021 - March 2022), the discharge rate of the Rhône River varied significantly with monthly fluctuations (Figure 5.2). The average river discharge during this period was about $1800\text{ m}^3\text{s}^{-1}$. Monthly discharges ranged from $553\text{ m}^3\text{s}^{-1}$ during the low flow period to $5045\text{ m}^3\text{s}^{-1}$ in January 2023. This maximum river discharge is 3 times higher than the mean discharge experienced during this period and 2 times higher than the other monthly peak observed in November, December and February. This highest discharge coincides with the maximum of suspended particulate matter (SPM) which is as high as 1420 mg L^{-1} . This high load of SPM is clearly discernible compared to the average SPM of 64 mg L^{-1} experienced within the 5-month duration of the sampling campaign. The other peak in SPM of November 2022 was small (91 mg L^{-1}).

5.4.2 Porewater composition of dissolved inorganic carbon, sulfate and methane and its comparison to model outputs

The depth profiles of measured and simulated concentrations of DIC, sulfate, and methane are presented in Figure 5.3 for all time points during the winter monitoring.

Prior to the flood deposition, porewater sulfate concentrations were constant in the first 5 cm of the sediment with concentration of 31-32 mM. Below, SO_4^{2-} concentrations decrease smoothly with depth to 40 cm where no/little sulfate was detected. The model reproduces a strong gradient of sulfate consumption between 5 and 30 cm. This gradient associated with sulfate reduction results in a modelled vertically-integrated sulfate consumption rate due to bacterial metabolism of $97\text{ mmol C m}^{-2}\text{ d}^{-1}$ prior to the deposition event. In contrast, methane was virtually zero in the upper 20 cm of the sediment. From 25 cm onward, methane builds up in the porewater with CH_4 rising up to 5 - 6 mM with depth. The trend in the data, supported by the model,

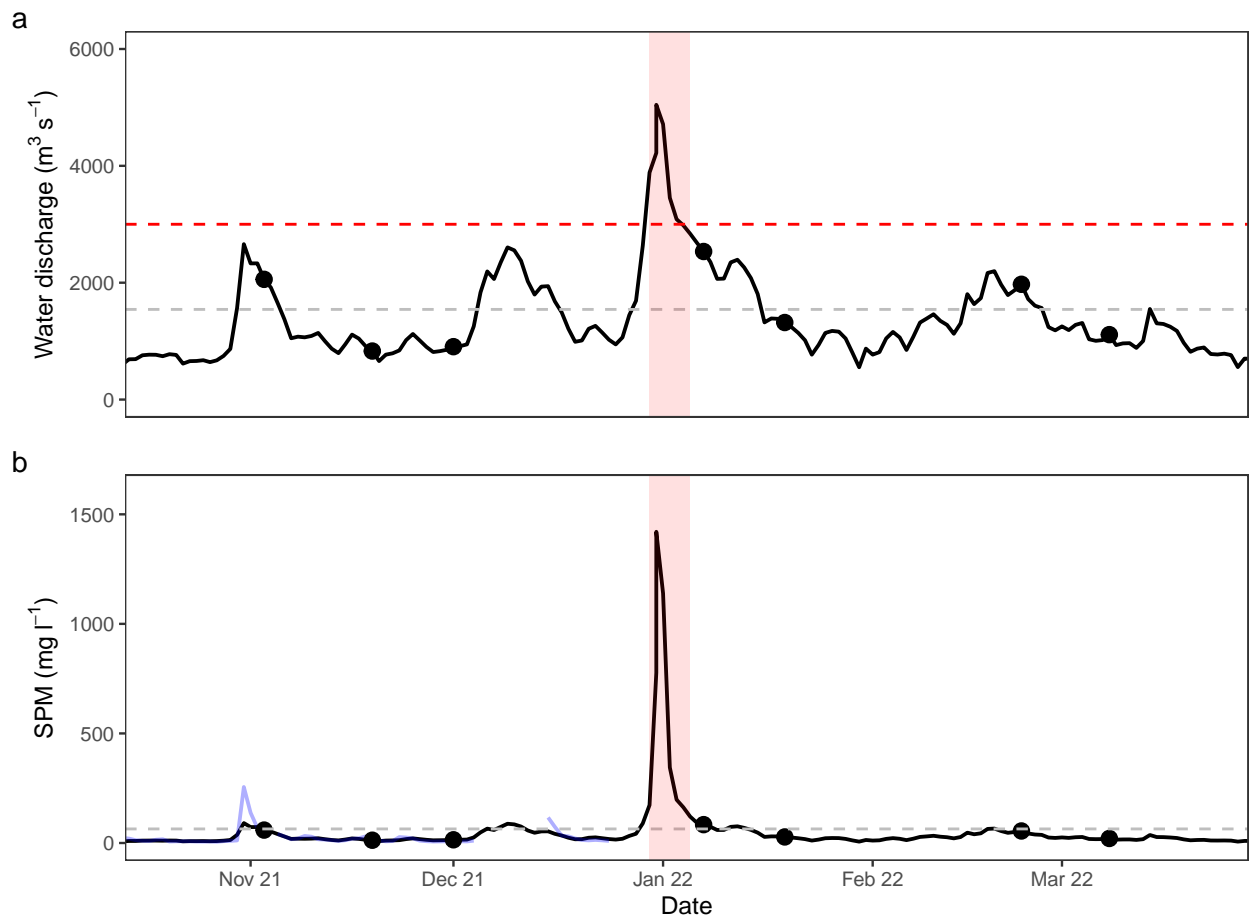


Figure 5.2: (a) Mean daily water discharge of the Rhône River at Beaucaire-Tarascon, located 60 km upstream the river mouth. The grey dotted line symbolizes the average water discharge level. The red dotted line symbolizes the flood level at Beaucaire-Tarascon with the flood period symbolizes with the red bar. (b) Total suspended particulate matters (SPM) in the Rhône River at Beaucaire-Tarascon. The 7 cruises are indicated by the black points.

indicates that a linearly diffusing methane gradient exists at depth (Figure 5.3). At depth, the entire contribution of methanogenesis to organic carbon mineralization as calculated by the model was $9 \text{ mmol C m}^{-3} \text{ d}^{-1}$.

The net product of reactions involving both methane and sulfate is DIC. The measured DIC concentrations in the bottom waters was 2.2 mM but gradually increases with depth up to 40 mM at the base of the sediment core. This DIC maximum at 40 cm was largely reproduced by model simulations as a result of organic matter mineralization. In general, DIC and sulfate profiles are symmetrical throughout the time series. In period of time preceding the major flood deposition, the changes of DIC, sulfate and methane profiles were limited. However, slight heterogeneity in porewaters leads to slightly less remarkable agreement between both model and data. Nonetheless, significant degrees of correspondence between the model and data were generally observed with correlation higher than 0.8.

After the flood deposition at the end of December 2022, all chemical species in the sediment porewater showed significant changes in their concentration profiles. The flood input resulted in the intrusion of sulfate-rich porewater ($> 25 \text{ mM}$) deep down to 25 cm together with relatively low DIC concentration ($< 10 \text{ mM}$). This nearly constant sulfate concentration in the data was clearly reproduced by the model (Figure 5.3). Below this depth, the profile is similar to the pre-flood situation with a slightly less steep gradient. This strong sulfate consumption between 40 and 75 cm is observed in the data and simulated by the model. For all three species (DIC, SO_4^{2-} and CH_4), the correlation between observed data and model was high ($r > 0.8$), with a consistent increase to 6 mM and 50 mM for CH_4 and DIC respectively while SO_4^{2-} reached zero at 60 cm. The depth of appearance of CH_4 is also shifted from an average position of 30 cm before the flood to a depth of 60 cm after the flood deposition. The maximum in both methane and DIC concentrations occur at 70 and 60 cm respectively. In addition, the model reproduced the sulfate-methane transition zone observed in the data. The model was able to obtain a satisfactory fit generally over the 60 cm depth. Below this depth, the simulated profiles obtained in January show a slight deviation from the measured profiles. The sediment barely changed profiles 15 days after its initial deposition. An excellent agreement between the model and data is observed. Furthermore, little change in the SMTZ was observed over the two months following flood deposition. The upward diffusion of methane was virtually not discernible on the methane profiles. Two months after the event, the slow sediment upward shift in methane was still undetectable and the depth of appearance of CH_4 was still around 60 cm.

In the upper layer, all solutes were slowly and steadily reorganized one month after deposition. Sulfate was still present up to 60 cm with significant decrease in the top 20 cm, and DIC accumulation in this layer of the sediment was obvious in both data and model results. However, the gradual establishment of a new gradient in this layer begins after that. As of February 2022, two gradients can be seen, one between 19 and 29 cm and the other between 40 and 61 cm.

5.4.3 Beryllium 7 (${}^7\text{Be}$)

The vertical distribution of Beryllium (${}^7\text{Be}$) measured after the flood showed significant activity with sediment depth down to 25 cm (Figure 5.4). The presence of ${}^7\text{Be}$ within this active upper zone suggests a recently deposited layer.

Examination of the ${}^7\text{Be}$ profile delineates two section within this active zone. In the upper section which extends from the surface to 10 cm of the sediment, ${}^7\text{Be}$ activities vary between 60 to 20 Bq kg^{-1} and decline linearly with depth. The uncertainty in these measurements was $\pm 20 \text{ Bq kg}^{-1}$. The lower section of the

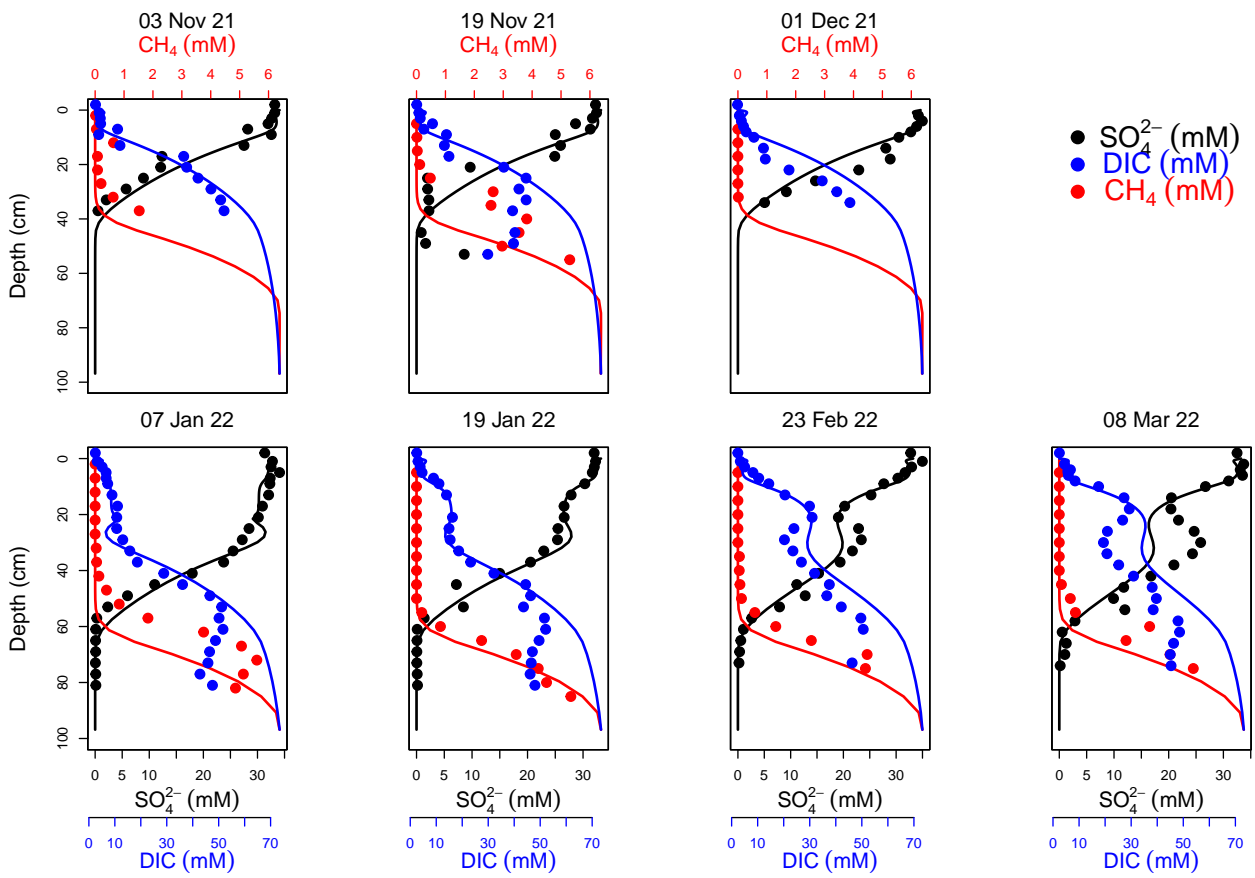


Figure 5.3: Vertical distribution of Dissolved Inorganic Carbon (DIC), sulfate (SO_4^{2-}) and methane (CH_4) concentrations in sediment pore waters. Dots represent the measured porewater data and lines denote the model result.

profile extends from 10 cm to 20 cm, with ${}^7\text{Be}$ profile slightly increasing with subsurface maximum of $50 \pm 15 \text{ Bq kg}^{-1}$ at 19 cm. The uncertainty in ${}^7\text{Be}$ activity (represented by the error bar) makes determining a significant decrease between 10 and 20 cm difficult. However, an examination of the profile reveals that ${}^7\text{Be}$ activity below 25 cm decreases, with no significant activity measured at 30 cm. Thus, the detection of ${}^7\text{Be}$ activities indicate a likely estimate of thickness of the flood layer. As large and constant ${}^7\text{Be}$ activities were measured, a significant and instantaneous deposition is likely.

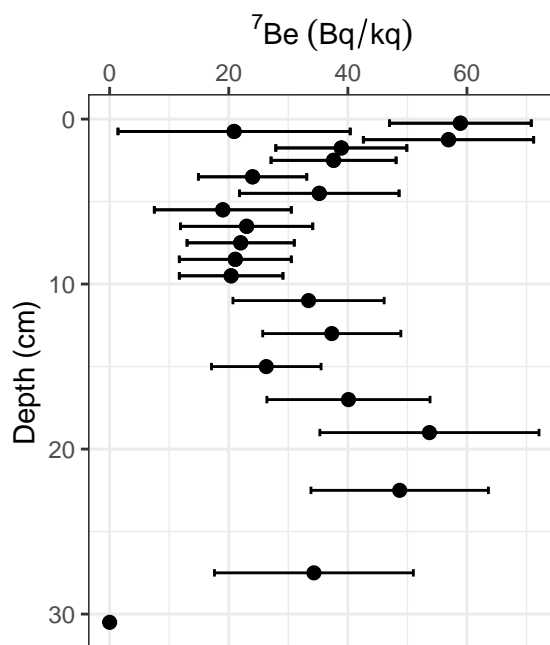


Figure 5.4: Vertical distributions of Beryllium-7 activities in the 01/07/2021 sediment core.

5.4.4 Organic carbon content

The average organic carbon (OC) content of sediment cores collected before and after the main flood event is shown Table 5.3. The pre-flood sediment has an average OC of $1.3 \pm 0.4 \%$ dw. The shape of the pre-flood OC profile shows a decrease with depth, starting at 1.8 % dw at the SWI and declining to 0.9 % dw at 22 cm.

In contrast to the pre-flood sediment, post-flood OC exhibits a less clear pattern in its variation with depth with overall larger OC content of $1.7 \pm 0.3 \%$ dw. Like the ${}^7\text{Be}$ profile, two possibly distinct regions are delineated in the OC content profile. In the upper 10 cm of sediment, organic carbon content after deposition varies from 2 to 1.3% dw. Below, a slight increase in OC concentration is observed with a subsurface maximum of 1.6 % dw. In the bottom layer, the average OC concentration is larger after the flood (1.5% dw) than before the flood (0.95% dw) and is similar to the average OC concentration in the top layer before the flood (1.6% dw). As the vertical resolution of the measurement of OC content is coarse in comparison to the beryllium profile, we did not attempt to correlate these two profiles.

Table 5.3: Organic carbon content at selected sediment depth (% dry weight) before and after the flood

Depth interval(cm)	Pre-flood OC content (%)	Post-flood OC content (%)
0-1	1.8	1.9
4-5	1.5	2.0
9-10	1.5	1.3

Depth interval(cm)	Pre-flood OC content (%)	Post-flood OC content (%)
20-25	0.9	1.5
25-30	1.0	1.6

5.5 Discussion

Extreme events, such as floods and storms, have measurable impacts on coastal benthic ecosystems near large river mouths and deltas (Tesi et al. 2012; Pastor et al. 2018). The present study provides a temporal picture of the dynamics of large sediment deposition during the winter flooding event of 2021-2022 at a shallow station in the Rhône River prodelta. Using a combined data-model approach, we describe prominent features of this flood and their implications for carbon cycling in sediments, the evolution of diagenetic pathways and sulfate/methane transformation during early diagenesis.

5.5.1 Disturbance identification, flood and its deposit

The massive deposition of fresh sediments deeply modifies the quantity and quality of the OM and defines the so-called flood layer. Accurate identification of the flood signature, its thickness and deposition timing which is essential for proper model calibration is challenging. In most instances, the exact specification of when and where the sediment delivered via flood event is permanently deposited on the seafloor is highly uncertain (Tesi et al. 2012) due to possible physical mixing with underneath layer or biomixing (Wheatcroft 1990). Furthermore, while the thickness of the massive deposited materials during this type of event is an important marker that can be clearly distinguished, it can be smudged by other related events such as fluctuating deposition-erosion event (Bentley and Nittrouer 2003; Wheatcroft et al. 2006). For large gauged rivers, water discharge that characterizes floods are generally well documented (Zebracki et al. 2015). However, the solid discharge is generally less known due to difficulties in accurately sampling particles during the flood periods.

The average Rhône River water flow was $1470 \text{ m}^3 \text{ s}^{-1}$ in the winter season of 2021-2022, with short periods of significant higher discharge. There were four periods of increased flow, but only one exceeded the flood threshold of $3000 \text{ m}^3 \text{ s}^{-1}$ at the end of December. This main winter flood corresponds well with the high concentrations of suspended particulate materials observed in the Rhône River (Figure 5.2). Furthermore, the work of (Pont et al. 2002) highlighted the non-linear relationship between flows and SPM concentrations which corresponds to large particle discharge at the end of December. Accordingly, a period of time with a single large flood (that is simulated in the model) in the Rhône River prodelta station characterizes this study. This assumption is furthermore supported by the work of Miralles et al. (2005).

In the absence of visual determination of the deposited flood layer, such as sediment color, we investigated multiple indicators to determine flood layer thickness. The downward shift of the gradient of sulfate (SO_4^{2-}) decrease as well as the gradient of DIC/CH_4 increase recorded 15 days after the flood is used to determine the extent of the flood deposition. Our estimate amounts to approximately 25 cm in agreement with the downward shift of methane gradient (Figure 5.5).

This deposition thickness was validated by analyzing ^7Be concentrations measured during this time period, which revealed significant radiotracer activities in the first 25 cm of the sediment (Figure 5.4). This latter method that allows for the identification of recent sediment deposition has been widely used in other studies document-

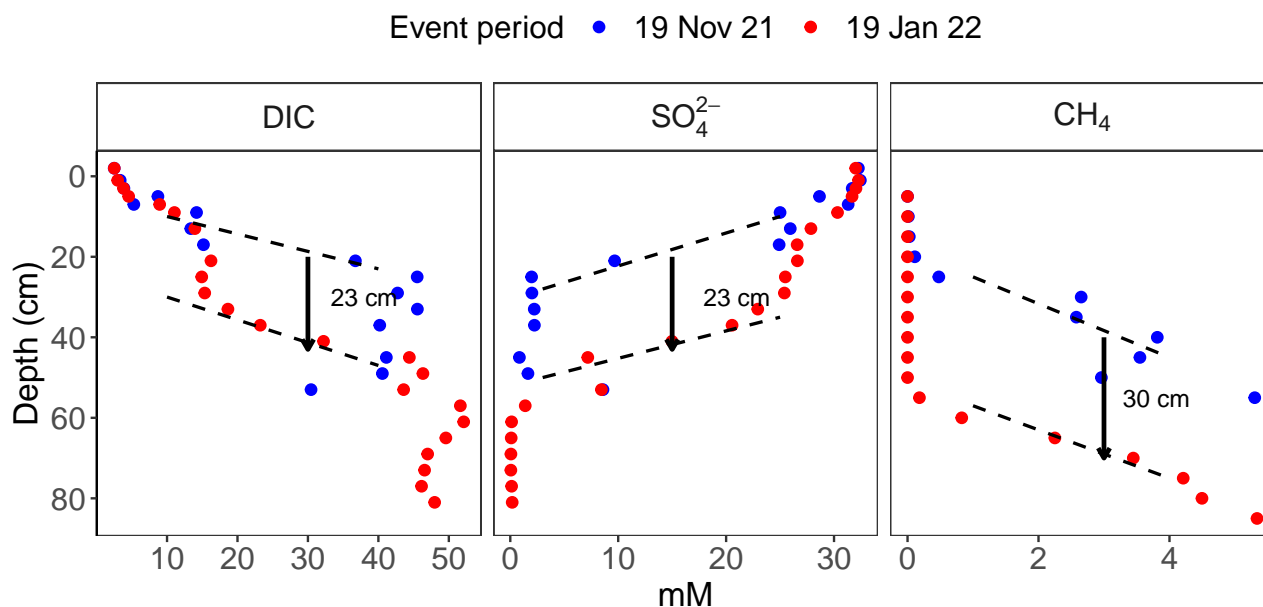


Figure 5.5: Concentration profiles of DIC, SO_4^{2-} and CH_4 in sediments porewaters from station Z. The dashed lines correspond to the position of the main gradient before (blue dots) and after (red dots) the flood. The arrow symbolizes the shift of this main gradient following the main winter flood.

ing flood deposition processes over short time scales (Feng et al. 1999; Palinkas et al. 2005; Wu et al. 2018). Indeed, the 7Be is significantly detected until 30 cm depth (Figure 5.4), which indicates newly deposited particles originating from the river down to this particular depth. However, the event layer thicknesses using 7Be can be overestimated in locations where bioturbation activity by benthic fauna is non-negligible. In the Rhône River prodelta, this is strictly not the case as previous studies have shown that bioturbation rate in this location is low (Pastor et al. 2011a; Pruski et al. 2015) and probably even lower during flood deposition due to habitat disturbance. In general, combining the qualitative assessment of the shift in the post-flood profile relative to the pre-flood, as well as 7Be event-based data, helps in defining our estimate for the deposit thickness. The accurate establishment of this thickness deposit by the flood provides an important constraint to the numerical model and increases its overall skillfulness.

The organic carbon concentration (Table 5.3) also indicate a change of concentration at depth due to the flood deposit. Indeed, the low concentration observed below 25 cm before the flood are refilled by larger OC concentration after the deposit. Furthermore, these new OC concentrations at depth are similar as those found in the top layer before the flood. This may indicate a downward shift of the former interface to a depth of 20-25 cm.

5.5.2 Transient evolution and mineralization pathways and rates

The accumulation of large amounts of terrigenous materials in the proximal region of deltaic depocenter has large implication on the carbon cycle (Hedges and Keil 1995). This routing of carbon to the depocenter sediments results in substantial organic matter degradation despite acting as accumulation site (Jahnke et al. 1990; Cathalot et al. 2010; Cai 2011; Blair and Aller 2012). The transformation and short-term fate of riverine-OC under episodic events, on the other hand, is largely unknown (Carlin et al. 2021). In the Rhône River prodelta, model estimate of total organic carbon mineralization is around $148 \text{ mmol C m}^{-2} \text{ d}^{-1}$ before the flood deposition. This estimate is comparable to the total mineralization rate reported in previous studies in the Rhône River prodelta. Under steady state condition, Pastor et al. (2011a) reported a total mineralization rate of 150

$mmol\ C\ m^{-2}\ d^{-1}$ while integrated mineralization rate in Ait Ballagh et al. (2021) averaged around $145\ mmol\ C\ m^{-2}\ d^{-1}$ for the proximal zone of the prodelta. As reported for other coastal systems with organic-rich sediments, anoxic diagenetic pathways involving organoclastic sulfate reduction (OSR) dominates in terms of contribution to total OC mineralization. In the present study, estimate of OSR indicate a contribution of nearly 65% to the total OC mineralization rate while methanogenesis accounts for only 8% (Figure 5.6).

Prior to the flood event, strong sulfate consumption in the surficial sediment was observed in the measured data, as evidenced by a significant decrease in concentration between 5 and 30 cm, accompanied by a significant increase of DIC concentration. DIC accumulation in intermediate sediment layers was also very large for this time period. This pre-flood situation hints at a system under steady state condition. This combined combination of sulfate reduction and methanogenesis (> 70% of total mineralization rate) corresponds with values observed in other studies in this shallow region of the prodelta where the anoxic contribution to OC mineralization ranged from 75 % to 89 % (Pastor et al. 2011a; Ait Ballagh et al. 2021).

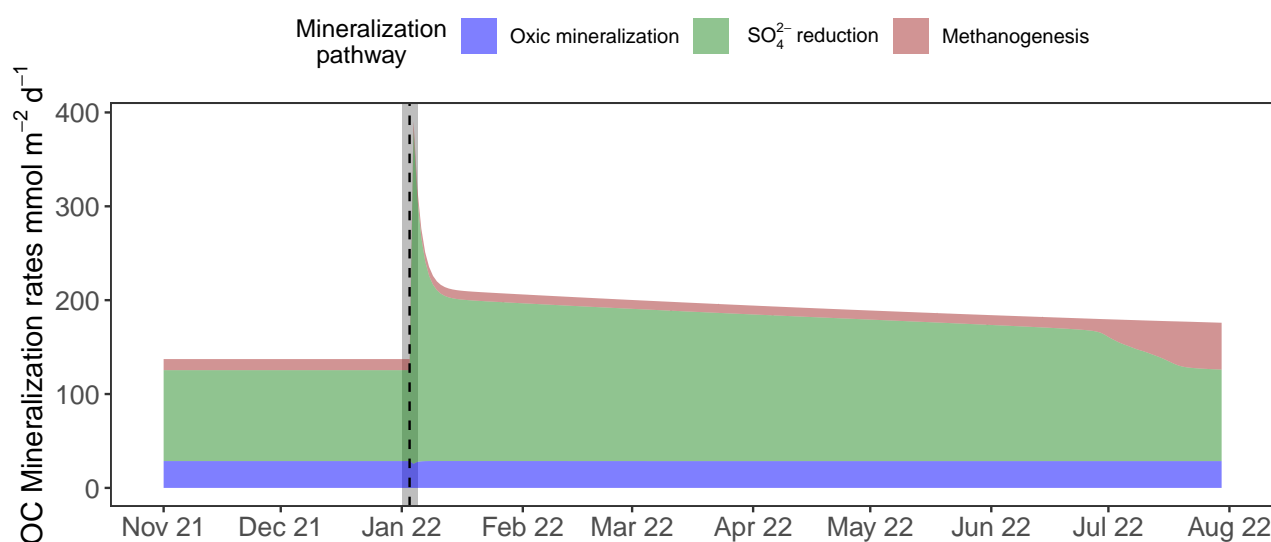


Figure 5.6: Vertically integrated rate of organic carbon mineralization and relative contribution by different pathways. The gray bar and dashed line reflect the date of the main flood (06/01/2022).

After the flood, the deposition of a thick sediment layer drastically alters the vertical distribution of all profiles with a deeper sulfate penetration, a lower DIC concentration in the top 25 cm of sediment porewaters and a deeper depth of CH_4 appearance. The addition of sulfate resulted in intense anoxic-favorable mineralization of degradable OC. As a result, model calculations suggest an immediate burst followed by an increase of sulfate reduction rates by 75% (Figure 5.6) in comparison to the pre-flood period. As the total rate of OC mineralization increases, the share of OSR in the total mineralization jumps from 65% before the flood to 81% after the flood. The relative contribution of methanogenesis to the total OC mineralization rate decreased from 4% to 2% after the flood. At the same time, oxic mineralization which accounts for around 19% of total mineralization before the flood is not modified after the flood due to its very short (daily) relaxation time (Nmor et al. 2022), and its share in total mineralization decreases to 11%. Thus, immediately after the flood and in the following two months, the organoclastic sulfate reduction is largely favored among the diagenetic pathways in the sediments. This can be related to the large quantity of sulfate available after the flood deposition which traps sulfate-rich bottom water over the 25 cm sedimentary column, and to its thermodynamically favorable energy yield compared to methanogenesis. These differences in carbon oxidation pathways before and after the flood also reflect the amount and quality of organic matter deposited in the sediment due to the flood input (Marvin-DiPasquale

and Capone 1998; Nmor et al. 2022; Smeaton and Austin 2022). Indeed, these winter floods carry large amounts of metabolizable organic matter originating from terrestrial organic debris or riverine organic matter (Cathalot et al. 2010; Bourgeois et al. 2011; Pozzato et al. 2018) which may trigger intense recycling once deposited in the sediment (Pastor et al. 2018). In a second time period, unfortunately not covered by the data set, model simulations indicate that methane contribution increases following complete sulfate relaxation to its pre-flood levels 5.5 month later. The rate of CH_4 production by methanogenesis increases, reaching $50 \text{ mmol C m}^{-2} \text{ d}^{-1}$, i.e. 27 % of total mineralization at until 8 months after the event. This secondary increase of methanogenesis needs to be confirmed with new data, it could maintain the long-term relaxation of the system over more than a year, therefore contributing to the accumulation of methane in prodelta sediments (Garcia-Garcia et al. (2006); Nmor et al., In prep)

5.5.3 Sulfate-Methane dynamics before and after the flood

In anoxic sediments, the carbon cycle is tightly coupled to sulfur/methane cycles (Jørgensen and Kasten 2006). The present dataset and model can be used to understand the impact of flood deposition on these coupled cycles. In the case of the sulfur cycle, 90 % of oceanic sulfate reduction takes place in sediments of the continental shelves (Jørgensen 1982; Jørgensen et al. 2019). The two main pathways for sulfate reduction is organoclastic sulfate reduction (OSR) that depends on the lability and amount of degradable organic matter and anaerobic oxidation of methane (AOM) where methane is anaerobically oxidized to bicarbonate using SO_4^{2-} as electron acceptor by a consortium of microbes including bacteria and archaea (Jørgensen et al. 2019). Although AOM and OSR can coexist, AOM frequently produces a second-deep sulfate reduction peak different from the near-surface maximum of sulfate reduction by carbon oxidation, and it requires considerably lower SO_4^{2-} concentrations. The relative degree of sulfate reduction in both modes regulates the flux of SO_4^{2-} and CH_4 across the SWI (Egger et al. 2018).

Because the sedimentary CH_4 flux is largely controlled by the rate of AOM, it is critical to understand how CH_4 and SO_4^{2-} fluxes are regulated (Dale et al. 2008b) especially during flood times and following evolution which disrupts the steady-state control of the CH_4 flux. In sediments of the Rhône River prodelta, while bacterial-mediated sulfate reduction is the main oxidation of OC, the quantification of the contribution of anaerobic oxidation of methane is missing from previous studies (Pastor et al. 2011a; Zhuang et al. 2018; Ait Ballagh et al. 2021). In this study, the data-model approach allows us to quantify the magnitude of the rate of AOM in the sediment.

The depth of maximum AOM before the winter deposition was situated at 35 cm (Figure 5.7). The rate of AOM at this depth was $16 \text{ mmol m}^{-3} \text{ d}^{-1}$. This is higher than values reported in marine sediments from the Skagerrat ($5 \text{ mmol m}^{-3} \text{ d}^{-1}$; Knab et al. (2008)), the Baltic sea ($14 \text{ mmol m}^{-3} \text{ d}^{-1}$; Treude et al. (2005)), but significantly lower than AOM activities in the Gulf of Mexico or the hydrate ridge off the coast of Oregon ($500 \text{ mmol m}^{-3} \text{ d}^{-1}$; Treude et al. (2003)).

After the deposition, the AOM maximum rates remains the same in intensity but occur deeper in the sediment (Figure 5.7). Further cross-examination of the sulfate and methane concentration profiles reveals physical imprint of the flood deposit on the porewater chemical composition. Our data show that penetration depth of SO_4^{2-} and appearance of methane exhibited a shift downward relative to the pre-flood situation confirming the AOM rate calculation by the model. This generated a downward shift of the sulfate-methane transition zone (SMTZ), defined as the area where sulfate and methane are consumed simultaneously. This SMTZ depth below

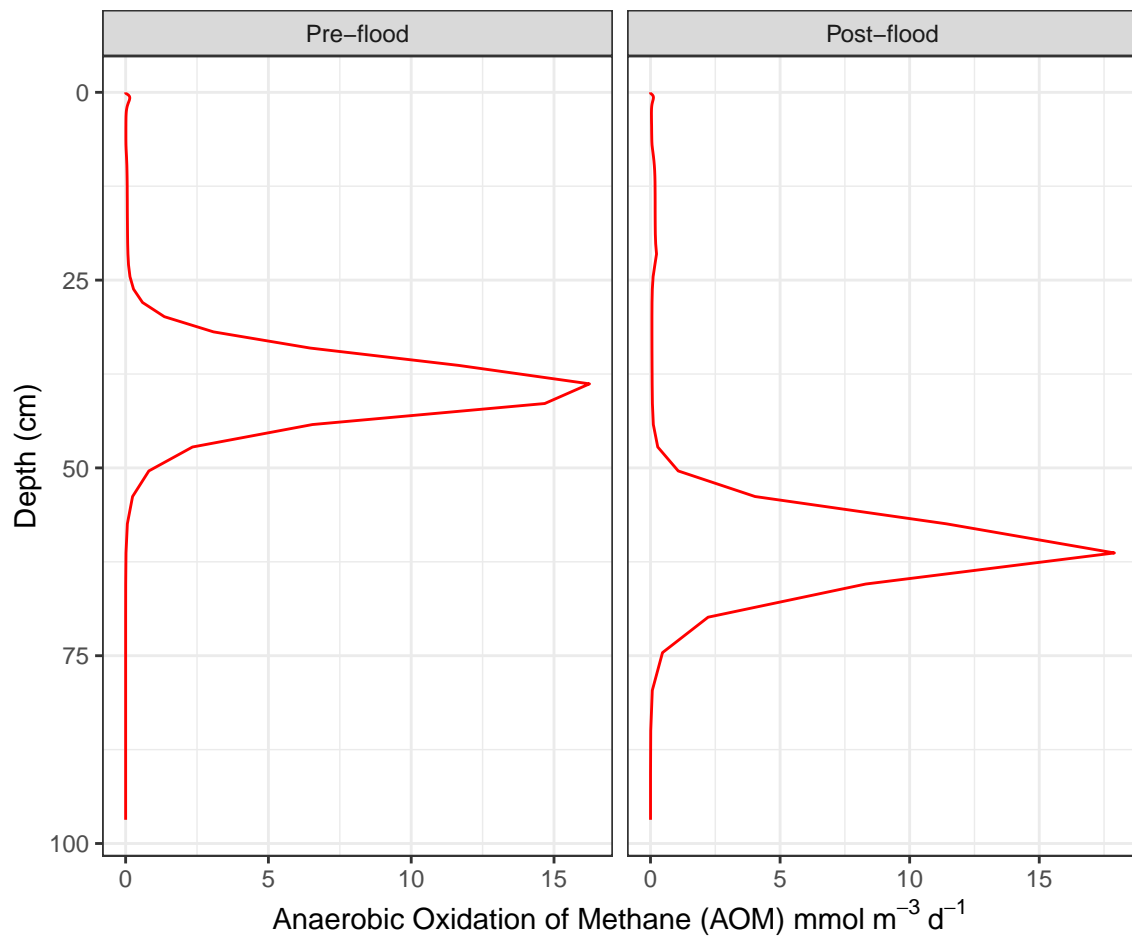


Figure 5.7: Vertical distribution of anaerobic oxidation of methane (AOM) for pre-flood and post-flood period.

the seafloor acts as a proxy for methane fluxes (Borowski et al. 1999). In general, the presence or absence of externally compressed upward fluid flow (Regnier et al. 2011), localized pockmark where advective transport occurs (Knab et al. 2008) and organic matter load all influence the depth of SMTZ. In our case, the observation of the porewater profiles and the SMTZ suggests a deepening with depth following the introduction of the flood 25 cm layer. Prior to the flood deposition, the SMTZ was located between 30 and 40 cm. The model estimated the location of SMTZ at 39 cm, which is within the interval of the data. This SMTZ depth shifted to 60 cm after the deposition. This vertical shift of the SMTZ in RiOMars system like Rhône prodelta differs from other coastal areas where a shoaling of the SMTZ is experienced as a result of high load of organic matter driven by eutrophication (Crill and Martens 1983). In our case, the deep penetration of bottom water sulfate following the event indicate that methane generating processes occurs much deeper. Furthermore, the upward diffusion of the released CH_4 (Borowski et al. 1999) is rather slow. This sluggish flux of methane to the SMTZ due to slow molecular diffusion of methane (Regnier et al. 2011) is linked to the long relaxation timescale associated with processes occurring deep in the sediment (Nmor et al. 2022). Our data provide support to this hypothesis, which shows that the SMTZ in the pre-flood profiles changed little. It is noteworthy that in some other rapidly accumulation setting, increased organic matter load can change the depth of the SMTZ by bringing it closer to the sediment surface (Crill and Martens 1983; Dale et al. 2019; Myllykangas et al. 2020). The dynamics of this change is unknown and depends on SO_4^{2-} exhaustion by early diagenesis processes. If this is the case, our observation here offers a different view on the role of instantaneous massive flood on sulfur-methane dynamics. This may be due to the “reactivity” of the organic matter or the short time scale associated with the present study but further investigation of this topic needs to be done to understand the impact of large deposition events.

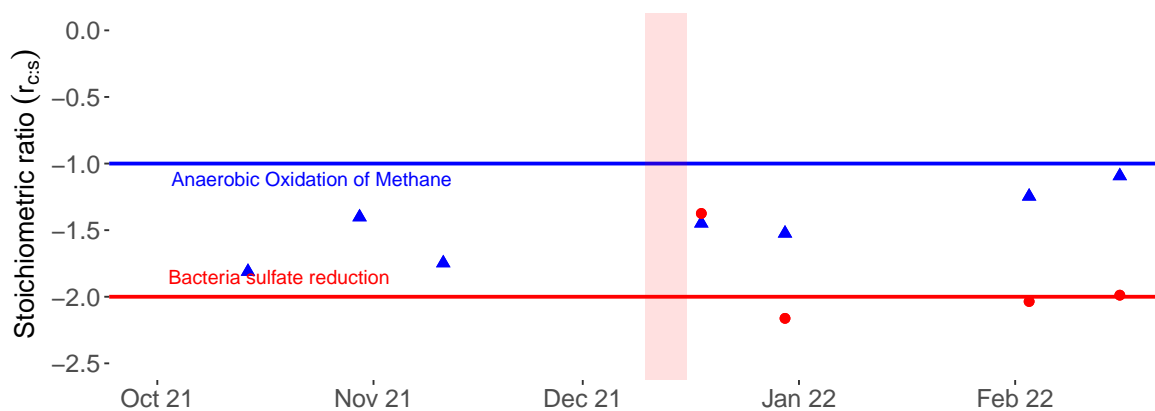


Figure 5.8: Temporal variation of DIC: SO_4^{2-} porewater ratio ($r_{c:s}$) calculated on the surface or depth layer. The red bar indicates the flood period, before the flood the entire core is considered like the surface layer. The blue line indicates the theoretical stoichiometric ratio of the anaerobic oxidation of methane (-1) and the red line indicates the theoretical stoichiometric ratio of the sulfate reduction (-2).

Qualitative assessment of DIC: SO_4^{2-} ratio ($r_{c:s}$) in the sediment core between pre- and post-flood profiles reveals an imbalance in the stoichiometric ratios involving sulfate reduction observed in the measured data partitioned by the depth of the new sediment layer (Figure 5.8). Before the winter flood, the $r_{c:s}$ varies between -1.7 and -1.4 with no clear pattern distinguishing between zones of the sediment favored by either organoclastic sulfate reduction or anaerobic methane oxidation. The sudden occurrence of this large deposition of materials triggers a post-flood bifurcation in sulfate reduction delineated by the SMTZ. In the newly deposited layer, the $r_{c:s}$ decreases from -1.8 to -2.0, thus showing a strong tendency toward OSR with time, whereas deeper sediment was AOM-favored with $r_{c:s}$ slowly drifting to -1.1 in February (Figure 5.8).

The implication of this event-driven drift between the upper and lower sediment is still unclear. However, the link between the temporal movement of the methane front and the migration of the AOM community adaptation to changing conditions has been highlighted (Regnier et al. 2011). While the model used here does not explicitly resolve the biomass involved in the reactions (Dale et al. 2007) or consider the impact of bioenergetics (Dale et al. 2006), we can show that a shift in the SMTZ seen correlated with the depth of model estimate of the maximum AOM zone before and after the deposition Figure 5.7. Since the SO_4^{2-} and CH_4 data are correctly reproduced by the model, the depth of the maximum rate of AOM is thus essentially controlled by substrate availability. This deepening of the AOM maximum suggests that in the advent of flood deposition, the AOM traps the upward flux of methane. It has been suggested that the shallower the SMTZ, the more chance of escape of methane from the sediment to the overlying water and, ultimately, to the atmosphere (Borges and Abril 2011). Thus, the occurrence of this large deposition could increase the efficiency of the trapping of methane in sediments.

5.5.4 Flood induced fluxes and link to carbonate chemistry

Because of their high load of mineralizable organic matter, coastal sediment represents an important source of CO_2 and methane to the coastal ocean and to the atmosphere (Egger et al. 2016). Changes in the intensity of various mineralization processes in response to flood deposition raise concerns about the consequences on fluxes of dissolved greenhouse gases at the sediment-water interface. These fluxes may have also a broader impact on benthic-pelagic biogeochemistry, such as ocean acidification (CO_2) of the coastal waters. Current estimate of solutes release does not explicitly account for these event-driven sedimentations which might have different geochemical properties depending on the type of flood (Cathalot et al. 2010; Pruski et al. 2015). For example, our results show that the event deposits have higher % OC values and drive larger mineralization rates (Figure 5.6) which result in substantial change of the sediment interstitial composition and possibly fluxes.

A remarkable change in the benthic exchange across the sediment-water interface was observed for DIC. Before the flood deposition, the DIC flux out of the sediment amounts to $101 \text{ mmol m}^{-2} \text{ d}^{-1}$. This calculated DIC efflux is larger than previous data based estimate but remains in the same order of magnitude as flux estimate reported in this proximal zone ($18 - 78 \text{ mmol m}^{-2} \text{ d}^{-1}$; Rassmann et al. (2020)) as well as other river deltas: Mississippi delta sediment ($36 - 53 \text{ mmol m}^{-2} \text{ d}^{-1}$; Rowe et al. (2002)), Fly River delta ($35 - 42 \text{ mmol m}^{-2} \text{ d}^{-1}$; Aller et al. (2008)) and Guadalquivir River estuary ($36 - 46 \text{ mmol m}^{-2} \text{ d}^{-1}$; Ferrón et al. (2009)). After the flood deposition, the model estimates of DIC benthic flux decreases from 101 to $55 \text{ mmol m}^{-2} \text{ d}^{-1}$ in response to the new input. This is largely related to the large decrease of the DIC gradient in porewaters after the flood (Figure 5.3) and represents a 45% reduction in DIC flux out of the sediment shortly after flood deposition. The reduced DIC flux quickly resumes to the previous situation after a week of lower fluxes and stabilizes to a value a few percent above the initial value. Yet, the production of DIC in the sediment column has increased by 43% due to the sudden increase of OC recycling activity following the introduction of fresh organic carbon contained in the flood deposit (Figure 5.9). The initial decrease of the flux of DIC followed by a slight increase of about 4% and then a stabilization at almost the same initial value as before the flood indicates that most of the DIC produced by the flood deposit is stored in the sediment porewaters. This is obvious from the DIC profile (Figure 5.3) which clearly indicates an accumulation of DIC in porewaters after the flood along the measurement period (from January to March).

This change of DIC flux in response to the abrupt introduction of flood-driven deposit can have an impact on the contribution of the coastal sediment to the release of CO_2 to the coastal zone and potentially later to the

atmosphere. The extent of this gas exchange is determined by several factors, including the DIC/TA flux ratio (Andersson and Mackenzie 2012). In the Rhône prodelta sediments at steady-state, the alkalinity flux ranges from 14 to 74 $mmol\ m^{-2}\ d^{-1}$ thus acting as an efficient counteracting mechanism controlling DIC fluxes to the overlying water (Rassmann et al. 2020). As most of the increase of DIC production arises from organoclastic sulfate-reduction which has a DIC/Alk production ratio of 1 (Rassmann et al. 2020), the flux of alkalinity out of the sediment will probably follow the DIC flux, therefore bringing little changes to the DIC/Alk ratio in the coastal bottom waters (Hu and Cai 2011). However other contributors to sediment alkalinity such as calcium carbonate dissolution as well as potential coupling processes involving FeS and FeS_2 burial might well affect the alkalinity during relaxation of the system after the flood (Nmor et al., in prep). This is likely the case in the Rhône River prodelta sediment where substantial pyrite burial at depth have been reported (Rassmann et al. 2020). As measurements of DIC and alkalinity flux at this winter flood are unavailable, and porewater iron and sulfide were not monitored during the time series, we can only speculate with the model results. In any case, this highlights the need to better study this phenomenon and provide better constraints on their contribution to coastal carbon cycle.

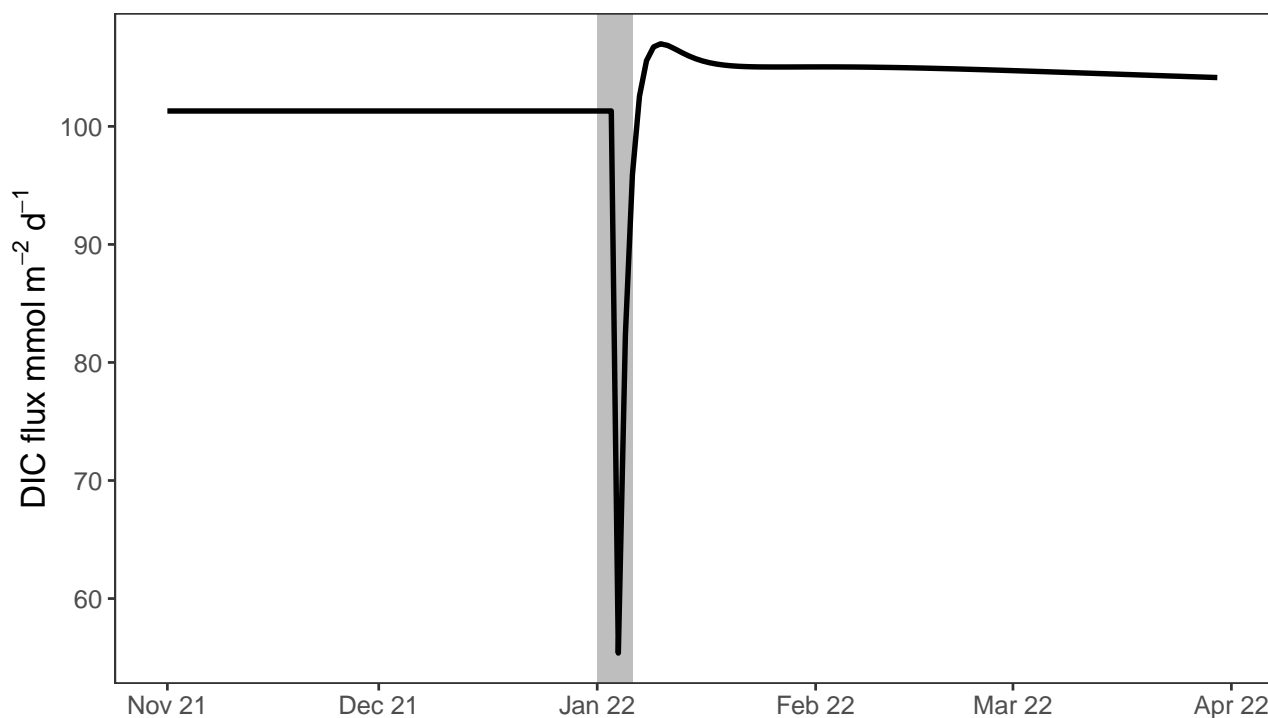


Figure 5.9: Flux of DIC across the sediment-water interface. Here, positive flux is directed out of the sediment. The gray bar reflects the date of the main flood (06/01/2022).

5.6 Conclusion

Extreme flood deposition events produce transient dynamics in biogeochemical processes in coastal marine environment. In this paper, we document the temporal features of porewater short-term response over 2 months to organic matter flood input at a station located in the Rhône prodelta. Using a data-model approach, we showed that the introduction of this new layer of OM input from flood deposition can alter the porewater profile of sulfate, DIC and methane. Although the model incorporates some simplifying assumptions, FESDIA is able to reproduce accurately the measured concentration depth profiles, including time and space variations. This reflects the capability of the model to capture nonsteady-state dynamics driven by abruptly changing boundary

condition.

Our modelling results indicate that large amounts of sediment can also trigger intense biogeochemical processes with stimulation of sulfate reduction and immediate decline of DIC flux out of the sediment. The internal storage of DIC in porewaters indicates a relative decoupling of sediment organic matter mineralization and fluxes to the water column. By considering the measured porewater profiles and the reactions stoichiometry, we showed that massive deposition of sediment can result in the disconnect between anaerobic oxidation of methane and organoclastic pathway for sulfate reduction in the sediment. This decoupling of AOM and OSR implies an increase in the efficiency of the sediment capacity to trap incoming flux of methane from below. The immediate consequence of the changes in the porewater chemistry and processes following these events highlights their importance in the short to medium term response and system functioning in the respective biogeochemical cycle. On a broader scale, the long-term fate of such events on sediment biogeochemical processes will require better and more continuous field monitoring to help future model development addressing the biogeochemical consequences of these flood events.

Code and data availability All data used in this study are available through SEANOE (<https://doi.org/10.17882/96514>) (Ferreira et al., 2023). The model version used to produce the results used in this paper is archived on Zenodo (<https://doi.org/10.5281/zenodo.6369288>) (Nmor et al., 2022).

Author contributions: EF, SN, EV, BB, BL, CG and CR conceptualized the study. EF, SN, BB, ER, GM, PvB and CR contributed to the data curation. EF, SN, CG, PvB performed the formal analysis. CR acquired the funds. EF, SN, EV, BB, BL, ER, CG, PvB and CR made the investigation. EF, SN, EV, BB, BL and CR contributed to the methodology. BB, CG and CR are behind the project administration and the supervision of the research planning. SN, EV and CR contributed to the software development. EF and SN contributed equally to the visualization and the writing of the original draft preparation. All authors contributed to the writing review, editing and validation.

Acknowledgements The authors would like to acknowledge Nolwenn Verpy, Laure Papillon and Deny Malengros for help collecting samples, Caroline Gauthier for help with OC analysis, Marc Souhaut, and Thomas Zambardi for help with 7-Beryllium analysis at the LAFARA underground laboratory. We would like to thank Hugo Lepage for discussing river flows and helping us obtain the SPM data and also the Observatoire des Sédiments du Rhône staff for the SPM results. Finally, we would also like to thank the various members of the RV Antédon II crew who were present on several campaigns. The map in this study was created with the ODV Software Schlitzer, Reiner, Ocean Data View, <https://odv.awi.de>, 2022.

Financial support This work was supported by a grant from the special call on estuaries from French National programme EC2CO under the name “DeltaRhône” and the French government grant managed by the Agence Nationale de la Recherche under the France 2030 program, RiOMar reference ANR 22 POCE 0006



Chapter 6

Conclusion and perspectives

Un peu de science éloigne de Dieu, beaucoup de science y ramène.

Louis Pasteur

The overarching goal of this thesis was to gain a better understanding of the influence of flood deposition on sediment biogeochemistry at river-dominated ocean margins. To that effect, this thesis attempted to advance the science of modelling early diagenetic processes by developing tools to address the numerous challenges surrounding large flood deposits with the end goal of understanding the biogeochemical implications of this phenomenon. The thesis was separated into three key sections, each of which built on the previous one, from the conceptual development of FESDIA to its implementation in the Rhône prodelta area across historical and present flood events. In the following sections, I present a synthesis of my current research, key findings from this project and future outlook.

6.1 Conclusion

This thesis concludes by providing new tools for investigating the impact of flood deposition on sediment biogeochemistry (Chapter 3). These tools have been applied to understand the dynamics of sediment porewaters during the floods of 2008 (Chapter 4) and 2021-22 (Chapter 5). Hereafter, I briefly review the main conclusion established during the thesis.

Given the importance of understanding extreme episodic deposition events on coastal river deltas and the lack of tools tailored to describing these phenomena (Chapter 1 - 2), this thesis seeks to develop a new framework for coupling early diagenesis processes in the sediment with explicit representation of event-driven sediment deposition (Chapter 3). This model, called FESDIA comprises 21 variables encompassing the carbon, nitrogen, manganese, iron and sulfur cycle. In Chapter 3, we showed how this model was developed and validated by a data snapshot of flood deposition in the Fall of 2008. The model post-flood evolution highlights salient features (e.g. slow but steady re-organization of the perturbed profiles) which characterized the sediment porewater behavior following these events. This re-organization resulted in the model predicted relaxation timescale of about a few days for oxygen and between 4-5 months for deeper solutes like DIC and SO_4^{2-} with variation in this estimate depending on deposition thickness and the reactivity of OM.

Numerical experiments performed on a suite of parameters demonstrated that the characteristics timescale of recovery of the porewater profiles to their pre-flood condition are in alignment with expectations observed in the natural world. These parameters - the nature of the newly deposited layer in terms of their carbon enrichment (which is associated with the quality and source-origin of the materials) and the thickness of the new layer (associated with the quantity of sediment deposited) - are responsible for the apparent quick relaxation of the coastal sediment under such extreme deposition. This is certainly the case for the Rhône prodelta sediment, where models and observations from field campaigns suggest a time-window of about 6 months for some porewater profiles (DIC and SO_4^{2-}) to show a rather steady-state behavior despite the occurrence of massive deposition from Rhône River floods. This finding highlights the possible occurrence of a so-called “biogeochemical attractor” pulling the system back to a stable state within a short period of time. This is a new understanding of the biogeochemical importance of flood deposition in deltaic sediment regarding its relaxation timescale, biogeochemical dynamics and impact on exchange fluxes with the water column.

In Chapter 4, using the FESDIA model, we demonstrate the utility of the model in explaining transient behaviors of two contrasting flood events. More specifically, the model result suggests that during the spring flood of May 2008 where 30 cm sediment comprising highly refractory carbon was deposited, a comparatively less biogeochemical modification of the examined porewater was found and can be characterized by low superficial sulfate reduction within the newly deposited layer in comparison to the buried layer as well as a moderate release of porewater dissolved metals induced by biotic and abiotic metal reduction. By contrast, in the fall of the same year, where a 10 cm sediment of mostly labile materials was deposited, more intense biogeochemical processes ensued, mostly marked by a strong oxygen consumption, a more substantial metal reduction, and strong anoxic diagenesis dominated by sulfate reduction. This contrast gave rise to a two-order of magnitude difference in the response of several biogeochemical pathways of carbon mineralization with remarkable changes observed in anoxic contribution to carbon mineralization rate (sulfate reduction >70% and methanogenesis >8%). In both instances, I demonstrated that the strong internal cycling and the role of secondary redox processes such as pyrite precipitation might be responsible for the maintenance of non-sulfidic conditions observed in Rhône prodelta sediment (Pastor et al. 2018; Rassmann et al. 2020). In addition, numerical experiments performed with scenarios of multiple sequential flood depositions show that the effect of flood interaction on biogeochemical processes (coined “*Memory effect*”) can be substantial for processes operating in the deeper layers (such as methanogenesis and sulfate reduction) but negligible for superficial oxic and suboxic processes on the timescale of the observed frequency of flood deposition. The biogeochemical ramifications of this might be more pronounced in the future, where an increasing frequency of these extreme events is likely.

In Chapter 5, I focused my attention on a more recent flood phenomenon, which occurred in the winter of 2021. Here, bi-weekly sampling campaigns were carried out to investigate the temporal evolution of the sediment porewater following a single massive flood deposition at the proximal station of the Rhône delta. The unique timeseries of porewater data for dissolved inorganic carbon, sulfate and methane was further analyzed with the model developed earlier in the thesis. Our data suggest that this winter flood can induce temporal modification of the interstitial porewater profile of DIC, SO_4^{2-} and CH_4 to a remarkable extent distinguishable from the pre-flood situation. An accurate estimation of the deposited layer thickness was confirmed (25 cm) using radionuclide and organic carbon data, thus fingerprinting the impact of this winter flood deposition. The model indicates that these winter events can result in as much as a 75% increase in total carbon mineralization resulting in a strong production of DIC and a longer term increase of DIC flux out of the sediment by 4%. With this data-model approach, we observed that in the event of the flood deposit, a decoupling of the two pathways

for sulfate reduction - organoclastic sulfate reduction and anaerobic oxidation of methane - ensued. This disconnection of both mechanisms of sulfate reduction correlated with a vertical migration of the sulfate-methane transition zone. The implication here is that the further deepening of the AOM maximum zone caused by the flood deposition could enhance the effective trapping of methane flux out of the sediment.

This thesis illustrates for the first time the role of this episodic event on the temporal and spatial dynamics of the biogeochemical processes operating in the sediment. Future works on extrapolating the results and methods obtained here on other similar river-ocean dominated regions will further build upon our understanding of these phenomena on sediment biogeochemistry. Upscaling our approach to a wider spatial extent and coupling with pelagic biogeochemistry will highlight the extent to which these events can affect coastal ecosystem functioning. With increasing frequency of these events due to changing environmental conditions, the long-term consequences of these events will be better understood. These future perspectives and pathways to approach them will be discussed in the next section.

6.2 Perspectives

Here, I present potential future perspectives on coastal biogeochemistry as it relates to episodic events. The immediate continuation of the study undertaken in this thesis may aim to concentrate on the three topics listed below: (1) Extend the main ideas and questions given in this thesis to additional coastal regions and time scales linked to typological features peculiar to River-dominated ocean margins (RiOMar) (2) Integrate and extend our 1D approach to improve spatial coverage by linking the benthic component to the pelagic domain (i.e a coupled benthic-pelagic biogeochemical model) for a better understanding of the impact of extreme events on coastal ecosystem functioning (3) Long simulations and futuristic scenarios to better understand the long-term consequences of an episodic event on inter-annual and climate change timescales. We proceed to briefly discuss these three research priorities and some preliminary steps taken in these directions during the thesis.

6.2.1 Event-driven flood typologies for Rhône River and beyond

The transport of suspended sediment from large rivers to marine environments has important environmental impacts on coastal zones. In this context, quantifying the sources of sediment supplying the Rhone River and, ultimately, the Mediterranean Sea is a critical prerequisite for better understanding riverine transfer and its potential role in global biogeochemical cycles, as well as for implementing effective control strategies to improve water and sediment quality (Walling and Collins 2008). Records of these flood events exist, and their role in the eventual transport of sedimentary particulate matter has been well-studied (Eyrolle et al. 2012; Zebracki et al. 2013; Pont et al. 2017).

To synthesise the work done in the thesis on the impact of Rhône River sediment deposition on the biogeochemical dynamics in the surrounding delta, we proposed a biogeochemical typology that incorporates the spectrum of flood features established in this region. To progress from the specific scenarios encountered in the dataset used in this thesis to a comprehensive coverage of all possible situations, previous studies must be aggregated and data describing the hydrological, geochemical and sedimentary properties of the deposition during this type of event must be integrated. For example, four types of climatological regimes can be distinguished based on the prior studies of flood types (Zebracki et al. 2013):

- Oceanic pluvial regime derived from northern tributaries in the winter (Saône and Ain rivers).

- Mediterranean flash flood coming from Mediterranean Sea and generally observed in autumn, that occur in the southeastern part of the watershed (Durance, Drôme and Ouvèze rivers)
- Extensive Cevenol Mediterranean rainfalls with similar characteristics as the mediterranean flood but with a sharper flow variation which occur early in fall season and are more located around the Cevennes mountains (Ardèche, Cèze and Gardon rivers).
- Generalized floods that encompasses a combination of floods coming from a majority of tributaries.

Furthermore, by combining the work of Zebracki et al. (2015) on tracing the origin of flood materials delivered to the Rhône basin and quantifying the relative contribution of the different catchment watersheds, as well as the recent work of (Bodereau et al. 2022) classifying $\Delta^{14}C - POC$ based on flood types, a meta-classification of the biogeochemical flood inputs can be established. Both classifications provide a hydrological (river flow rate, sediment export, and suspended particle matter) and geochemical (radionuclide) marker typology that is closely related to the flood typology and its carbon load. To upscale beyond this independent but related classification, a combination of both data to yield a linear superposition of typology can be achieved. For example, we can combine the two typologies to derive a biogeochemical typology defined from the linear combination between the “flood-hydrology” space typology and “flood-carbon” typology. To obtain this biogeochemical typology, we proceed by calculating the total carbon mineralization rate expected from the distribution of sediment export from 2001 to 2011 for each flood type (Zebracki et al. 2015). This sediment load is normalized to the range of thicknesses deposited from field observation discussed in previous chapters. Similar mapping from the $\Delta^{14}C - POC$ - denoting the sediment source contribution derived from clustering analysis (Bodereau et al. 2022) to the carbon enrichment factor (as discussed in Chapter 3) was done. Together, the thickness and carbon enrichment proxy can be used to estimate the expected rate of carbon mineralization from the observed intensity and composition of the flood materials as discussed in chapter 3. Hierarchical clustering of the OC mineralization rates derived from these simulations can provide a simple classification of the sediment response intensity to the flood deposition, with the result serving as a basis for extrapolating the biogeochemical implication of the deposition.

In Figure 6.1, the range of expression in terms of the flood type and sediment source on the total carbon mineralization rate is shown. Clearly, we see a linear tendency between sediment thickness linked to flood-hydrology and the flood-carbon typologies related to the enrichment factor on the biogeochemical rate with a stronger effect at higher flood-hydrology-carbon type (see inset in Figure 6.1). This typology suggests that for the Rhône area, the river input to the deltas with its associated source-type modulated by the varying age and degree of reactivities of sediment carbon deposited could have a substantial range of impact on biogeochemistry. This preliminary analysis is in agreement with previous work in this area and the works of chapter 4-5 demonstrating that the carbon arriving from the Rhone river in the prodeltaic area carry sediment of different properties related to the flood history (type of flood, the composition of the eroded catchment area), which exhibit a wide range of biogeochemical response (Lansard et al. 2009a; Bourgeois et al. 2011; Cathalot et al. 2013).

Furthermore, clustering analysis of the total carbon oxidation rate reveal three degree of the intensity of sediment response induced by these flood depositions: A low intensity response characterized by lower carbon mineralization rate possibly driven by refractory materials (e.g. sediment delivered in spring 2008), a high intensity response modulated by enriched organic matter in high deposited sediment (e.g. sediment input in the fall 2008) and an intermediate biogeochemical type response possibly comprising the mixture of both sediment characteristics (e.g. winter 2021-22 Figure 6.1). Although, the processes operating in the sediment are often

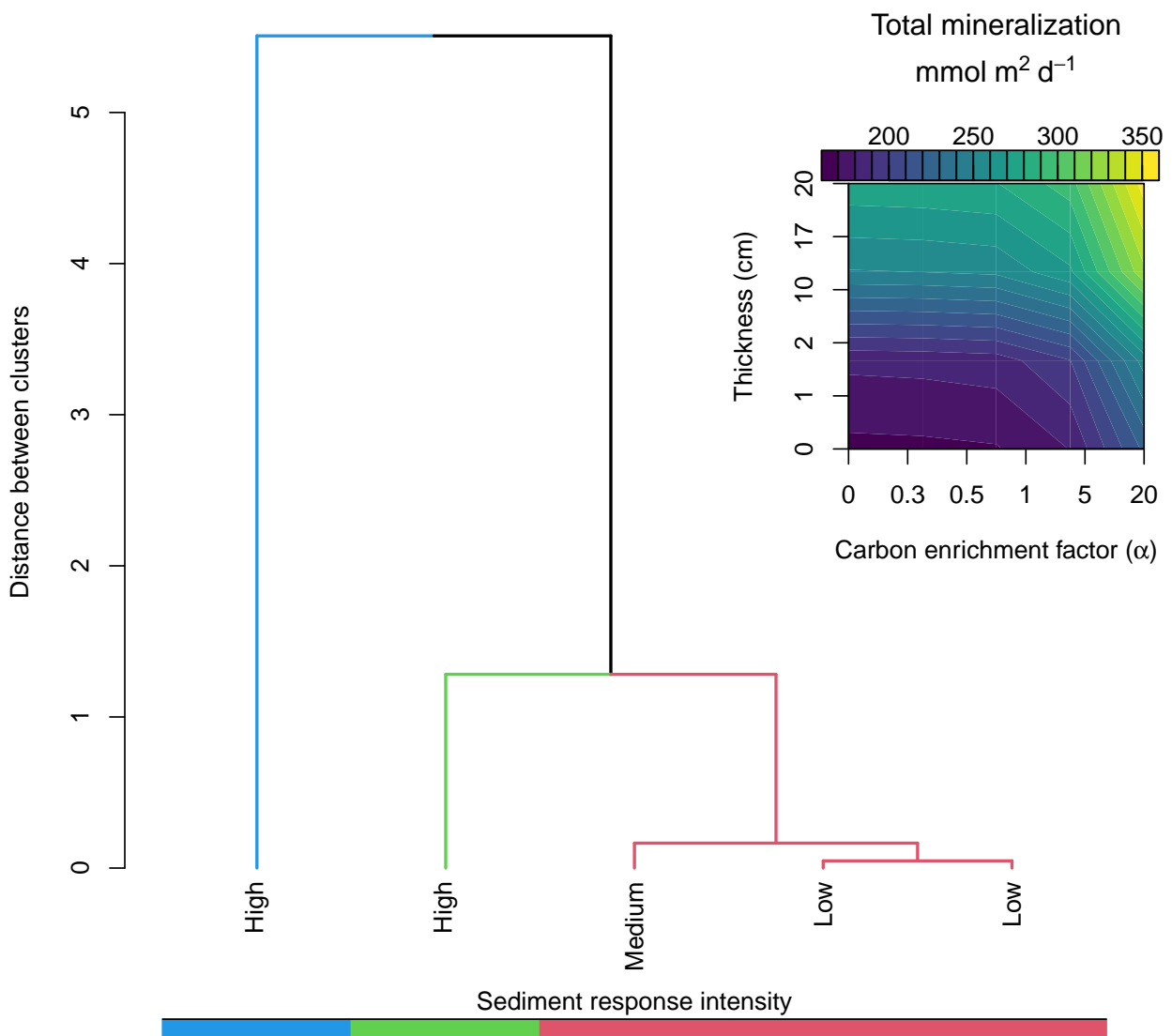


Figure 6.1: Biogeochemical typology from the Rhône prodelta sediment. A preliminary result from hierarchical clustering analysis of the total carbon mineralization range (insert) across the expectation of carbon enrichment and sediment deposition thickness in the prodelta area.

non-linear and complex, such classification underscores how the intensity of flood deposition and its history upon deposition can affect biogeochemical processes in the sediment. Beyond this ad-hoc analysis of the typology of sediment response, future work for a better understanding of the coupling between the flood history, characteristics of the deposited sediment and the sediment biogeochemistry needs to be prioritized.

Table 6.1: : Major characteristics of some major river systems classified by annual river and sediment discharge, drainage basin area and flux of particulate organic carbon. ^aMilliman and Meade (1983); McKee et al. (2004), Milliman and Farnsworth (2013). ¹Cai et al. (2008) and references herein, ²Moreira-Turcq et al. (2003), ³Ludwig et al. (1996) and references herein, ⁴Dittmar and Kattner (2003), ⁵Gebhardt et al. (2004), ⁶Sempéré et al. (2000)

Rivers	Sediment discharge ^a (10 ⁶ t yr ⁻¹)	Fresh water discharge (10 ⁹ m ³ yr ⁻¹)	Drainage basin area (10 ⁶ km ²)	Degradable POC flux (t km ⁻² yr ⁻¹)
Lena, Russia ^{1,4,5}	11	510	2.49	0.5
St Lawrence, Canada ^{1,3}	3	450	1.03	0.4
Yangtze, China ^{1,3}	480	900	1.94	5.7
Mekong, Vietnam ¹	160	470	0.79	
Pearl, China	80	300	0.44	
Mississippi, USA ^{1,3}	210	530	3.27	0.3
Amazon, Brazil ^{1,2}	1150	6300	6.15	1.0
Rhône, France⁶	10	53	0.98	0.2

In addition, simple extrapolation to other coastal and shelf area can be done. For example, Table 6.1 shows how the Rhône river compares with other river-dominated ocean margin (RiOMar) regions. Although the Rhône river is comparatively different from other RiOMar systems in terms of its functioning (Rabouille et al. 2008), we can speculate how flood deposition might affect biogeochemical processes in the adjacent coastal zone. As the Rhône River has similar sediment load to drainage surface area ratio with the Yangtze and Pearl River, we can expect some similarity in the biogeochemical classification. However, such transfer of knowledge from the Rhône prodelta sediment to other similar region ought to be taken with caution as the drivers of some of these RiOMar systems are different (Rabouille et al. 2008). For examples, the Rhone River and its adjacent basin differs in terms of their basin area, seasonality in their discharge, magnitude of sediment export, nutrient input as well as physical and biogeochemical functioning (Estournel et al. 2001; Yin et al. 2004; Rabouille et al. 2008). These differences would make such extrapolation difficult as site-specific assumption have to be accounted for in models (Mieleitner and Reichert 2006). Indeed, this demands that more in-depth research should be conducted in order to understand how coastal deltas behave under episodic deposition of sediment.

6.2.2 Benthic-pelagic coupling

The pelagic and benthic ecosystems are strongly connected in shallow coastal and shelf areas, where a large portion of primary production occurs. This is due to the fact that organic matter that escapes degradation in the water column and reaches the sediment undergoes biogeochemical transformation in the sediment, as well as the existence of a dual exchange of materials between both compartments. Furthermore, lateral transport of

particulate matter across the river-ocean continuum results in considerable POC transfer in coastal locations (Aufdenkampe et al. 2011). The extent and unpredictability of this vertical and horizontal coupling which very often occurs as events (storms and dense water cascading (Ulses et al. 2008a), algal bloom (Karlson et al. 2021; Li et al. 2022)) have significant implications for coastal issues such as eutrophication, carbon capture, and deoxygenation.

As the flux of solutes (e.g. oxygen, sulfate, DIC) across the sediment-water interface determined via measurements such in-situ benthic chambers, or ex-situ core-incubation are limited in space and time and only offers a snapshot of benthic-pelagic exchanges, the need of augmenting observational data with numerical models is increasingly emphasized (Middelburg and Soetaert 2004; Brady et al. 2013; Lessin et al. 2018). Despite this thesis showcasing the use of sediment biogeochemical model for understanding the temporal variability of the sediment response to external perturbation, only a limited spatial information is offered and the feedback with the overlying bottom water is crudely modelled. Future progression of this thesis ought to consider the horizontal distribution of these fluxes on a basin scale as organic carbon distribution and the resulting diffusive flux of solutes can display variability with respect to proximity to the coast and the associated carbon flux (Cathalot et al. 2010; Many et al. 2021; Estournel et al. 2023). The next frontier of challenge to overcome lies in upscaling FESDIA model towards the entire prodelta area and possibly the shelf portion of the Gulf of Lion.

To achieve this goal, it is important to acknowledge that although pelagic and benthic models have both substantially progressed, their coupling (especially in 3D models) is by far less advanced. In most coupled model, the choice of a lower boundary condition in water column models is often simplified without careful representation of the essentials of sediment-water exchange (Soetaert et al. 2000). In these simplified models, benthic systems are generally under-represented and mostly modelled as a simple closure term for mass conservation (Lessin et al. 2018). Despite these drawbacks, attempts at fully coupled regional 3D pelagic-benthic models have been successfully developed and applied (Baretta et al. 1995; Wakelin et al. 2012; Capet et al. 2016; Moriarty et al. 2017) illustrating that there is no fundamental barrier between the two domains.

In the Rhône area, we have begun attempting to push this limit further (Figure 6.2). Here, work is currently underway to integrate the hydrodynamic regional ocean circulation SYMPHONIE (Marsaleix et al. 2008), a 3D primitive equation, free surface, and generalized sigma vertical coordinate model. This model has previously been used to simulate Mediterranean Sea hydrodynamic conditions and specific processes such as Rhône River plume dynamics (Estournel et al. 2001), coastal dense water formation (Ulses et al. 2008c), wind-induced circulation over the Gulf of Lion shelf (Estournel et al. 2003; Ulses et al. 2008a), shelf-slope exchanges, and along-slope circulation (Mikolajczak et al. 2020).

This model has been coupled to the pelagic ecosystem model Eco3M-S, a multi-plankton and multi-nutrient dynamics model that simulates the dynamics of biogenic element (carbon, nitrogen, phosphorus, silicon, and oxygen) and plankton group biogeochemical cycles (Auger et al. 2011; Ulses et al. 2016). This model includes seven compartments: one with four dissolved nutrients (nitrate, ammonium, phosphate, and silicate), a three phytoplankton size classes (pico-, nano-, and micro-phytoplankton), a three zooplankton size classes (nano-, micro-, and meso-zooplankton), a bacterial compartment, a dissolved organic matter compartment, a compartment with particulate organic matter, and a compartment with dissolved oxygen.

For this ongoing project, the attempt to couple the pelagic biophysical model with the sediment model have been prototyped for OMEXDIA model (Soetaert et al. 1996a) with the next step toward implementing the full FESDIA model developed in this thesis. Preliminary results from our analysis are shown in Figure 6.2 highlight-

ing the regional scale distribution of the benthic variables. Here, the importance of the transported particulate organic carbon (POC) on the prodelta superficial chemistry is obvious. The response of oxygen, nutrient and reduced species shows an offshore gradient in agreement with observation in the prodeltaic (Lansard et al. 2009b). Further work beyond this thesis will continue to extend this model to provide greater realism of the processes operating in this region and better understanding of the system complexity and feedbacks with pelagic ecosystem dynamics.

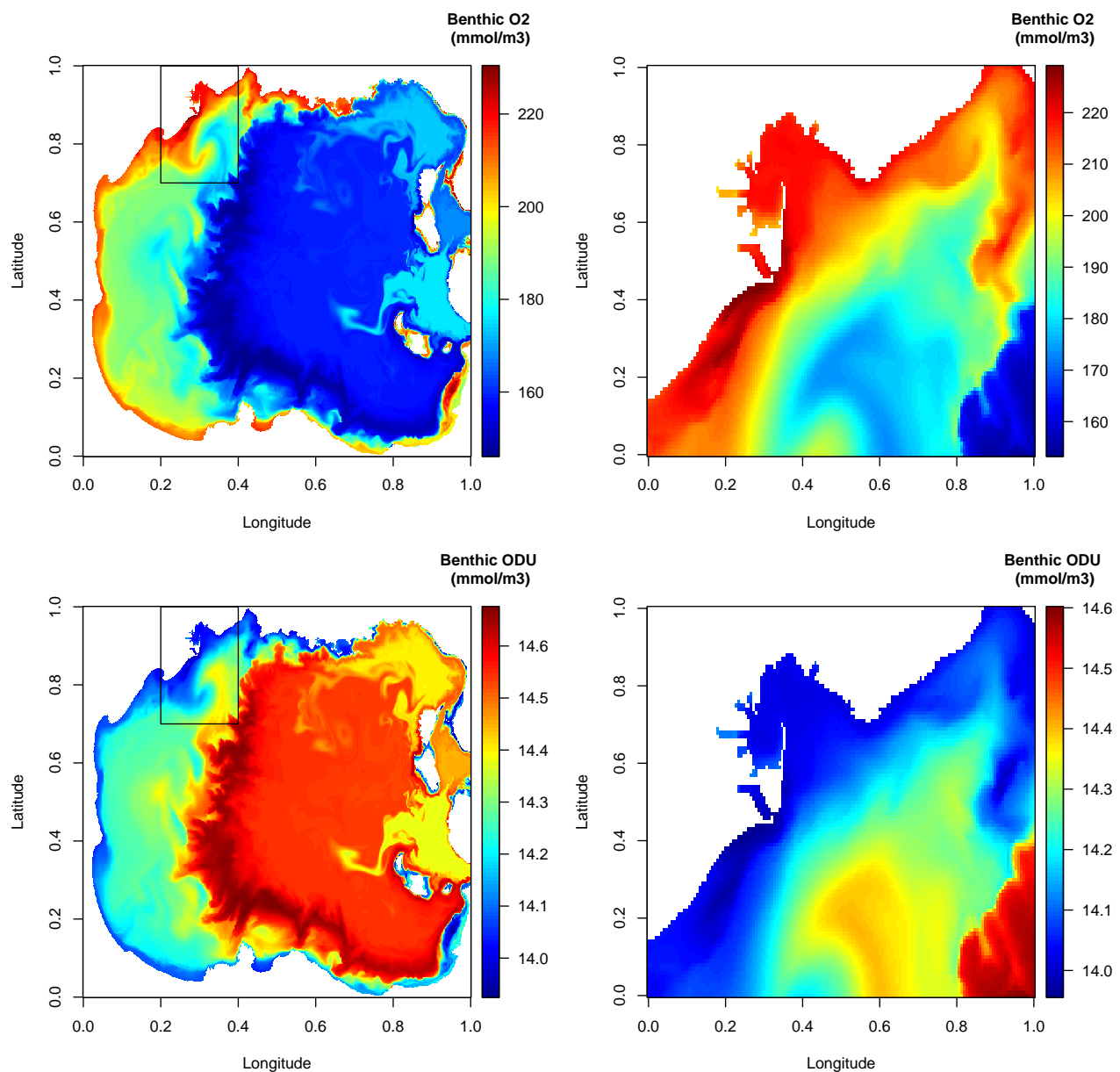


Figure 6.2: (Left) Basin scale sediment porewater surface composition from a coupled early diagenetic model (OMEXDIA) with 3D hydrodynamic model (SYMPHONIE / ECO3M). (Right) Zoom into the prodelta region. Preliminary output from a 5 year simulation over the Gulf of Lions.

6.2.3 Long-term impact of flood deposition

With the entire thesis outcome limited to the short to intermediate-term effects of the massive flood deposition (< 1 year), another near-term goal for the advancement of this work will be to investigate the multi-year impact of the extreme events on the sediment biogeochemistry. To go beyond the site-specific studies outlined in

previous chapters and analyse past, present and future changes of the marine biogeochemistry (Arndt et al. 2013), model simulations with longer timescale are required. This is important because sediment burial is the ultimate sink for the biogeochemical cycle of carbon, iron and sulfur as well as other cycles not considered in this thesis (e.g. silica), and is thus a crucial factor in the establishment of the long-term mass balance of elements in the coastal ocean. Unfortunately, the temporally short simulation done in prior chapters does not effectively depict this long-term burial sink.

In addition, the future trajectory of the different biogeochemical pathways in sediment following this increasing frequency of large flood deposition is still unclear. Questions of the eventual fate of some deep-lying diagenetic processes (e.g. Methanogenesis or mineral precipitation/dissolution) were not easily diagnosed from the simulations performed in earlier chapters. For some processes, the final convergence or divergence to a stable, pre-flood situation or an entirely new state is still largely unknown.

To overcome this limitation, and evaluate the long-term response and fate of associated biogeochemical processes affecting the sediment porewater and solid phase, work on longer timescale simulations should be conducted. For example, a reanalysis of model simulation without multi-flood interaction, such as that performed in Chapter 4, at a longer timescale revealed that within the order of a year, most pathways for carbon mineralization rate are well within their pre-flood value. However, in the absence of other flood deposition during the five-year simulation, methanogenesis takes a substantially longer time to reach a stable pre-flood state (almost 2 years) (Figure 6.3). This example highlights the importance of lengthier simulations, particularly for investigations concentrating on diagenetic processes working in deeper sediment or biogeochemical cycles with long-term fate (e.g., carbon, silicate (Heinze et al. 2003; Bernard et al. 2010)). Indeed, this simplistic scenario ignores the effect of increasing flood frequency or the intensity and amount of deposited sediment. It still provides insights into the type of behaviour shown by porewater in terms of organic carbon oxidation over longer timescales.

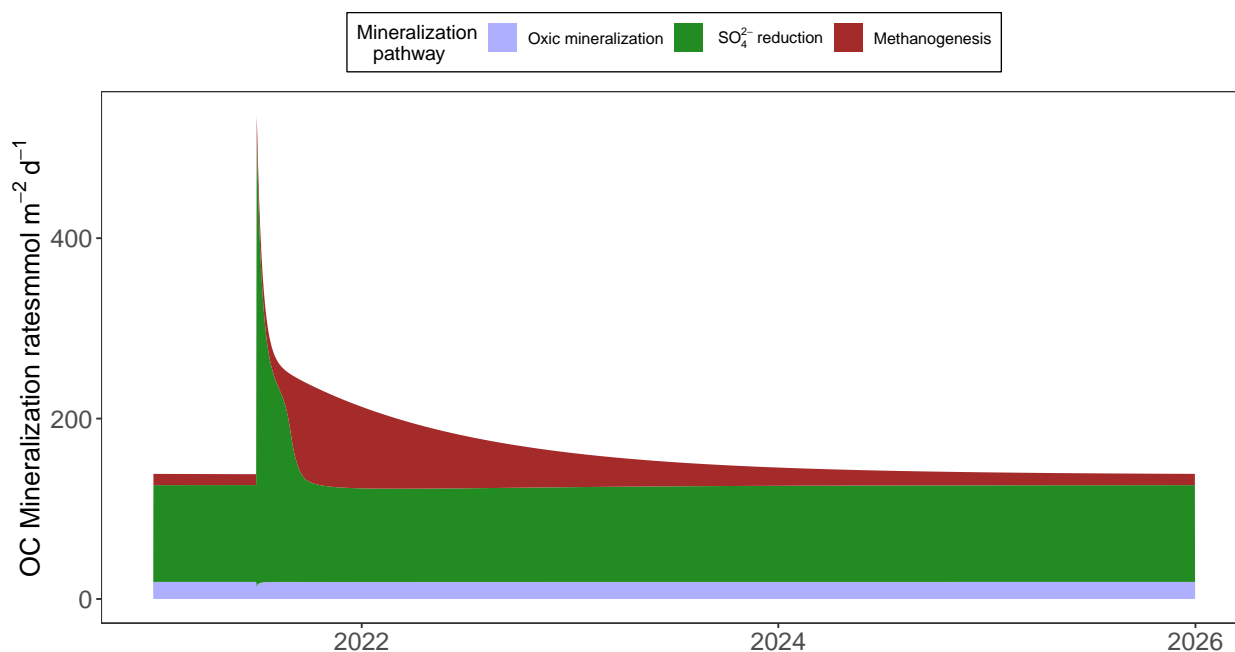


Figure 6.3: Long term view of carbon cycling following a single depositional event. Parameters and forcing is similar to model simulation performed in Chapter 6 but over a five-year period.

In addition, the intrinsic characteristics of the Rhône prodelta sediment such as its apparent stability (thus the aforementioned term - “*biogeochemical attractors*”) despite such large quantities of sediment deposition can

only be diagnosed properly by simulation forecasting the long-term fate of the different chemical species. While, the outcome of this thesis provides preliminary insights into the short and intermediate fates of only a few variables (e.g. oxygen, sulfate, DIC - Chapter 3) as well as carbon-centric pathways, more effort should be made to quantify the response of other diagenetic variables in terms of the magnitude of their rate and flux at appropriate timescales, post-flood dynamics, and possibly relaxation timescales. This long-term perspective necessitates concurrent improvements in monitoring these flood depositions in order to properly constrain the prediction of the model. In recent years, the community has made significant efforts to create equipment and techniques for continuous research on transient events impacting benthic mineralization rates and associated relaxation processes (Berg et al. 2013; Toussaint et al. 2014). The integration of these measurements techniques over the long term and model should be the next frontier.

To conclude this subsection, in anticipating longer diagenetic simulation under this massive deposition and changing environmental condition, certain factors which might affect organic matter upon deposition need to be considered. For example, the temperature dependency of organic matter mineralization needs to be accounted for (Arnosti et al. 1998; Robador et al. 2010), although there are observational evidences that the effect of seasonal temperature variations cannot be easily translated to long-term temperature increases induced by either slow burial of organic matter along geothermal gradient or by climate change (Tabuchi et al. 2010; Kirschbaum 2013). Better model parameterization, as well as including the source-origin and reactivity of organic matter arriving at the depocenter, are also required (Magen et al. 2010; Arndt et al. 2013; Toussaint et al. 2013b; Zhang et al. 2014) whereas calibration data is required for accurately comparing the model output (Smeaton and Austin 2022). Our ability to quantify carbon cycling in deep sediments or under changing climate conditions will thus be heavily reliant on a better mechanistic understanding of the effect of long-term environmental changes, relevant high-throughput data, and modelling advances (Arndt et al. 2013).

References

- Aguilera, D., P. Jourabchi, C. Spiteri, and P. Regnier. 2005. A knowledge-based reactive transport approach for the simulation of biogeochemical dynamics in earth systems. *Geochemistry, Geophysics, Geosystems* **6**.
- Ait Ballagh, F. E., C. Rabouille, F. Andrieux-Loyer, and others. 2021. Spatial variability of organic matter and phosphorus cycling in rhône river prodelta sediments (NW mediterranean sea, france): A model-data approach. *Estuaries and Coasts* **44**: 1765–1789.
- Aller, R. C. 1980. Diagenetic processes near the sediment-water interface of long island sound. I.: Decomposition and nutrient element geochemistry (s, n, p), p. 237–350. *In Advances in geophysics*. Elsevier.
- Aller, R. C. 1982. The effects of macrobenthos on chemical properties of marine sediment and overlying water. *Animal-sediment relations: the biogenic alteration of sediments* 53–102.
- Aller, R. C. 1998. Mobile deltaic and continental shelf muds as suboxic, fluidized bed reactors. *Marine Chemistry* **61**: 143–155.
- Aller, R. C. 2004. Conceptual models of early diagenetic processes: The muddy seafloor as an unsteady, batch reactor. *Journal of Marine Research* **62**: 815–835.
- Aller, R. C., and J. Y. Aller. 1992. Meiofauna and solute transport in marine muds. *Limnology and oceanography* **37**: 1018–1033.
- Aller, R. C., N. E. Blair, and G. J. Brunskill. 2008. Early diagenetic cycling, incineration, and burial of sedimentary organic carbon in the central gulf of papua (papua new guinea). *Journal of Geophysical Research: Earth Surface* **113**.
- Aller, R., N. Blair, Q. Xia, and P. Rude. 1996. Remineralization rates, recycling, and storage of carbon in amazon shelf sediments. *Continental Shelf Research* **16**: 753–786.
- Allison, M. A., M. T. Lee, A. S. Ogston, and R. C. Aller. 2000. Origin of amazon mudbanks along the northeastern coast of south america. *Marine Geology* **163**: 241–256.
- Almroth, E., A. Tengberg, J. H. Andersson, S. Pakhomova, and P. O. Hall. 2009. Effects of resuspension on benthic fluxes of oxygen, nutrients, dissolved inorganic carbon, iron and manganese in the gulf of finland, baltic sea. *Continental Shelf Research* **29**: 807–818.
- Andersson, A., and F. Mackenzie. 2012. Revisiting four scientific debates in ocean acidification research. *Biogeosciences* **9**: 893–905.
- Anschutz, P., F. Jorissen, G. Chaillou, R. Abu-Zied, and C. Fontanier. 2002. Recent turbidite deposition in the eastern atlantic: Early diagenesis and biotic recovery. *Journal of Marine Research* **60**: 835–854.
- Antonelli, C., F. Eyrolle, B. Rolland, M. Provansal, and F. Sabatier. 2008. Suspended sediment and ^{137}Cs fluxes during the exceptional december 2003 flood in the rhone river, southeast france. *Geomorphology* **95**: 350–360.
- Archer, D., J. Morford, and S. Emerson. 2002. A model of suboxic sedimentary diagenesis suitable for auto-

-
- matic tuning and gridded global domains. *Global Biogeochemical Cycles* **16**: 17–1.
- Arndt, S., B. B. Jørgensen, D. E. LaRowe, J. Middelburg, R. Pancost, and P. Regnier. 2013. Quantifying the degradation of organic matter in marine sediments: A review and synthesis. *Earth-science reviews* **123**: 53–86.
- Arnosti, C., B. B. Jørgensen, J. Sagemann, and B. Thamdrup. 1998. Temperature dependence of microbial degradation of organic matter in marine sediments: Polysaccharide hydrolysis, oxygen consumption, and sulfate reduction. *Marine Ecology Progress Series* **165**: 59–70.
- Aufdenkampe, A. K., E. Mayorga, P. A. Raymond, J. M. Melack, S. C. Doney, S. R. Alin, R. E. Aalto, and K. Yoo. 2011. Riverine coupling of biogeochemical cycles between land, oceans, and atmosphere. *Frontiers in Ecology and the Environment* **9**: 53–60.
- Auger, P.-A., F. Diaz, C. Ulses, C. Estournel, J. Neveux, F. Joux, M. Pujo-Pay, and J. Naudin. 2011. Functioning of the planktonic ecosystem on the gulf of lions shelf (NW mediterranean) during spring and its impact on the carbon deposition: A field data and 3-d modelling combined approach. *Biogeosciences* **8**: 3231–3261.
- Ballagh, F. E. A., C. Rabouille, F. Andrieux-Loyer, K. Soetaert, K. Elkalay, and K. Khalil. 2020. Spatio-temporal dynamics of sedimentary phosphorus along two temperate eutrophic estuaries: A data-modelling approach. *Continental Shelf Research* **193**: 104037.
- Baretta, J., W. Ebenhöf, and P. Ruardij. 1995. The european regional seas ecosystem model, a complex marine ecosystem model. *Netherlands Journal of Sea Research* **33**: 233–246.
- Bauer, J. E., W.-J. Cai, P. A. Raymond, T. S. Bianchi, C. S. Hopkins, and P. A. Regnier. 2013. The changing carbon cycle of the coastal ocean. *Nature* **504**: 61–70.
- Bell, P., A. Mills, and J. Herman. 1987. Biogeochemical conditions favoring magnetite formation during anaerobic iron reduction. *Applied and Environmental Microbiology* **53**: 2610–2616.
- Bentley, S. J., and C. A. Nittrouer. 2003. Emplacement, modification, and preservation of event strata on a flood-dominated continental shelf: Eel shelf, northern california. *Continental Shelf Research* **23**: 1465–1493.
- Berg, P., M. H. Long, M. Huettel, and others. 2013. Eddy correlation measurements of oxygen fluxes in permeable sediments exposed to varying current flow and light. *Limnology and Oceanography* **58**: 1329–1343.
- Berg, P., S. Rysgaard, and B. Thamdrup. 2003. Dynamic modeling of early diagenesis and nutrient cycling. A case study in an arctic marine sediment. *American journal of science* **303**: 905–955.
- Bernard, C., G. G. Laruelle, C. Slomp, and C. Heinze. 2010. Impact of changes in river fluxes of silica on the global marine silicon cycle: A model comparison. *Biogeosciences* **7**: 441–453.
- Berner, R. A. 1964. An idealized model of dissolved sulfate distribution in recent sediments. *Geochimica et Cosmochimica Acta* **28**: 1497–1503.
- Berner, R. A. 1980. *Early Diagenesis: A Theoretical Approach*, Princeton University Press.
- Berner, R. A. 1982. Burial of organic carbon and pyrite sulfur in the modern ocean: Its geochemical and environmental significance. *Am. J. Sci.:(United States)* **282**.
- Bianchi, T. S., R. C. Aller, T. B. Atwood, and others. 2021. What global biogeochemical consequences will marine animal–sediment interactions have during climate change? *Elem Sci Anth* **9**: 00180.
- Bianchi, T. S., X. Cui, N. E. Blair, D. J. Burdige, T. I. Eglinton, and V. Galy. 2018. Centers of organic carbon burial and oxidation at the land-ocean interface. *Organic Geochemistry* **115**: 138–155.
- Bianucci, L., K. Balaguru, R. W. Smith, L. R. Leung, and J. M. Moriarty. 2018. Contribution of hurricane-induced sediment resuspension to coastal oxygen dynamics. *Scientific reports* **8**: 1–10.

-
- Bissett, A., C. Burke, P. L. Cook, and J. P. Bowman. 2007. Bacterial community shifts in organically perturbed sediments. *Environmental Microbiology* **9**: 46–60.
- Blair, N. E., and R. C. Aller. 2012. The fate of terrestrial organic carbon in the marine environment. *Annual review of marine science* **4**: 401–423.
- Blair, N. E., E. L. Leithold, and R. C. Aller. 2004. From bedrock to burial: The evolution of particulate organic carbon across coupled watershed-continental margin systems. *Marine Chemistry* **92**: 141–156.
- Bodereau, N., A. Delaval, H. Lepage, F. Eyrolle, P. Raimbault, and Y. Copard. 2022. Hydrological classification by clustering approach of time-integrated samples at the outlet of the Rhône river: Application to $\Delta^{14}\text{C}$ -POC. *Water Research* **220**: 118652.
- Boetius, A., K. Ravenschlag, C. J. Schubert, and others. 2000. A marine microbial consortium apparently mediating anaerobic oxidation of methane. *Nature* **407**: 623–626.
- Bonifácio, P., S. Bourgeois, C. Labrune, and others. 2014. Spatiotemporal changes in surface sediment characteristics and benthic macrofauna composition off the Rhône river in relation to its hydrological regime. *Estuarine, Coastal and Shelf Science* **151**: 196–209.
- Borges, A., and G. Abril. 2011. 5.04-carbon dioxide and methane dynamics in estuaries. 9780080878850.
- Borowski, W. S., C. K. Paull, and W. Ussler III. 1999. Global and local variations of interstitial sulfate gradients in deep-water, continental margin sediments: Sensitivity to underlying methane and gas hydrates. *Marine Geology* **159**: 131–154.
- Boudet, L., F. Sabatier, and O. Radakovitch. 2017. Modelling of sediment transport pattern in the mouth of the Rhône delta: Role of storm and flood events. *Estuarine, Coastal and Shelf Science* **198**: 568–582. doi:10.1016/j.ecss.2016.10.004
- Boudreau, B. P. 1994. Is burial velocity a master parameter for bioturbation? *Geochimica et Cosmochimica Acta* **58**: 1243–1249.
- Boudreau, B. P. 1996. A method-of-lines code for carbon and nutrient diagenesis in aquatic sediments. *Computers & Geosciences* **22**: 479–496.
- Boudreau, B. P. 1997. *Diagenetic models and their implementation*, Springer, Berlin.
- Boudreau, B. P. 1999. Metals and models: Diagenetic modelling in freshwater lacustrine sediments. *Journal of Paleolimnology* **22**: 227–251.
- Boudreau, B. P., and B. B. Jørgensen. 2001. The benthic boundary layer: Transport processes and biogeochemistry.
- Boudreau, B. P., and B. R. Ruddick. 1991. On a reactive continuum representation of organic matter diagenesis. *American Journal of Science* **291**: 507–538.
- Bourgeois, S., A. Pruski, M.-Y. Sun, and others. 2011. Distribution and lability of land-derived organic matter in the surface sediments of the Rhône prodelta and the adjacent shelf (Mediterranean Sea, France): A multi proxy study. *Biogeosciences* **8**: 3107–3125.
- Bourrin, F., P. L. Friend, C. L. Amos, E. Manca, C. Ulses, A. Palanques, X. D. De Madron, and C. E. Thompson. 2008. Sediment dispersal from a typical Mediterranean flood: The Têt river, Gulf of Lions. *Continental Shelf Research* **28**: 1895–1910.
- Brady, D. C., J. M. Testa, D. M. Di Toro, W. R. Boynton, and W. M. Kemp. 2013. Sediment flux modeling: Calibration and application for coastal systems. *Estuarine, Coastal and Shelf Science* **117**: 107–124.
- Braeckman, U., C. Van Colen, K. Soetaert, M. Vincx, and J. Vanaverbeke. 2011. Contrasting macrobenthic activities differentially affect nematode density and diversity in a shallow subtidal marine sediment. *Marine Ecology Progress Series* **422**: 179–191.

-
- Burdige, D. 2011. 5.09 estuarine and coastal sediments–coupled biogeochemical cycling. *Treatise on estuarine and coastal science* **5**: 279–308.
- Burdige, D. J. 1991. The kinetics of organic matter mineralization in anoxic marine sediments. *Journal of Marine Research* **49**: 727–761.
- Burdige, D. J. 1993. The biogeochemistry of manganese and iron reduction in marine sediments. *Earth-Science Reviews* **35**: 249–284.
- Burdige, D. J. 2005. Burial of terrestrial organic matter in marine sediments: A re-assessment. *Global Biogeochemical Cycles* **19**.
- Burdige, D. J. 2007. Preservation of organic matter in marine sediments: Controls, mechanisms, and an imbalance in sediment organic carbon budgets? *Chemical reviews* **107**: 467–485.
- Burdige, D. J., and J. M. Gieskes. 1983. A pore water/solid phase diagenetic model for manganese in marine sediments. *American Journal of Science* **283**.
- Burdige, D. J., and T. Komada. 2011. Anaerobic oxidation of methane and the stoichiometry of remineralization processes in continental margin sediments. *Limnology and Oceanography* **56**: 1781–1796.
- Cai, W.-J. 2011. Estuarine and coastal ocean carbon paradox: CO₂ sinks or sites of terrestrial carbon incineration? *Annual review of marine science* **3**: 123–145.
- Cai, W.-J., X. Guo, C.-T. A. Chen, and others. 2008. A comparative overview of weathering intensity and HCO₃⁻ flux in the world's major rivers with emphasis on the changjiang, huanghe, zhujiang (pearl) and mississippi rivers. *Continental Shelf Research* **28**: 1538–1549.
- Canfield, D. E. 2004. The evolution of the earth surface sulfur reservoir. *American Journal of Science* **304**: 839–861.
- Canfield, D. E., R. Raiswell, and S. H. Bottrell. 1992. The reactivity of sedimentary iron minerals toward sulfide. *American Journal of Science* **292**: 659–683.
- Canfield, D. E., and B. Thamdrup. 2009. Towards a consistent classification scheme for geochemical environments, or, why we wish the term 'suboxic' would go away. *Geobiology* **7**: 385–392.
- Canfield, D. E., B. Thamdrup, and J. W. Hansen. 1993. The anaerobic degradation of organic matter in danish coastal sediments: Iron reduction, manganese reduction, and sulfate reduction. *Geochimica et Cosmochimica Acta* **57**: 3867–3883.
- Capet, A., F. J. Meysman, I. Akoumianaki, K. Soetaert, and M. Grégoire. 2016. Integrating sediment biogeochemistry into 3D oceanic models: A study of benthic-pelagic coupling in the Black Sea. *Ocean Modelling* **101**: 83–100.
- Carlin, J. A., K. M. Schreiner, T. M. Dellapenna, A. McGuffin, and R. W. Smith. 2021. Evidence of recent flood deposits within a distal shelf depocenter and implications for terrestrial carbon preservation in non-deltaic shelf settings. *Marine Geology* **431**: 106376.
- Carter, R., P. Larcombe, J. Dye, M. Gagan, and D. Johnson. 2009. Long-shelf sediment transport and stormbed formation by cyclone winifred, central great barrier reef, australia. *Marine Geology* **267**: 101–113.
- Cathalot, C., C. Rabouille, L. Pastor, and others. 2010. Temporal variability of carbon recycling in coastal sediments influenced by rivers: Assessing the impact of flood inputs in the Rhône River prodelta. *Biogeochemistry* **7**: 1187–1205. doi:10.5194/bg-7-1187-2010
- Cathalot, C., C. Rabouille, N. Tisnérat-Laborde, and others. 2013. The fate of river organic carbon in coastal areas: A study in the Rhône river delta using multiple isotopic ($\delta^{13}\text{C}$, $\Delta^{14}\text{C}$) and organic tracers. *Geochimica et Cosmochimica Acta* **118**: 33–55.
- Centler, F., H. Shao, C. De Biase, C.-H. Park, P. Regnier, O. Kolditz, and M. Thullner. 2010. GeoSysBRNS—

-
- a flexible multidimensional reactive transport model for simulating biogeochemical subsurface processes. *Computers & Geosciences* **36**: 397–405.
- Chaillou, G., P. Anschutz, C. Dubrulle, and P. Lecroart. 2007. Transient states in diagenesis following the deposition of a gravity layer: Dynamics of O₂, Mn, Fe and N-species in experimental units. *Aquatic Geochemistry* **13**: 157–172.
- Chakrapani, G. J. 2005. Factors controlling variations in river sediment loads. *Current Science* 569–575.
- Charmasson, S., O. Radakovitch, M. Arnaud, P. Bouisset, and A.-S. Pruchon. 1998. Long-core profiles of ¹³⁷Cs, ¹³⁴Cs, ⁶⁰Co and ²¹⁰Pb in sediment near the Rhone river (northwestern Mediterranean Sea). *Estuaries* **21**: 367–378.
- Cheng, P., M. Li, and Y. Li. 2013. Generation of an estuarine sediment plume by a tropical storm. *Journal of Geophysical Research: Oceans* **118**: 856–868.
- Copard, Y., F. Eyrolle, O. Radakovitch, A. Poirel, P. Raimbault, S. Gairoard, and C. Di-Giovanni. 2018. Badlands as a hot spot of petrogenic contribution to riverine particulate organic carbon to the Gulf of Lion (NW Mediterranean Sea). *Earth Surface Processes and Landforms* **43**: 2495–2509. doi:10.1002/esp.4409
- Couture, R.-M., R. Fischer, P. Van Cappellen, and C. Gobeil. 2016. Non-steady state diagenesis of organic and inorganic sulfur in lake sediments. *Geochimica et Cosmochimica Acta* **194**: 15–33.
- Couture, R.-M., B. Shafei, P. Van Cappellen, A. Tessier, and C. Gobeil. 2010. Non-steady state modeling of arsenic diagenesis in lake sediments. *Environmental Science & Technology* **44**: 197–203.
- Crill, P. M., and C. S. Martens. 1983. Spatial and temporal fluctuations of methane production in anoxic coastal marine sediments. *Limnology and Oceanography* **28**: 1117–1130.
- Dagg, M., R. Benner, S. Lohrenz, and D. Lawrence. 2004. Transformation of dissolved and particulate materials on continental shelves influenced by large rivers: Plume processes. *Continental Shelf Research* **24**: 833–858.
- Dai, M., J. Su, Y. Zhao, and others. 2022. Carbon fluxes in the coastal ocean: Synthesis, boundary processes, and future trends. *Annual Review of Earth and Planetary Sciences* **50**: 593–626.
- Dai, Z., X. Mei, S. E. Darby, Y. Lou, and W. Li. 2018. Fluvial sediment transfer in the Changjiang (Yangtze) river-estuary depositional system. *Journal of Hydrology* **566**: 719–734.
- Dale, A. W., S. Flury, H. Fossing, P. Regnier, H. Røyt, C. Scholze, and B. Jørgensen. 2019. Kinetics of organic carbon mineralization and methane formation in marine sediments (Aarhus Bay, Denmark). *Geochimica et Cosmochimica Acta* **252**: 159–178.
- Dale, A. W., L. Nickelsen, F. Scholz, C. Hensen, A. Oschlies, and K. Wallmann. 2015. A revised global estimate of dissolved iron fluxes from marine sediments. *Global Biogeochemical Cycles* **29**: 691–707.
- Dale, A. W., P. Regnier, N. J. Knab, B. B. Jørgensen, and P. Van Cappellen. 2007. Anaerobic oxidation of methane (AOM) in marine sediments from the Skagerrak (Denmark): II. Further insights with a reaction-transport model. *Controls of anaerobic oxidation of methane in ocean margin sediments* 91.
- Dale, A. W., P. Regnier, N. Knab, B. Jørgensen, and P. Van Cappellen. 2008a. Anaerobic oxidation of methane (AOM) in marine sediments from the Skagerrak (Denmark): II. Reaction-transport modeling. *Geochimica et Cosmochimica Acta* **72**: 2880–2894.
- Dale, A. W., P. Regnier, and P. Van Cappellen. 2006. Bioenergetic controls on anaerobic oxidation of methane (AOM) in coastal marine sediments: A theoretical analysis. *American Journal of Science* **306**: 246–294.
- Dale, A. W., P. Van Cappellen, D. Aguilera, and P. Regnier. 2008b. Methane efflux from marine sediments in passive and active margins: Estimations from bioenergetic reaction-transport simulations. *Earth and Planetary Science Letters* **265**: 329–344.

-
- Day, J. W., C. Ibáñez, D. Pont, and F. Scarton. 2019. Status and sustainability of mediterranean deltas: The case of the ebro, rhône, and po deltas and venice lagoon, p. 237–249. *In* *Coasts and estuaries*. Elsevier.
- De Borger, E., J. Tiano, U. Braeckman, A. D. Rijnsdorp, and K. Soetaert. 2021a. Impact of bottom trawling on sediment biogeochemistry: A modelling approach. *Biogeosciences* **18**: 2539–2557.
- De Borger, E., J. Tiano, U. Braeckman, A. D. Rijnsdorp, and K. Soetaert. 2021b. Impact of bottom trawling on sediment biogeochemistry: A modelling approach. *Biogeosciences* **18**: 2539–2557. doi:10.5194/bg-18-2539-2021
- Deflandre, B., A. Mucci, J.-P. Gagné, C. Guignard, and B. Jørn Sundby. 2002. Early diagenetic processes in coastal marine sediments disturbed by a catastrophic sedimentation event. *Geochimica et Cosmochimica Acta* **66**: 2547–2558.
- Dezzeo, N., R. Herrera, G. Escalante, and N. Chacón. 2000. Deposition of sediments during a flood event on seasonally flooded forests of the lower orinoco river and two of its black-water tributaries, venezuela. *Biogeochemistry* **49**: 241–257.
- Dhillon, G. S., and S. Inamdar. 2013. Extreme storms and changes in particulate and dissolved organic carbon in runoff: Entering uncharted waters? *Geophysical research letters* **40**: 1322–1327.
- Dittmar, T., and G. Kattner. 2003. The biogeochemistry of the river and shelf ecosystem of the arctic ocean: A review. *Marine chemistry* **83**: 103–120.
- Dittrich, M., B. Wehrli, and P. Reichert. 2009. Lake sediments during the transient eutrophication period: Reactive-transport model and identifiability study. *Ecological Modelling* **220**: 2751–2769.
- Dufois, F., P. Garreau, P. Le Hir, and P. Forget. 2008. Wave-and current-induced bottom shear stress distribution in the gulf of lions. *Continental Shelf Research* **28**: 1920–1934.
- Dufois, F., R. Verney, P. Le Hir, F. Dumas, and S. Charmasson. 2014. Impact of winter storms on sediment erosion in the rhone river prodelta and fate of sediment in the gulf of lions (north western mediterranean sea). *Continental Shelf Research* **72**: 57–72.
- Dumoulin, J., L. Pozzato, J. Rassman, and others. 2018. Isotopic signature ($\delta^{13}C,^{14}C$) of DIC in sediment pore waters: An example from the rhone river delta. *Radiocarbon* **60**: 1465–1481.
- Efron, B. 1992. Bootstrap methods: Another look at the jackknife, p. 569–593. *In* *Breakthroughs in statistics*. Springer.
- Egger, M., W. Lenstra, D. Jong, and others. 2016. Rapid sediment accumulation results in high methane effluxes from coastal sediments. *PloS one* **11**: e0161609.
- Egger, M., N. Riedinger, J. M. Mogollón, and B. B. Jørgensen. 2018. Global diffusive fluxes of methane in marine sediments. *Nature Geoscience* **11**: 421–425.
- Eglinton, T. I. 2008. Tempestuous transport. *Nature Geoscience* **1**: 727–728.
- Eppley, R. W., and B. J. Peterson. 1979. Particulate organic matter flux and planktonic new production in the deep ocean. *Nature* **282**: 677–680.
- Estournel, C., P. Broche, P. Marsaleix, J.-L. Devenon, F. Auclair, and R. Vehil. 2001. The rhone river plume in unsteady conditions: Numerical and experimental results. *Estuarine, Coastal and Shelf Science* **53**: 25–38.
- Estournel, C., X. Durrieu de Madron, P. Marsaleix, F. Auclair, C. Julliard, and R. Vehil. 2003. Observation and modeling of the winter coastal oceanic circulation in the gulf of lion under wind conditions influenced by the continental orography (FETCH experiment). *Journal of Geophysical Research: Oceans* **108**.
- Estournel, C., G. Mikolajczak, C. Ulses, and others. 2023. Sediment dynamics in the gulf of lion (NW mediterranean sea) during two autumn–winter periods with contrasting meteorological conditions. *Progress in Oceanography* **210**: 102942.

-
- Eyrolle, F., O. Radakovitch, P. Raimbault, and others. 2012. Consequences of hydrological events on the delivery of suspended sediment and associated radionuclides from the Rhône River to the Mediterranean Sea. *Journal of Soils and Sediments* **12**: 1479–1495. doi:10.1007/s11368-012-0575-0
- Fenchel, T., H. Blackburn, G. M. King, and T. H. Blackburn. 2012. *Bacterial biogeochemistry: The ecophysiology of mineral cycling*, Academic press.
- Feng, H., J. K. Cochran, and D. J. Hirschberg. 1999. ²³⁴Th and ⁷Be as tracers for transport and sources of particle-associated contaminants in the Hudson River estuary. *Science of the Total Environment* **237**: 401–418.
- Ferreira, E., S. Nmor, E. Viollier, and others. 2023. Characterization of the benthic biogeochemical dynamics after flood events in the Rhône river prodelta: A data-model approach. *Biogeosciences Discussions* **2023**: 1–27.
- Ferrón, S., F. Alonso-Pérez, T. Ortega, and J. M. Forja. 2009. Benthic respiration on the northeastern shelf of the Gulf of Cádiz (SW Iberian Peninsula). *Marine Ecology Progress Series* **392**: 69–80.
- Fiadeiro, M. E., and G. Veronis. 1977. On weighted-mean schemes for the finite-difference approximation to the advection-diffusion equation. *Tellus* **29**: 512–522.
- Finstér, K., W. Liesack, and B. Thamdrup. 1998. Elemental sulfur and thiosulfate disproportionation by *Desulfocapsa sulfoexigens* sp. nov., a new anaerobic bacterium isolated from marine surface sediment. *Applied and Environmental Microbiology* **64**: 119–125.
- Froelich, P. N. 1988. Kinetic control of dissolved phosphate in natural rivers and estuaries: A primer on the phosphate buffer mechanism 1. *Limnology and Oceanography* **33**: 649–668.
- Froelich, P. N., G. P. Klinkhammer, M. L. Bender, and others. 1979a. Early oxidation of organic matter in pelagic sediments of the eastern equatorial Atlantic: Suboxic diagenesis. *Geochimica et Cosmochimica Acta* **43**: 1075–1090. doi:10.1016/0016-7037(79)90095-4
- Froelich, P., G. Klinkhammer, M. L. Bender, and others. 1979b. Early oxidation of organic matter in pelagic sediments of the eastern equatorial Atlantic: Suboxic diagenesis. *Geochimica et Cosmochimica Acta* **43**: 1075–1090.
- García-García, A., D. Orange, T. Lorenson, and others. 2006. Shallow gas off the Rhône prodelta, Gulf of Lions. *Marine Geology* **234**: 215–231.
- Gebhardt, A., B. Gaye-Haake, D. Unger, N. Lahajnar, and V. Ittekkot. 2004. Recent particulate organic carbon and total suspended matter fluxes from the Ob and Yenisei rivers into the Kara Sea (Siberia). *Marine Geology* **207**: 225–245.
- Ghil, M. 2019. A century of nonlinearity in the geosciences. *Earth and Space Science* **6**: 1007–1042.
- Glud, R. N. 2008. Oxygen dynamics of marine sediments. *Marine Biology Research* **4**: 243–289. doi:10.1080/17451000801888726
- Goldberg, E. D., and M. Koide. 1962. Geochronological studies of deep sea sediments by the ionium/thorium method. *Geochimica et Cosmochimica Acta* **26**: 417–450.
- Gooday, A. J. 2002. Biological responses to seasonally varying fluxes of organic matter to the ocean floor: A review. *Journal of Oceanography* **58**: 305–332.
- Got, H., and J. Aloisi. 1990. The Holocene sedimentation on the Gulf of Lions margin: A quantitative approach. *Continental Shelf Research* **10**: 841–855.
- Grenz, C., L. Denis, G. Boucher, L. Chauvaud, J. Clavier, R. Fichez, and O. Pringault. 2003. Spatial variability in sediment oxygen consumption under winter conditions in a lagoonal system in New Caledonia (South Pacific). *Journal of Experimental Marine Biology and Ecology* **285**: 33–47.

-
- Group, T. M., X. D. de Madron, C. Guieu, and others. 2011. Marine ecosystems' responses to climatic and anthropogenic forcings in the mediterranean. *Progress in Oceanography* **91**: 97–166.
- Gruber, N. 2015. Carbon at the coastal interface. *Nature* **517**: 148–149.
- Guinasso Jr, N., and D. Schink. 1975. Quantitative estimates of biological mixing rates in abyssal sediments. *Journal of Geophysical Research* **80**: 3032–3043.
- Haese, R., R. 2000. The reactivity of iron, in marine geochemistry, p. 233–261. *In* H.D. Schulz [ed.], *Marine geochemistry*. Springer.
- Hedges, J. I., and R. G. Keil. 1995. Sedimentary organic matter preservation: An assessment and speculative synthesis. *Marine chemistry* **49**: 81–115.
- Heinze, C., A. Hupe, E. Maier-Reimer, N. Dittert, and O. Ragueneau. 2003. Sensitivity of the marine biospheric si cycle for biogeochemical parameter variations. *Global biogeochemical cycles* **17**.
- Hensel, P. F., J. W. Day, D. Pont, and J. N. Day. 1998. Short-Term Sedimentation Dynamics in the Rhône River Delta, France: The Importance of Riverine Pulsing. *Estuaries* **21**: 52. doi:10.2307/1352546
- Hindmarsh, A. C. 1983. ODEPACK: A systemized collection of ODE solvers. *Scientific computing* 55–64.
- Horowitz, A. J. 2003. An evaluation of sediment rating curves for estimating suspended sediment concentrations for subsequent flux calculations. *Hydrological processes* **17**: 3387–3409.
- Hu, X., and W.-J. Cai. 2011. The impact of denitrification on the atmospheric CO₂ uptake potential of seawater. *Marine Chemistry* **127**: 192–198.
- Hülse, D., S. Arndt, S. Daines, P. Regnier, and A. Ridgwell. 2018. OMEN-SED 1.0: A novel, numerically efficient organic matter sediment diagenesis module for coupling to earth system models. *Geoscientific Model Development* **11**: 2649–2689.
- Ilyina, T., K. D. Six, J. Segsneider, E. Maier-Reimer, H. Li, and I. Núñez-Riboni. 2013. Global ocean biogeochemistry model HAMOCC: Model architecture and performance as component of the MPI-earth system model in different CMIP5 experimental realizations. *Journal of Advances in Modeling Earth Systems* **5**: 287–315.
- Jahnke, R. A., C. E. Reimers, and D. B. Craven. 1990. Intensification of recycling of organic matter at the sea floor near ocean margins. *Nature* **348**: 50–54.
- Jørgensen, B. B. 1982. Mineralization of organic matter in the sea bed—the role of sulphate reduction. *Nature* **296**: 643–645.
- Jørgensen, B. B., A. J. Findlay, and A. Pellerin. 2019. The biogeochemical sulfur cycle of marine sediments. *Frontiers in microbiology* **10**: 849.
- Jørgensen, B. B., and S. Kasten. 2006. Sulfur cycling and methane oxidation. *Marine geochemistry* 271–309.
- Jørgensen, B. B., and N. P. Revsbech. 1985. Diffusive boundary layers and the oxygen uptake of sediments and detritus 1. *Limnology and oceanography* **30**: 111–122.
- Jourabchi, P., P. Van Cappellen, and P. Regnier. 2005. Quantitative interpretation of pH distributions in aquatic sediments: A reaction-transport modeling approach. *American Journal of Science* **305**: 919–956.
- Karlson, B., P. Andersen, L. Arneborg, and others. 2021. Harmful algal blooms and their effects in coastal seas of Northern Europe. *Harmful Algae* **102**: 101989. doi:10.1016/j.hal.2021.101989
- Katsev, S., B. Sundby, and A. Mucci. 2006. Modeling vertical excursions of the redox boundary in sediments: Application to deep basins of the Arctic Ocean. *Limnology and Oceanography* **51**: 1581–1593. doi:10.4319/lo.2006.51.4.1581
- Kirschbaum, M. U. 2013. Seasonal variations in the availability of labile substrate confound the temperature dependence of organic matter decomposition. *Soil Biology and Biochemistry* **57**: 568–576.

-
- Kittel, T., J. Heitzig, K. Webster, and J. Kurths. 2017. Timing of transients: Quantifying reaching times and transient behavior in complex systems. *New Journal of Physics* **19**: 083005.
- Klump, J. V., and C. S. Martens. 1989. The seasonality of nutrient regeneration in an organic-rich coastal sediment: Kinetic modeling of changing pore-water nutrient and sulfate distributions. *Limnology and Oceanography* **34**: 559–577.
- Knab, N. J., B. A. Cragg, C. Borowski, R. J. Parkes, R. Pancost, and B. B. Jørgensen. 2008. Anaerobic oxidation of methane (AOM) in marine sediments from the skagerrak (denmark): I. Geochemical and microbiological analyses. *Geochimica et Cosmochimica Acta* **72**: 2868–2879.
- Kristensen, E., G. Penha-Lopes, M. Delefosse, T. Valdemarsen, C. O. Quintana, and G. T. Banta. 2012. What is bioturbation? The need for a precise definition for fauna in aquatic sciences. *Marine ecology progress series* **446**: 285–302.
- Krumins, V., M. Gehlen, S. Arndt, P. Van Cappellen, and P. Regnier. 2013. Dissolved inorganic carbon and alkalinity fluxes from coastal marine sediments: Model estimates for different shelf environments and sensitivity to global change. *Biogeosciences* **10**: 371–398.
- Lansard, B., C. Rabouille, L. Denis, and C. Grenz. 2008. In situ oxygen uptake rates by coastal sediments under the influence of the Rhône River (NW Mediterranean Sea). *Continental Shelf Research* **28**: 1501–1510. doi:10.1016/j.csr.2007.10.010
- Lansard, B., C. Rabouille, L. Denis, and C. Grenz. 2009a. Benthic remineralization at the land–ocean interface: A case study of the Rhône river (NW mediterranean sea). *Estuarine, Coastal and Shelf Science* **81**: 544–554.
- Lansard, B., C. Rabouille, L. Denis, and C. Grenz. 2009b. Benthic remineralization at the land–ocean interface: A case study of the Rhône River (NW Mediterranean Sea). *Estuarine, Coastal and Shelf Science* **81**: 544–554. doi:10.1016/j.ecss.2008.11.025
- LaRowe, D. E., S. Arndt, J. Bradley, and others. 2020. The fate of organic carbon in marine sediments-new insights from recent data and analysis. *Earth-Science Reviews* **204**: 103146.
- Lasaga, A., and H. Holland. 1976. Mathematical aspects of non-steady-state diagenesis. *Geochimica et Cosmochimica Acta* **40**: 257–266.
- Lee, T.-Y., J.-C. Huang, J.-Y. Lee, S.-H. Jien, F. Zehetner, and S.-J. Kao. 2015. Magnified sediment export of small mountainous rivers in taiwan: Chain reactions from increased rainfall intensity under global warming. *PloS one* **10**: e0138283.
- Lepage, H., A. Gruat, F. Thollet, and others. 2022. Concentrations and fluxes of suspended particulate matter and associated contaminants in the Rhône river from lake geneva to the mediterranean sea. *Earth System Science Data* **14**: 2369–2384.
- Lessin, G., Y. Artioli, E. Almroth-Rosell, and others. 2018. Modelling Marine Sediment Biogeochemistry: Current Knowledge Gaps, Challenges, and Some Methodological Advice for Advancement. *Frontiers in Marine Science* **5**: 19. doi:10.3389/fmars.2018.00019
- Li, R., M. Li, and P. M. Glibert. 2022. Coupled carbonate chemistry - harmful algae bloom models for studying effects of ocean acidification on *Prorocentrum* minimum blooms in a eutrophic estuary. *Frontiers in Marine Science* **9**. doi:10.3389/fmars.2022.889233
- Lionello, P., G. Sannino, and I. Vilibić. 2023. Surface wave and sea surface dynamics in the mediterranean, p. 161–207. *In Oceanography of the mediterranean sea*. Elsevier.
- Lorenz, E. N. 1963. Deterministic nonperiodic flow. *Journal of atmospheric sciences* **20**: 130–141.
- Ludwig, W., J.-L. Probst, and S. Kempe. 1996. Predicting the oceanic input of organic carbon by continental erosion. *Global Biogeochemical Cycles* **10**: 23–41.

-
- Luff, R., and A. Moll. 2004. Seasonal dynamics of the north sea sediments using a three-dimensional coupled sediment–water model system. *Continental Shelf Research* **24**: 1099–1127.
- Luff, R., K. Wallmann, S. Grandel, and M. Schlüter. 2000. Numerical modeling of benthic processes in the deep arabian sea. *Deep Sea Research Part II: Topical Studies in Oceanography* **47**: 3039–3072.
- Mackenzie, F. T. 1999. Global biogeochemical cycles and the physical climate system. University Corporation for Atmospheric Research 1–76.
- Mackenzie, F., A. Lerman, and A. Andersson. 2004. Past and present of sediment and carbon biogeochemical cycling models. *Biogeosciences* **1**: 11–32.
- Madron, X. D. de, A. ABASSI, S. HEUSSNER, and others. 2000. Particulate matter and organic carbon budgets for the gulf of lions (NW mediterranean). *Oceanologica acta* **23**: 717–730.
- Madron, X. D. de, P. L. Wiberg, and P. Puig. 2008. Sediment dynamics in the gulf of lions: The impact of extreme events. *Continental Shelf Research* **28**: 1867–1876.
- Magen, C., G. Chaillou, S. A. Crowe, A. Mucci, B. Sundby, A. Gao, R. Makabe, and H. Sasaki. 2010. Origin and fate of particulate organic matter in the southern beaufort sea–amundsen gulf region, canadian arctic. *Estuarine, Coastal and Shelf Science* **86**: 31–41.
- Maier-Reimer, E., I. Kriest, J. Segschneider, and P. Wetzel. 2005. The hamburg ocean carbon cycle model HAMOCC5. 1-technical description release 1.1.
- Maillet, G. M., C. Vella, S. Berné, P. L. Friend, C. L. Amos, T. J. Fleury, and A. Normand. 2006. Morphological changes and sedimentary processes induced by the december 2003 flood event at the present mouth of the grand rhône river (southern france). *Marine Geology* **234**: 159–177.
- Manh, N. V., N. V. Dung, N. N. Hung, B. Merz, and H. Apel. 2014. Large-scale suspended sediment transport and sediment deposition in the mekong delta. *Hydrology and Earth System Sciences* **18**: 3033–3053.
- Many, G., F. Bourrin, X. D. De Madron, A. Ody, D. Doxaran, and P. Cauchy. 2018. Glider and satellite monitoring of the variability of the suspended particle distribution and size in the rhône ROFI. *Progress in oceanography* **163**: 123–135.
- Many, G., C. Ulses, C. Estournel, and P. Marsaleix. 2021. Particulate organic carbon dynamics in the gulf of lion shelf (NW mediterranean) using a coupled hydrodynamic–biogeochemical model. *Biogeosciences* **18**: 5513–5538.
- Marin, B., and P. Giresse. 2001. Particulate manganese and iron in recent sediments of the gulf of lions continental margin (north-western mediterranean sea): Deposition and diagenetic process. *Marine geology* **172**: 147–165.
- Marion, C., F. Dufois, M. Arnaud, and C. Vella. 2010. In situ record of sedimentary processes near the rhône river mouth during winter events (gulf of lions, mediterranean sea). *Continental Shelf Research* **30**: 1095–1107.
- Marsaleix, P., F. Auclair, J. W. Floor, M. J. Herrmann, C. Estournel, I. Pairaud, and C. Ulses. 2008. Energy conservation issues in sigma-coordinate free-surface ocean models. *Ocean Modelling* **20**: 61–89.
- Marvin-DiPasquale, M., and D. Capone. 1998. Benthic sulfate reduction along the chesapeake bay central channel. I. Spatial trends and controls. *Marine Ecology Progress Series* **168**: 213–228.
- Mayer, L. M. 1994. Surface area control of organic carbon accumulation in continental shelf sediments. *Geochimica et Cosmochimica Acta* **58**: 1271–1284.
- McKee, B. A., R. Aller, M. Allison, T. Bianchi, and G. Kineke. 2004. Transport and transformation of dissolved and particulate materials on continental margins influenced by major rivers: Benthic boundary layer and seabed processes. *Continental Shelf Research* **24**: 899–926.

-
- McMillan, S. K., H. F. Wilson, C. L. Tague, and others. 2018. Before the storm: Antecedent conditions as regulators of hydrologic and biogeochemical response to extreme climate events. *Biogeochemistry* **141**: 487–501.
- Meybeck, M., H. Dürr, S. Roussennac, and W. Ludwig. 2007. Regional seas and their interception of riverine fluxes to oceans. *Marine Chemistry* **106**: 301–325.
- Middelburg, J. J. 1989. A simple rate model for organic matter decomposition in marine sediments. *Geochimica et Cosmochimica acta* **53**: 1577–1581.
- Middelburg, J. J., and J. J. Middelburg. 2019. Carbon processing at the seafloor. *Marine carbon biogeochemistry: A primer for Earth system scientists* 57–75.
- Middelburg, J. J., and K. Soetaert. 2004. The role of sediments in shelf ecosystem dynamics. *The sea* **13**: 353–373.
- Middelburg, J. J., K. Soetaert, and P. M. Herman. 1997. Empirical relationships for use in global diagenetic models. *Deep Sea Research Part I: Oceanographic Research Papers* **44**: 327–344.
- Middelburg, J. J., T. Vlug, F. Jaco, and W. Van der Nat. 1993. Organic matter mineralization in marine systems. *Global and Planetary change* **8**: 47–58.
- Middelburg, J., and L. Levin. 2009. Coastal hypoxia and sediment biogeochemistry. *Biogeosciences* **6**: 1273–1293.
- Mieleitner, J., and P. Reichert. 2006. Analysis of the transferability of a biogeochemical lake model to lakes of different trophic state. *Ecological Modelling* **194**: 49–61.
- Mikolajczak, G., C. Estournel, C. Ulses, and others. 2020. Impact of storms on residence times and export of coastal waters during a mild autumn/winter period in the gulf of lion. *Continental Shelf Research* **207**: 104192.
- Milliman, J. D., and K. L. Farnsworth. 2013. *River discharge to the coastal ocean: A global synthesis*, Cambridge University Press.
- Milliman, J. D., and R. H. Meade. 1983. World-wide delivery of river sediment to the oceans. *The Journal of Geology* **91**: 1–21.
- Miralles, J., O. Radakovitch, and J.-C. Aloisi. 2005. ²¹⁰Pb sedimentation rates from the Northwestern Mediterranean margin. *Marine Geology* **216**: 155–167. doi:10.1016/j.margeo.2005.02.020
- Misrocchi, S., L. Langone, and T. Tesi. 2007. Content and isotopic composition of organic carbon within a flood layer in the po river prodelta (adriatic sea). *Continental Shelf Research* **27**: 338–358.
- Montanher, O. C., E. M. L. de M. Novo, and E. E. de Souza Filho. 2018. Temporal trend of the suspended sediment transport of the amazon river (1984–2016). *Hydrological sciences journal* **63**: 1901–1912.
- Moreira-Turcq, P., P. Seyler, J. L. Guyot, and H. Etcheber. 2003. Exportation of organic carbon from the amazon river and its main tributaries. *Hydrological processes* **17**: 1329–1344.
- Moriarty, J. M., M. A. Friedrichs, and C. K. Harris. 2021. Seabed resuspension in the chesapeake bay: Implications for biogeochemical cycling and hypoxia. *Estuaries and Coasts* **44**: 103–122.
- Moriarty, J. M., C. K. Harris, K. Fennel, M. A. Friedrichs, K. Xu, and C. Rabouille. 2017. The roles of resuspension, diffusion and biogeochemical processes on oxygen dynamics offshore of the rhône river, france: A numerical modeling study. *Biogeosciences* **14**: 1919–1946.
- Moriarty, J. M., C. K. Harris, M. A. Friedrichs, K. Fennel, and K. Xu. 2018. Impact of seabed resuspension on oxygen and nitrogen dynamics in the northern gulf of mexico: A numerical modeling study. *Journal of Geophysical Research: Oceans* **123**: 7237–7263.
- Morse, J. W., and P. M. Eldridge. 2007. A non-steady state diagenetic model for changes in sediment bio-

-
- geochemistry in response to seasonally hypoxic/anoxic conditions in the “dead zone” of the louisiana shelf. *Marine Chemistry* **106**: 239–255.
- Morse, J. W., and G. T. Rowe. 1999. Benthic biogeochemistry beneath the mississippi river plume. *Estuaries* **22**: 206–214.
- Mucci, A., B. Boudreau, and C. Guignard. 2003. Diagenetic mobility of trace elements in sediments covered by a flash flood deposit: Mn, fe and as. *Applied geochemistry* **18**: 1011–1026.
- Mucci, A., and H. M. Edenborn. 1992. Influence of an organic-poor landslide deposit on the early diagenesis of iron and manganese in a coastal marine sediment. *Geochimica et Cosmochimica Acta* **56**: 3909–3921.
- Mucci, A., B. Sundby, M. Gehlen, T. Arakaki, S. Zhong, and N. Silverberg. 2000. The fate of carbon in continental shelf sediments of eastern canada: A case study. *Deep Sea Research Part II: Topical Studies in Oceanography* **47**: 733–760.
- Mudroch, A., and S. D. MacKnight. 1994. *Handbook of techniques for aquatic sediments sampling*, CRC press.
- Munhoven, G. 2021. Model of early diagenesis in the upper sediment with adaptable complexity–MEDUSA (v. 2): A time-dependent biogeochemical sediment module for earth system models, process analysis and teaching. *Geoscientific Model Development* **14**: 3603–3631.
- Mylykangas, J.-P., S. Hietanen, and T. Jilbert. 2020. Legacy effects of eutrophication on modern methane dynamics in a boreal estuary. *Estuaries and Coasts* **43**: 189–206.
- Newton, A., T. J. Carruthers, and J. Icely. 2012. The coastal syndromes and hotspots on the coast. *Estuarine, Coastal and Shelf Science* **96**: 39–47.
- Nick, H., A. Raouf, F. Centler, M. Thullner, and P. Regnier. 2013. Reactive dispersive contaminant transport in coastal aquifers: Numerical simulation of a reactive henry problem. *Journal of contaminant hydrology* **145**: 90–104.
- Nmor, S. I., E. Viollier, L. Pastor, B. Lansard, C. Rabouille, and K. Soetaert. 2022. FESDIA (v1. 0): Exploring temporal variations of sediment biogeochemistry under the influence of flood events using numerical modelling. *Geoscientific Model Development* **15**: 7325–7351.
- Olafsson, E. 2003. Do macrofauna structure meiofauna assemblages in marine soft-bottoms? A review of experimental studies. *Vie et Milieu/Life & Environment* 249–265.
- Osburn, C. L., J. C. Rudolph, H. W. Paerl, A. G. Hounshell, and B. R. Van Dam. 2019. Lingering carbon cycle effects of hurricane matthew in north carolina’s coastal waters. *Geophysical Research Letters* **46**: 2654–2661.
- Palinkas, C., C. Nittrouer, R. Wheatcroft, and L. Langone. 2005. The use of ⁷Be to identify event and seasonal sedimentation near the po river delta, adriatic sea. *Marine Geology* **222**: 95–112.
- Paraska, D. W., M. R. Hipsey, and S. U. Salmon. 2014. Sediment diagenesis models: Review of approaches, challenges and opportunities. *Environmental modelling & software* **61**: 297–325.
- Pastor, L., C. Cathalot, B. Deflandre, and others. 2011a. Modeling biogeochemical processes in sediments from the Rhône River prodelta area (NW Mediterranean Sea). *Biogeosciences* **8**: 1351–1366. doi:10.5194/bg-8-1351-2011
- Pastor, L., B. Deflandre, E. Viollier, and others. 2011b. Influence of the organic matter composition on benthic oxygen demand in the Rhône River prodelta (NW Mediterranean Sea). *Continental Shelf Research* **31**: 1008–1019. doi:10.1016/j.csr.2011.03.007
- Pastor, L., C. Rabouille, E. Metzger, A. Thibault de Chanvalon, E. Viollier, and B. Deflandre. 2018. Transient early diagenetic processes in Rhône prodelta sediments revealed in contrasting flood events. *Continental Shelf Research* **166**: 65–76. doi:10.1016/j.csr.2018.07.005

-
- Pena, M., S. Katsev, T. Oguz, and D. Gilbert. 2010. Modeling dissolved oxygen dynamics and hypoxia. *Biogeosciences* **7**: 933–957.
- Pont, D., J. W. Day, and C. Ibáñez. 2017. The impact of two large floods (1993–1994) on sediment deposition in the Rhône delta: Implications for sustainable management. *Science of The Total Environment* **609**: 251–262. doi:10.1016/j.scitotenv.2017.07.155
- Pont, D., J.-P. Simonnet, and A.-V. Walter. 2002. Medium-term changes in suspended sediment delivery to the ocean: Consequences of catchment heterogeneity and river management (Rhône river, France). *Estuarine, Coastal and Shelf Science* **54**: 1–18.
- Poulton, S. W., M. D. Krom, and R. Raiswell. 2004. A revised scheme for the reactivity of iron (oxyhydr) oxide minerals towards dissolved sulfide. *Geochimica et Cosmochimica Acta* **68**: 3703–3715.
- Poulton, S., and R. Raiswell. 2002. The low-temperature geochemical cycle of iron: From continental fluxes to marine sediment deposition. *American Journal of Science* **302**: 774–805.
- Pozzato, L., J. Rassmann, B. Lansard, J.-P. Dumoulin, P. van Breugel, and C. Rabouille. 2018. Origin of remineralized organic matter in sediments from the Rhône river prodelta (NW Mediterranean) traced by $\Delta^{14}\text{C}$ and $\delta^{13}\text{C}$ signatures of pore water DIC. *Progress in Oceanography* **163**: 112–122.
- Press, W. H., B. P. Flannery, S. A. Teukolsky, and W. T. Vetterling. 1992. *Numeric Recipes in C: The Art of Scientific Computing*. Camb. Univ. Press Camb.
- Pruski, A. M., R. Buscail, S. Bourgeois, G. Vétion, J. Coston-Guarini, and C. Rabouille. 2015. Biogeochemistry of fatty acids in a river-dominated Mediterranean ecosystem (Rhône river prodelta, Gulf of Lions, France): Origins and diagenesis. *Organic Geochemistry* **83**: 227–240.
- Pusceddu, A., A. Dell'Anno, M. Fabiano, and R. Danovaro. 2009. Quantity and bioavailability of sediment organic matter as signatures of benthic trophic status. *Marine Ecology Progress Series* **375**: 41–52.
- R Core Team. 2021. *R: A Language and Environment for Statistical Computing*, R Foundation for Statistical Computing.
- Rabouille, C., D. Conley, M. Dai, and others. 2008. Comparison of hypoxia among four river-dominated ocean margins: The Changjiang (Yangtze), Mississippi, Pearl, and Rhône rivers. *Continental Shelf Research* **28**: 1527–1537.
- Rabouille, C., and J.-F. Gaillard. 1990. The validity of steady-state flux calculations in early diagenesis: A computer simulation of deep-sea silica diagenesis. *Deep Sea Research Part A: Oceanographic Research Papers* **37**: 625–646.
- Rabouille, C., and J.-F. Gaillard. 1991. Towards the EDGE: Early diagenetic global explanation. A model depicting the early diagenesis of organic matter, O₂, NO₃, Mn, and PO₄. *Geochimica et Cosmochimica Acta* **55**: 2511–2525.
- Rabouille, C., F. T. Mackenzie, and L. M. Ver. 2001a. Influence of the human perturbation on carbon, nitrogen, and oxygen biogeochemical cycles in the global coastal ocean. *Geochimica et Cosmochimica Acta* **65**: 3615–3641.
- Rabouille, C., R. Witbaard, and G. Duineveld. 2001b. Annual and interannual variability of sedimentary recycling studied with a non-steady-state model: Application to the North Atlantic Ocean (Bengal site). *Progress in Oceanography* **50**: 147–170.
- Radakovitch, O., S. Charmasson, M. Arnaud, and P. Bouisset. 1999. ²¹⁰Pb and Caesium Accumulation in the Rhône Delta Sediments. *Estuarine, Coastal and Shelf Science* **48**: 77–92. doi:10.1006/ecss.1998.0405
- Radakovitch, O., V. Roussiez, P. Ollivier, W. Ludwig, C. Grenz, and J.-L. Probst. 2008. Input of particulate heavy metals from rivers and associated sedimentary deposits on the Gulf of Lion continental shelf. *Estuarine,*

-
- Coastal and Shelf Science **77**: 285–295.
- Radtke, H., M. Lipka, D. Bunke, and others. 2019. Ecological ReGional Ocean Model with vertically resolved sediments (ERGOM SED 1.0): Coupling benthic and pelagic biogeochemistry of the south-western Baltic Sea. *Geoscientific Model Development* **12**.
- Raiswell, R., and D. E. Canfield. 1998. Sources of iron for pyrite formation in marine sediments. *American Journal of Science* **298**: 219–245.
- Rassmann, J., E. M. Eitel, B. Lansard, C. Cathalot, C. Brandily, M. Taillefert, and C. Rabouille. 2020. Benthic alkalinity and dissolved inorganic carbon fluxes in the Rhône River prodelta generated by decoupled aerobic and anaerobic processes. *Biogeosciences* **17**: 13–33. doi:10.5194/bg-17-13-2020
- Rassmann, J., B. Lansard, L. Pozzato, and C. Rabouille. 2016. Carbonate chemistry in sediment porewaters of the Rhône river delta driven by early diagenesis (northwestern mediterranean). *Biogeosciences* **13**: 5379–5394.
- Raymond, P. A., and J. J. Cole. 2003. Increase in the export of alkalinity from north america's largest river. *Science* **301**: 88–91.
- Rayner, R., C. Jolly, and C. Gouldman. 2019. Ocean observing and the blue economy. *Frontiers in Marine Science* **6**: 330.
- Reed, D. C., C. P. Slomp, and B. G. Gustafsson. 2011. Sedimentary phosphorus dynamics and the evolution of bottom-water hypoxia: A coupled benthic–pelagic model of a coastal system. *Limnology and Oceanography* **56**: 1075–1092.
- Regnier, P., A. W. Dale, S. Arndt, D. LaRowe, J. Mogollón, and P. Van Cappellen. 2011. Quantitative analysis of anaerobic oxidation of methane (AOM) in marine sediments: A modeling perspective. *Earth-Science Reviews* **106**: 105–130.
- Regnier, P., P. Friedlingstein, P. Ciais, and others. 2013. Anthropogenic perturbation of the carbon fluxes from land to ocean. *Nature geoscience* **6**: 597–607.
- Regnier, P., J. O'kane, C. Steefel, and J.-P. Vanderborght. 2002. Modeling complex multi-component reactive-transport systems: Towards a simulation environment based on the concept of a knowledge base. *Applied Mathematical Modelling* **26**: 913–927.
- Regnier, P., L. Resplandy, R. G. Najjar, and P. Ciais. 2022. The land-to-ocean loops of the global carbon cycle. *Nature* **603**: 401–410.
- Reichert, P. 1994. AQUASIM—a tool for simulation and data analysis of aquatic systems. *Water Science and Technology* **30**: 21.
- Rickard, D. 1997. Kinetics of pyrite formation by the H₂S oxidation of iron (II) monosulfide in aqueous solutions between 25 and 125 °C: The rate equation. *Geochimica et Cosmochimica Acta* **61**: 115–134.
- Rickard, D. 2006. The solubility of FeS. *Geochimica et Cosmochimica Acta* **70**: 5779–5789.
- Robador, A., V. Brüchert, A. D. Steen, and C. Arnosti. 2010. Temperature induced decoupling of enzymatic hydrolysis and carbon remineralization in long-term incubations of arctic and temperate sediments. *Geochimica et Cosmochimica Acta* **74**: 2316–2326.
- Romans, B. W., S. Castelltort, J. A. Covault, A. Fildani, and J. Walsh. 2016. Environmental signal propagation in sedimentary systems across timescales. *Earth-Science Reviews* **153**: 7–29.
- Roussiez, V., W. Ludwig, O. Radakovitch, J.-L. Probst, A. Monaco, B. Charrière, and R. Buscail. 2011. Fate of metals in coastal sediments of a mediterranean flood-dominated system: An approach based on total and labile fractions. *Estuarine, Coastal and Shelf Science* **92**: 486–495.
- Rowe, G. T., M. E. C. Kaegi, J. W. Morse, G. S. Boland, and E. G. Escobar Briones. 2002. Sediment community

-
- metabolism associated with continental shelf hypoxia, northern gulf of mexico. *Estuaries* **25**: 1097–1106.
- Ruardij, P., and W. Van Raaphorst. 1995. Benthic nutrient regeneration in the ERSEM ecosystem model of the north sea. *Netherlands Journal of Sea Research* **33**: 453–483.
- Sadaoui, M., W. Ludwig, F. Bourrin, and P. Raimbault. 2016. Controls, budgets and variability of riverine sediment fluxes to the gulf of lions (NW mediterranean sea). *Journal of Hydrology* **540**: 1002–1015.
- Sciberras, M., J. G. Hiddink, S. Jennings, and others. 2018. Response of benthic fauna to experimental bottom fishing: A global meta-analysis. *Fish and Fisheries* **19**: 698–715.
- Seeberg-Elverfeldt, J., M. Schlüter, T. Feseker, and M. Kölling. 2005. Rhizon sampling of porewaters near the sediment-water interface of aquatic systems. *Limnology and oceanography: Methods* **3**: 361–371.
- Sempéré, R., B. Charrière, F. Van Wambeke, and G. Cauwet. 2000. Carbon inputs of the Rhône River to the Mediterranean Sea: Biogeochemical implications. *Global Biogeochemical Cycles* **14**: 669–681. doi:10.1029/1999GB900069
- Shafei, B. 2012. Reactive transport in natural porous media: Contaminant sorption and pore-scale heterogeneity, Georgia Institute of Technology.
- Slomp, C. P., H. P. Mort, T. Jilbert, D. C. Reed, B. G. Gustafsson, and M. Wolthers. 2013. Coupled dynamics of iron and phosphorus in sediments of an oligotrophic coastal basin and the impact of anaerobic oxidation of methane. *PloS one* **8**.
- Smeaton, C., and W. Austin. 2022. Quality not quantity: Prioritizing the management of sedimentary organic matter across continental shelf seas. *Geophysical Research Letters* **49**: e2021GL097481.
- Smith, D. A., and G. Matisoff. 2008. Sediment oxygen demand in the central basin of lake erie. *Journal of Great Lakes Research* **34**: 731–744.
- Smith, K. L., H. A. Ruhl, C. L. Huffard, M. Messié, and M. Kahru. 2018. Episodic organic carbon fluxes from surface ocean to abyssal depths during long-term monitoring in NE pacific. *Proceedings of the National Academy of Sciences* **115**: 12235–12240.
- Soetaer, K., P. M. Herman, and J. J. Middelburg. 1996. Dynamic response of deep-sea sediments to seasonal variations: A model. *Limnology and Oceanography* **41**: 1651–1668.
- Soetaert, K. 2014. Package rootSolve: Roots, gradients and steady-states in r. Google Scholar.
- Soetaert, K., and P. M. Herman. 2009. A practical guide to ecological modelling: Using r as a simulation platform, Springer.
- Soetaert, K., P. M. Herman, and J. J. Middelburg. 1996a. A model of early diagenetic processes from the shelf to abyssal depths. *Geochim. Cosmochim. Acta* **60**: 1019–1040.
- Soetaert, K., P. M. Herman, and J. J. Middelburg. 1996b. Dynamic response of deep-sea sediments to seasonal variations: A model. *Limnology and Oceanography* **41**: 1651–1668.
- Soetaert, K., and F. Meysman. 2012a. Reactive transport in aquatic ecosystems: Rapid model prototyping in the open source software R. *Environmental Modelling & Software* **32**: 49–60.
- Soetaert, K., and F. Meysman. 2012b. Reactive transport in aquatic ecosystems: Rapid model prototyping in the open source software r. *Environmental Modelling & Software* **32**: 49–60.
- Soetaert, K., J. J. Middelburg, P. M. Herman, and K. Buis. 2000. On the coupling of benthic and pelagic biogeochemical models. *Earth-Science Reviews* **51**: 173–201.
- Soetaert, K., and T. Petzoldt. 2010. Inverse modelling, sensitivity and monte carlo analysis in r using package FME. *Journal of statistical software* **33**: 1–28.
- Soetaert, K., and T. Petzoldt. 2020. Marelac: Tools for aquatic sciences,.
- Soetaert, K., T. Petzoldt, and F. Meysman. 2010a. Marelac: Tools for aquatic sciences.

-
- Soetaert, K., T. Petzoldt, and R. W. Setzer. 2010b. Solving Differential Equations in R: Package deSolve. *Journal of Statistical Software* **33**: 1–25. doi:10.18637/jss.v033.i09
- Sohma, A., Y. Sekiguchi, T. Kuwae, and Y. Nakamura. 2008. A benthic–pelagic coupled ecosystem model to estimate the hypoxic estuary including tidal flat—Model description and validation of seasonal/daily dynamics. *Ecological modelling* **215**: 10–39.
- Sommerfield, C. K., A. S. Ogston, B. L. Mullenbach, and others. 2007. Oceanic dispersal and accumulation of river sediment. *Continental margin sedimentation: from sediment transport to sequence stratigraphy* 157–212.
- Steinsberger, T., B. Müller, C. Gerber, B. Shafei, and M. Schmid. 2019. Modeling sediment oxygen demand in a highly productive lake under various trophic scenarios. *PLoS One* **14**: e0222318.
- Strogatz, S. H. 2018. *Nonlinear dynamics and chaos: With applications to physics, biology, chemistry, and engineering*, CRC press.
- Stumm, W., and J. J. Morgan. 2012. *Aquatic chemistry: Chemical equilibria and rates in natural waters*, John Wiley & Sons.
- Sulpis, O., M. P. Humphreys, M. M. Wilhelmus, D. Carroll, W. M. Berelson, D. Menemenlis, J. J. Middelburg, and J. F. Adkins. 2022. RADIV1: A non-steady-state early diagenetic model for ocean sediments in Julia and MATLAB/GNU octave. *Geoscientific Model Development* **15**: 2105–2131.
- Sundby, B. 2006. Transient state diagenesis in continental margin muds. *Marine chemistry* **102**: 2–12.
- Tabuchi, K., H. Kojima, and M. Fukui. 2010. Seasonal changes in organic matter mineralization in a sublittoral sediment and temperature-driven decoupling of key processes. *Microbial ecology* **60**: 551–560.
- Taylor, K. E. 2001. Summarizing multiple aspects of model performance in a single diagram. *Journal of Geophysical Research: Atmospheres* **106**: 7183–7192.
- Tengberg, A., E. Almroth, and P. Hall. 2003. Resuspension and its effects on organic carbon recycling and nutrient exchange in coastal sediments: In situ measurements using new experimental technology. *Journal of Experimental Marine Biology and Ecology* **285**: 119–142.
- Tesi, T., L. Langone, M. Goñi, R. Wheatcroft, S. Miserocchi, and L. Bertotti. 2012. Early diagenesis of recently deposited organic matter: A 9-yr time-series study of a flood deposit. *Geochimica et Cosmochimica Acta* **83**: 19–36.
- Tesi, T., S. Miserocchi, F. Acri, L. Langone, A. Boldrin, J. Hatten, and S. Albertazzi. 2013. Flood-driven transport of sediment, particulate organic matter, and nutrients from the Po river watershed to the Mediterranean sea. *Journal of Hydrology* **498**: 144–152.
- Thamdrup, B. 2000. Bacterial manganese and iron reduction in aquatic sediments. *Advances in microbial ecology* 41–84.
- Thamdrup, B., H. Fossing, and B. B. Jørgensen. 1994. Manganese, iron and sulfur cycling in a coastal marine sediment, Aarhus Bay, Denmark. *Geochimica et Cosmochimica Acta* **58**: 5115–5129.
- Thill, A., S. Moustier, J.-M. Garnier, C. Estournel, J.-J. Naudin, and J.-Y. Bottero. 2001. Evolution of particle size and concentration in the Rhône river mixing zone: Influence of salt flocculation. *Continental Shelf Research* **21**: 2127–2140.
- Thullner, M., P. Van Cappellen, and P. Regnier. 2005. Modeling the impact of microbial activity on redox dynamics in porous media. *Geochimica et Cosmochimica Acta* **69**: 5005–5019.
- Tockner, K., and J. A. Stanford. 2002. Riverine flood plains: Present state and future trends. *Environmental conservation* **29**: 308–330.
- Toussaint, F., C. Rabouille, C. Cathalot, and others. 2014. A new device to follow temporal variations of oxygen

- demand in deltaic sediments: The LSCE benthic station. *Limnology and oceanography: Methods* **12**: 729–741.
- Toussaint, F., N. Tisnérat-Laborde, C. Cathalot, R. Buscail, P. Kerhervé, and C. Rabouille. 2013b. Depositional Processes of Organic Matter in the Rhône River Delta (Gulf of Lions, France) Traced by Density Fractionation Coupled with $\delta^{14}\text{C}$ and $\delta^{13}\text{C}$. *Radiocarbon* **55**: 920–931. doi:10.1017/S0033822200058070
- Toussaint, F., N. Tisnérat-Laborde, C. Cathalot, R. Buscail, P. Kerhervé, and C. Rabouille. 2013a. Depositional processes of organic matter in the Rhône river delta (gulf of lions, france) traced by density fractionation coupled with $\Delta^{14}\text{C}$ and $\delta^{13}\text{C}$. *Radiocarbon* **55**: 920–931.
- Treude, T., A. Boetius, K. Knittel, K. Wallmann, and B. B. Jørgensen. 2003. Anaerobic oxidation of methane above gas hydrates at hydrate ridge, NE pacific ocean. *Marine Ecology Progress Series* **264**: 1–14.
- Treude, T., M. Krüger, A. Boetius, and B. B. Jørgensen. 2005. Environmental control on anaerobic oxidation of methane in the gassy sediments of eckernförde bay (german baltic). *Limnology and oceanography* **50**: 1771–1786.
- Ulses, C., P.-A. Auger, K. Soetaert, and others. 2016. Budget of organic carbon in the north-western mediterranean open sea over the period 2004–2008 using 3-d coupled physical-biogeochemical modeling. *Journal of Geophysical Research: Oceans* **121**: 7026–7055.
- Ulses, C., C. Estournel, J. Bonnin, X. Durrieu de Madron, and P. Marsaleix. 2008a. Impact of storms and dense water cascading on shelf-slope exchanges in the gulf of lion (NW mediterranean). *Journal of Geophysical Research: Oceans* **113**.
- Ulses, C., C. Estournel, X. D. De Madron, and A. Palanques. 2008b. Suspended sediment transport in the gulf of lions (NW mediterranean): Impact of extreme storms and floods. *Continental shelf research* **28**: 2048–2070.
- Ulses, C., C. Estournel, P. Puig, X. Durrieu de Madron, and P. Marsaleix. 2008c. Dense shelf water cascading in the northwestern mediterranean during the cold winter 2005: Quantification of the export through the gulf of lion and the catalan margin. *Geophysical Research Letters* **35**.
- Van Beek, P., M. Souhaut, B. Lansard, M. Bourquin, J.-L. Reyss, P. Von Ballmoos, and P. Jean. 2013. LAFARA: A new underground laboratory in the french pyrénées for ultra low-level gamma-ray spectrometry. *Journal of environmental radioactivity* **116**: 152–158.
- Van Cappellen, P., and J.-F. Gaillard. 2018. Biogeochemical dynamics in aquatic sediments, p. 335–376. *In* Reactive transport in porous media. De Gruyter.
- Van Cappellen, P., J.-F. Gaillard, and C. Rabouille. 1993. Biogeochemical transformations in sediments: Kinetic models of early diagenesis, p. 401–445. *In* Interactions of c, n, p and s biogeochemical cycles and global change. Springer.
- Van Cappellen, P., and Y. Wang. 1996. Cycling of iron and manganese in surface sediments; a general theory for the coupled transport and reaction of carbon, oxygen, nitrogen, sulfur, iron, and manganese. *American Journal of Science* **296**: 197–243.
- Velde, S. J. van de, C. T. Reinhard, A. Ridgwell, and F. J. Meysman. 2020. Bistability in the redox chemistry of sediments and oceans. *Proceedings of the National Academy of Sciences* **117**: 33043–33050.
- Velde, S. van de, V. Van Lancker, S. Hidalgo-Martinez, W. M. Berelson, and F. J. R. Meysman. 2018. Anthropogenic disturbance keeps the coastal seafloor biogeochemistry in a transient state. *Scientific Reports* **8**: 5582. doi:10.1038/s41598-018-23925-y
- Vidal, M., and J.-A. Morgui. 1995. Short-term pore water ammonium variability coupled to benthic boundary layer dynamics in alfacs bay, spain (ebro delta, NW mediterranean). *MARINE ECOLOGY-PROGRESS*

SERIES **118**: 229–229.

- Viollier, E., C. Rabouille, S. E. Apitz, and others. 2003. Benthic biogeochemistry: State of the art technologies and guidelines for the future of in situ survey. *Journal of Experimental Marine Biology and Ecology* **285**: 5–31.
- Wakelin, S., J. Holt, J. Blackford, J. Allen, M. Butenschön, and Y. Artioli. 2012. Modeling the carbon fluxes of the northwest european continental shelf: Validation and budgets. *Journal of Geophysical Research: Oceans* **117**.
- Walling, D., and A. Collins. 2008. The catchment sediment budget as a management tool. *environmental science & policy* **11**: 136–143.
- Wang, Y., and P. Van Cappellen. 1996. A multicomponent reactive transport model of early diagenesis: Application to redox cycling in coastal marine sediments. *Geochimica et Cosmochimica Acta* **60**: 2993–3014.
- Westerhold, T., N. Marwan, A. J. Drury, and others. 2020. An astronomically dated record of earth's climate and its predictability over the last 66 million years. *Science* **369**: 1383–1387.
- Westrich, J. T., and R. A. Berner. 1984. The role of sedimentary organic matter in bacterial sulfate reduction: The G model tested 1. *Limnology and oceanography* **29**: 236–249.
- Wheatcroft, R. A. 1990. Preservation potential of sedimentary event layers. *Geology* **18**: 843–845.
- Wheatcroft, R. A., and D. E. Drake. 2003. Post-depositional alteration and preservation of sedimentary event layers on continental margins, i. The role of episodic sedimentation. *Marine Geology* **199**: 123–137.
- Wheatcroft, R. A., A. W. Stevens, L. M. Hunt, and T. G. Milligan. 2006. The large-scale distribution and internal geometry of the fall 2000 po river flood deposit: Evidence from digital x-radiography. *Continental Shelf Research* **26**: 499–516.
- Wheatcroft, R., and C. Sommerfield. 2005. River sediment flux and shelf sediment accumulation rates on the pacific northwest margin. *Continental shelf research* **25**: 311–332.
- Wijsman, J., P. Herman, J. Middelburg, and K. Soetaert. 2002. A model for early diagenetic processes in sediments of the continental shelf of the black sea. *Estuarine, Coastal and Shelf Science* **54**: 403–421.
- Wollast, R. 1993. Interactions of carbon and nitrogen cycles in the coastal zone, p. 195–210. *In Interactions of c, n, p and s biogeochemical cycles and global change*. Springer.
- Wu, J., C. Rabouille, S. Charmasson, J. L. Reyss, and X. Cagnat. 2018. Constraining the origin of recently deposited particles using natural radionuclides ⁷Be and ²³⁴Thex in deltaic sediments. *Continental Shelf Research* **165**: 106–119. doi:10.1016/j.csr.2018.06.010
- Yakushev, E. V., E. A. Protsenko, J. Bruggeman, P. Wallhead, S. V. Pakhomova, S. K. Yakubov, R. G. Bellerby, and R.-M. Couture. 2017. Bottom RedOx model (BROM v. 1.1): A coupled benthic–pelagic model for simulation of water and sediment biogeochemistry. *Geoscientific Model Development* **10**: 453–482.
- Yin, K., J. Zhang, P.-Y. Qian, W. Jian, L. Huang, J. Chen, and M. C. Wu. 2004. Effect of wind events on phytoplankton blooms in the pearl river estuary during summer. *Continental shelf research* **24**: 1909–1923.
- Yuan-Hui, L., and S. Gregory. 1974. Diffusion of ions in sea water and in deep-sea sediments. *Geochimica et cosmochimica acta* **38**: 703–714.
- Zebracki, M., F. Eyrolle-Boyer, A. De Vismes-Ott, C. Antonelli, X. Cagnat, and V. Boullier. 2013. Radionuclide contents in suspended sediments in relation to flood types in the lower rhone river. *Procedia Earth and Planetary Science* **7**: 936–939.
- Zebracki, M., F. Eyrolle-Boyer, O. Evrard, D. Claval, B. Mourier, S. Gairoard, X. Cagnat, and C. Antonelli. 2015. Tracing the origin of suspended sediment in a large mediterranean river by combining continuous river monitoring and measurement of artificial and natural radionuclides. *Science of the Total Environment* **502**:

122–132.

- Zhang, Y., K. Kaiser, L. Li, D. Zhang, Y. Ran, and R. Benner. 2014. Sources, distributions, and early diagenesis of sedimentary organic matter in the pearl river region of the south china sea. *Marine Chemistry* **158**: 39–48.
- Zhao, M., S. Zhang, L. G. Tarhan, C. T. Reinhard, and N. Planavsky. 2020. The role of calcium in regulating marine phosphorus burial and atmospheric oxygenation. *Nature communications* **11**: 1–8.
- Zhuang, G.-C., V. B. Heuer, C. S. Lazar, and others. 2018. Relative importance of methylotrophic methanogenesis in sediments of the western mediterranean sea. *Geochimica et Cosmochimica Acta* **224**: 171–186.
- Zindorf, M., J. Rooze, C. Meile, C. März, G. Jouet, R. Newton, C. Brandily, and L. Pastor. 2021. The evolution of early diagenetic processes at the mozambique margin during the last glacial-interglacial transition. *Geochimica et Cosmochimica Acta* **300**: 79–94.

